PSO Elkraft FU-4205

SCR Catalsyt Deactivation by Additives

Final Report

F. Castellino, A.D. Jensen, J.E. Johnsson

CHEC Research Center
Department of Chemical and Biochemical Engineering
Technical University of Denmark

R. Fehrmann

Center for Sustainable and Green Chemistry
Department of Chemisty
Technical University of Denmark

July 2008

Contents

Preface

This work has been carried out in collaboration between the CHEC (Combustion and Harmful Emission Control) Research Center, Department of Chemical and Biochemical Engineering (KT) of the Technical University of Denmark, and the Center for Sustainable and Green Chemistry, Department of Chemisty (KEMI), Technical University of Denmark.

The project has involved

- one Ph.D. project, "Deactivation of SCR Catalysts by Additives", by Francesco Castellino;
- one 40 ECTS points M.Sc. project, "Deactivation of SCR Catalysts by Additives", by Sonia Pueyo Sin;
- one 2x20 ECTS points B.Sc. project, "Kinetics and Diffusion in DeNO$_x$ Catalysts", by Camilla Berg and Maria Friberg Andersen.

The reports of the above listed projects are available at the Department of Chemical and Biochemical Engineering of the Technical University of Denmark.

The work has been supervised by Professor Anker Degn Jensen from KT.

Summary

Biomass (co)-combustion has been for more than one decade practiced in countries like Denmark and Sweden. For instance, straw and wood chips are replacing as much coal as possible in the Danish heat and power production. However, biomass combustion presents different issues, which may reduce the efficiency of the process and make its operation rather complicated. For instance, fouling and corrosion of the superheater exchangers are the main problems encountered during straw combustion. Both these two effects are due to the particular composition of the fly ash produced, which is particularly rich in potassium chloride, KCl. This salt has a relatively low melting point temperature (i.e. 776 ℃) and is therefore found in a liquid phase at the temperature of the superheater exchangers. This fact makes the fly ash particularly sticky and deposition on the metal surfaces of the heat exchangers causing the formation of a fouling layer is then favoured. Subsequently fast chloride induced corrosion may occur.

In order to overcome these problems, the use of different additives to the biomass has been proposed. The objective of the addition process is to change the fly ash composition produced during combustion and thereby favor (i) the release of Cl in the gas phase; (ii) the formation of ashes melting at higher temperatures (i.e. 1000 ℃), and therefore minimize deposition on the superheater exchangers. In particular, Danish power companies sees as promising additives those involving P and Ca compounds proposed by Sørensen et al. (US Patent No. US6615751). However, little is known about their effects on the lifetime of the vanadia-based SCR catalysts. Both P and Ca are in fact known as deactivating compounds and therefore some concerns about their utilization at full scale have risen.

In order to estimate the potential impact of the addition process on the SCR catalysts, deactivation tests with the potential products of the additives reaction have been performed both at a SCR pilot plant and in the laboratory.

The first part of the experimental work mainly focused on Phosphorus. In order to simulate the release of gaseous phosphorus during combustion, phosphoric acid was added to a natural gas flue gas and the resulting flue gas

was let through a SCR commercial vanadia-based monolith. Three different monoliths were exposed to 10, 100 and 1000 ppmv H_3PO_4. Polyphosphoric acids were formed due to the exposure at high temperatures (i.e. > 800 ℃) of the injected acid. According to their concentration in the flue gas, both chemical and physical deactivation may occur as shown by the performed tests. These are the first well-controlled experiments in the literature showing the real deactivation potential of phosphorus.

In the second part of the work, commercial SCR monolith were exposed to a flue gas doped with K_3PO_4. This compound was tested since it is one of the possible products forming during reaction between the alkali fraction released by the biomass, and the P introduced by the additives. Furthermore, the test has served the scope of better understanding the mechanism of deactivation by K. From the results obtained, it can be concluded that binding K to P in potassium phosphates will not reduce the rate of deactivation normally experienced during biomass firing.

In the third part of the work, both H_3PO_4, KCl, $Ca(OH)_2$ and H_2SO_4 have been added to the flue gas in order to have the P/K and P/Ca molar ratios equal to 2 and 0.8 as suggested from previous combustion test with straw and P,Ca-additives. During the test here reported, K was effectively bound to P-Ca-K species and did not deactivate the catalyst. Considering the fact that all the Cl was released in the gas phase, it can be concluded that the addition process may have some potential also in reducing the fast rates of deactivation observed during biomass combustion. On the other hand, part of the total P introduced in the system formed polyphosphoric acids that accumulated in the catalyst walls and enhanced fouling on the outer surface. It is therefore important to reduce their formation, probably by optimising the P/K and P/Ca molar ratios adopted at full scale.

Chapter 1

Introduction

In this section both the SCR process and the Additives are briefly introduced. A more comprehensive literature report concerning the SCR process, the vanadia-based SCR catalysts and the known deactivation mechanisms is present in Appendix A. Here, further information and detailed references to the facts here cited can be found. Regarding the Additives, all the data reported in the present work are taken from Sørensen et al., US Patent No. US6615751, and P.A. Jensen et al., Technical University of Denmark (2005) KT-Report No. 0504.

1.1 Background

Nitrogen oxides emitted from combustion and high temperature processes have been regarded during the last three decades as a major environmental concern, thus supporting a great amount of research to develop clean combustion techniques. Among the various technologies available nowadays for removing NO_x from stationary sources, the Selective Catalytic Reduction (SCR) process applied to fossil fuel combustion is the best-developed and worldwide applied. In this process, the NO_x fraction of the flue gas is reduced to nitrogen by ammonia on a catalyst surface. The commercial SCR catalysts normally employed at central power stations constituted by vanadia (the active phase) supported on high surface titania. WO_3 and MoO_3 are also added to the final composition in order to improve their physical and chemical properties.

Understanding of the mechanisms of catalyst deactivation has also been the aim of many investigations. Since the appearance of the SCR catalysts in the 1980s, many of the possible causes of both chemical and physical deactivation have been investigated. These studies have always been strictly

correlated to the problems encountered at full-scale applications and have often led to the development of better catalysts. Nowadays, the number of these investigations is still increasing due to the requirement of NO_x abatement in processes where alternative fuels are burnt, and where the catalyst life is not as long as desired due to the presence of different deactivating compounds in the resulting flue gas. Since both the use of alternative fuels and the removal of the NO_x fraction from the flue gases are more often regulated by local environmental policy, research is needed to make the co-existence of these two practices economically feasible for the power operators.

In the case of straw combustion, the application of the SCR is rather problematic due to the fast deactivation rates experienced. Straw is rich in K, which is one of the strongest poisons for the vanadia-based SCR catalysts. Deactivation rates up to 1%/day have been reported during straw firing at a Danish power plant.

On the other hand, biomass (co)-combustion has been for more than one decade practiced in countries like Denmark and Sweden. For instance, straw and wood chips are partially replacing coal in the Danish heat and power production. Owing to government demand, since the year 2000, 1.2 million tones of straw and 200 000 tones of wood chips are to be used annually in the power plants, providing approximately 6% of the annual energy consumption in the danish power stations. In the long term, the Danish government is planning to increase even more the use of biomass at central power stations.

However, biomass combustion presents different issues, which may reduce the efficiency of the process and make its operation rather complicated. For instance, fouling and corrosion of the superheater exchangers are the main problems encountered during straw combustion. Both these two effects are due to the composition of the fly ash produced, which is particularly rich in potassium chloride, KCl. This salt has a relatively low melting point temperature (i.e. 776 ℃) and is therefore found in a liquid phase at the temperature of the superheater exchangers. This fact makes the fly ash particularly sticky and deposition on the metal surfaces of the heat exchangers causing the formation of a fouling layer is then favoured. Heat transfer through the heat exchanger is consequently decreased, and so is the efficiency in energy production. Due to the presence of chlorine in the deposits, these are particularly corrosive and may irreversibly damage the heat exchangers.

In order to overcome these problems, the use of different additives to the biomass has been proposed. The objective of the addition process is to change the fly ash composition produced during combustion and thereby favor (i) the release of Cl in the gas phase; (ii) the formation of ashes melting at temperatures higher than e.g. 1000℃, and therefore minimize sticking on the superheater exchangers. In particular, Danish power companies sees as

Table 1.1: Theoretical products of biomass combustion in the presence of additives

	T_m, ℃	P/K	P/Ca
$K_4P_2O_7$	1105	0.5	-
$K_2CaP_2O_7$	1143	1.0	2
K_3PO_4	1340	0.33	-
$KCaPO_4$	1560	1.0	1
$K_4Ca(PO_4)_2$	1645	0.5	2
$Ca_3(PO_4)_2$	1670	-	0.66

promising additives those involving P and Ca compounds proposed in the above mentioned patent by Sørensen et al.. According to the invention, the addition process creates the reacting conditions at which all the potassium released during biomass combustion is bound in a phase consisting of K_2O-CaO-P_2O_5, that have melting points above 1000 ℃, and eventually K_3PO_4, that have a melting point of 1340℃, while releasing the Cl in the gas phase. In order to meet these conditions, a fuel analysis is required and the amount of P and Ca to be added is calculated with the following formulas:

$$\mathrm{P}_{added} = q_1(31/39\mathrm{K}_w + 31/23\mathrm{Na}_w - \mathrm{P}_w - 31/35.4\mathrm{Cl}_w) \quad (1.1)$$

$$\mathrm{Ca}_{added} = q_2(40/31(\mathrm{P}_{added} + \mathrm{P}_w) - \mathrm{Ca}_w) \quad (1.2)$$

where E_w indicates the amount of the element E in parts by weight per 100 parts by weight of the non combustible inorganic portion of fuel material before addition of additives. According to the invention, the two parameters q_1 and q_2 are ranging between 0.33 and 5 and 0 and 3 respectively. Based on the adopted values, the ash resulting from the combustion of the biomass containing fuel will be dominated by the compositions showed in Table 1.1.

Tests using a macro-TGA (thermo-gravimetric analysis) and a bench scale atmospheric fluidized bed, involving wheat samples impregnated by aqueous solutions of H_3PO_4 and/or $Ca(H_2PO_4)_2H_2O$, have been giving good results in terms of sintering, indicating higher melting temperatures. The ash produced by heating up the pretreated fuel was in the worse case only partially sintered, containing few fused ash particles at temperature around 1000 ℃. In these tests the major products measured using X-ray diffraction were the ones showed in Table 1.1. Addition of monocalcium phosphate monohydrate as crushed dry particles showed also good results.

Different types of biomass pretreated with Ca and P additives have been tested at the CHEC research center solid fuel flow reactor modified in order

to make some deposit tests. Here, a very high reduction (-98%) of Cl deposit contents was observed when the obtained ratios in the prepared fuel and additive mixture were approximately: P/(Na+K) = 2 and P/Ca = 0.8.

While the here mentioned preliminary combustion tests of biomass with the additives have shown their potential for solving the above mentioned fouling and corrosion problems, little is known about their effects on the lifetime of the vanadia-based SCR catalysts. Both P and Ca are known as deactivating compounds and therefore some concerns about their utilization at full scale have risen.

1.2 Objectives

The main objective of this work has been to study the potential effects of the P and Ca additives on vanadia-based commercial SCR catalysts by clarifying their mechanism of deactivation under well defined and realistic conditions. For this purpose, deactivation tests have been carried out in a pilot-scale SCR reactor by exposing commercial SCR monoliths to a flue gas doped with P, K and Ca, both independently and as a mixture.

The experimental work has been divided into the following three parts:

1. *Deactivation by Phosphorus*
2. *Deactivation by Potassium phosphates*
3. *Simultaneous deactivation by K, P and Ca*
4. *Studies of Diffusion in Fresh Catalysts*

In the first part, the deactivating effects due to P have been studied both in the laboratory, by doping the catalyst according to the conventional wet impregnation methods, and in the pilot plant. Here P, which was injected as H_3PO_4, was exposed to more realistic combustion temperatures and underwent important both chemical and physical changes, which revealed its real deactivation strength. The work carried out in this part can be considered the first reference of deactivation by P under combustion conditions and have improved the understanding of various deactivation mechanisms experienced at full scale during combustion of P-rich fuels.

The second part of the work dealt with deactivation by potassium phosphate and mainly served two purposes. According to the invention by Sørensen et al., K_3PO_4 may be one of the most desired products of the addition process, since it has a relatively high melting point temperature (i.e. 1340 ℃) and would require the release of Cl in the gas phase during its formation.

Therefore the first purpose of the tests was to verify the poisoning strength of this compound. Since in previous works the strong K-deactivation has been related to the melting point of the compounds in which K is included, this test has also served the purpose to verify this relation and thereby increase the understanding of K-deactivation.

In the third part of the experimental work a deactivation test simulating the suggested ratios P/K=2 and P/Ca=0.8 has been carried out.

The main findings of the above mentioned parts are presented in this report. Based on these findings, their practical applications, both concerning the addition process, the different potentially *SCR-friendly* co-firing solutions and the more general aspect about deactivation of SCR catalysts are addressed. For further details about the investigations carried out, the three papers written for publication on peer-reviewed international journals have been attached in the Appendix.

Finally, the diffusion in fresh catalysts has been studied as part of a 2x20 ECTS points B.Sc. project by Camilla Berg and Maria Frieberg Andersen. The report is available at the Department of Chemical and Biochemical Engineering of DTU.

Chapter 2

Deactivation by P

The results reported in this section have been published in the peer-reviewed international journal *Applied Catalysis B: Environmental*. The paper is included in Appendix B.

2.1 Polyphosphoric Acids Formation and Deposition

When exposed to the high temperatures of combustion, gaseous phosphoric acid, H_3PO_4, undergoes condensation reactions leading to the formation of chains of poly-, pyro-, tri-, and meta-phosphoric acids. These reactions can be explained as follows. The ortho-phosphoric acid molecule can be written as $0.5P_2O_5{\cdot}3H_2O$ and thus be considered as a 72.5% P_2O_5 solution having a boiling point temperature at 255 ℃. When exposed to higher temperatures, water can evaporate until an azeotropic mixture consisting of 92.4% P_2O_5 is formed. This azeotropic mixture has a much higher boiling point at 864 ℃. Due to their higher boiling point temperatures, the polyphosphoric acids may condense due to homogeneous nucleation according to their vapor pressure when the gas cools down to the SCR reactor temperature. Figure 2.1 shows a plot of the partial pressure of different polyphosphoric acids as a function of P_2O_5 content. As it can be seen, for temperatures around 350 ℃, a liquid phase of the polyphosphoric acids at azeotropic composition is already in equilibrium with a vapor having a partial pressure of 10 ppm. Once those polyphosphoric acids are formed, their condensation may happen already at concentrations of few ppm.

Polyphosphoric acid condensation has been confirmed during our tests at the SCR pilot plant. Aerosol measurements with a Scanning Mobility Particle Sizer (SMPS) have been made at the SCR reactor inlet at different

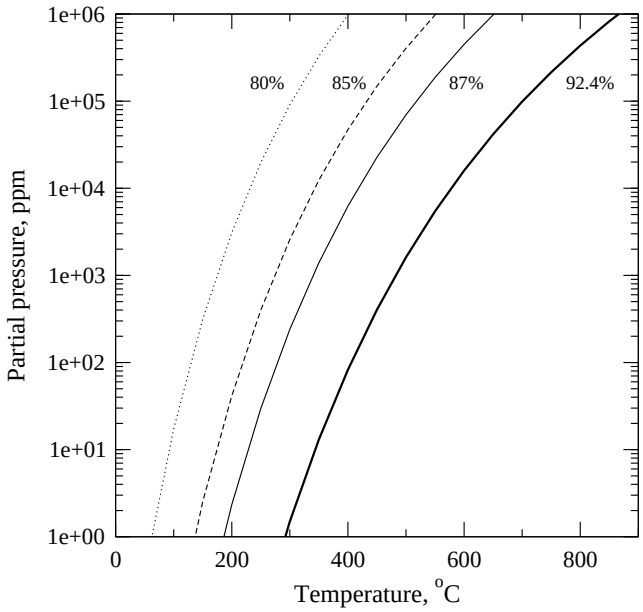

Figure 2.1: Vapor pressure of polyphosphoric acids as a function of temperature at different P_2O_5 weight content.

H_3PO_4 concentrations in the flue gas (i.e. 10-400 ppmv). In Figure 2.2 the particle size distribution (PSD) for some of the tests are shown. In all the measurements the PSD consisted of only one clear peak. The mean particle size, which was calculated from the total number concentration, was found to vary in the range 25-70 nm and was increasing with the acid concentration in the flue gas. The order of magnitude of the total particle number concentration was equal to $1{\cdot}10^{14}$ particles/m^3. Both the low particle diameters and the high concentration numbers clearly indicate the occurrence of homogeneous nucleation in the gas phase. Based on the plot showed in Figure 2.1, particle formation has been assumed occurring at temperatures < 500 ℃. From the deposits found in the setup, these particles were constituted by a green viscous liquid phase.

2.2 Deactivation by Polyphosphoric Acids

Three commercial vanadia-based monoliths have been exposed at the pilot plant to a flue gas doped with 10, 100 and 1000 ppmv H_3PO_4 respectively.

The first test carried out was the one with 1000 ppmv. Due to a massive formation of polyphosphoric acids, the entire catalyst pore structure was

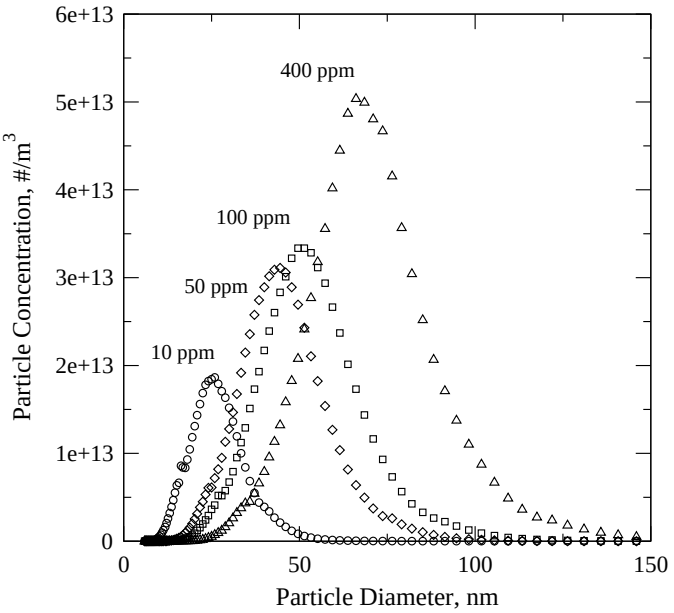

Figure 2.2: Particle size distribution of polyphosphoric acids measured at the SCR reactor inlet at different H_3PO_4 addition by SMPS. T = 350 ℃.

filled and the exposed element was practically dead after only 24 hours of exposure. Figure 2.3 shows the loss of 33% of initial activity during the first 2 hours of exposure. This test clearly shows how, at very high P concentrations, the catalyst can be physically deactivated by pore blocking and condensation.

When the H_3PO_4 concentration in the flue gas was decreased to only 10 ppmv, the relative activity of a fresh catalyst element stabilized at around 65% (Figure 2.4) indicating the occurrence of a pseudo steady state. At the end of the exposure, the total P-concentration was found equal to about 3.1%wt. However, as it is shown in Figure 2.4, most of the deactivation took place before starting the acid addition. This fact was due to re-entraining of deposits that accumulated in the setup during the exposure to 1000 ppmv H_3PO_4 and that were found in the the monolith channels at the end of the test. The relative decrease in activity from the start of the addition was equal to 10%.

When the H_3PO_4 concentration in the flue gas was increased to 100 ppmv, the P-accumulation was again very fast: After 38 h of exposure the element accumulated 4.2%wt. P. The relative activity measured at the end of the exposure was equal to 42%. However, during the activity measurements, a transient in NO was measured as a function of NH_3 exposure, as shown in Figure 2.5. As it can be seen, at the beginning of the NH_3 addition (i.e. at

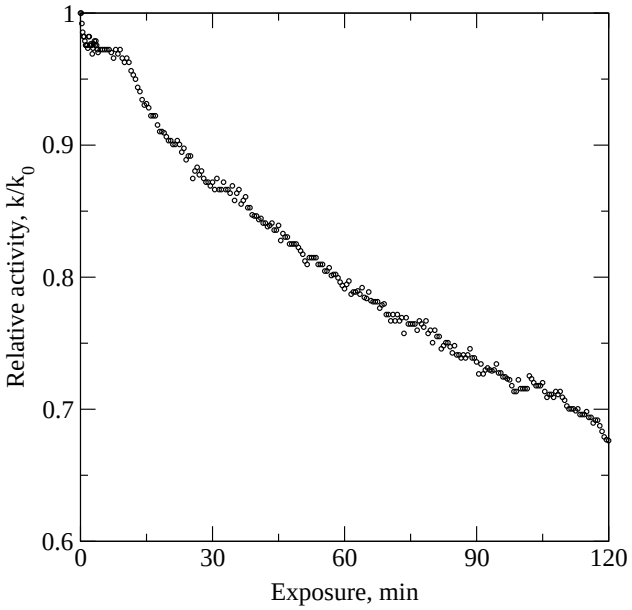

Figure 2.3: Relative activity of the P1000 element during the first 2 hours of exposure. T = 350 ℃. Total flow: 40 Nm^3/h. Gas composition on dry basis: NO = 496 ppmv, NH_3 = 735 ppmv, O_2 = 10%v, CO_2 = 6%v, N_2 balance. 10%v H_2O.

the time 0 in the plot), the element was converting 55% of the inlet NO, corresponding to a relative activity of 90%. After 40 minutes of continuous addition of NH_3, however, the NO reached a steady-state level at about 340 ppmv, corresponding to a NO conversion of 31% and a relative activity of 42%.

In order to understand the reasons causing the NO transient, in situ Electron Paramagnetic Resonance (EPR) measurements have been carried out using both a fresh catalyst, a sample exposed to 10 ppmv H_3PO_4 and a sample exposed to 100 ppmv H_3PO_4. The results have shown that the V(IV) sites on the catalyst, which according to the accepted mechanism of reaction are produced as intermediate of reaction during the NO reduction, are not readily re-oxidized to the active V(V) in the presence of the polyphosphoric acids. This NO transient is believed to be the main characteristic indicating poisoning by polyphosphoric acids.

Deposition of polyphosphoric acids also had another consequence. The amount of chemisorbed NH_3 was found higher on the catalysts doped with polyphosphoric acids, and the NO conversion rate was dependent on the NH_3 partial pressure in the flue gas. In Figure 2.5 it is shown how doubling the NH_3 concentration increased the NO conversion. This fact has been associ-

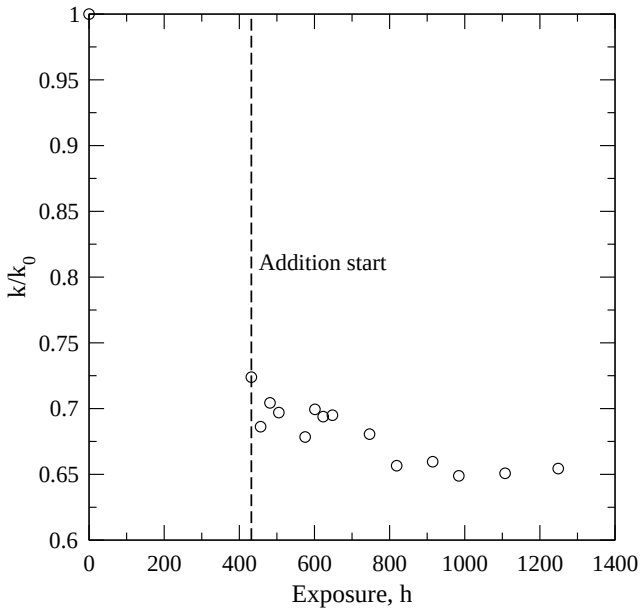

Figure 2.4: Relative activity of P10 at 350 ℃as a function of exposure time. Total flow: 40 Nm^3/h. Average gas composition: NO = 500 ppmv, NH_3 = 735 ppmv, O_2 = 10%v, CO_2 = 6%v, and 10%v H_2O in N_2.

ated to a decrease in NH_3 coverage at the standard experimental conditions of our tests (i.e. 350 ℃ and 600 ppmv NH_3).

2.3 Conclusions

When exposed to the high temperatures of a combustion process, the H_3PO_4 molecules eventually released in the gas phase start condensation reactions forming polyphosphoric acids. This process has been simulated in the present investigations and the deactivation mechanism by polyphosphoric acid have been clarified.

This deactivation mechanism has been found to follow both a physical and a chemical deactivation. Surface masking, fouling, pore blocking and condensation are definitely important contributions to catalyst deactivation. Once deposited on the catalyst outer surface, they are very mobile and can even be sucked into the walls by capillary forces. The P-accumulation, and consequently the implied deactivation, is however limited by the rate of hydrolysis of the deposits themselves. The H_2O present in the flue gas, at the SCR temperatures can break down the polyphosphoric acid chains and

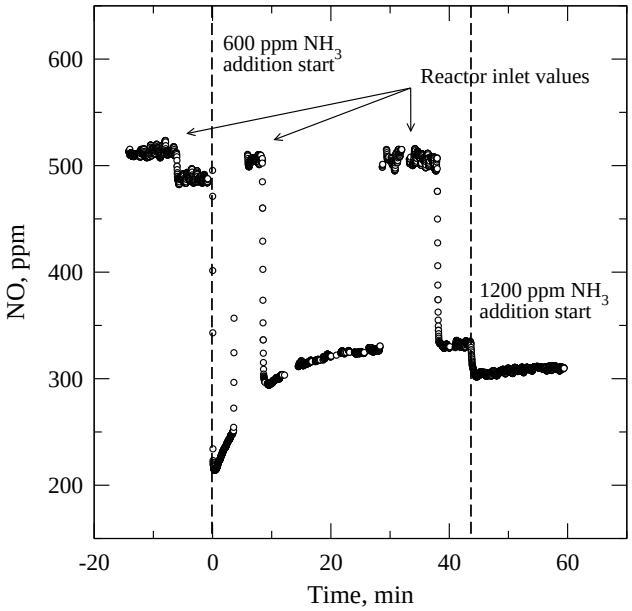

Figure 2.5: Activity measurement for P100 at 350C and 50 Nm^3/h after 134 hours of operating time. Gas composition on dry basis: NO = 515 ppmv, NH_3 = 600 - 1200 ppmv, O_2 = 11%v, CO_2 = 5.6%v, N_2 balance. 10%v H_2O.

free some H_3PO_4 back in the gas-phase. Therefore P deactivation may be controlled if the concentration is less than a few tens of ppm.

The physical deactivation, however is not the only effect responsible for the overall measured deactivation levels. Supported by the transient behaviour in NO reduction measured during activity tests with mass transfer-limited-catalysts, and in-situ EPR analysis of the spent catalysts, it has been found that the deposited polyphosphoric acids tend to both increase and stabilize the number of non active V(IV) species, which are formed as intermediate during the SCR reaction. Moreover, part of the NH_3 present in the gas phase preferentially adsorbs on the polyphosphoric acids and is only less active in the reduction of NO.

The results obtained in this work constitute the first reference about deactivation of vanadia-based catalysts explicitly due to polyphosphoric acid alone. It is believed they show the real deactivating potential of P, when this is present in the flue gas during post-treatment of combustion processes, which has been found much more poisonous than indicated by wet impregnated tests.

Chapter 3

Deactivation by Potassium Phosphate

In this chapter, the main results obtained from the exposure of commercial vanadia-based monoliths to a flue gas doped with K_3PO_4 are reported. The complete work has been submitted to the peer-reviewed international journal *Applied Catalysis B: Environmental* and can be found in Appendix C of this report.

3.1 Deactivation by K_3PO_4

Two commercial full length vanadia-based catalysts have been exposed to a flue gas doped with 100 and 200 mg/Nm^3 K_3PO_4 respectively and their activities have been followed as a function of exposure time. They will be referred to as KP100 and KP200 in the following.

The activity decrease measured in the two tests is shown in Figure 3.1. Overall the measured deactivation rate was increasing according to the K_3PO_4 concentrations in the flue gas. In both cases, the deactivation was very fast at the beginning of the exposure: The two elements lost respectively 26 and 31% of their original activity during the first 72 h. After this initial period, the deactivation proceeded at slower but still appreciable rates.

The addition of 100 mg/Nm^3 was carried out for 720 h. After this period of time, the element was exposed to clean flue gas for additional 288 h, before it was taken out and characterized. The relative activity at the end of the addition time was 62%, corresponding to an overall deactivation rate of about 1.3%/day. During the subsequent exposure to the clean flue gas, the element regained 9% of relative activity. In particular, 7% was regained after the first 24 h after the addition was shut off. During these 24 hours, the pressure

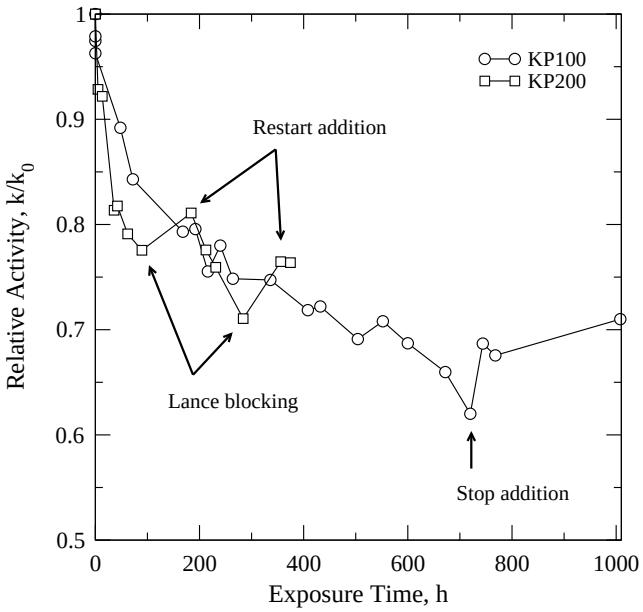

Figure 3.1: Relative activity as a function of exposure time. Total flow: 40 Nm^3/h. Gas composition: NO = 500 ppmv, NH_3 = 600 ppmv, O_2 = 10%v, CO_2 = 6%v, and 10%v H_2O in N_2.

drop along the monolith decreased of 11% indicating some cleaning of the channels due to the soot blowing system, which was in the meantime left on.

The addition of 200 mg/Nm^3 was carried out for only 280 h and was more problematic than the previous test. Due to the higher K_3PO_4 load, the two-fluid nozzle used for atomizing the water solution tended to clog due to salt deposition. Clogging of the nozzle mainly happened two times: After 89 and 284 h from the addition start. In both cases, the activity measurement performed after the clogging showed an increased relative activity of the element compared to the previous test. These facts are in agreement with the result obtained with the previous element, when this latter was exposed to a clean flue gas as discussed before. Overall, at the end of the experiment, the exposure to 200 mg/Nm^3 K_3PO_4 caused the loss of 22% of the original activity. However, the minimum relative activity was measured after 284 h during the last activity measurement before the nozzle clogged for the second time. Here the relative activity was equal to 73%, corresponding to a deactivation rate equal to about 2.3 %/day.

At the end of the exposures, the K-content in the catalyst bulk was varying in the range 0.8-2.5 wt%, whereas the P-content was varying in the range 0.4-0.8 wt%. About double levels of K were found on the sample exposed for

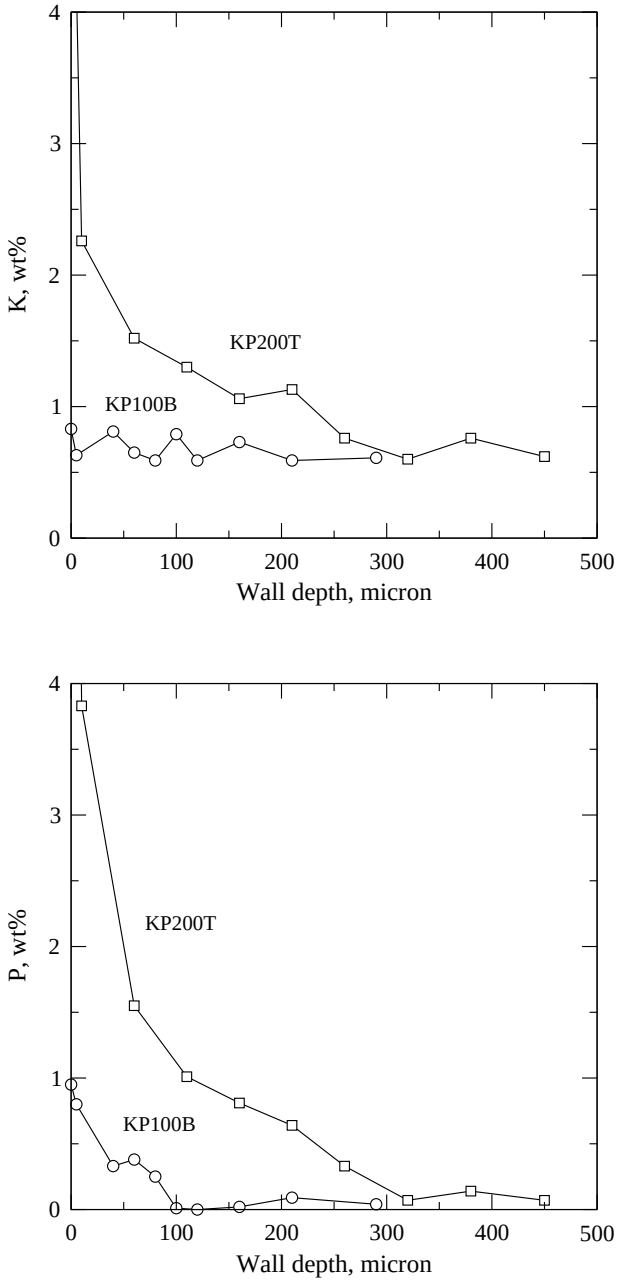

Figure 3.2: K- and P-content along the KP100B and KP200T walls as measured by SEM-EDX.

720 hours to 100 mg/Nm^3 K_3PO_4, whereas the levels of P were roughly the same. The calculated bulk K:P molar ratios were in the range 0.85-2.52 and

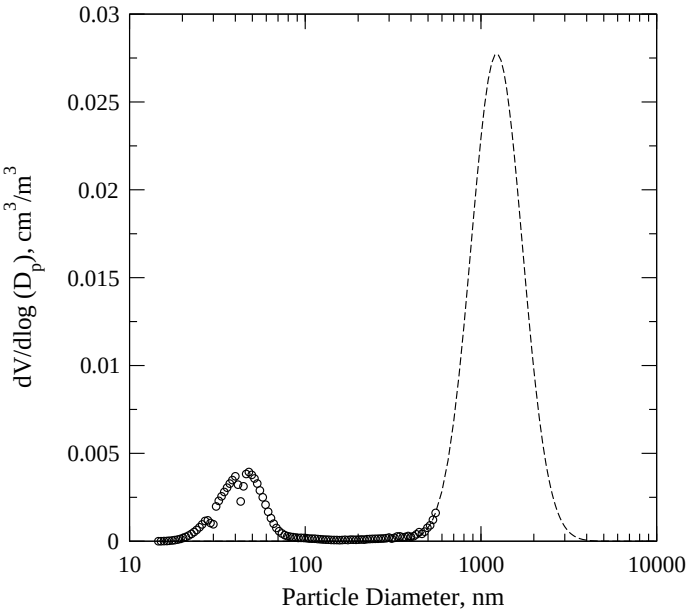

Figure 3.3: Volume-based particle size distributions measured by SMPS at the reactor inlet during addition of 100 mg/Nm^3 K_3PO_4. T = 350 ℃.

therefore less than 3, which is the value introduced into the system by the K_3PO_4 molecule.

The distributions of both K and P in the catalyst wall cross section have been measured by SEM-EDX. The results are shown in Figure 3.2. As shown in the plots, both the K- and P-content decrease as a function of catalyst wall depth, assuming the typical distribution of diffusion limited processes. Only in the case of KP100B, the K-content is almost constant around 0.7 %wt throughout the analyzed wall thickness, indicating that the rate of diffusion in the wall is similar to the rate of deposition. Moreover, higher P-concentrations on the outer surface compared to the K-content were found. However, the major difference between the K- and P-distributions is that, in the case of K, the concentration in the walls always appears to level off at a finite K-level (i.e. 0.7 %wt in the cases shown in Figure 3.2), whereas the P-concentration decreases to zero.

By assuming that K and P are not evenly distributed in the formed particles, it is possible to explain the results obtained from both the chemical and the SEM-EDX analysis. SMPS measurements were performed during the addition of 100 mg/Nm^3 K_3PO_4. The results, which are shown in Figure 3.3, indicated the presence in the flue gas of two distinct particle populations. The first one was characterized by a volume-based mean diameter at

around 40 nm, whereas the second one was characterized by particle diameters exceeding the detectable range of the SMPS (in the plot, the dashed line represents a lognormal distribution fitted on the available data). Based on these results, and taking into account the results of the chemical analysis, it is possible to assume that the small particles consisted of polyphosphoric acids, whereas the larger ones consisted of K-P salts formed during water evaporation from the added solution. Since the small particles are mainly constituted by P and they are depositing faster due to their higher diffusivity, more P than K will then accumulate in the catalyst wall compared to the case in which the particle were simply constituted by K_3PO_4. In this way it is possible to explain the K/P ratios lower than 3 found in the catalyst.

According to NH_3 chemisorption tests made during the exposure to the doped flue gas, the deactivation proceeded via blocking of V-sites involved in the adsorption of NH_3. This mechanism of deactivation is known for K and not for the polyphosphoric acids. Therefore it can be concluded that poisoning by K was responsible for the fast deactivation measured.

3.2 Conclusions

K_3PO_4 has been indicated as a potential product of combustion of biomass mixed with P- and Ca-based K-getter additives for reducing fouling and corrosion problems on superheater surfaces at power stations. However, the results presented here show that K_3PO_4 is a very harmful poison to SCR catalysts. Deactivation rates up to 3%/day have beeen measured. K has been found to penetrate the whole catalyst wall indicating that this is not strongly bound to the solid particles and instead preferentially reacts with the catalyst surface and subsequently penetrates the catalyst wall by surface diffusion. The NH_3 chemisorption studies have shown that the deactivation has mainly proceeded via K-poisoning by blocking the sites for NH_3 adsorption. All these data recall the mechanism of deactivation previously reported during exposure to KCl and K_2SO_4 and therefore indicate that binding K to P by the addition process does not seem to be an advantageous solution with respect to the vanadia-based SCR catalysts.

Even though the formation of the polyphosphoric acid aerosols have been strongly indicated by the particle size measurements, poisoning by polyphosphoric acids has not been seen in this investigation due to both the relatively low P-content in the bulk and low poisoning strenght compared to K. However, Hg-porosimetry has revealed the occurrence of fouling and pore mouth blocking at the outer catalyst surface. It is believed that the polyphosphoric acids play an important role in the formation of this layer by gluing together

the deposited particles and has therefore to be considered a fouling promoter.

Chapter 4

Deactivation by Additives

In this chapter, the main results obtained from the exposure of commercial vanadia-based monoliths to a flue gas doped with KCl, H_3PO_4, $Ca(OH)_2$ and H_2SO_4 are reported. The P/K and P/Ca molar ratios in the flue gas have been fixed to 2 and 0.8 respectively as suggested by initial tests made with biomass and P, Ca additives.

The complete work has been submitted to the peer-reviewed international journal *Applied Catalysis B: Environmental* and can be found in the Appendix D of this report.

4.1 Particle Measurements

Figure 4.1 shows the volume-based particle size distribution measured by a SMPS at the SCR reactor inlet. This is characterized by a peak at around 12 nm and a second one around 300 nm. This second peak is clearly representing most of the volume/mass of the total PSD. The dual-mode volume-based PSD measured by SMPS indicate the presence of mainly two classes of compounds:

1. The first one is constituted by small particles and high concentration numbers due to homogeneous nucleation of gaseous species. This class of particles accounts for about 6% of the total volume measured by the SMPS.

2. The second class is constituted by bigger particles with low total concentration numbers. Their formation is likely due to salt crystallization during water evaporation from the atomized solution at the injection point. This class accounts for about 94% of the total volume measured

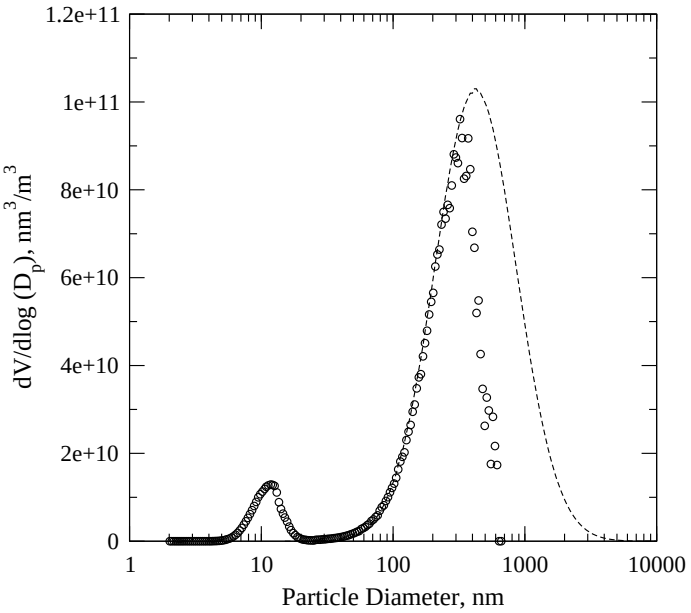

Figure 4.1: Volume-based particle size distributions measured by a SMPS at the reactor inlet during simulatneous addition of KCl (10 mg/Nm^3), $Ca(OH)_2$ (13 mg/Nm^3), H_3PO_4 (26 mg/Nm^3) and H_2SO_4 (20 mg/Nm^3). T = 350 ℃. The dashed line represents the lognormal distribution obtained by interpolation of experimental data.

by the SMPS. Due to their different mobility and number concentrations, these two particle classes contribute differently to the species accumulation and penetration into the catalyst walls.

Based on the results discussed in the previous chapters and the chemical analysis that will be shown in the following, it is very likely that the small particles were constituted by polyphosphoric acids. In particular, the number concentration and particle mean diameter would correspond to around 3-4 ppmv H_3PO_4, i.e. about half of the total acid injected.

A low pressure cascade impactor (LPI) has also been used to characterize the particles entering the SCR reactor. The particles collected on the different stages have then been analyzed by SEM-EDX. The results of the measurements are shown in Figure 4.2. Here a mass based particle size distribution with a peak at around 200 nm can be seen. This value is lower than the one measured by the SMPS, and the difference is believed to be due to experimental uncertainties and principal differences associated with the different sampling techniques and equipments. Particle deposition was found to happen at every single impactor stage as indicated by the non-zero particle concentration in the whole particle diameter range. The total mass

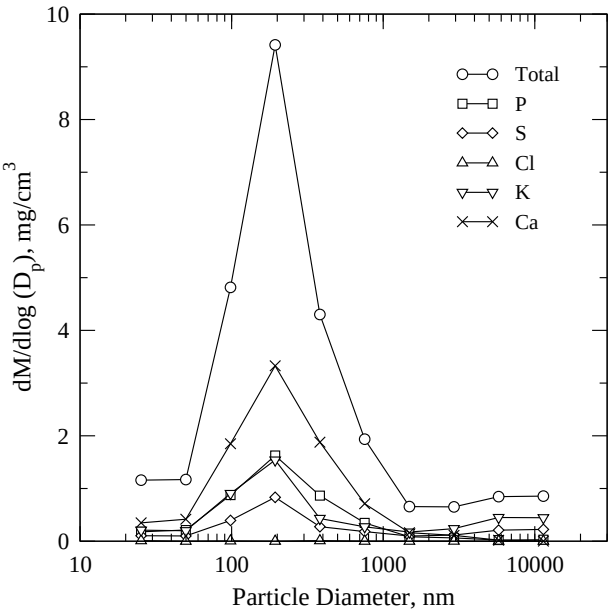

Figure 4.2: Particle size distribution measured by a low pressure impactor at the reactor inlet during simulatneous addition of KCl (10 mg/Nm^3), $Ca(OH)_2$ (13 mg/Nm^3), H_3PO_4 (26 mg/Nm^3) and H_2SO_4 (20 mg/Nm^3). T = 90 ℃. The curves for each single element have been obtained knowing their concentration on each single stage from EDX analysis.

concentration was about 10 mg/Nm3. The EDX chemical analysis of the collected deposits showed no Cl in any of the impactor stage, indicating that Cl was effectively released to the gas phase prior to enter the SCR reactor. From the analysis of the element distribution shown in Figure 4.2, it can be seen that both Ca and P are distributed in the particle diameter range 25-3000 nm but not at higher diameters, where only K and S are found, probably due to the formation of some K_2SO_4.

From the analysis of each impactor stage, both P:Ca and K:S molar ratios have been found constant at around 0.65 and 1.55 respectively throughout the whole particle size range. Simply based on these values it is not possible to identify the exact composition of the formed salts. However, by comparing the results with both the P:K and P:Ca injected, it is possible to conclude that some P is missing. This result might indicate again the formation of particles with diameters out of the impactor range, for instance having the volume-based mean diameter at 12 nm measured by the SMPS, thereby supporting the formation of polyphosphoric acids.

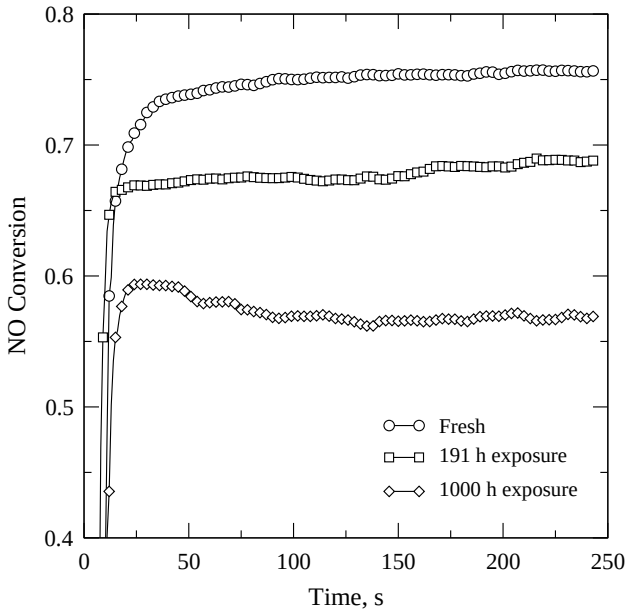

Figure 4.3: Activity measurement made on fresh and spent monolith at 350 ℃. Gas dry composition: NO = 500 ppmv, NH_3 = 600 ppmv, O_2 = 10 %v, CO_2 = 6 %v. H_2O = 10 %v. Flow: 40 Nm^3/h.

4.2 Deactivation

A full-length commercial SCR monolith has been exposed to the flue gas containing the particles characterized in the previous section. The total exposure to the doped flue gas was of 1000 hours. After the first 453 hours, two pieces of the monolith were cut off and analyzed for chemical composition and surface and SEM-EDX. The rest of the monolith was then exposed for rest of the exposure time.

Three activity measurements made after 0, 191 and 1000 hours of exposure respectively are shown in Figure 4.3. As it can be seen, apart from the different final conversions obtained, which are also dependent on different total catalyst mass due to the cut after 453 h, the conversion curve obtained at 1000 hours differs from the other two curves because it first goes through a maximum value right after the NH_3 introduction, and then reaches a steady state value after about 2 minutes of exposure to NH_3. All the activity measurements made after around 300 h of exposure to the additive mixture have shown this behavior. No NO conversion transient was instead measured at shorter exposure times, as shown by the activity tests made at 0 and 191 hours of exposure. According to the results reported in Chapter 2, this is

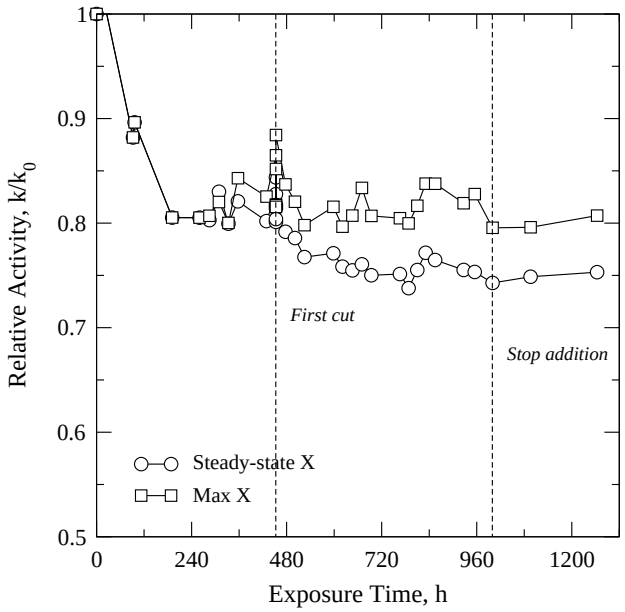

Figure 4.4: Relative activity as a function of exposure time. The activity measurement were made at 350 °C. Gas dry composition: NO = 500 ppmv, NH_3 = 600 ppmv, O_2 = 10 %v, CO_2 = 6 %v. H_2O = 10 %v. Flow: 40 Nm^3/h.

a clear indication that deactivation by polyphosphoric acids contributed to the observed decrease in activity at the 1000 h exposure test.

In order to isolate the PO_x effect on the overall degree of deactivation, for each activity measurement both a maximum and a steady-state relative activity have been calculated. The results of the calculation are shown in Figure 4.4. As it can be seen, the catalyst element lost 19% of activity during the first 191 hours, but no polyphosphoric acid effect was seen at that time. This was instead clear after about 300 hours, when the two curves shown in Figure 4.4 started been distinguishable from each other.

Apart from rending the quantification of the polyphosphoric acids possible, another important conclusion can be made from Figure 4.4. Since the appearance of the NO conversion transient, the Max X relative activity has constantly remained around 8% throughout the whole exposure, indicating that the components causing the fast drop of activity at the beginning of the exposure did not cause any further deactivation during the rest of exposure.

An explanation for the steep decrease in activity measured at the beginning of the test comes from the combined analysis of the elemental composition of the spent catalyst samples shown in Table 4.1, the SEM pictures taken at the end of the exposure (Figure 4.6) and the poresize distribution

Table 4.1: Bulk and surface analysis for the fresh and spent monoliths.

	Fresh	ADD1T	ADD2T	ADD2B	ADD1B
Axial Position, cm		5	10	40	45
Additive Exposure, h		453	1000	1000	453
Bulk chemical analysis					
V %, wt/wt	1.6	2.4	1.9	1.8	1.7
K %, wt/wt	-	0.1	0.2	0.1	< 0.1
P %, wt/wt	-	0.7	1.8	1.3	0.5
Ca %, wt/wt	1.7	2.1	1.9	1.7	1.8
S %, wt/wt	0.3	0.4	0.4	0.3	0.3
Cl %, wt/wt	< 0.1	< 0.1	< 0.1	< 0.1	< 0.1
Surface chemical analysis					
V %, wt/wt	2.10	3.84	3.35	1.93	2.04
K %, wt/wt	-	0.22	0.25	0.33	0.12
P %, wt/wt	-	1.67	4.67	3.10	1.72
Ca%, wt/wt	-	0.41	0.36	1.17	0.11
S %, wt/wt	0.66	0.67	0.71	1.39	0.36
Cl %, wt/wt	-	-	-	-	-

measured by Hg-porosimetry with the spent samples shown in Figure 4.5. According to Table 4.1, the bulk chemical analysis did not show any important enrichment of either K or Ca during the whole exposure that could explain the lost activity by chemical deactivation. These elements were not found inside the catalyst wall. They were instead accumulated on the outer catalyst surface, therefore suggesting the presence of a fouling layer. In particular, up to 1.2 %wt Ca was found at the end of the exposure.

The formation of a fouling layer has been confirmed by both the SEM and the Hg-porosimetry analysis made at the end of the exposure. This is in fact visible in Figure 4.6 where the porous catalyst structure clearly looks covered by a 2 μm-thick-layer. The Hg-porosimetry analysis of the same sample did not show any pores in the range 0.3-8 μm. However the total intrusion volume did not differ between the two samples. This fact indicates that the outer surface of the sample only presents pores smaller than 0.3 μm due to the formation of the fouling layer.

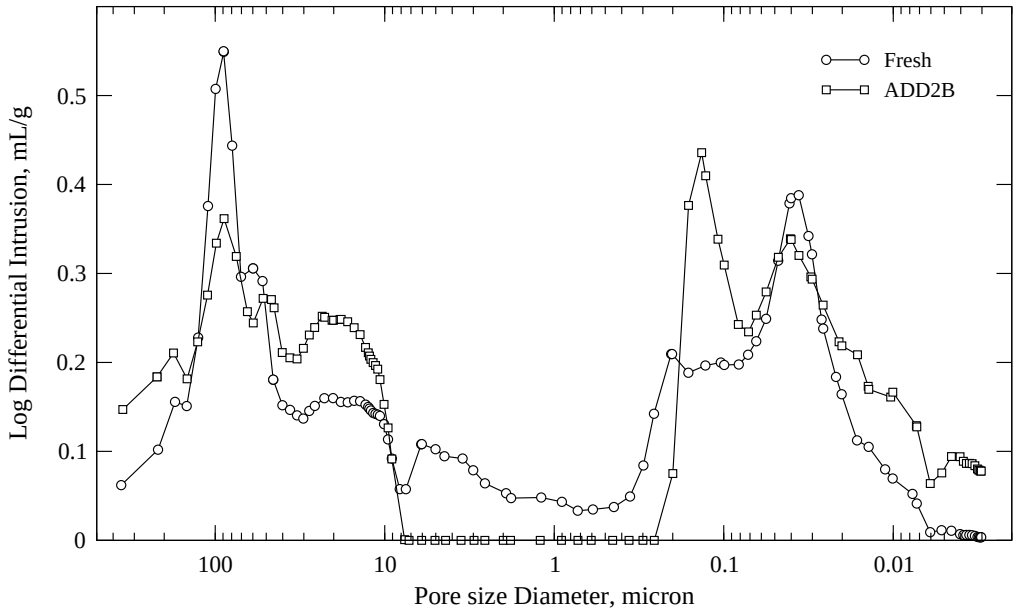

Figure 4.5: Pore size distribution measured by Hg-porosimetry.

4.3 Conclusions

The activity of a commercial SCR catalyst has been followed during simultaneous addition of KCl, H_3PO_4, $Ca(OH)_2$ and H_2SO_4 in a hot flue gas for 1000 h in a SCR pilot plant. In the test carried out, the P/K and P/Ca molar ratios have been fixed to values of 2 and 0.8 respectively suggested in the literature.

Either K or Ca penetrated the catalyst walls but only accumulated on the external catalyst surface. At the chosen experimental conditions, formation of polyphosphoric acids has been favoured and about half of the total P has been estimated to be present in these compounds, which formed aerosols with volume-based mean diameter equal to 12 nm. The known deactivating effects of the polyphosphoric acids (i.e. NO transient, reduced NH3 coverage) have been identified: After the initial loss of activity, they controlled the overall deactivation rate, which was about 0.2 %/day. However, due to their relatively low concentration, a steady-state between deposition and hydrolysis was reached and no additional deactivation was measured after about 750 h of exposure.

Based on the results obtained in this work, it can be concluded that binding K into P-K-Ca compounds is an effective way of reducing the deactivation rates normally experienced during biomass combustion. Reactions between

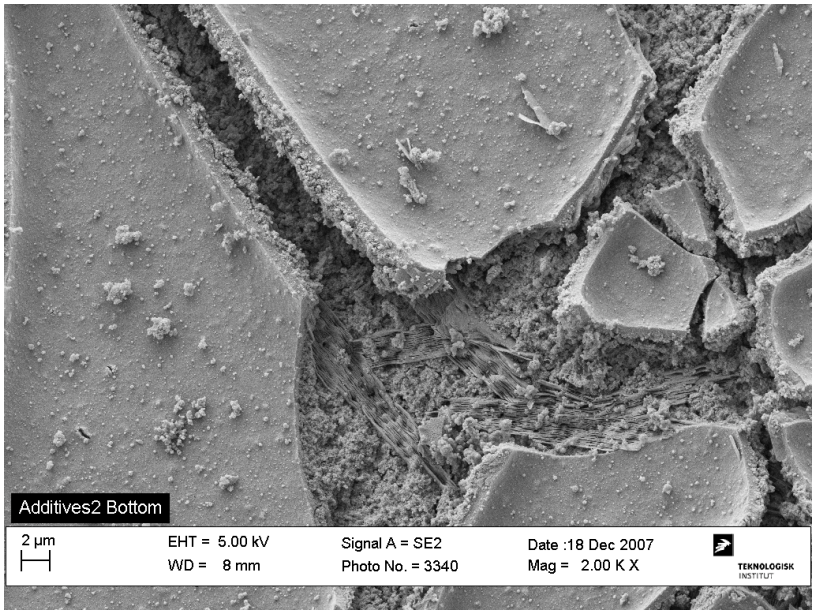

Figure 4.6: SEM images of catalyst sample taken after 1000 h of exposure (ADD2B).

K and the V active sites are in fact prevented, and so is the penetration of K in the catalyst walls by surface diffusion. However, in real applications, the formation of polyphosphoric acids needs to be controlled, since this may counterbalance the just mentioned positive effects. PO_x levels in the range 1-10 ppmv may still be acceptable since their deposition will be limited by their simultaneous hydrolysis, and a steady-state level implying low deactivation degrees may be reached. This situation could however be different in the presence of higher K-concentrations in the flue gas. If the fraction of P forming the PO_x is mainly controlled by the P/K and P/Ca ratios, at higher K-contents the amount of formed PO_x could be higher and thereby lead to faster deactivation rates. More tests at different P/K and P/Ca ratios would be necessary to understand the formation of PO_x, and suggest the optimal conditions to limit it.

Chapter 5

Conclusions and Recommendations

The potential effects of the P,Ca-additives on commercial SCR catalysts have been studied both in the laboratory and in a SCR pilot plant. By carrying out the tests under well defined and realistic conditions, it has been possible to obtain a better understanding of the deactivation mechanisms involved.

The effect of phosphorus on the vanadia-based catalysts have been extensively investigated by adding H_3PO_4 in a hot flue gas. In this way, the release of gaseous P during combustion has been simulated and the deactivation due to P has been isolated and identified. According to the results obtained, gaseous P, when exposed to temperatures higher than 800 ℃, forms polyphosphoric acids that are liquid at the typical SCR temperatures. These species can then deposit in the catalyst walls and deactivate the catalyst both physically and chemically. However, reaction of these compounds with the water content of the flue gas at the SCR temperature leads to hydrolysis of these species with release of gaseous P. This mechanism counterbalance the deposition and may, according to their concentration in the flue gas, limit the deactivation. According to our tests, up to 10-20 ppmv of free-P in the flue gas may be acceptable. At higher concentrations, the observed deactivation will be too fast.

From heat transfer surface deposition and corrosion point of view, one of the most desired products of the addition process is constituted by K_3PO_4. In this way, all the Cl initially bound to KCl will be released to the gas phase and K will be bound to a particle with high melting point temperature (i.e. 1340 ℃) and therefore low tendency in sticking on the superheat exchangers and low corrosion potential. From our tests, the presence of K_3PO_4 in the flue gas entering the SCR reactor will not be advantageous. In particular, about the same rates of deactivation known for KCl will be experienced. The

reasons for this enhanced deactivation have been found in the ability of K in reacting with the catalyst surface and penetrate the catalyst wall by surface diffusion. In order to limit this deactivation, the reaction between K and the catalyst surface needs to be limited by binding K in more chemically stable compounds.

A flue gas containing the recommended P/K and P/Ca molar ratios have also been prepared and a commercial monolith have been exposed to it for 1000 hours in total. The results of this test have shown that when K is bound into P-Ca-K particles, reactions with the catalyst surface with release of K have not been favoured. During this test, K was found to deposit only on the outer catalyst surface and did not penetrate into the catalyst wall. In this way, the highly undesired poisoning by K has been avoided. This is believed to be a clear evidence that firing of biomass with the P,Ca-additives may reduce the fast deactivation rates normally experienced during biomass combustion. However, part of the P introduced in the system was found to form polyphosphoric acids. P then accumulated in the catalyst wall and enhanced the formation of a fouling layer on the outer surface. The levels of free-P were still in the acceptable range discussed above (i.e. a few ppmv) and therefore the deactivation due to P only accounted for 8% and it was not expected to increase further. This fact, however, may indicate that the used P/K and P/Ca molar ratios may be further optimised in order to further limit the formation of these species. These tests could be carried out using the techniques applied in this study. Eventually, verification in full scale will be necessary.

Acknowledgment

This work is part of the CHEC (Combustion and Harmful Emission Control) Research Center funded a.o. by the Technical University of Denmark, the Danish Technical Research Council, the European Union, the Nordic Energy Research, Dong Energy A/S, Vattenfall A.B., F L Smidth A/S, and Public Service Obligation funds from Energinet.dk and the Danish Energy Research program.

Supply of the catalyst samples by Haldor Topsøe A/S is gratefully acknowledged.

Appendix A

Literature Study

Part of this report will be submitted to an international journal as a review paper about deactivation of SCR catalysts.

Selective Catalytic Reduction of Nitric Oxide by Ammonia over Vanadia-based Catalysts

Francesco Castellino, Anker Degn Jensen, Jan Erik Johnsson

June 2006

Contents

1 Introduction

Nitrogen oxides emitted from combustion and high temperature processes have been regarded during the last three decades as a major environmental concern, thus supporting a great amount of research to develop clean combustion techniques. Among the various technologies available nowadays for removing NO_x from stationary sources, the Selective Catalytic Reduction (SCR) process applied to fossil fuel combustion is the best-developed and worldwide applied [1, 2]. In this process, the NO_x fraction of the flue gas is reduced to nitrogen by ammonia on a catalyst surface.

The commercial SCR catalysts are normally constituted by vanadia (the active phase) supported on high surface titania. WO_3 and MoO_3 are the most common compounds added to the catalysts in order to improve its performance both chemically and physically. The composition of the industrial catalyst varies according to the particular application and it is the result of a comprehensive research carried out in the last two decades. This research have extensively covered all the aspects involved in catalysis, such as physical and chemical characterization, surface studies, activity studies and kinetic modeling, by using all the known techniques.

Understanding of the mechanisms of catalyst deactivation has also been the aim of many investigations. Since their appearance in the 1980s, all the possible causes of both chemical and physical deactivation have been investigated. These studies have always been strictly correlated to the problems encountered at full-scale applications and have often conducted to the development of better catalysts. Moreover, the number of these investigations

is nowadays still increasing due to the requirement of NO_x abatement in processes (*e.g.* biofuels and wastes combustion) where the catalyst life is not as long as desired. The interest in these *alternative* processes is in the last years increasing due to local environmental policy and regulations. In some cases, very fast rates of deactivation are observed resulting in great investments of resources aimed at overcoming the encountered problems by developing new and more resistant catalysts.

The objective of the present work is to review the open literature concerning the industrial SCR catalysts with a particular attention to the present knowledge about their deactivation mechanisms and promoters.

The present paper is composed by three parts. In the first part (Chapter 2 and 3) the NO_x sources and the available control technologies are presented. This part mainly deals with coal combustion, since the development of these technologies was mainly related to this fuel. The SCR process is also introduced in this first part.

The second part (Chapter 4) extensively deals with the vanadia-based catalysts. This is an attempt to point out from the open literature the characteristics and properties of this family of catalysts, which are relevant only for typical SCR conditions. The different proposed mechanisms of reaction and the respective kinetic models are also presented and discussed.

Finally, the third part (Chapter 5) deals with deactivation of vanadia-based catalysts. The different mechanisms of deactivation and the deactivation promoters are presented in this part. An attempt to correlate the different deactivation mechanisms to the particular SCR application is also made in this part.

2 NO_x Control Technologies

Nitric oxide and nitric dioxide, collectively termed NO_x, are acid rain precursors and participate in the generation of photochemical smog, thus constituting a major environmental concern. The need to comply with increasingly stringent regulations for the NO_x emissions has motivated a vast amount of research. Different methods of NO_x control have been developed during the last decades. These methods are known as *primary measures* when they act directly on the formation of NO_x in the boiler and furnace. The technologies that reduce the concentration of NO_x in the flue gas are known as *secondary measures*.

In the present section, after introducing the sources of nitrogen oxides, both primary and secondary control measures of industrial interest are briefly presented.

Table 1: Global inventory of NO_x sources. Data from [3].

NO_x sources	Magnitude, TgN/year	
Fossil fuel combustion	22	(15-29)
Biomass Burning	6.7	(3-10.4)
Lightning	2	(1-4)
Stratospheric injection	0.5	(0.4-0.6)
Aircraft emissions	0.55	(0.5-0.6)
Ammonia oxidation	1.0	(0.5-1.5)
Total	38.2	(23.7-53.8)

2.1 Sources of Nitrogen Oxides

Fossil fuel combustion is identified as a major source of nitrogen oxides, NO and NO_2. Another important source is biomass combustion. Together, these two *anthropogenic* sources cover 75% of the total NO_x emission [3]. Beside these, biogenic emissions from soil are a third important source of NO_x. In this case, NO_x is the result of the natural process of nitrogen cycling. However, fertilizers and other agricultural practices perturb the natural process increasing the amount of NO_x emitted. Finally, other significant sources of NO_x are due to lightning, ammonia oxidation and aircraft exhausts. A global inventory of NO_x sources is presented in Table 1 [3].

The flue gas resulting from combustion processes mainly consists of NO and NO_2, with the former accounting for about 95% of the NO_x emissions from combustion. There are three different mechanisms for NO_x formation in combustion processes [4]:

1. *Thermal NO_x.* It is formed as a result of the reaction of nitrogen with molecular oxygen in the combustion air at peak flame temperature. Thermal NO_x increases according to the combustion temperature and generally accounts for about 5-25% of the NO_x formed during coal combustion.

2. *Fuel NO_x.* Its formation is due to oxidation of the nitrogen bound in the fuel. It highly depends on the local flame stoichiometry, whereas the temperature does not affect its production to any great extent. The nitrogen content in coal, ranging between 0.5 and 2%, can contribute up to 70-80% of NO_x formed during coal combustion.

3. *Prompt NO_x.* The formation of prompt NO_x takes place in the front of the flame first by reactions between nitrogen in the air and hydrocarbon fuel fragments forming intermediate HCN. This reaction is then followed by the oxidation of the HCN to NO. Prompt NO_x has a weak temperature dependence and is significant only in fuel-rich

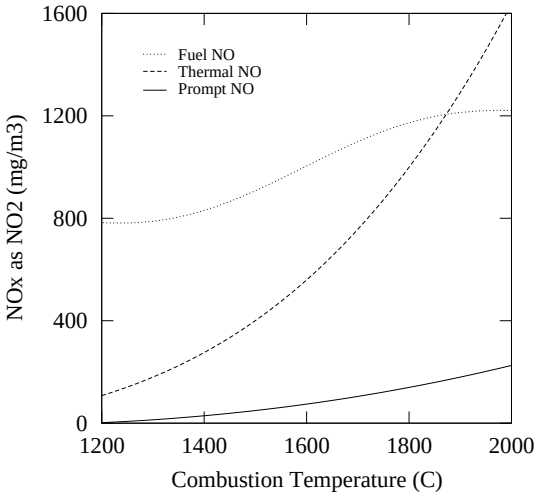

Figure 1: Temperature influence on the amount of NO_x produced from the three NO_x formation mechanism in the case of coal combustion. Data from [6].

flames. In fact, for typical conditions the prompt NO_x portion from coal combustion accounts for only 5% of the total NO_x emissions.

In solid fuel systems, fuel NO is generally the major source of NO_x, with some contribution from thermal NO (Figure 1). The fuel nitrogen formation and conversion in solid fuel fired system was recently reviewed by Glarborg *et al.* [5].

2.2 Primary Measures

Primary measures, also known as combustion controls or clean technologies, are the first taken into consideration to lower the NO_x emissions due to their high effective-cost ratio compared to other control technologies.

The main targets for these measures are:

1. decreasing the oxygen level at peak temperature;
2. reducing the peak temperature and the residence time in the combustion zone;
3. reducing the level of fuel nitrogen.

The first two issues are in general achieved by adopting so-called *low-NO_x* burners. These are designed to control fuel and air mixing at each burner in order to create larger and more branched flames, reducing peak flame temperature.

The most effective combustion control is the *reburning* technique (Figure 2) [6]. It consists of a three stage system and requires the injection of

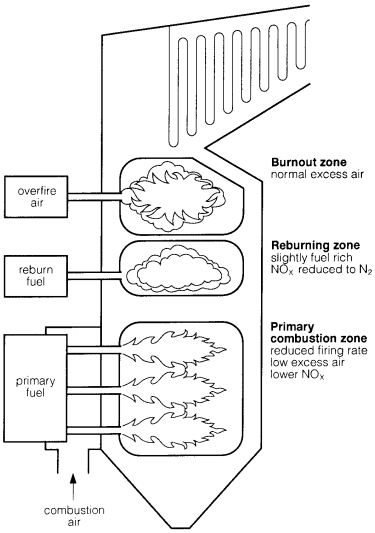

Figure 2: The three combustion zones in a reburning process [6].

a secondary fuel, typically natural gas (also coal, oil and biomass can be used). In the first stage, the so-called "primary combustion zone", the fuel is burnt at low excess air conditions, reducing initial NO_x formation. The secondary fuel is then introduced in the furnace at the second stage (the "reburning zone") without combustion air. Here, the secondary fuel breaks down to produce hydrocarbon fragments which reduce NO_x from the first stage to HCN and NH_3. Then, according to the operating conditions at this stage, the formation of molecular nitrogen from these is favored. Finally, at the third stage, overfire air is injected in order to consume the CO and the unreacted hydrocarbons leaving the reburning zone. This final stage is referred to as the "burnout zone". The operating cost of this combustion control is highly influenced by the cost of the secondary fuel.

Another effective primary technique is *air staging*. It consists of the introduction of combustion air in two separate (primary and secondary) flow sections, in order to encourage the formation of N_2 rather than NO_x. Primary air (70-90%) is mixed with the fuel producing a relative low temperature, oxygen deficient, fuel-rich zone. In this manner, only moderate amounts of NO_x are formed. Secondary air (10-30%) is then injected above the combustion zone in order to complete the combustion of the fuel.

Finally, other techiques are the *flue gas recirculation* and the *addition of steam or water*. Both of them decrease the peak temperatures in the combustion chamber and accordingly the production of thermal NO_x.

By combining different primary measures, NO_x removal up to 70% are possible [7]. Table 2 presents a list of primary methods and their respective NO_x reduction capabilities [6]. However, some of these methods may not be

Table 2: Primary measure reduction capabilities in coal-fired boilers [6].

Primary measure	De-NO_x (%)
flue gas recirculation	<20
burner fuel staging	10-30
low NO_x burners	30-55
low NO_x burners and overfire air	35-70
coal reburning	40-60
natural gas reburning with flue gas recirculation	55-65
natural gas reburning without flue gas recirculation	<60
low NO_x burners with natural gas reburning	60-70

viable for fuels like biomass or waste. These fuels are commonly burned on grates or in fluized beds, and these technologies do not support, for example, the use of low-NO_x burners.

2.3 Secondary Measures

The secondary measures, also referred to as post-combustion control or flue gas treatment, offer moderate to high NO_x removal efficiency. They are categorised as follow:

- Selective Catalytic Reduction systems (SCR);
- Selective Non Catalytic Reduction systems (SCNR);
- hybrid SNCR/SCR systems;
- combined SO_2 and NO_x removal processes.

All these methods can be used independently or in combination with primary measures. In general, most of them relies on the injection of ammonia, urea or other compounds to react with the NO_x in the flue gas and reduce it to molecular nitrogen.

In the SCR process, the reaction is carried out in the presence of a catalyst, which strongly enhances the rate of NO conversion at lower temperatures. This post-combustion control is capable of providing NO_x reductions in excess of 90%. The SCR process will be extensively discussed in the next chapters.

On the contrary, in the SNCR process, nitric oxide and ammonia react in the absence of a catalyst. High conversions are only possible at higher temperatures (800-1000°C) than the ones required by the SCR process (300-400°C). For this reason, the reducing agent is introduced directly in the boiler, above the flame zone. NO_x removal up to 70% is possible using an

Table 3: Simultaneus removal of SO_x and NO_x processes [6].

Dry Processes	Wet Processes
Mitsui-BF actived carbon	CombiNO_x process
RTI-Waterloo actived carbon	SOXAL process
Copper oxide process	Tri-NOx-NoxSorb process
SNAP alumina-sodium process	LTO process
SNOX process	Iron-chelate process
SNRB process	
DESONOX process	
E-Beam process	
ANL alkali dry spray process	
LILAC process	

efficient reagent injection control that avoids the decomposition of ammonia at higher temperatures, and an appropriate residence time in the reaction temperature range.

A hybrid SNCR/SCR system combines the injection of ammonia into the boiler with a SCR catalyst where the reaction between residual NO_x and ammonia slip takes place. In other words, the SNCR removes part of the NO_x while supplying the ammonia reagent required for the catalytic removal of more NO_x.

In order to achieve more cost effective systems with both high NO_x and SO_2 removal, several combined processes have been developed [1,6], and are generally classified in dry and wet processes. Table 3 presents a list of the most important processes [6].

3 The SCR Process

Among flue gas treatment methods the Selective Catalytic Reduction (SCR) is the most world-wide used for controlling NO_x emissions from stationary combustion sources. It was first installed in Japan in the late 1970s on industrial and utility plants, whereas in Europe, the first commercial SCR process appeared in 1985. Based on the Japanese and European experience, the process was then adopted in the USA during the 1990s where it was first confined to gas turbines primarily located in California. [8–10].

The commercial use of the SCR process in the years has followed the introduction of stringent limits to regulate NO_x emissions in each country. In 2001, SCR commercial installations were in operation in the Japanese and European power companies for an estimated overall capacity close to 100,000 and 60,000 MW respectively [10]. However, in the last years the use of the SCR process has further increased due to its introduction to processes such

as industrial and municipal waste incinerators, chemical plants and cement industries among the others. Moreover, SCR catalysts are also increasingly employed in biomass-fired boilers, stationary and non-stationary diesel and gas engines (*i.e.* marine propulsion engines and locomotive engines) [10,11].

3.1 The Reactions

In the SCR process, NO_x is reduced by ammonia directly injected into the flue gas over a catalyst in the presence of sufficient oxygen. The operating temperature is typically ranging between 300 and 400℃. The NO_x reduction is then possible according to the following overall reactions:

$$4\ NO + 4\ NH_3 + O_2 \rightarrow 4\ N_2 + 6\ H_2O \quad (1)$$

$$2\ NO_2 + 4\ NH_3 + O_2 \rightarrow 3\ N_2 + 6\ H_2O \quad (2)$$

$$4\ NH_3 + 5\ O_2 \rightarrow 4\ NO + 6\ H_2O \quad (3)$$

Since NO constitutes more than 95% of NO_x in the flue gas, reaction (1) is the main SCR reaction and thus accounts for the overall stoichiometry of the process.

The ability of ammonia to react selectively with the NO_x fraction of the flue gas instead of being oxidized according to reaction (3) is a unique feature of this system, not observed in the case of other reagents such as CO and hydrocarbons [10].

The potentially most troublesome side reaction is the oxidation of SO_2 to SO_3 by the catalyst, which is greatly increased at temperatures above approximately 370℃. Sulphur oxides in the flue gas may react in the presence of unreacted ammonia forming $(NH_4)_2SO_4$ and NH_4HSO_4. The formation of NH_4HSO_4 is possible at 235℃ in the usual SCR operating condition of 5 ppm NH_3 and 10 ppm SO_3, whereas $(NH_4)_2SO_4$ is formed if the temperature drops below 200℃. These compounds are responsible for both (reversible) deactivation of the catalyst and damage of downstream equipments. This is a major problem with high sulphur coals.

From all this, it is clear that:

1. unreacted ammonia (ammonia slip) has to be avoided;
2. besides a high NO_x removal activity, selectivity is an extremely important parameter for SCR catalysts.

The first issue is complished by injecting around 0.9 parts of ammonia for each part of nitric oxide. The temperature is typically kept below 370℃, to avoid the oxidation of SO_2, but above 300℃, to minimize ammonia slip and ensure efficient NO_x removal. Figure 3 shows the correlation between NO_x removal and ammonia slip [12]. From this, it is clear that to keep the ammonia slip below 5 ppm the NH_3/NO_x ratio have to be below 1.

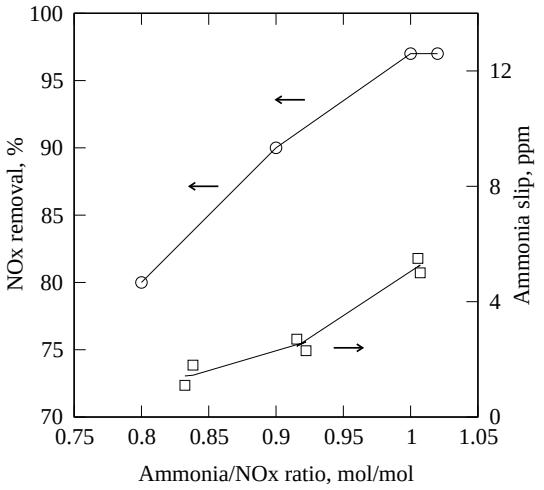

Figure 3: NO_x reduction (circles) and ammonia slip (squares) as a function of reagent normalized stoichiometric ratio. NO_x inlet: 425 ppm; temperature: 368°C. Data from [12].

Different catalysts based on zeolite, iron oxide or activated carbon have been tested in laboratory scale. However, the most widely adopted are based on vanadia on a titanium oxide carrier [1, 2]. The characterization of this family of catalysts and their behavior in the SCR reaction are discussed in Chapter 4.

3.2 Process Design and Optimization

A typical SCR system includes: a storage, delivery, vaporization, and injection system for reagents; an SCR reactor housing the catalyst; soot blowers; and additional instrumentation. There are mainly three typical layout arrangements of SCR systems applied to fossil-fuel-fired power stations (Figure 4). The best configuration strongly depends on the particular application. *High dust* configuration is the most widely used SCR configuration in coal-fired plants. The main advantage is that the temperature right after the boiler economizer is in the range suitable for the SCR reaction. The name "high dust" indicates that no particulates have been removed from the flue gas prior to the de-NO_x process. In this configuration, the catalyst is thus exposed to fly ash and chemical compounds present in the flue gas that can both plug the catalyst and degrade it mechanically and chemically. However, appropriate design of a high-dust SCR system can mitigate the impacts on the catalyst. If this was not the case, the cost of a high temperature electrostatic precipitator (H-ESP) placed in between the boiler and the SCR reactor could still be a convenient investment. This solution is known as *low dust* configuration. In a *tail end* configuration, the SCR reactor is placed between the Flue Gas Desulphurization plant (FGD) and the stack. In this

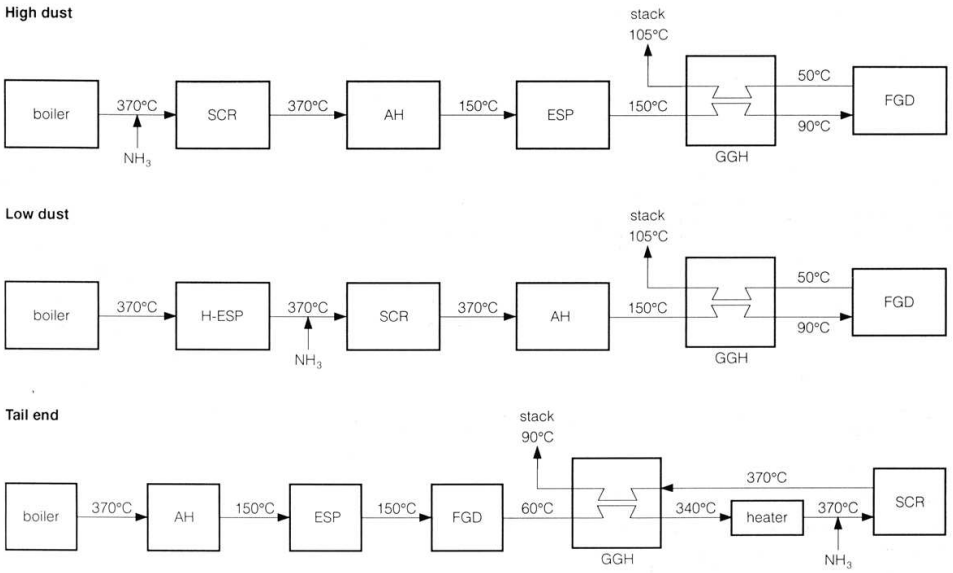

Figure 4: SCR process arrangements. SCR:selective catalytic reduction; AH: air preheater; ESP: electrostatic precipitator; H-ESP: high temperature ESP; GGH: gas-gas heater; FGD: flue gas desulphurisation [13].

case, the absence of SO_2 in the flue gas allows the use of more reactive catalyst formulations, mainly because the oxidation of SO_2 to SO_3 is not a problem. At the same time, the lifetime of the catalyst is also increased because of the low dust loading. Anyway, the lower catalyst costs need to be compared with the investment in the heat exchangers and the energy needed in order to reheat the flue gas from about 60 to 370°C.

Liquid ammonia is vaporized, diluted with air and injected into the flue gas through a grid located in the ductwork leading to the SCR reactor. The distance from the reactor is kept to a relative high value in order to ensure complete mixing of the reactants across the catalyst cross-section. The amount of ammonia injected is controlled by measuring the NO_x concentration in the flue gas at the economizer outlet, whereas the temperature of the flue gas reaching the SCR reactor is controlled by mixing the flue gas exiting the economizer with the flue gas from the economizer by-pass.

Industrial SCR reactors contain up to four catalyst layers with spacing in between (Figure 5). Each layer consists of different catalysts assembled in modules. The configuration of the applied SCR catalyst element and reactor depends on several factors. The SCR catalysts are designed for use in parallel flow and various types of geometry can be used. Figure 6 presents the different possible configurations. The main features of monolithic catalysts are: (i) low pressure drop, (ii) large external surface, and (iii) uniform flow. Another feature, very important in the treatment of flue gases, is the good

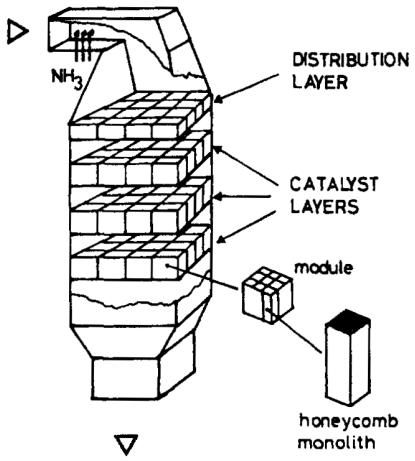

Figure 5: Structure of SCR reactors [14].

resistance to attrition and dust deposition.

Each module contains a large number of parallel straight channels with openings of a few millimeters depending on dust concentration and properties. In high dust configurations, the channels have large channel openings (6-7 mm) and wall thickness (up to 1.5 mm) in order to prevent channel blocking and erosion by ash. In low dust and tail end configurations, the relative absence of particulate allows the use of catalysts with higher geometric surface. In all configurations, a typical honeycomb catalyst block is 50-100 cm long with a face area up to 50 cm by 50 cm. The flue gas normally has gas hourly space velocities (GHSV) in the 2000-7000 h^{-1} (STP) range [15].

In order to ensure high NO_x removal efficiency and low ammonia slip great attention is paid to the fluid dynamics of the entire reactor. A uniform distribution of the reagents, and temperature and flat velocity profile of the flue gas need to be obtained over the entire cross-section of the catalyst layer. For these reasons, the SCR reactor is provided by guided vanes and distribution layers.

4 Supported-Vanadia Catalysts in the SCR of NO by NH_3

Among all the metal oxide catalysts applied in the SCR process of NO by NH_3, the TiO_2(anatase)-supported V_2O_5 catalyst is the most efficient one due to its high selectivity and high activity at relative low temperature [1]. Consequently, it has been subject to a great number of studies concerning mechanisms and kinetics.

In the present section, a review of the information in the open literature about the catalyst properties and its behavior in the selective catalytic

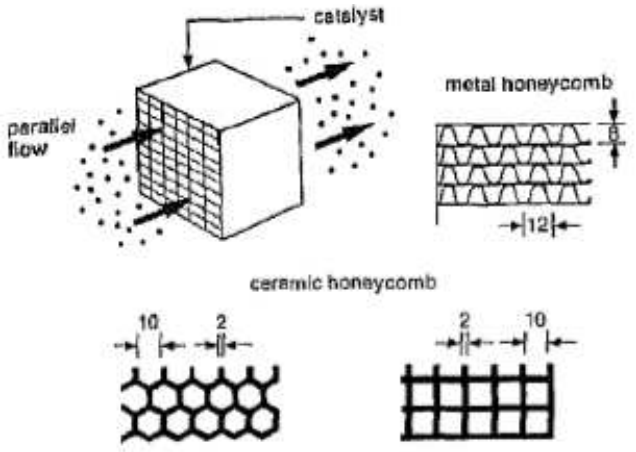

Figure 6: Different geometries and reactor designs used in SCR [16].

reduction on NO by NH_3 is presented.

4.1 Characterization of the Catalysts

The name "supported vanadia catalyst" indicates a wide number of different systems that have in common the vanadium oxide as active component in the SCR reaction. The commercial catalysts present both different kind of supports and amounts of active component. Moreover, additives are used in order to improve their physicochemical properties and catalytic activity. On the other hand, in order to understand the influence of each single component in the global catalyst, simplified systems have been studied. Pure vanadia catalysts and binary vanadia-titania systems have been prepared and characterized in order to clarify the role of the structure of the active phase and its influence on the behavior of the catalyst [17, 18]. The behavior of the single promoter has been displayed by analyzing the activity in the SCR reaction of its pure phase [19]. Different authors have compared vanadia-titania system with promoters-titania and vanadia-promoter-titania systems [20–27] in order to address the optimal composition of the catalyst. Others have characterized commercial catalysts and compared them with the previous *ideal* systems [28, 29].

In the following sections, the properties of the support, the active phase and the most common promoters have been extracted and resumed from the evidences found in the open literature.

4.1.1 The Support

Pure titania catalysts have a low activity in the SCR reaction [30]. Titania becomes only weakly and reversibly sulfated under SCR conditions

[1]. Moreover, titania in the anatese form, despite its thermal instability, presents the highest surface area (BET $\approx$ 70-100 m^2/g). For all these reasons, this latter has been preferred as optimal support for the active phase.

IR studies of a pure titania catalyst after oxygen pretreatment revealed the presence on the surface of Ti–OH bonds mainly due to water molecules included in the atmosphere [30–32]. These species are the sites where the interaction between titania and vanadia takes place. Thus, their concentration determines the vanadia amount necessary to cover the support surface with a single monolayer and the dispersion of the vanadia species. As it will be clearer in the next section, both the amount of vanadia and its dispersion are determining for the SCR activity and N_2 selectivity of the catalyst. A way to control the support properties is the preparation technique [33]. Among the others, the hydrolysis of titanium isopropoxide provides supports with the greatest surface area and highest concentration of Ti–OH sites [34].

4.1.2 The Active Phase

It is generally accepted that vanadia constitutes the active phase in the SCR process [1, 25, 35–40]. A comprehensive review of the role and chemistry of supported vanadium oxides in heterogeneous catalysis has been recently published [41].

Supported vanadium oxides can be present in the following molecular configurations [41] depending on the load:

- isolated vanadium ions;
- dimeric or polymeric species;
- two-dimensional layer of supported vanadium oxides;
- crystalline or amorphous, three-dimensional vanadium oxides;
- mixed metal oxide phases with the support.

Each one of the previous species, shown in Figure 7, presents a different behavior in the catalytic process. Went *et al.* [35] have first studied the dependence of vanadia load on the different molecular configurations and their behavior in the SCR reactions. By means of Raman spectra, they showed that at low vanadia contents (1% w/w) only *isolated* monomeric species are present on the support. For loading around 2% w/w, *less isolated* monomers start reacting together producing polymeric vanadyl species. Finally, when the vanadia content is further raised, the polymeric species increase in vanadia terminals and crystallites are also observed. In particular, the formation of the crystallites takes place at the expense of the polymeric entities as shown in Figure 8. According to the Raman spectra obtained by the authors, both mono- and polymeric vanadates are characterized by V=O bands at different frequencies. The crystallites, in addition, present

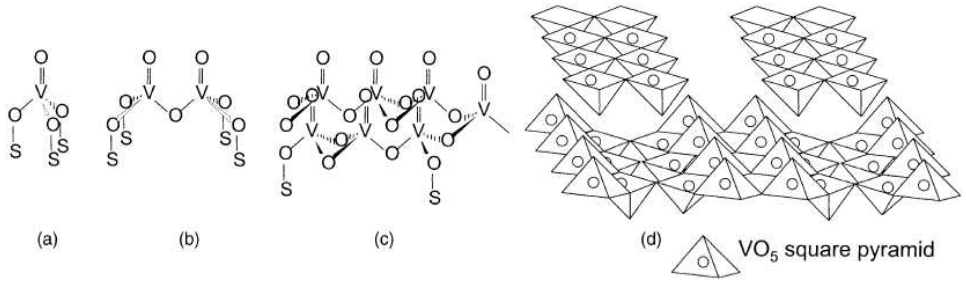

Figure 7: Possible molecular configurations for supported vanadium oxides (with S the support cation): (a) isolated vanadium oxide species; (b) dimeric vanadium oxide species; (c) two-dimensional vanadium oxide chains; (d) V_2O_5 crystals. From [41].

V–O–V bonds, where the O atoms are more labile than the ones present in the Ti–O–Ti bonds of the support. The different energies of formation associated with the vanadate species were then used to explain the values of activity and N_2 selectivity according to the vanadia loading. These have been found to be optimal when one monolayer of vanadia is dispersed on the support surface [25, 35, 36], indicating a strong activity of the polymeric species characterized by terminal V=O bonds in dry conditions and V–OH bonds in wet atmospheres.

As a direct consequence of this result, and considering that vanadia is active in the undesired oxidation of SO_2 to SO_3, the vanadia content in the commercial catalysts for the SCR of NO by NH_3 usually does not exceed about 2% w/w.

Topsøe *et al.* [31], analyzing pure titania and vanadia-titania samples at different loads by means of Fourier Transform IR (FT-IR), have found that the deposition of vanadia takes place on the sites previously occupied by the Ti–OH bonds. Moreover, the resulting species are characterized by V–OH bonds (3500-3700 cm^{-1}), not observed on pure V_2O_5. The concentration of V–OH bonds is also very sensitive to the sample pretreatments and enhanced by oxidation. In fact extensive reduction in H_2 eliminated the V–OH species, reexposing the surface Ti–OH ones.

4.1.3 Additional Components

The industrial catalysts for the SCR process are based mainly on TiO_2(a)-supported V_2O_5-WO_3 and/or V_2O_5-MoO_3. WO_3 and MoO_3 have been selected since they increase the acidity and reactivity of the V_2O_5/TiO_2 catalysts and can limit the oxidation of SO_2 to SO_3. Moreover, they also provide thermal stability to the catalyst, widening its temperature window and avoiding both the surface area loss of anatase and its transformation to the more stable rutile configuration [1, 42]. In addition to these compounds,

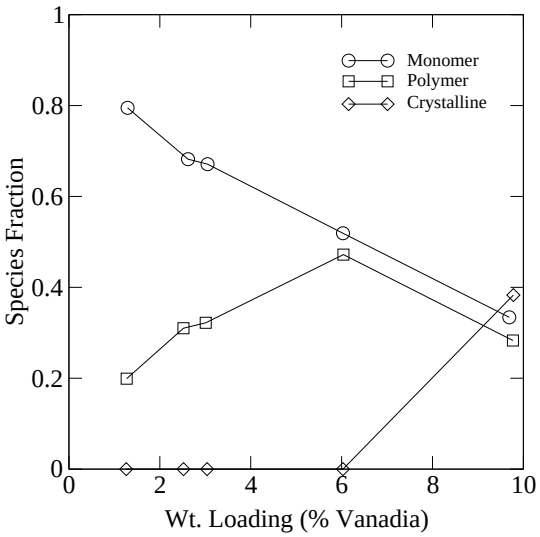

Figure 8: Distribution of monomeric, polymeric and crystalline V_2O_5 species as a function of the vanadia surface density. Data from [35].

silico-aluminates and glass-fibres are also added to improve the mechanical properties and strenght of the catalysts.

WO_3 is added in substancial amounts (≈10% w/w). While pure WO_3 or WO_3 supported on titania shows only limited SCR activity, when added to vanadia/titania catalysts it strongly improves their activity, as shown in Figure 9. The properties of this compound in the SCR reaction can be extracted from different studies on pure WO_3 [19], WO_3/TiO_2 [25, 27] and TiO_2(a)-supported V_2O_5-WO_3 [20,21,26,28,29] catalysts. From these studies, it is seen that WO_3 interacts with the titania supports forming W_xO_y clusters containing W–O–Ti and terminal W–OH and W=O bonds, the latter with a coordinative unsaturation [27]. On the other hand, it does not interact with vanadia. When tungsten and vanadia are both present on the titania support, they form the same W=O and V=O bonds observed on the tungsten-titania and vanadia-titania catalysts respectively [26]. Furthermore, no evidence is found for V-W mixed oxides [29] indicating that interactions take place only through the support.

With an extensive characterization of V_2O_5-MoO_3/TiO_2 catalysts, Lietti *et al.* [43] showed that the addition of MoO_3 to V_2O_5/TiO_2 produces similar effects to those produced by the addition of WO_3. In this case, the surface is characterized by Mo=O and Mo–OH bonds. Compared to the catalyst with tungsten, the V_2O_5-MoO_3/TiO_2 at high temperature becomes less active. Furthermore, in the presence of a dry feed, it also becomes less selective due to the formation of N_2O. However, this additive has had a great success since it permitted to overcome the problems due to arsenic deactivation (Section

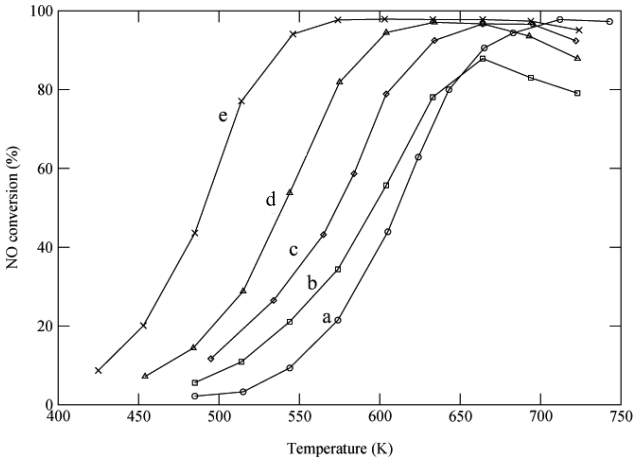

Figure 9: NO conversion versus temperature: (a) $WO_3(9)/TiO_2$; (b) $V_2O_5(0.78)/TiO_2$; (c) $V_2O_5(1.4)/TiO_2$; (d) $V_2O_5(0.78)$-$WO_3(9)/TiO_2$; (e) $V_2O_5(1.4)$-$WO_3(9)/TiO_2$. Feed: He, 800 ppm NH_3, 800 ppm NO, 1% O_2. Data from Ref. [42].

5.5.2).

Finally, regarding the use of sulfated TiO_2 supports, Choo *et al.* [32] found that they enhance the activity of the catalyst by improving the polymer vanadate fraction on the surface. This fact was explained by the authors to be caused by the reduced surface area available for vanadia deposition in the presence of sulfates.

4.2 Adsorption and Surface Reaction Studies

From the characterization presented above, it is clear that, according to the vanadia loading and the addition of promoters, the surface of the catalyst presents an increasing concentration of (V,W,Mo)–OH, (V,W,Mo)=O and V–O–V bonds. On the other hand, the Ti–OH bonds disappear with the formation of a monolayer of vanadia. Additionally, Ti–O–Ti bonds are present on the uncovered titania. All these species are responsible in different ways for the adsorption of the reacting compounds.

To elucidate such aspects, the adsorption characteristics of SCR reactants over vanadia-based catalysts have been extensively investigated in the literature by means of Laser Raman (LR) spectra and Fourier Transform IR (FT-IR) [21, 25, 28, 30, 31, 40, 44, 45], Diffuse Reflectance Infrared Fourier Transform Spectroscopy (DRIFTS) [46, 47] and isotopic labeling [48]. Temperature Programmed Desorption (TPD) and Temperature Programmed Surface Reaction (TPSR) studies have also been performed to display the reactions activated by the catalyst [20, 25, 38, 39]. In order to better follow the adsorption process under typical reaction conditions, *in situ* techniques have also been applied and the surface reaction was analyzed combining on-

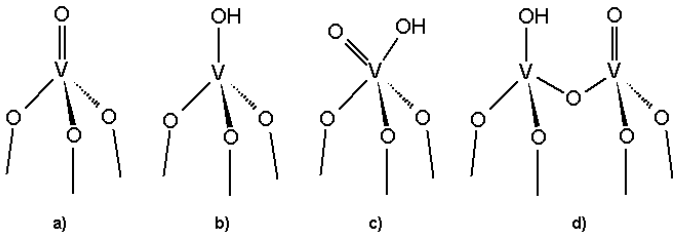

Figure 10: Possible acid sites structures on vanadia-based catalysts.

line mass spectroscopy (MS) [38, 39]. Transient respons methods have also been performed [11, 20, 49–51]. The following sections present the most relevant evidences in order to introduce the mechanistic and kinetic discussion that will follow. A short introduction about the possible site structures is first made in order to better follow the discussion presented.

4.2.1 Acid Site Structure on Vanadia-based Catalysts

As it will be clearer in section 4.2.4, the nature of the *active* sites in the SCR reactions has been for many years subject of discussion. The main point of controversion has been whether the sites which host the reactions are *Brønsted* or *Lewis* acid sites. However, the discussion has not been focused enough on their *chemical* structure. Very often it has been discussed about V–OH and V=O species, without clearly mentioning the link between these species and the BA and LA sites, thus causing confusion to the reader. In order to prevent such confusion when analyzing the surface studies, a brief discussion about the possible structures of the acid sites is presented.

There is general agreement about the structure of the Lewis acid site (LA). According to the definition given by Gilbert Lewis, a Lewis acid is a specie which can accept a pair of electrons and form a coordinate covalent bond. All the metal atom with an oxygen atom double bonded present on the catalyst surface (*i.e.* (Ti,V)=O) are thus regarded as LA sites. They are shown in Figure 10a. Also the structures shown in Figure 7 could act as LA sites.

For the Brønsted species (BA), instead, the situation is not very clear since their structure is mentioned more vaguely in the literature. According to its definition, a Brønsted-Lowry acid is a specie that donates a hydrogen ion to another compound. Thus every metal atom presenting an attached hydroxyl group (*e.g.* (Ti,V)–OH for vanadia-based catalysts) could be regarded as a BA site. Its basic chemical structure is shown in Figure 10b. However, other BA sites structures are chemically possible and most of them, as the ones shown in Figure 10c-d, also present V=O species which are tipical of LA sites. Recently density functional theory (DFT) calcula-

tions are being adopted in order to clearify the structure of these acid sites and get insight into their process of formation [52–54]. Moreover, the stability of the adsorbed species is evaluated and mechanistic implications are adressed [55–57].

It is then clear that, when analyzing the results of surface studies presented below, it is necessary to keep in mind that the BA and LA sites are identified based on the products of adsorption (*i.e.* covalent or coordinated species respectively). Their chemical structures are of course important but not sufficient in order to determine the exact acid nature of the site. Moreover, it is very important to carefully take into account the experimental conditions adopted and the techniques used during the investigations, since it could be imagined that a specie like the one shown in Figure 10c could in principle behaves both as BA and LA site according to different temperatures and reaction atmospheres.

4.2.2 NH_3 Adsorption

The different ways ammonia can adsorb on vanadia-titania catalysts are shown in Figure 11 [42]. Ammonia readily adsorbs at room temperature on the TiO_2 support in the coordinated form [30, 31, 36, 38], indicating the presence of only LA sites on pure titania. No evidence was found by different authors for NH_4^+ species, showing the absence on the support of Brønsted acid sites. H-bonding between NH_3 and Ti–OH groups were detected by Topsøe *et al.* [31, 38].

On the contrary, pure vanadia is characterized mainly by Brønsted acid sites as indicated by the presence of ammonium ions upon ammonia adsorption. Besides the BA sites, small amounts of coordinated ammonia are present on pure vanadia catalysts. Their total amount increases after a reduction pretreatment due to more anion vacancies being created during reduction [31].

As expected from these results, titania-vanadia catalysts present both Lewis and Brønsted acid sites depending on the vanadia loading. In fact ammonia adsorbs on these catalysts both as coordinated ammonia and ammonium ions [31, 40]. Moreover, the relative amount of these sites is a function of the oxidation state of the catalyst: an oxidized catalyst will present much more BA sites than a reduced one. The contrary is true for the LA sites. H-bonding with oxide sites is also possible.

The effects of vanadia load on ammonia adsorption have been reported in several pubblications [31, 38–40]. The results showed that for catalysts with different vanadia loading treated with ammonia at room temperature the Brønsted acidity is greatly enhanced by the addition of vanadia [31, 38, 39]. The disappearance of the V–OH bands during the ammonia treatment suggests that the BA sites are directly associated to these species. Additionally, the upwards shifts of the frequencies due to NH_4^+ species in the vana-

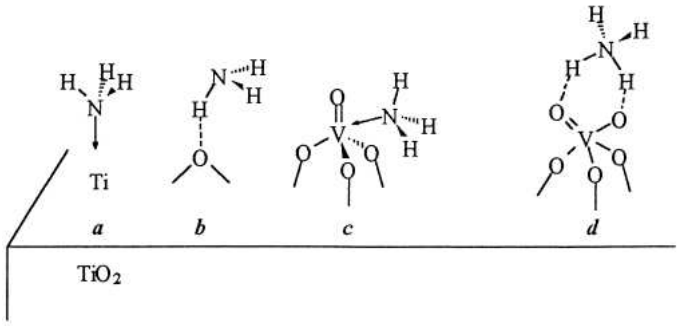

Figure 11: Proposed structures for ammonia adsorbed on V2O5-TiO2: (a) Lewis-bonded NH_3 at Ti sites; (b) H-bonded NH_3 on oxide sites; (c) Lewis-bonded NH_3 at vanadyl sites; (d) ammonium ions bonded at V Brønsted acid sites. From [42].

dia/titania catalysts indicate that the interaction between titania and vanadia enhances the strength of the total Brønsted acidity [31]. Also the original Lewis acidity due to the support was found to increase somewhat by adding vanadia to the catalyst [31]. The disapperence in the recorded adsorption spectra of the peaks due to the V=O bonds indicated that ammonia is coordinated on vanadyl groups [40].

The influence of additional compounds on the ammonia adsorption was also investigated [20,25,27,45]. All authors agree that the W=O and Mo=O species lead to the formation of Lewis acid sites stronger than the ones present on V_2O_5/TiO_2 surface. Additionally, protonated ammonia also adsorbs on the W–OH and Mo–OH sites, increasing the Brønsted acidity of the surface. Furthermore, under typical SCR conditions, the ammonia coverage of the WO_3-free catalyst is significantly lower [11].

Regarding the thermal stability of these acid sites, all the authors agree that LA sites are much stronger than BA sites: upon evacuation at 520 K, ammonium ions are not present on the catalyst, while coordinated ammonia is still observed [40]. Ammonia is more strongly adsorbed on the catalyst in the presence of WO_3 [11].

4.2.3 NO Adsorption

In principle, NO can adsorb on the titania support at least in three different ways [30, 40]: i) it can coordinate on the Lewis sites of the titania oxide as nitrosyls; ii) it can react on the catalyst surface and adsorb as coordinated N_2O; or iii) as nitrate ions. On the other hand, vanadia-titania catalysts adsorb NO on exposed Ti^{4+} centers as NO_3^- species, the latter being produced by oxidation of NO on vanadyl cations. The oxidation state of the surface also plays an important role on NO adsorption [31]. In fact, no adsorption is possible on oxidized samples, whereas extensive adsorption is detectable

only upon strong reduction in H_2 flow due to increased presence of Ti–OH bonds.

In any case, the interaction of NO with the surface is very weak and, as it will be clearer in the following section, it is negligible under typical SCR conditions, particularly due to the presence of ammonia.

4.2.4 Surface Reaction Studies: Active Sites in the SCR Reaction

In order to better understand the mechanisms of the reaction, NH_3 and NO co-adsorption experiments were carried out by many investigators [11, 20, 21, 23, 31, 38–40, 44, 46–49]. From all these, it appears that under typical SCR conditions NO does only slightly adsorb on the catalyst surface. On the other hand, most authors agree that ammonia strongly adsorbs both as coordinated on Lewis acid sites and as protonated on Brønsted acid sites. However there is still not complete agreement on which one is the active site during the SCR reaction or whether both of them are involved.

Ramis *et al.* [40] using a standard FT-IR cell found that with increasing temperature, coordinated ammonia disappeared faster than the ammonium ions, in contrast to the evidences discussed in the ammonia desorption studies. At the same time, the bands assigned to adsorbed nitrosamide (NH_2NO) and to hydroxyl groups, possibly due to the adsorption of water, were growing. They concluded that these two facts implied the presence of the SCR reaction: *coordinated ammonia* and gaseous NO were identified as the active species in the reaction, with the latter passing through the formation of NH_2NO identified as a possible intermediate.

Contrarily, Topsøe *et al.* [38] concluded that *ammonium ions* are involved in the SCR reaction, mostly adsorbed on V–OH sites that are then indicated as the active sites of the reaction. To better follow the surface reaction and the formation of the products, they combined *in situ* FT-IR and Mass Spectroscopy and performed TPSR in O_2, NO and O_2+NO atmosphere. As Ramis *et al.* [40], they also noticed the disappearance of the coordinated ammonia, but in their opinion under SCR conditions coordinated ammonia desorbs and readily re-adsorbs on BA sites. Furthermore, LA sites are also converted to BA sites by the water present in the feed. In any case, an important role in the catalytic activity of the catalyst was assigned to the V=O terminals. According to [38], these are responsible for the activation of adsorbed ammonia on BA sites.

The ammonia adsorbed on sites provided by the additional components does not seem to be directly involved in the SCR reaction. On the contrary, it has been shown by means of Transient Response Method that these sites provide an ammonia reservoir [11, 28, 49]. This ammonia needs to be transferred over the surface or desorb and re-adsorb on vanadia sites prior to reaction.

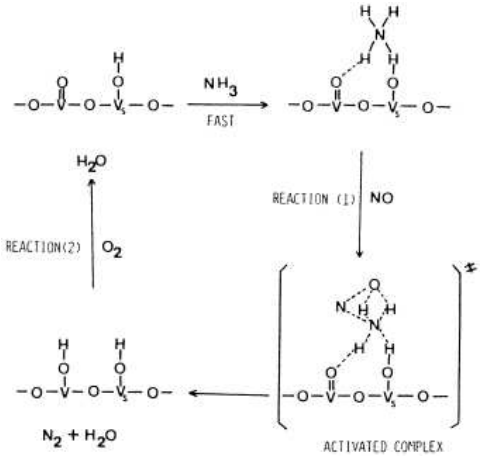

Figure 12: Mechanism of the NO-NH_3 reaction on vanadium oxide in the presence of oxygen. Miyamoto *et al.* [58].

4.3 Reaction Mechanism

Since the first mechanism proposed by Takagi *et al.* [59] in 1977, a great number of different proposals have been presented in the literature, based both on experimental and theoretical studies [2,42,60]. In the present section a brief review of the main mechanisms is presented.

Since there is a general agreement that no NO adsorption is possible under typical SCR conditions, the reaction follows an Eley-Rideal mechanism between strongly adsorbed NH_3 and gaseous or weakly adsorbed NO. The possibility that the reaction would follow a Langmuir-Hinshelwood mechanism with both the reactants adsorbed on the catalyst, as first supposed by Takagi *et al.*, has been completely excluded at high temperatures.

The first mechanism supposing a reaction between gaseous NO and ammonia adsorbed on vanadia catalysts as ammonium ions was proposed by Miyamoto *et al.* [58]. Ammonia was supposed to adsorb on O=V–O–V–OH species and then react with NO forming an activated complex. After the release of N_2 and H_2O, the starting species on vanadia were reestablished by gaseous oxygen (Figure 12). Similar mechanisms were later proposed by Gasior *et al.* [61] and Odenbrand *et al.* [62].

The first mechanism based on the reaction between gaseous NO and *coordinated* NH_3 was proposed by Ramis *et al.* [40], referred to as the "amide-nitrosamide" mechanism (Figure 13). The mechanism consists of the fol-

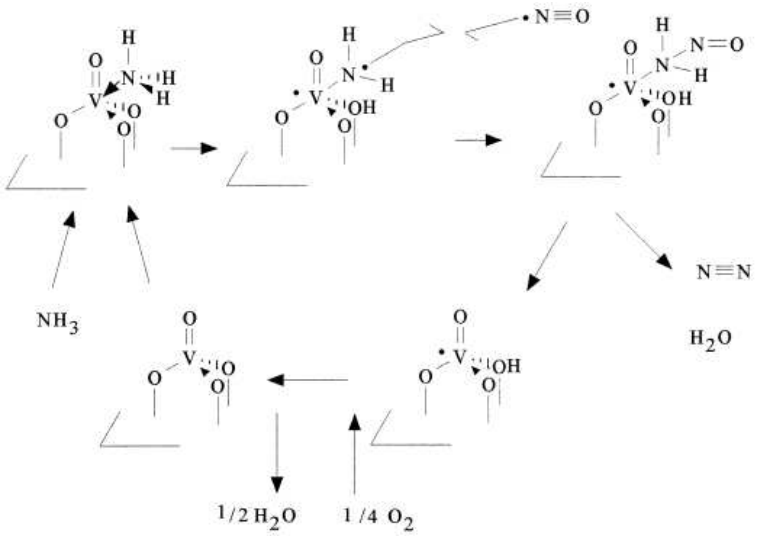

Figure 13: Mechanism of the NO-NH_3 reaction on vanadium oxide in the presence of oxygen. Ramis *et al.* [40].

lowing steps:

$$NH_{3,g} + VO^{2-} \rightleftharpoons H_3N\text{-}V^{5+}O^{2-} \tag{4}$$

$$H_3NV^{5+}O^{2-} \rightarrow V^{4+}O^{2-}NH_2 + {}^{-}OH \tag{5}$$

$$V^{4+}O^{2-}NH_2 + NO \rightarrow V^{4+}NH_2NO \tag{6}$$

$$V^{4+}NH_2NO \rightarrow V^{4+} + N_2 + H_2O \tag{7}$$

$$2V^{4+} + 0.5\ O_2 \rightarrow 2V^{5+}{=}O \tag{8}$$

$$2OH^{-} \rightarrow H_2O + O^{2-} \tag{9}$$

In the first step ammonia is adsorbed reversibly on the surface of the catalyst both on Lewis and Brønsted acid sites, MO^{2-} and M–OH respectively. Then, only the ammonia adsorbed on vanadium Lewis sites reacts producing N_2 and H_2O via NH_2NO formation and decomposition (reactions (5), (6) and (7)). In reactions (8) and (9) the catalyst is finally reoxidized by gaseous oxygen.

In 1993, Topsøe *et al.* [63] showed that a simple two-step Eley-Rideal mechanism involving reaction between adsorbed NH_3 and gaseous NO is not able to describe correctly the experimental evidences obtained at typical SCR conditions. They thus proposed the following three-step mechanism:

$$NH_3 + M \rightleftharpoons NH_3\text{-}M \tag{10}$$

$$NH_3\text{-}M + S \rightleftharpoons NH_3\text{-}S + M \tag{11}$$

$$NH_3\text{-}S + NO \rightarrow \text{Products} + S \tag{12}$$

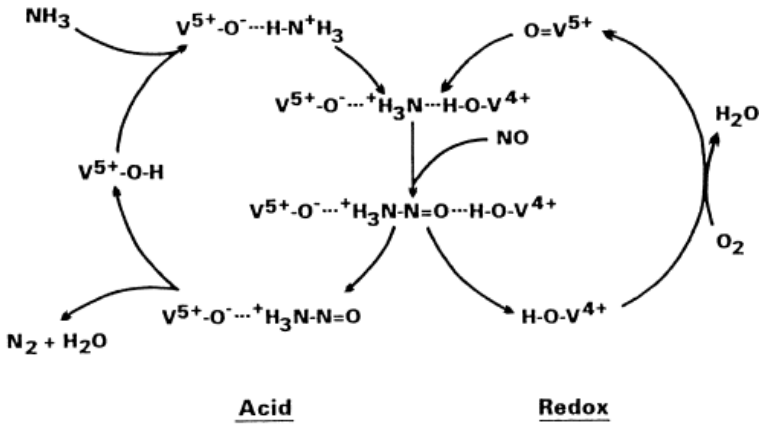

Figure 14: Mechanism of the NO-NH_3 reaction on vanadium oxide in the presence of oxygen. Topsøe *et al.* [39].

consisting of equilibrated ammonia adsorbtion, followed by an activation step of the adsorbed ammonia and a subsequent reaction between the activated ammonia species and NO to form the products. The three-step mechanism was found to quantitavely describe both the ammonia conversion and the ammonia slip (*see* Section 4.4). However the authors pointed out that the three-step mechanism had to be regarded as semi-empirical in nature, since information concerning the nature of the M and S sites was still lacking.

In view of this situation, *in situ* FTIR spectroscopic studies of the surface chemistry for different vanadia-based catalysts were performed [38, 39] and the following mechanistic scheme was proposed (1995):

$$NH_3 + V^{5+}OH \rightleftharpoons V^{5+}ONH_4 \tag{13}$$

$$V^{5+}ONH_4 + V^{5+}{=}O \rightleftharpoons V^{5+}ONH_3^+V^{4+}OH \tag{14}$$

$$V^{5+}ONH_3^+V^{4+}OH + NO \rightarrow N_2 + H_2O + V^{5+}OH + V^{4+}OH \tag{15}$$

$$2V^{4+}OH \rightarrow H_2O + V^{3+} + V^{5+}{=}O \tag{16}$$

$$O_2 + 2V^{3+} \rightarrow 2V^{5+}{=}O \tag{17}$$

$$H_2O{+}V^{5+}OH \rightleftharpoons V^{5+}OH_3O \tag{18}$$

Clearly, the M-sites and S-site (reactions (10)-(12)) were associated to the V–OH and V=O sites respectively. Thus, the *BA sites* were found to be responsible for adsorption of *reacting* ammonia, whereas the V=O species, normally associated to LA sites, were found responsible for the required activation of the adsorbed ammonia (reaction 14): only this activated adsorbed ammonia can further react with gaseous NO giving the products of reaction. During this activation, the vanadyl groups are reduced and addi-

tional reduced V–OH are released upon reaction with NO (reactions 14 and 15). Again, the gaseous oxygen is then responsible for the reoxidation of the surface (reaction 17). The mechanism proposed then involves an acid cycle and a redox cycle clearly shown in Figure 14: this fact strongly underlines the important role played in the SCR reaction by the redox state of the catalyst. In particular, when the oxygen concentration in the flue gas is high ($> 5\%$) the acid cycle controls the overall reaction rate: this will be then faster at increasing number of V–OH sites. On the other hand, at low oxygen concentrations, the redex cycle is the one controlling the reaction rate since the reoxidation of the surface is slow (reactions (16)-(17)).

The main criticism revolved to the mechanism proposed by Topsøe has been the lack of information about the chemical structure and the kinetic role of the intermediate specie NH_3^+. According to Busca *et al.* [42], it is difficult to accept on a chemistry basis that this radical-cation specie, produced by the extraction of an electron from ammonia, is involved as such in the reaction with gaseous NO. In this sense, the research which the group of Topsøe is currently carrying out by using DFT calculations [52–54] is seen as a step toward an improvement of the mechanism proposed. From their results, more insight into both the nature of the BA sites and the intermediates are already available:

1. BA sites are favored by the titania support by i) stabilizing H atoms bonded to vanadium oxide moieties; ii) transferring H atoms from a Ti-OH group to a vanadium oxide moiety;

2. ammonia preferentially adsorbs on V-OH species as NH_4 which is then stabilized between two V=O species;

3. the NH_2NO species are the intermediate of reaction, as already stated in the mechanisms of Ramis, but in this case their formation involves the participation of both V=O and V-OH groups, and the formation of NH_4 species. Their decomposition to N_2 and water is then favoured by the transfer back and forth of hydrogen atoms.

While the mechanisms proposed by Takagi *et. al.* and Miyamoto *et. al.* still present interest only for their historical importance, the ones from Topsøe *et. al.* and Ramis *et. al.* are the ones on which the debate is nowadays still open. It is not the object of this work to decide which one is the right one, but some discussion is considered necessary.

1. It has first to be mentioned that both the Ramis *et al.* [40] and Topsøe *et al.* [39] mechanism are supported by surface studies performed in the absence of water and SO_2 that can alter the acidity and redox state of the catalyst. Thus, care must be taken when extrapolating data to the real operating conditions.

2. The two mechanisms are in general very similar. They both have in common the fact that an acid cycle is coupled with a redox cycle. In particular the authors underline the importance of this redox cycle in order to clarify the influence of water and oxygen on the observed rate of reaction. This fact should even more stress what just said in the previous item.

3. While Ramis *et al.* include in their mechanism discussion and derivation a detailed structure of the chemical species involved bringing evidences for the formation of the intermediates, Topsøe *et al.* referred too generally to V=O and V–OH species. They are now bringing theoretical evidences to further support their mechanism.

4. The surface studies were conducted using different techniques. In this sense the results obtained by Topsøe *et al.* are more interesting since were obtained *in situ*.

5. The deactivation experience with vanadia-based catalysts should be considered as a viable way to better support a proposed mechanism of reaction. None of the authors has considered it.

4.4 Kinetics of the SCR Reaction

Several kinetic studies have been reported in the literature for the SCR reaction, based on both empirical expressions [64–66] and mechanistic approaches [67–73]. The catalysts used were both model and commercial vanadia-based catalysts. In all cases, these were crushed and sieved to small particles (generally with diameters in the range 100-300 μm) in order to avoid internal mass transfer limitations. The NO and NH_3 concentrations were varying in the range 50-2500 ppm. Kinetic expressions were generally proposed for temperatures in the range 120-350°C. Only in few cases, the kinetic behavior of the reaction was studied at higher temperatures. Even though water was not always added into the feed, in all the studies no evidence was found for the formation of N_2O and NO_2 and the only reaction considered was the following:

$$NO + NH_3 + 1/4\ O_2 \rightarrow N_2 + 3/2\ H_2O \tag{19}$$

From an empirical point of view, without adopting any detailed reaction mechanism, the NO conversion rate can be simply assumed to depend on the concentrations of the reactants (*i.e.* NO, NH_3 and O_2) and water according to the following expression:

$$-r_{NO} = kC_{NO}^{\alpha}C_{NH_3}^{\beta}C_{O_2}^{\gamma}C_{H_2O}^{\delta}. \tag{20}$$

Different authors [64–66] have reported values for α in the range 0.5-0.8 for temperatures less than 300°C. The order of dependence on C_{NH_3} also

appeared with values of β larger than zero when the ratio NH_3/NO was less than 1, typical in the industrial applications. Moreover, γ was found to vary in the range 0.25-0.5 for vanadia-based catalysts.

On the other hand, for temperatures in the 300-380℃ range, working with NH_3/NO≥1, more than 5%v of oxygen and 5%v of water, the rate of NO conversion is found to be independent of ammonia, oxygen and water. At these conditions, the following expression is then considered a good approximation:

$$-r_{NO} = kC_{NO}. \tag{21}$$

The use of this expression is supported by the evidences showed in Figure 15, in which the effects of the reagents on the NO conversion measured on a commercial monolith are presented [74].

In order to obtain an expression that physically explains the behavior of the catalyst in the SCR reaction in a wider domain, adsorption, surface reaction and mechanistic studies have to be considered. In particular, the effects due to ammonia, oxygen, nitric oxide and water concentrations need to be included in the kinetic model, since their effects become relevant.

In the following sections, each of these effects and the way they have been taken into account in the kinetic expressions found in the literature is presented. Furthermore, a summary of these expressions together with the conditions where they were validated is presented in Table 4.

4.4.1 Ammonia Effects

As discussed previously, ammonia is adsorbed on the catalyst prior to reaction, thus the coverage of ammonia under reaction conditions has to be considered. At low NH_3/NO, the coverage of NH_3 is not unity. At high temperatures (≥300℃), the exothermicity of the adsorption reaction also implies that the coverage is not total.

In order to consider the ammonia effects, most authors have added in their rate expression a term due to the ammonia coverage θ_{NH_3}. When the adsorption reaction is assumed to follow a Langmuir-type isotherm, the following expression can be derived:

$$\theta_{NH_3} = \frac{K_{NH_3}C_{NH_3}}{1 + K_{NH_3}C_{NH_3}} \tag{22}$$

If a simple Eley-Rideal mechanism is assumed with strongly adsorbed ammonia reacting with gaseous nitric oxide, the following expression is derived by considering the surface reaction as the limiting step and the ammonia concentration in equilibrium on the surface:

$$-r_{NO} = kC_{NO}\theta_{NH_3} \tag{23}$$

Figure 16 shows the progress of θ_{NH_3} versus the partial pressure of ammonia at different temperatures [66]. The values were obtained from activity

measurements on powders assuming θ_{NH_3}=1 in the case of maximum conversion, and comparing the conversion rate under different conditions as follow:

$$\theta_{NH_3} = \frac{k}{k_{max}} \tag{24}$$

Figure 16 clearly shows a typical Langmuir-type isotherm for the adsorption curve.

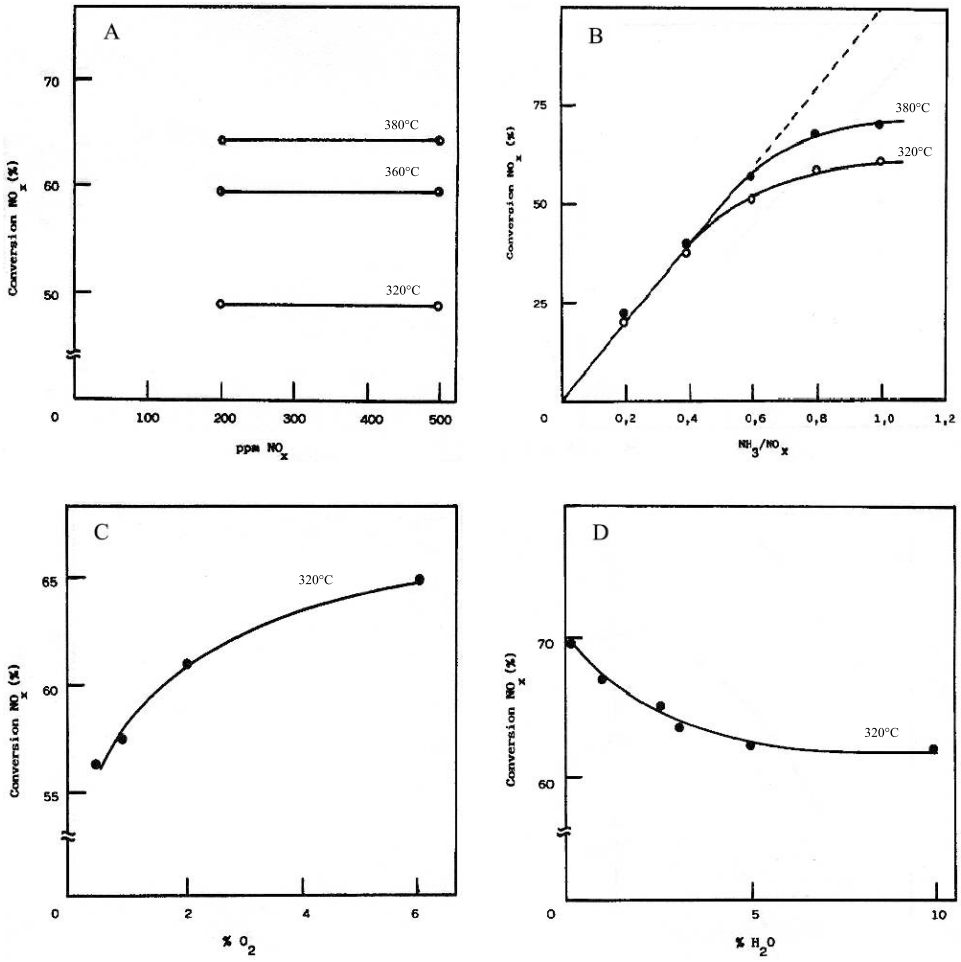

Figure 15: A: Effect of NO_x concentration on NO_x conversion; B: effect of NH_3/NO_x ratio, NO_x=500 ppm, on NO_x conversion; C: effect of O_2 concentration on NO_x conversion; D: effect of water concentration on NO_x conversion. From [74].

Table 4: Proposed rate expressions for the SCR of NO by NH_3.

	$-r_{NO}$	NO, ppm	NH_3/NO	O_2, %v	H_2O, %v	T, ℃	Ref.
a.	$\frac{4k_R C_t P_{NO}}{1+\frac{k_R P_{NO}}{8k_O P_{O_2}^{0.71}}+\sqrt{\frac{k_R P_{NO}}{8k_O P_{O_2}^{0.71}}\left(2+\frac{k_R P_{NO}}{8k_O P_{O_2}^{0.71}}\right)}}$	400-1600	1-4	0.5-12	-	195-310	[67]
b.	$k\frac{K_{NO}K_{NH_3}P_{NO}P_{NH_3}}{1+K_{NH_3}P_{NH_3}(1+K_{NO}P_{NO})}$	100-1100	0.02-2	excess	-	200-250	[68]
c.	$k\frac{K_{NO}K_{NH_3}P_{NO}P_{NH_3}}{1+K_{NH_3}P_{NH_3}(1+K_{NO}P_{NO})+K_{H_2O}P_{H_2O}}$	100-1100	0.02-2	excess	-	250-350	[68]
d.	$k\frac{K_{NH_3}C_{NH_3}}{1+K_{NH_3}C_{NH_3}}\frac{K_{O_2}C_{O_2}}{1+K_{O_2}C_{O_2}}$	50-1000	0.05-20	0.2-6.5	-	225-325	[69]
e.	$k\frac{K_{NO}P_{NO}}{1+K_{NO}P_{NO}}\frac{\frac{K_{O_2}P_{O_2}}{1+K_{O_2}P_{O_2}}}{\frac{K_{O_2}P_{O_{2,10\%}}}{1+K_{O_2}P_{O_{2,10\%}}}}$	300-1000	0.3-3.3	0-11.5	0-7.5	120-200	[70]
f.	$kP_{NO}\frac{\frac{K_{O_2}P_{O_2}}{1+K_{O_2}P_{O_2}}}{\frac{K_{O_2}P_{O_{2,10\%}}}{1+K_{O_2}P_{O_{2,10\%}}}}$	300-1000	0.3-3.3	0-11.5	0-7.5	200-290	[70]
g.	$k_{10}P_{NO}\frac{K_{10}P_{NH_3}/P_{NO}}{1+K_{10}P_{NH_3}/P_{NO}+K_{11}/P_{NO}+KNH_3P_{NH_3}}$	SCR typical conditions					[63]
h.	$\frac{\alpha}{\beta}\left[\gamma-\left(\gamma^2+\beta m/\alpha\right)^{1/2}\right]^2$	100-500	0.2-1	4	0-10	250-350	[71]
i.	$\frac{m}{(1+m)^2}\frac{k_1\theta_{NH_3}}{1+\frac{P_{H_2O}^{1/2}}{K_{OX}P_{O_2}^{1/4}}+\frac{k_1\theta_{NH_3}}{(1+m)k_2P_{NO}}}$	80-1080	0-26	0.05-5	-	240-280	[73]
l.	$kC_{NO}\theta^*_{NH_3}\left[1-\exp\left(-\frac{\theta_{NH_3}}{\theta^*_{NH_3}}\right)\right]$	0-700	0-1	1	0-5	220-400	[75]

$m = S_{V^{5+}=O}/S_{V^{5+}OH}$

$\alpha = k_9k_{10}P_{NO}K_8P_{NH_3}/\left[\left(k_{-9}+k_{10}P_{NO}\right)\left(1+K_{13}P_{H_2O}+K_8P_{NH_3}\right)+k_9K_8P_{NH_3}\right]$

$\beta = 16k_{11}k_{12}P_{O_2}$

$\gamma = \left(2k_{12}P_{O_2}\right)^{1/2}+k_{11}^{1/2}$

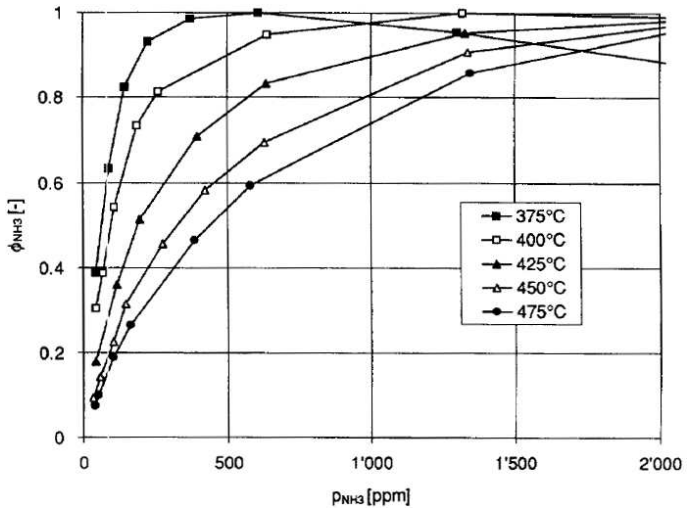

Figure 16: Experimental values of θ_{NH_3}, NO: 100ppm. From [66].

An expression similar to (23) was proposed by Nova *et al.* [75, 76], presented in Table 4 (expression (l)). By analysing the ammonia adsorption and the surface reaction on model vanadia-based catalysts by transient methods, they showed that the ammonia coverage affects the reaction rate only if θ is less than a critical NH_3 coverage value θ^* with $\theta^* < \theta$. This phenomenon is well shown in Figure 17-A, where the NO outlet concentration is measured against step changes in the NH_3 inlet concentration. Notably, when NH_3 is added to the feed, the NO outlet concentration reaches its steady-state value well before NH_3. Furthermore, when the ammonia inlet concentration is again decreased (trace b), NO concentration remains unaffected for several minutes. All these facts demonstrate that NH_3 is stored on surface *spectator* sites as *non reacting* ammonia, from which is transferred to these active sites, as already affirmed by Kleemann *et al.* [11] and discussed in Section 4.2.4.

In any case, it is worth noting that, when the ammonia coverage can be assumed total (low temperatures/high ammonia partial pressures), equation (23) reduces to the first-order expression (21).

Topsøe *et al.* [63] found that a three-step Eley-Rideal mechanism (Equations (10-12) was more consistent with the data from typical SCR conditions than a simple two-step Eley-Rideal mechanism. They thus proposed the expression (g) presented in Table 4, assuming a fast ammonia adsorption and slow rates for the two remaining steps. This expression was found to quantitavely describe both the NO reduction and the ammonia slip for NH_3/NO varying in the range 0.7-1.1.

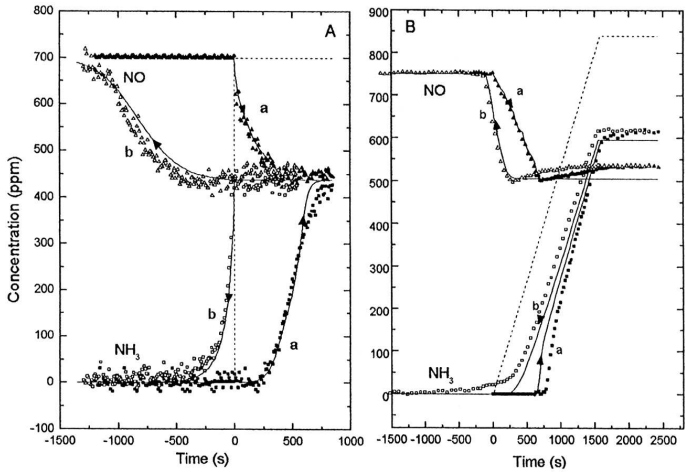

Figure 17: Dynamics of the NH_3 + NO reaction. (A) Step changes of the NH_3 inlet concentration ($0 \rightarrow 700 \rightarrow 0$ ppm) in He + NO + O_2 at 493 K over model V_2O_5-WO_3/TiO_2 catalyst. (B) Linear changes of the NH_3 inlet concentration ($0 \rightarrow 840 \rightarrow 0$ ppm) in He + NO + O_2 at 573 K over model V_2O_5-WO_3/TiO_2 catalyst. From [75].

4.4.2 Oxygen Effects

All authors agree that oxygen has an enhancing effect on the NO conversion, as shown in Figure 15C. This effect is especially pronounced at low oxygen concentrations and levels off above $\approx 10\%$ [69,70]. It is directly linked to the oxidation state of the catalyst surface. Some authors [77] proposed that the oxidation reaction of the catalyst is the limiting step in the SCR reaction.

The effects due to oxygen are considered in two different ways. By plotting the rate of NO conversion vs the oxygen concentration at different temperatures for a vanadia-tungsta-titania/sepiolite catalyst, Odenbrand *et al.* [69] showed that the oxygen adsorption follows a Langmuir behavior comparable to that of ammonia. Thus they assumed that also the oxygen concentration was in equilibrium on different sites than NH_3 and added to the rate expression an oxygen coverage θ_{O_2} term:

$$\theta_{O_2} = \frac{K_{O_2} C_{O_2}}{1 + K_{O_2} C_{O_2}}, \tag{25}$$

obtaining expression (d) in Table 4. In the presence of excess oxygen, the previous term can be neglected and the rate expression takes the Eley-Rideal form (23). In a similar way, the effect of oxygen was taken into account by Willi *et al.* [70]. In this case, the θ_{O_2} was normalized to 10% oxygen in the exhaust gas to allow an independent estimation of the constant k (expressions (e) and (f)). Figure 18 presents their experimental data and a good agreement between experimental results and simulations is seen.

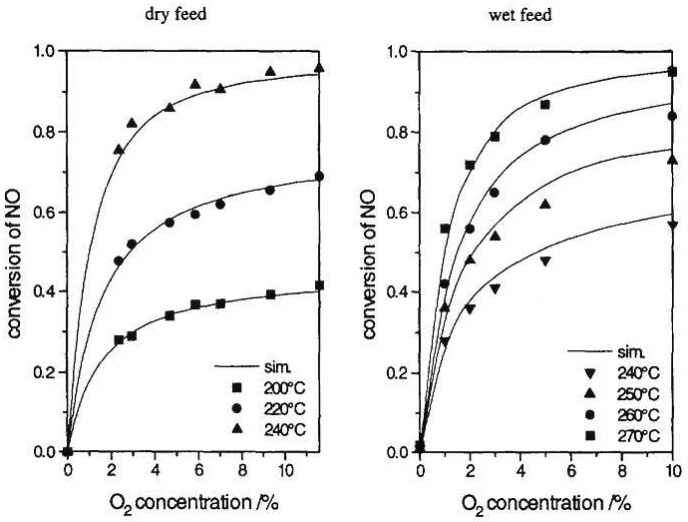

Figure 18: Conversion of NO versus oxygen concentration. Feed: 0-11.5% O_2, 1000 ppm NO, 1000 ppm NH_3, 5% H_2O, balance N_2. From [70].

On the other hand, other authors [67, 71, 73] considered the effects of oxygen by assuming the re-oxidation of the catalyst as a rate determining step in the global SCR reaction rate. They assumed the reaction following a simplified version of the mechanism proposed by Inomata *et al.* [58] and the Acid-Redox mechanism proposed by Topsøe *et al.* [39]. The results are presented in Table 4 (expressions (a) and (i) respectively).

4.4.3 Nitric Oxide Effects

At typical SCR conditions, NO does not adsorb on the catalyst. At lower temperatures, evidences for NO adsorbed species were found [66, 72].

As already mentioned before, the order with respect to NO in expression (21) was found to decrease from unity with decreasing temperatures. This fact was explained by different authors [66] assuming a weak adsorption of NO on the catalyst. In particular, according to Koebel *et al.* [66] at low temperatures, a much better description of the kinetic behavior of the catalyst is possible taking into consideration the adsorption of both NH_3 and NO on different sites. The same conclusion was reached by Willi *et al.* [70] and Tufano *et al.* [68]. As a matter of fact, the first group added to their rate expression valid for low temperature (expression (e)) the following term:

$$\theta_{NO} = \frac{K_{NO}C_{NO}}{1 + K_{NO}C_{NO}} \tag{26}$$

thus assuming that also the concentration of NO is equilibrated on the surface through a Langmuir-type isotherm on different sites than NH_3.

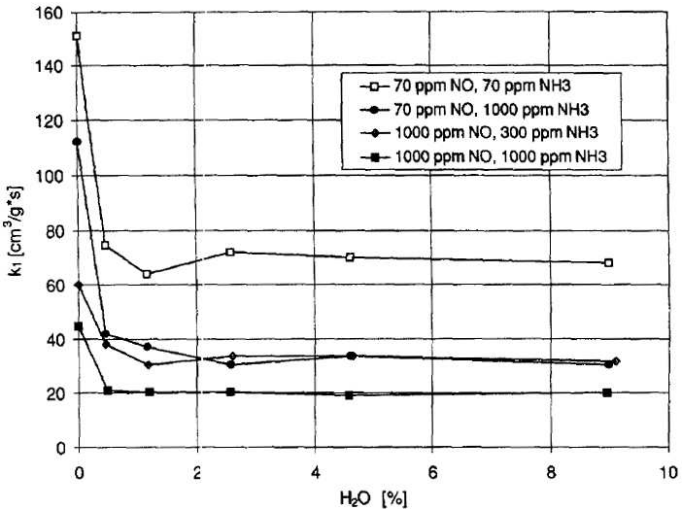

Figure 19: Influence of water on reaction rate, O_2=10%, T=250°C. From [66].

On the contrary, Tufano *et al.* derived a rate expression directly from the nitro-nitrosamide mechanism (reactions (4)-(9)) assuming the rate of decomposition of the amine species (reaction (7)) as the limiting step, resulting in the rate expression (b) in Table 4. This expression best fitted the experimental data in the whole range of temperatures examined. However, at higher temperatures (*i.e.* 300-350°C), a similar fitting accuracy was obtained assuming instead the surface reaction (6) as the rate limiting of the global reaction, thus obtaining from the same mechanism a simple Eley-Rideal model (expression (23)). This fact was interpreted by the authors affirming that at lower temperatures the amide species are more strongly adsorbed on the catalyst surface and thus their decomposition becomes the limiting step in the global SCR reaction. Again, the strong influence of temperature on the reaction behavior was pointed out.

4.4.4 Water Effects

The addition of water in the feed has an inhibiting effect on the NO conversion. A relative activity ($k_{obs,wet}/k_{obs,dry}$) of less than 0.50 was found in the presence of 2%v of water compared to the case in absence of water [66, 70]. However, this effect was found to level off at increasing concentrations (Figure 19).

This inhibiting effect has been considered in different ways. In the earlier studies, it was considered by assuming water competing with ammonia on the active sites [78]. Tufano *et al.* [68] found that at high temperatures this effect, if included in the rate expression by considering an adsorption constant for water, could better fit the experimental data. They thus proposed

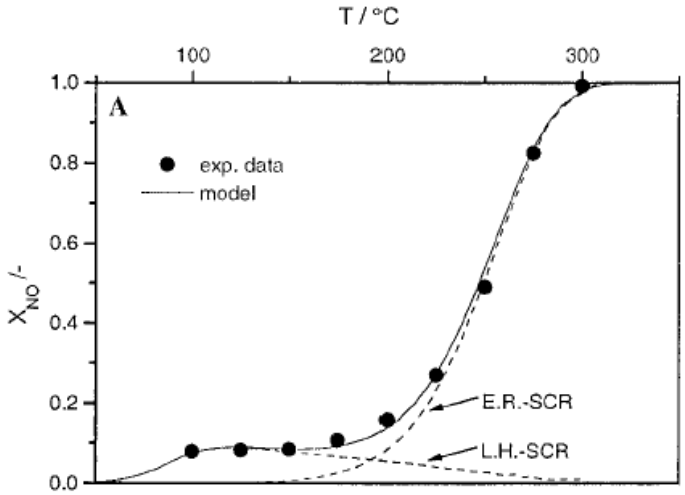

Figure 20: Conversion of NO versus temperature, LH-SCR and ER-SCR paths. Feed: 10% O_2, 5% H_2O, 1000 ppm NO, 1000 ppm NH_3, balance N_2. Catalyst weight: 4.41 g; particle size: 250 μm; flow 260 L/h (NTP). From [72].

expression (c) in Table 4 at temperatures above 250°C. However, water was not reported to have been added into the feed [68].

Nowadays, the possibility that water could compete with ammonia on the active sites is still matter of discussion. All authors agree that the interactions between water and the active sites are weak compared to ammonia-vanadia interactions. On the other hand, water is present at higher concentrations, so that eventually the observed inhibiting effects of water appears reasonable.

Recently, Nova *et al.* [75] observed the effect of water on the transient behavior of the SCR reaction. They added 5% of water vapor into the feed and showed that the inhibiting effect could not be explained by the competitive adsorption of water. They rather concluded that this effect should be explained by considering the changes in the redox state of the catalyst due to the presence of water, as already affirmed by Topsøe [79], which is then the main responsible for the overall rate of reaction.

The models directly derived from the SCR mechanism proposed by Topsøe *et al.* [39] are the ones that better can account for the redox state of the catalyst. Kamata *et al.* [73] derived directly from equations (13)-(18) the expression (i) in Table 4. In this, m is defined as the ratio of $S_{V^{5+}=O}$ to $S_{V^{5+}OH}$ sites, considered as a function of P_{O_2} and P_{H_2O}. The authors calculated by data fitting the dependence of m with the oxygen pressure and found that this is proportional to $P_{O_2}^{1/4}$ at all temperatures. Dumesic *et al.* [71] also validated the mechanism under typical SCR conditions (5%v H_2O, 300°C) and proposed expression (h), valid only if the water concentra-

Table 5: Correlations for estimating the external mass transfer in monolith catalysts.

Correlation	Type	Reference
$Sh_{av} = 0.766/\left[z^*\right]^{0.483}$	empirical	Ullah
$Sh_{av} = 2.976\left[1 + 0.139/z^*\right]^{0.81}$	empirical	Uberoi & Pereira
$Sh_{av} = 2.976\left[1 + 0.095/z^*\right]^{0.45}$	semi-theoretical	Hawthorn
$Sh = 2.976\left[1 + 0.206/z\right]^{0.545}$	theoretical	Tronconi & Forzatti

tion is sufficiently low that reaction (16) is irreversible.

4.4.5 Temperature Effects

As already discussed in section 4.4.3, the temperature has a direct influence on the general mechanism of reaction. At lower temperatures (*i.e.* < 250℃), the mechanism follows a Langmuir-Hinshelwood path with both ammonia and nitric oxide reacting as adsorbed species [66], whereas at higher temperatures the Eley-Rideal path is the one followed by the reaction. This fact was clearly showed by Roduit *et al.* [72] by simulating the reaction assuming both the two possible paths. Figure 20 shows the results of their calculations and the good fitting with experimental data.

4.5 Catalyst Design and Reactor Modeling

From the previous discussion it is clear that the SCR reaction is dependent on various parameters and a single expression valid in a wide domain of temperatures (150-450℃) and different flue gas compositions is not yet available. However, when limiting the domain at the conditions relevant for industrial applications, most of the expressions presented in Table 4 can be implemented in a general model simulating the entire SCR reactor.

Different authors [14, 15, 74, 80–84] have modeled the entire SCR reactor taking into account the reaction kinetics and both external and internal mass transfer limitations. A good introduction to the role of mass transfer in the SCR reaction over catalysts of different shapes can be found in [85].

The entire SCR reactor can be described with a one-dimensional model, neglecting axial diffusion and pressure drop [85]. Regarding the external mass transfer, at typical industrial conditions the flow in the channel is laminar with significant mass transfer limitation between the gas phase and the monolith wall. In order to evaluate the contribution of this external resistance, both experimental and theoretical approaches have been considered. Some correlations for the Sherwood number available in the literature are shown in Table 5. In the case of empirical expressions, the Sherwood number is given as an *average* number ($Sh_{av} = (k_{mt} d_h / D)$) over the entire monolith length ($z^* = LD/(d_h^2 u)$).

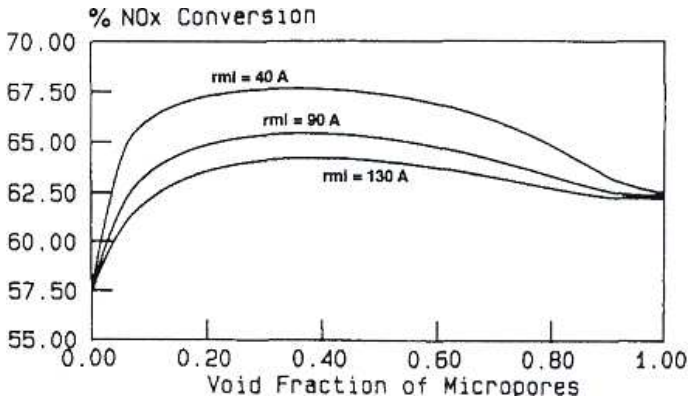

Figure 21: Calculated NO conversion vs. micropore void fraction for different values of micropore radius r_{mi}; macropore radius = 200 nm. From [14].

Besides the external mass transfer limitations, monoliths also present intraporous diffusion limitations which strongly limit the performance of commercial SCR catalysts. This resistance is a function of the effective diffusivity of the reactants into the catalytic pores and, in order to model correctly the observed reaction rate, it is important to measure or predict its value [86]. Beeckman *et al.* [87] developed an experimental technique to measure the effective diffusion coefficient of nitric oxide through the porous walls of a monolith-type ceramic catalyst. It involves the passage of gas streams inside and outside of a particular monolith channel and measuring the net flux across its walls. The experimental data were then successfully compared with the prediction of the random pore model of Wakao and Smith [88] based on Hg porosimetry measurements.

This finding had mainly two consequences. The first one was that it was possible to estimate the effective diffusivity by Hg porosimetry measurements, which is easy to obtain. The second one was that the internal mass transfer limitations were then modelled as a function of micro- and macroporosity (expressed as volume fractions) and the volume-integral-averaged micro- and macropore radii [14, 15, 74, 82, 83, 85]. From the analysis of the numerical solutions, it is seen that SCR catalysts normally operate under inter- and intra-phase mass transfer limitations. The NO intra-phase diffusion coefficient has been found about two-orders of magnitude smaller than molecular diffusivity [85]. Accordingly, the effectiveness factor of the monolith catalyst is in the range 0.01-0.1, indicating that only a very thin layer (0.2 mm) of catalyst is active in the SCR reaction [83].

The adoption of the random pore model of Wakao and Smith [88] had also another important consequence. By the analysis of the influence of the pore distribution on the SCR activity, it was shown that the introduction of macroporosity strongly enhanced the effective diffusion coefficient. The

reason was found in a larger effective diffusion coefficient provided by the macropores, which are able to more than offset the drop in volume-specific area, caused by the reduction of micropores. The necessity of a new pore structure was then revealed. In particular, Beeckman *et al.* [15] suggested to include a matrix of silica in the catalyst, which is able to satisfy the calculated bimodal pore structure. Tronconi *et al.* [14] showed that up to 17% of the total catalyst volume can be saved by limiting the micropore fraction to 0.4 with a micropore radius of 4 nm, as shown in Figure 21. The total void fraction was fixed to 0.7 for mechanical reasons.

Based on these results it can be concluded that in order to increase the global efficiency of the whole SCR process different roads are possible:

1. From a chemical point of view, the development of new catalyst compositions should aim at increasing the activity of the catalyst at lower temperatures. In this case it would be more convinient to adapt a tail-end configuration limiting the problems due to deactivation by particulates. Another reason to develop new compositions should be to obtain catalysts which are more poison-resistant. This would favour the application of the SCR process to systems where nowadays the deactivation rate is so fast that the SCR process is not feasible.

2. From an engineering point of view, the reactor should permit a complete and uniform mixing of the reactants. The use of 3-D modeling during the design process has already given good results [89]. Moreover, both the micro- and macro-structure of the catalyst monolith could be even more improved by developing monoliths with optimal channels geometries and pore sizes distributions, according to the results of the simulations. In this sense it could be more interesting to develop complete two- or three-dimensional models for the monoliths instead of using simplified one-dimensional models. The problems due to the high computational time due to these more complex models should nowadays not be an issue anymore, as it was in the past when these models were first developed.

5 Deactivation of Vanadia-based Catalysts

5.1 General Aspects

Catalyst deactivation is defined as the loss over time of catalytic activity and/or selectivity. Due to the high costs for catalyst replacement and process shutdown, this is one of the major problems related to the operation of catalytic processes. Deactivation is inevitable, but in a well-controlled process some of its consequences may be slowed, postponed or even prevented. Hence, research and understanding of the deactivation mechanisms are needed in order to optimize the development, design and operation of

commercial processes.

There are many mechanisms of catalyst deactivation, both chemical and physical (thermal and mechanical) [90–92]. *Poisoning* is the strong chemisorption of reactants, products or impurities present in the feed on the active sites, which are then deactivated. A species act as a poison only if its adsorption strength is high compared to other species competing for catalytic sites. A poison may act simply by geometrically blocking an active sites, or by electronically altering the adsorption of other species. Moreover, in the presence of a poison, the chemical nature of the active sites can be altered by the formation of new compounds.

The loss of activity due to blockage of active sites and/or pores caused by the physical deposition of species from the fluid phase onto the catalyst surface is known as *fouling*. This deactivation mechanism is particularly important in the case of catalytic reactions involving hydrocarbons and/or carbon oxides. Here, carbonaceous residues (coke and carbon) are produced by side reactions, and cover a great part of the catalyst surface (*coking*).

Deactivation via structural modification of the catalyst is referred to as *sintering*. This mechanism generally takes place at high temperatures (*e.g.* >500°C) and involves the agglomeration and coalescence of small crystallites into larger ones with lower surface-to-volume ratio. In general, sintering processes are difficult to reverse, but at moderate reaction temperatures their kinetics is slow.

Also a *solid-state transformation* can lead to the transformation of a crystalline phase into a different one with less surface area, thus deactivating the catalyst. This process is favored at high temperatures and could be considered as an extreme form of sintering. Moreover, it may occur due to the presence of foreign compounds in the lattice or even on the surface.

Beside these, other deactivation mechanisms include *volatilization*, *erosion* and *attrition*.

SCR catalysts were mainly developed for purely fossil-fuel-fired systems with a lifetime up to 5 years in the case of HD-SCR reactor. In this case, the main deactivating causes reported in the literature are the following [94]:

1. loss of surface area due to sintering and rutilization of titania after long-term operation at high temperature in *gas firing*;
2. poisoning by alkali metals in *oil firing*;
3. pore and channel blocking by calcium compounds in *coal firing*;
4. poisoning by As in the case of *wet bottom or recirculating boilers*;
5. accumulation of P components in lubricating oil in the case of *diesel engines*.

Table 6: Fuel analysis: bituminous coals [93].

	Colombian	Illinois No. 6	Polish
Proximate analysis, wt.%			
Water (raw)	7	2	4
Ash (dry)	11.3	12.9	8
Volatiles (dry)	32.3	33.1	30.5
Ultimate analysis, wt.%			
Carbon, C	66.9	63.3	72.5
Hydrogen, H	4.6	4.1	4.5
Oxygen, O	8	13.4	9
Nitrogen, N	1.4	1.27	1.25
Sulphur, S	0.93	2.84	0.67
Chlorine, Cl	0.012	0.119	0.073
Elemental analysis, mg/kg$_{dry}$			
Potassium, K	2600	3610	1420
Sodium, Na	440	1420	450
Ash composition, wt.% (ash)			
SiO_2	59.9	53.5	42.4
Fe_2O_3	7.9	12.4	11.3
Al_2O_3	18.1	16.4	21.7
CaO	1.8	4.6	7
MgO	1.5	0.7	4.2
Na_2O	0.4	1.2	0.8
K_2O	1.8	2.8	1.7
TiO_2	0.8	0.8	1.4

Recently, the thermal recycling of residues as secondary fuel is of increasing interest for power plant operators. Consequently, a variety of secondary fuels such as straw, wood, sewage sludge, meat and bone meal (MBM) and municipal waste are combusted. In all these cases, the lifetime of a normal HD-SCR catalyst has been found to be drastically reduced and the major deactivating mechanism according to the different application are under study. Table 6 and 7 present chemical analysis of some coals and secondary fuels normally used in the power plants. It can be seen that in most of the cases the different constituent of coal are found to quantitavely vary according to the different fuels. Based on these chemical analysis of the fuel, it is possible to initially provide a list of *potential* deactivation promoters and foresee and prevent undesired effects, which may affect the efficiency and practicability of the whole process when adopting a particular fuel or mixture of fuels.

In the following sections, each of the previously mentioned mechanisms of

Table 7: Fuel analysis: biomass and waste. Data from ECN's Phyllis database.

	Wheat straw	Untrea. Wood	Sewage sludge
Proximate analysis, wt.%			
Water (raw)	10.3	-	3
Ash (dry)	4.2	-	6.9
Volatiles (dry)	69.7	-	-
Ultimate analysis, wt.%			
Carbon, C	42.5	47.8	25
Hydrogen, H	5.3	5.4	4.5
Oxygen, O	37.1	36.3	13.6
Nitrogen, N	0.52	0.45	4.5
Sulphur, S	0.06	0.06	1.4
Chlorine, Cl	0.153	0.009	1.4
Elemental analysis, mg/(kg_{dry})			
Potassium, K	5480	2370	20000
Sodium, Na	140	1444	20000
Phosphorus, P	-	41	50000

deactivation are discussed according to the evidences available in the open literature in the case of vanadia-based SCR catalysts. The deactivating effects of the different compounds shown in Table 6 and 7 are also reviewed.

5.2 Poisoning

In the case of vanadia-based catalysts applied at biomass firing, poisoning represents the main mechanism of deactivation. As discussed previously, the vanadia-based catalysts are characterized by both BA and LA sites on the active phase, the support and the promoters. Ammonia adsorbs on all these acid sites, but reacts with gaseous NO only if adsorbed on the vanadia sites. From this point of view, a poison is a species that can strongly adsorb on the vanadia sites, thus reducing the number of sites available for the adsorption of *reacting* ammonia. However, the same poison can adsorb on the different acid sites present on the support and/or due to the promoters, competing with the adsorption of *non-reacting* ammonia. Accordingly, the *total* amount of ammonia adsorbed decrease with the increasing level of poison. Care must be taken when correlating the strength of a poison with the total amount of adsorbed ammonia without considering the *selectivity* of the poison itself.

Alkali and alkaline earth metals, arsenic, phosphorus, HCl, zinc and lead are the main poisons for the vanadia-based catalysts. Their different contributions to the total deactivation rate strongly depend on the particular

application, the fuel and the combustion process. In general, since the activity of the catalyst depends on its acidity, the poisoning strength is directly correlated to the basicity of the poison [95, 96]. Moreover, since vanadia is present in small concentrations on the commercial catalyst, even small amounts of poisons can produce drastic effects on the activity of the catalyst.

In order to prevent the effects of poisoning, two ways are available. The first one is the *partial* elimination of the poison from the flue gas. To this first class belong all the possible modifications of the combustion process and the fuel (*e.g.* using additives) that can either avoid the release or favor the recapture of the poison. The second one is the reduction of the interactions between the poison and the active sites. This solution is mainly constituted by chemical modification of the catalyst composition. Introducing a component in the catalyst that forms non-active sites where the poison preferentially adsorbs, can preserve the active sites from the attacks. When prevention is not possible, the regeneration of the doped catalyst could still be an available way to reduce the cost compared to complete replacement of the catalyst unit.

5.3 Fouling

Catalyst plugging in the SCR process is primarily caused by both salt and fly ash deposition. The decrease of NO_x reduction associated with an increased pressure drop is the main indication of catalyst fouling. The determination of catalyst surface area, total pore volume and pore size distribution by mercury porisometry and BET helps in distinguishing between pore blocking by ash and pore condensation.

Different compounds present in the flue gas are able to form salts that can solidify at SCR temperature and deposit on the catalyst. The most important are CaO, HCl, $CaCO_3$, NH_3 and SO_3. Free CaO in the fly ash reacts with SO_3 adsorbed on the catalyst forming $CaSO_4$, which is solid at SCR typical temperatures (*i.e.* $CaSO_4$ melting point 1450°C) and can plug the catalyst. Also NH_3 in the presence of SO_3 and H_2O can react forming ammonia bisulphate (NH_4HSO_4) and ammonium sulphate ($(NH_3)_2SO_4$). However, since these two ammonium salts have melting points lower than the typical SCR temperature (147 and 235°C respectively), their deposition is a major concern for the equipments downstream the SCR reactor or at partial load. The ammonium chloride has a similar behavior: it is formed from the reaction between gaseous NH_3 and HCl and has a melting point at 338°C. Blockage of surface area and pores by phosphorus and arsenic were also reported [95, 97, 98]. However care must be taken when considering the melting points of the pure compounds, since in reality these compounds may not be pure and form a liquid phase at lower temperatures.

According to the previous evidences, two ways are effective in order to

decrease the effects of fouling. The first one is the proper selection of catalyst pitch and cell opening size according to the properties of dust and fly ash. Moreover, a temperature control in the SCR reactor can avoid the deposition of ammonium salts. The second one is the limitation of the SO_2 oxidation, since SO_3 is the main responsible for the formation of the most dangerous salts. In any case, efficient soot blowing systems installed at the inlet of each catalyst layers in the SCR reactor can strongly enhance the performance of the reactor and its resistence against fouling and channel blocking.

5.4 Sintering and Solid-state Transformation

Sintering and solid-state transformation due to ageing are the main mechnisms of deactivation for vanadia-based catalysts in the case of gas firing. In other applications (*e.g.* coal and biomass/waste combustion) its importance is minor compared to poisoning and/or fouling, but not negligible considering the long life-time desired for the catalyst.

For the vanadia-based catalysts, both sintering and solid-state transformation are associated with the TiO_2 support and strongly depend on the thermal history [94] and on the composition of the catalyst [18,37]. Titania is employed as support in the anatase form which presents a higher surface area than the rutile form. However, anatase is not a stable configuration and tends to convert into the rutile configuration.

The temperature has a direct influence on both sintering and rutilization. A catalyst which has experienced high temperatures (>500℃, either during its initial calcination or during normal operation) presents bigger crystals and more rutile phase, and thus less specific surface area than a catalyst treated at lower temperatures [18,37,94].

Vanadia-loading also has an important influence on both sintering and rutilization. The influence of vanadia-loading on titania sintering has been studied by Alemany *et al.* [18] on model V_2O_5-TiO_2 and by Madia *et al.* [37] on model V_2O_5-WO_3-TiO_2, using X-ray diffraction (XRD), X-ray photoelectron spectroscopy (XPS), Raman spectroscopy and BET surface area determination. Figure 22 shows the different values of relative BET surface area obtained by the authors. It can be noted that this latter was found to linearly decrease at increasing vanadia-loading. In particular, the specific surface area of the catalyst employed by Alemany *et al.* decresead from 85 m^2/g (sample without vanadia) to 30 m^2/g by adding only 3.5%wt. of vanadia. Since at the calcination temperatures adopted in these experiments (*i.e* 500℃ for the experiments of Alemany *et al.* and 600℃ for those of Madia *et al.*) anatase was the only phase detected, it was concluded by both the authors that vanadia is a sintering promoter. This fact was further confirmed by the corresponding changes in the average crystal size, pore volume, and pore radius.

Vanadia is also able to lower the temperature of rutilization. Alemany

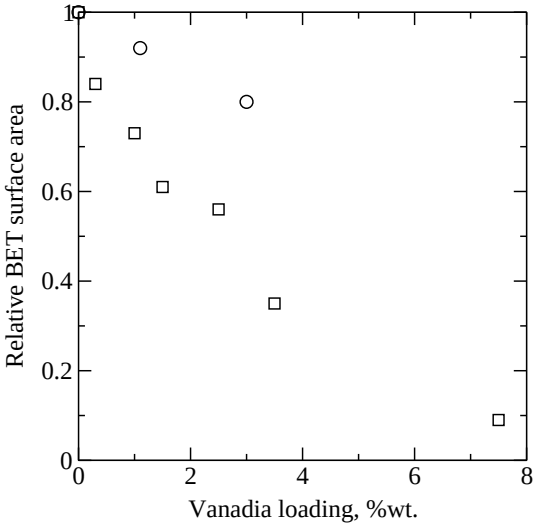

Figure 22: Effect of vanadia-loading on the relative BET surface area of model V_2O_5-WO_3-TiO_2 (circles) [37] and model V_2O_5-TiO_2 (squares) [18] calcined at 500 and 600℃ respectively.

et al. [18] found that a 1.5% V_2O_5-TiO_2 catalyst calcined at 700℃ presented only 4% of rutile phase. When the vanadia content was raised to 7.5%, already at 600℃ the support was constituted by 72% of rutile. Its BET surface area was 8 m^2/g.

The activity of a commercial (0.62%)V_2O_5-(9%)WO_3-TiO_2 calcined in the range 500-900℃ was tested in the laboratory by Nova *et al.* [94], in order to correlate the sintering caused by temperature with the activity and selectivity of the catalyst. By analysing the catalysts by FT-IR, FT-Raman spectroscopy, it was concluded that the sintering of the support favours the aggregation of isolated vanadium ions. This fact resulted in higher activity at lower temperatures, but lower selectivity (*i.e.* -20% of the initial) at high temperatures, demonstrating the unapplicability of the common commercial catalysts in long-term high-temperature gas firing applications. Moreover the catalysts became more active in the SO_2 to SO_3 oxidation. However, it must be noted that the temperatures investigated in this work were higher than the melting point of V_2O_5 (690℃).

Similar results were obtained by Madia *et al.* [37], further demonstrating that the temperature window of the vanadia-based catalysts decreases with the exposure time rending the whole SCR process less flexible.

5.5 Performed Investigations on Deactivating Compounds

Due to their commercial success, vanadia-based catalysts have been subjected to numerous studies in order to understand and prevent the causes

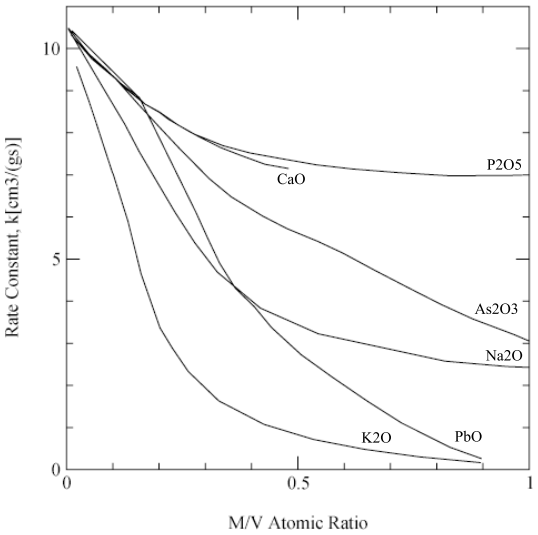

Figure 23: Activities of 5% V_2O_5/TiO_2 doped with different amounts of metal oxide poisons. Operating conditions: NO=NH_3=1000 ppm, O_2=2%, T=300°C, space velocity=15000 hr^{-1} [95].

of their deactivation. Great part of the research has been carried out in the laboratory. Both model and commercial catalysts have been doped *in situ* by wet impregnation and their activities have been measured in lab-scale reactors [95, 96, 99–102]. Although with this particular method of doping the results are far from simulating the real effects of a poison in the SCR reactor, these investigations can provide an useful first estimation of the *potential* poisoning effects of the single compound and they normally constitute the first step of a wider research program. However, since the deposition of a poison on the catalyst surface strongly depends on both the physical state (gaseous, solid, particle size, etc.) of the poison in the flue gas and the fluid dynamics within the SCR reactor, both pilot- and full-scale experiments have been performed. Here commercial catalyst module in full size have been exposed either to model flue gases containing the poisons under investigation [103] or to real flue gases from power plants [104, 105].

In the following sections, evidences reported in the literature about deactivation of vanadia-based catalysts are reviewed.

5.5.1 Alkali and Alkaline Earth Metals

Alkali (K, Na) metals are strong poisons for the vanadia-based catalysts. When the SCR is applied at biomass (co)-combustion, this is a major concern due to the high amount of water soluble alkali metal oxides present in the flue gas. As a matter of fact, for purely coal-fired power plants, the effect of alkali deactivation is negligible since alkali content is relatively low

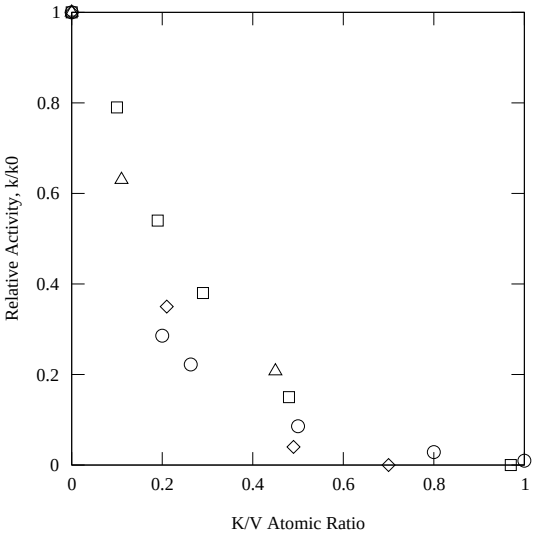

Figure 24: Potassium effect on SCR activity of vanadia-based catalyst. Circles: powderized lab-catalysts (5% V_2O_5-TiO_2) doped with KNO_3 [95]. Squares: powderized commercial catalyst (1% V_2O_5-8%WO_3-TiO_2) doped with KNO_3 [101]. Diamonds: powderized commercial catalyst (1.8% V_2O_5-8.5%WO_3-TiO_2) doped with KNO_3 [102]. Triangles: commercial catalyst (1.78% V_2O_5-WO_3-TiO_2), plates doped with KCl [100].

and the alkali fractions in the fuel are usually bound as silicate and alumina, which are very stable at even high temperatures and are thus found in the ash. On the other hand, in biomass combustion the alkali (mainly potassium) are released to form sulphates and chlorides which are water soluble and able to penetrate the catalyst pore structure [106].

According to Chen *et al.* [95, 96], the strength of the poison follows the scale of basicity:

$$K_2O > Na_2O > CaO$$

as shown in Figure 23.

The effects of potassium were studied by different authors on both model vanadia/titania [95,96,99] and commercial catalysts [100–102]. The K-doped catalysts were prepared in laboratory by wet impregnation with aqueous solution of KNO_3 [95, 96, 101, 102], KOH and K_2CO_3 [99], and KCl and K_2SO_4 [100]. Only in this last case, the activity tests were performed on plates instead of powders. All the tests were conducted by measuring the rate of NO reduction at increasing K content. Ammonia adsorption studies were also carried out. The amount of adsorbed ammonia was measured by TPD methods or by measuring the amount of NO reduced by a catalyst pre-covered with ammonia. Both fresh and doped catalysts were then analyzed by means of FT-IR in order to point out the active sites in the SCR

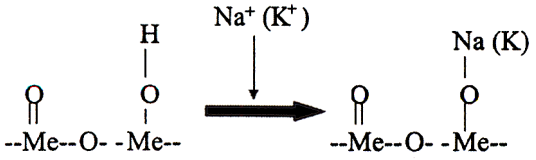

Figure 25: Model of alkali deactivation [98].

reaction and thus correlate their number to the amount of K deposited on the catalyst.

All authors find that due to K-doping a much lower amount of ammonia adsorbs on the vanadia-based catalyst, both in the coordinated and protonated form. The rate constants for the K-doped catalyst were calculated at temperatures between 250 and 400℃, by assuming a first-order kinetic for the SCR reaction and a plug flow behavior for the packed-bed reactor. The conversion of NO was found to highly decrease for even small addition of poison (*i.e.* 0.1 wt.%), as shown in Figure 24. By comparing the progress of rate constants with the amount of ammonia adsorbed by the different K-doped catalysts, the reaction was still found first-order [95, 96]. Hence, potassium simply reduce the number of active sites by strongly interacting with them.

The FT-IR evidences suggested that the potassium preferentially reacts with the V-OH species, whereas the LA sites were not affected to great extent by the poisoning [101]. The BA sites associated with the V-OH species were thus proposed as the active species in the SCR reaction. Figure 25 shows a schematic representation of alkali poisoning [98]. However, especially when considering commercial catalysts, it is not possible to well distinguish the contribution of each single species present on the surface in the total absorbance. For this reason, Kamata *et al.* [101] concluded that K_2O preferentially adsorbs on the V-OH *and/or* W-OH groups, without considering that the active sites are only associated with the former group.

Similar behaviors were found for Na_2O and CaO poisoning [95, 96, 102] when doping the catalysts by wet impregnation with aqueous solution of $NaNO_3$ and $Ca(Ac)_2$.

As stated above, alkali metals are considered the main deactivating agents when the SCR process is employed in plants burning biomass both pure and mixed with fossil fuels. The use of biomass as fuel in the power production is very common in countries like Sweden and Denmark. Here straw and wood are burned in the power plants in order to obey to the national regulations resulting in a lower performance of the whole combustion process [104,105,107]. The results obtained in the laboratory by wet impregnation are of course far from simulating the situation at full-scale. Here the alkali fraction is present as aerosol particles formed during homogeneus and

heterogeneous condensation of alkali metals evaporated from the fuel during the combustion [108, 109]. Their interaction with the monolith could thus be dependent on several different phenomena (*e.g.* diffusion, evaporation, condensation, etc.). For this reason, investigations using catalysts exposed under more realistic conditions have recently started [103–105].

Moradi *et al.* [103] exposed vanadia-supported monolith and wire-mesh catalysts to aerosol particles of KCl, K_2SO_4 and K_2CO_3 produced by a spray method. The de-NO_x activity of the exposed samples was then determined in the laboratory, and their surfaces were characterized by scanning electron microscopy and X-ray mapping. Hg-porosimetry and BET surface area determination were also performed. The aerosol particles produced had a constant average diameter around 0.066 μm and the load was around 15-20 mg/m^3 at room temperature: compared to the aerosol distribution measured at full-scale (straw grate-firing), both the load and the mean particle diameter were very low [108,109]. After 31 hours of exposure at 300°C, K-salts were found to penetrate the catalyst wall to a depth of 1-1.5 μm. Since at that temperature these salts are solid, it was concluded that the fine particles were able to penetrate by diffusion. This conclusion was further supported by the increased amount of deposited K found when the exposure temperature was raised at 500°C. The Hg-porosimetry and the BET analysis showed an increased value of the average pore diameter which suggested the occurence of loss of meso- and micro-pores. Pore blocking by K-salts was then indicated as the main mechanism of deactivation. However, no significant decrease in activity was observed when the treated samples were used in the SCR reaction. Considering both the small load of particles and the very short exposure time adopted in these experiments, this result is not surprising. It only suggests that more experiments at higher loads and exposure times are required in order to further clearify the whole process of deactivation.

The few references available in the open literature about SCR applied to biomass combustion are from Sweden [104] and Denmark [105, 107] where, as said before, the use of biomass in the power plant is highly motivated by local regulations. These references are the most important ones concerning the deactivation by alkali, in particular potassium.

Khodayari *et al.* [104] studied the activity of commercial V_2O_5-WO_3-TiO_2 ceramic honeycombs and plates as a function of exposure time (max 2100 hours) at full-scale flue gases. The catalysts contained a higher amount of V_2O_5 than the one normally used in coal combustion, due to the lower SO_2 levels in biomass combustion. The tests were carried out in a 125 MW_e circulating fluidised bed (CFB) plant burning forest residues, and in a 75 MW_e plant burning pulverised wood (PC). The catalysts were exposed either in a by-pass rig or in a test bench directly introduced into the flue gas duct. Activity measurements were performed on mini monoliths (3x3 channels) in an aluminum reactor chamber at a fixed temperature of 300°C,

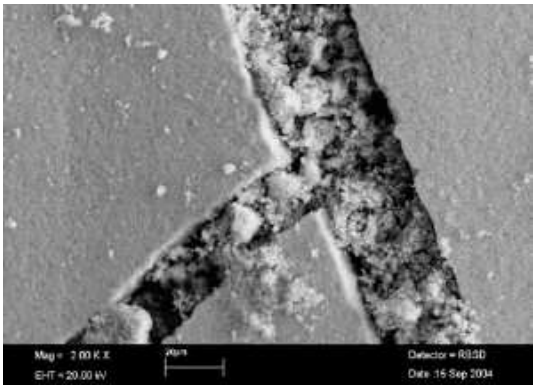

Figure 26: Surface of commercial type V_2O_5-WO_3-TiO_2 monolith exposed for 1621 hours at full straw/wood combustion. From [105].

and the exposed samples were characterized by BET surface analysis and SEM/EDX. In the case of the CFB plant where forest residues were burned, the catalysts lost 20% of their initial activity. Here K was found well distributed in the walls and constituted the 0.27 wt% of the whole catalyst mass. In the case of wood combustion at the PC plant, after only 1400 hours of exposure, the catalysts lost up to 80% of their initial activity. Here the total amount of K depositated was 0.8 wt%. The difference in deactivation between the two plants was found in the different composition of the fuels. Contrary to wood, forest residues present an ash with more than 40 wt% constituted by SiO_2. Part of the K is then supposed to be bound to this silica in high-temperature melting point fly ash, which simply go through the catalyst without chemically interacting with the active sites. These findings are in agreement with the experience developed in Denmark in cofiring coal and straw (20% on energy basis) [107].

By a fast comparison of these data with Figure 24 it is hypotizable that in the case of potassium the wet impregnation method overestimate the deactivation measured at full-scale. A reason for this behavior could be found in the fact that when present in an aqueous solution, K can more efficiently react with the active sites rending them inactive, whereas, in solid phase, less K than the one present in the wall can really *chemically* react with an active site. However, it is worth noting how fast potassium is able to accumulate in the catalysts pores; this makes the conventional SCR catalyst unsuitable for cleaning of flue gases from biomass combustion. Eventhough this was clear, the mechanism of accumulation of K inside the catalysts walls was not discussed.

This mechanism was instead developed by Zheng *et al.* [105] studying the behavior of commercial type V_2O_5-WO_3-TiO_2 monolith catalysts under straw/wood combustion at a full-scale grate-fired power plant. The

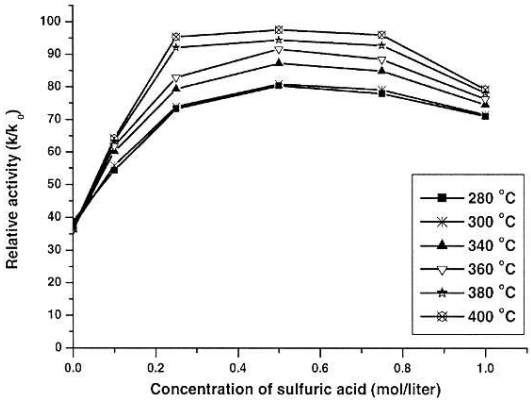

Figure 27: Relative activity vs. concentration of sulphuric acid at different temperatures. From [110].

work involved aerosol measurements, periodic activity tests and ammonia chemisoption, and characterizations by SEM-EDX and BET of the exposed catalysts. The exposure time to power plant flue gas was up to 1600 hours: at that time the catalysts lost more than 50% of their initial activity, corresponding to an unacceptable deactivation rate of 1.1% per day. Based on the results obtained, it was concluded that both physical and chemical deactivation are due to alkali aerosols. The physical deactivation was showed by SEM-EDX pictures of exposed surfaces. Figure 26 clearly shows how the catalyst pores were filled with deposits resulting in slower transport of reactants into the walls. The chemical deactivation was clear when analyzing the accumulation and distribution of potassium in the catalyst. This was able to penetrate the catalyst structure and K/V ratio higher than 0.3 were found. According to Figure 24 this ratio is already able to reduce the catalyst activity to its 30%.

The following mechanism of deactivation was then proposed:

1. The water soluble alkali fraction present in the biomass is released in the gas-phase during combustion;

2. At lower temperatures the alkali fraction present in the gas-phase forms aerosols. Part of the aerosols present in the gas stream, depending on their size and the external mass transfer limitations, can reach the catalyst walls by diffusion in the gas phase.

3. Due to their mobility at SCR temperatures (both the Huttig and Tamman temperature for KCl and K_2SO_4 are lower than 400°C) the most fine particles can further penetrate the walls by *surface diffusion* and either interact with the active sites or block the pores.

Based on these results it is now clear that both the high chemical affinity between K and V and the ability of K-salts in forming pure submicron particles are the main causes of deactivation by K in biomass combustion. In this sense the experimental set up developed by Moradi *et al.* [103] looks very interesting if both the load, the particle size and the exposure time can be increased. Moreover, in order to better quantify the influence of chemical and physical deactivation, it would be interesting to start measuring the effective diffusion of NO and NH_3 in exposed catalysts. The Hg-porosometry and the BET techniques applied so far do not seem to be able to solve the question since in the results the surface area and the pores of the deposits are of course taken into consideration, rending the reading of the data more complicated.

In general it can be said that overcoming K-deactivation is a very challenging process, since it should include changes both in the chemical composition and the pore structure of the catalysts. So far, regeneration of K-poisoned catalysts has been indicated as a viable solution for minimising the total cost of the SCR process applied to biofuels (co)-combustion. Khodayari *et al.* [110,111] studied the regeneration effects of washing with different aqueous solutions (i.e. of sulphuric acid, sulphuric acid and vanadyl sulphate, sulphuric acid and vanadyl sulphate and ammonium paratungstate) and sulphation with SO_2. From their activity tests on a commercial vanadia-based catalyst, they concluded that the most effective method is washing with aqueous solution of H_2SO_4. As shown in Figure 27, at 400℃, a catalyst washed with 0.5 M of H_2SO_4 almost regained its initial activity. A similar result was obtained by Zheng *et al.* [100]. Again the regeneration by 0.5 M H_2SO_4 resulted an effective way to regenerate the catalyst. Beside this, the regeneration by 1 M NH_4Cl also showed good results (Figure 28). However, the textural properties of the catalyst after regeneration were found to degrade, indicating a limit in the number of possible regenerations [110].

5.5.2 Arsenic

Arsenic is a coal mineral matter constituent with serious impact on SCR design and operation [112–115]. Arsenic deactivation was first identified as a problem mainly in wet bottom boilers or in the presence of ash recirculation: in some German installations, 50% loss of activity has been reported after 10,000 operating hours in the case of vanadia-tungsten based catalysts [113]. Due to this great impact of arsenic on the activity of SCR catalysts, many investigations have been carried out in order to elucidate the mechanism of As-deactivation and propose some solutions [98, 115–119].

All authors agree that the poison is constituted by gaseous As_2O_3 released during fuel combustion. It is thus clear that the problems experienced in the presence of ash recirculation were related to the concentrating mechanism due to recirculation, which was able to cause high gaseous arsenic

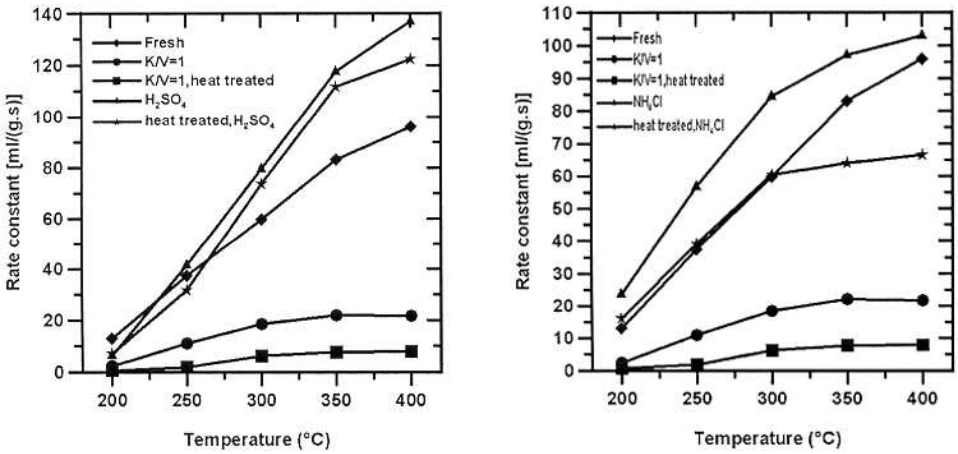

Figure 28: Effects of washing by 0.5 M H_2SO_4 and 1 M NH_4Cl on the activity of K-poisoned 1 wt% $V_2O_5(WO_3)/TiO_2$ catalysts. From [100].

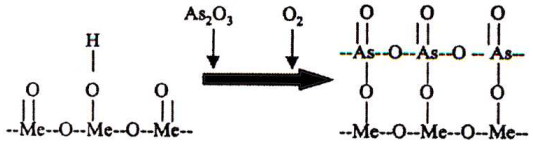

Figure 29: Model of gaseous arsenic deactivation [98].

levels (10 times the initial level) in the flue gas. However it was also found that a correlation between gaseous As and Ca in the fuel exists [112]. By analysing the ash composition, it was concluded that in the presence of free CaO in the gas, much of the As_2O_3 reacts with this to form calcium arsenide $Ca(As_2O_3)_2$. Since this compound is a stable solid material, it becomes boiler bottom ash or fly ash. In this case, only a small part of the As_2O_3 remains gaseous and reaches the SCR catalyst. Experience now indicates that if free CaO in the fly ash is below 2%, all the arsenic present in the fuel contributes to gaseous As_2O_3 [112]. In this case the addition of limestone to the fuel is necessary.

Research on the mechanism of deactivation by gaseous As_2O_3 lead to the development of the so-called As-resistant SCR catalysts [98,115–119]. It was found that gaseous As tends to condense on the catalytic surface blocking the active sites (as shown in Figure 29) and altering the pore structure of the catalyst. However, a general linear relationship of As_2O_3 adsorption to deactivation was not found for all the catalysts under investigation, thus indicating that was not possible to correlate decreasing of activity with catalyst physical properties over operating time [119]. The co-presence of

Table 8: Ash analysis: MBM and sewage sludge. Data from CATDEACT final report.

	Sewage Sludge	MBM
Ash composition, wt.% (ash)		
P_2O_5	20.4	32.7
SiO_2	29.9	0.92
Fe_2O_3	13.0	0.47
Al_2O_3	12.8	0.09
CaO	14.3	56.0
MgO	3.0	1.1
Na_2O	0.61	2.2
K_2O	1.8	1.7
TiO_2	1.1	<0.03

both chemical and physical deactivation mechanisms due to As was then showed [116].

Further research on the deactivating effects of As on different catalysts compositions showed that vanadia-molibdenum-titania catalysts were more resistant to As poisoning than vanadia-tungsten-titania catalysts [118]: it is now demonstrated that arsenic preferentially reacts with MoO_3 and, while there are free Mo-OH on the catalyst surface, the vanadia sites are not attacked.

Based on these findings, arsenic poisoning was best abated by both catalyst formulation and pore design. Molibdenum was added to the catalyst up to 6% w/w and a deactivation rate up to three times slower compared to the V_2O_5-WO_3/TiO_2 catalyst was obtained. Moreover, by reducing the average pore diameter, the diffusion of gaseous As_2O_3 was also limited due to the high volume occupied by the molecules [98,112,113]. However, the resulting catalysts were less active compared to vanadia-tungsten-titania catalysts.

5.5.3 Phosphorus

Phosphorus is a typical constituent of coal. It reaches levels ≈ 1 wt% of the total concentration and its deactivating effects are not relevant compared to other poisons like the alkali metals. However, the increasing interest in (co-)combustion of sewage sludge or meat and bone meal (MBM), which introduce in the system high amounts of phosphorus as shown in Table 8, has made that its effect on the SCR activity is nowadays under study [120].

The deactivating effect of P were studied on both model (5 wt%)V_2O_5-TiO_2 [95] and commercial (1 wt%)V_2O_5-WO_3-TiO_2 catalysts [121]. Phosphorus was added to the catalysts by wet impregnation of aqueous solution of H_3PO_4. The activity of the doped catalysts was then measured in the lab-

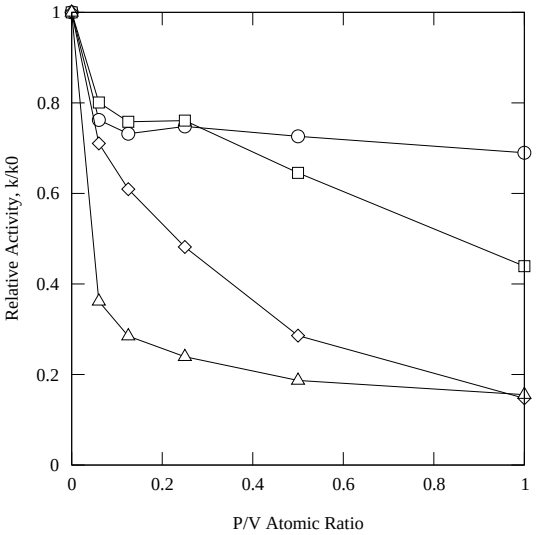

Figure 30: Effects of P_2O_5 doped on 5% V_2O_5/TiO_2 catalyst in the SCR reaction at 150 (triangles), 200 (diamonds), 250 (squares) and 300°C (circles). Data from [95].

oratory and the samples were characterized by means of FT-IR and Raman spectroscopy, XPS and N_2 adsorption.

The poison was found to disperse well over the catalyst surface without significant agglomeration up to 5 wt% load [121]. The activity tests performed on model high-vanadia-content catalysts [95] showed that P_2O_5 formed during heating is a very weak poison as compared with the alkali metal oxides (Figure 23) at typical SCR temperatures. At lower temperatures, however, its poisoning strength was found relatively higher as shown by Figure 30 [95]. Low addition of P_2O_5 to commercial $V_2O_5(WO_3)/TiO_2$ catalyst did not cause a pronounced deactivation effect either [121]. This effect was found to gradually increase according with the P_2O_5 content.

The following deactivating mechanisms by phosphorus were proposed by Kamata *et al.* [121]:

- by decreasing the specific surface area and pore volume of the catalyst, in agreement with previous observation by Blanco *et al.* [97] on vanadia catalysts extruded with H_3PO_4;
- by replacing surface hydroxyl groups (V-OH and W-OH) with P-OH groups: FT-IR evidences of ammonia adsorption showed that these groups still present a Brønsted acidity and participate in the activation of adsorbed ammonia [121], but this acidity is much weaker than the one due to the replaced groups;
- by removing sulfur species from the catalyst surface which are known

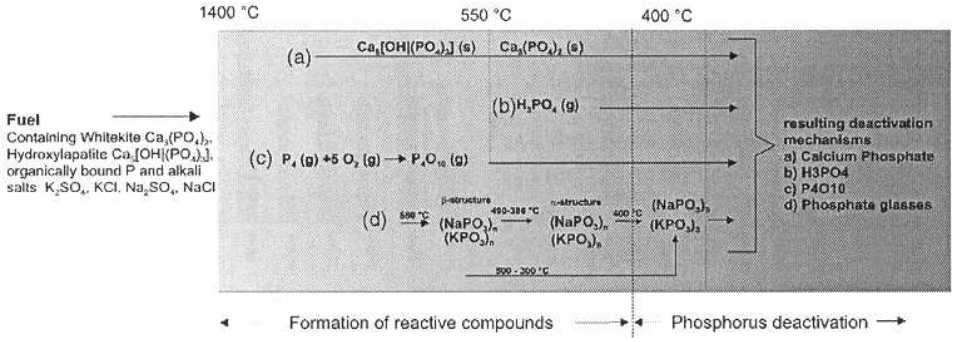

Figure 31: Proposed reactions of calcium phosphates along the flue gas path. From [120].

to contribute to some extent to the acidity of the catalytic surface.

Recently, Beck *et al.* [120] analyzed different high-dust vanadia-based catalysts employed in the treatment of flue gas produced by sewage sludge and MBM co-combustion. From the results of BET analysis of the exposed samples, they concluded that pore condensation in combination with pore blocking is the prevaling deactivation mechanism by phosphorus. The main responsibles for this mechanism were identified by equilibrium calculations considering primary flue gas constituents (i.e. SO_2, H_2O and CO) together with the fly ash components (i.e. CaO, Al_2O_3 and SiO_2) in the temperature range of 400-1400℃. The results are shown in Figure 31. As it can be seen from this, the four following deactivating species were proposed:

- *Solid calcium phosphates.* These compounds are due to heterogeneous reactions between gasesous P and fly ash, or they come directly from the fuel, especially in the case of MBM were great part of the P is bound to high melting point calcium phosphates. These particles can be regarded as pore- and channel-blocking agents.

- *Condensed phosphoric acid.* When present in the gas-phase at high temperatures, the phosphoric acid forms poly-phosphates which have melting points higher than the typical SCR temperature. They can thus form aerosols which can diffuse into the pore structure and deactivate the catalysts both by poisoning and pore-condensation. Furthermore, these poly-phosphates are known to form insolouble salts with ammonia and the alkali fraction present in the flue gas and give glassy deposits on the catalyst surface.

- *Gaseous phosphorus oxide* and *phosphoric acid.* Since these compounds are present in the gas phase, they can *easily* diffuse into the wall and poison the catalyst.

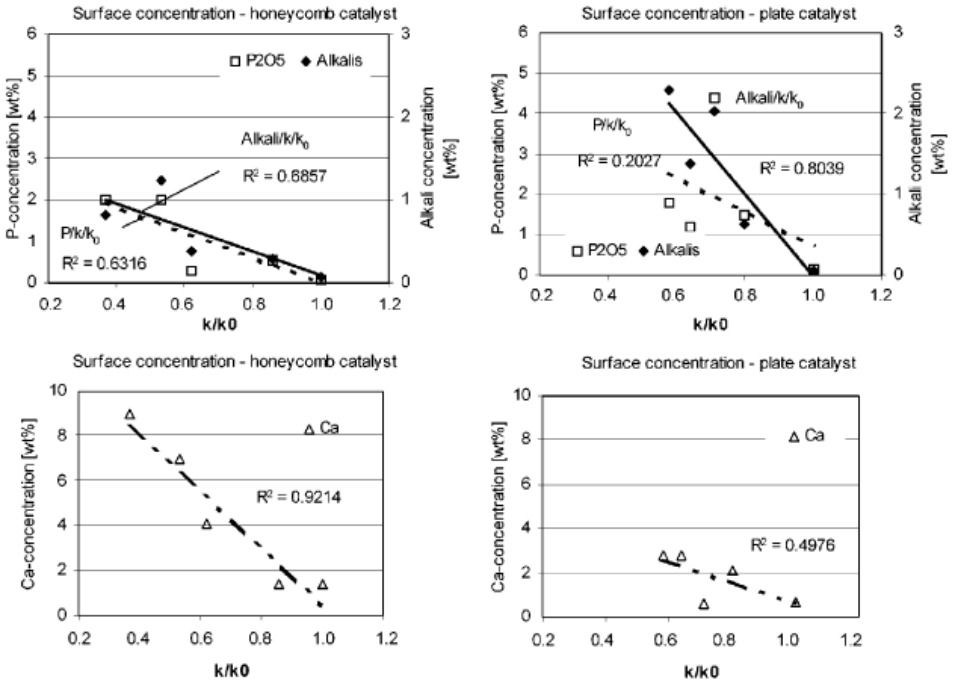

Figure 32: Relation of surface P, alkali and Ca concentration compared to k/k_0 of honeycomb and plate catalysts exposed to MBM and sewage sludge co-combustion. From [120].

The relative activities of the different catalysts analysed were also plotted against the amount of phosphorus found on the surface of the exposed catalyst (*i.e.* without considering the total amount of P deposited *in* the catalysts) in order to verify any relation between the two variables. However, in the case of P the test was not really successfull as shown in Figure 32: in some cases better correlations were instead found for the alkali and alkaline earth metals. In general, considering that bulk concentrations for K_2O were found in the range 0.2-0.7 wt%, which may be expected to cause significant deactivation, it is really difficult to address the influence of P on the measured deactivation. Moreover, the catalysts were in fact poisoned under the most undefined conditions: both honeycomb and plate type catalysts were exposed to flue gases from either wet bottom or dry ash boilers burning coal mixed to either MBM or sewage sludge. The exposure times were also varying between 2000 and 55000 hours.

From this work, however, it was clear that the P-chemistry could be an issue in the upcoming years since more interest has been focusing on the utilization of P-rich secondary fuels for energy production. Recently another work from Beck *et al.* concerning the behaviour of P in flue gases from coal and MBM and sewage sludge co-combustion and the SCR catalysts has

been published [122]. In this, by analyzing at full-scale both the flue gas and particle composition at both the inlet and outlet of the SCR reactor, an increase of S-content in the particles at the outlet of the reactor was noted. Correspondingly an increase in phosphoric acid concentration at the outlet was also measured. The following reaction occurring on the SCR catalyst was then proposed:

$$Me_3(PO_4)_2(s) + 3\ H_2SO_4(g) \rightarrow 3\ MeSO_4(s) + 2\ H_3PO_4(g) \qquad (27)$$

where a possible influence of P on SO_2 capture due to the SCR catalyst were hypothesized. More research in this field is expected in the future.

5.5.4 Lead, Zinc and Hydrogen Chloride

The poisoning effects of PbO, ZnO and $ZnCl_2$ are reported as the worst poisons for the SCR catalysts used at waste incineration plants [123]. Moreover, the flue gases from these plants can contain significant amount of hydrogen chloride [102].

Elemental analysis of the catalysts employed in the Swedish incinerator located in Sysav after 2000 hours of exposure revealed deposition of Pb and Zn on the catalyst *surface* up to 0.15 and 0.36 wt%.

Khodayari *et al.* [124] studied the effects of lead on the reduction of NO over a commercial vanadia-based catalyst by SCR activity tests and ammonia chemisorption determination. The samples were doped by wet impregnation with different aqueous solutions of $Pb(NO_3)_2$. In order to grant complete decomposition of the nitrate into the oxide, the samples were calcinated at 420℃ for 14 h. At this temperature all lead should exist as PbO. In order to lessen the influence of mass transfer on the reaction rate for the fresh and impregnated catalysts, activity test were performed also over crushed and sieved samples. In the case of monolith samples, low lead loads (comparable with the amount found in the Swedish incinerator plant) caused only small changes in the activity. For higher lead coverages, a more significant drop (*i.e.* $k/k_0 \approx 0.35$ at 400℃ as calculated from the NO conversion data reported and assuming first order reaction in a plug flow) was observed when 1.85 wt% of PbO were deposited in the catalyst. At even higher lead concentrations (*i.e.* 2.31 and 2.88 wt%) no additional decrease in activity was found, indicating a saturation point. As expected, the crushed samples were found to be deactivated more than the monolith: only 10 wt% of the original activity was still present at 400℃ when again 1.85 wt% of PbO was present. The ammonia chemisorption tests reveled that the amount of NH_3 adsorbed and the activity of the catalysts were decreasing in the same way according to the Pb-load. Based on this result, it is possible to conclude that Pb does not *selectively* react with the active sites but does deposit indistinguishly on the surface area, rending the the active sites unaccessible to the gas phase.

Khodayari *et al.* [123] also tested in the laboratory the deactivating effects of $ZnCl_2$. Commercial catalysts were doped by $ZnCl_2$ using a gas phase impregnation technique at 650℃. To avoid oxidation of $ZnCl_2$ to ZnO, the activity measurements were performed at temperature lower than 340℃. At this temperature, the relative activity for the catalyst with the same concentration found in the Swedish incinerator plant was around 10-15%. A minimum in relative activity at the same temperature was then found at a concentration around 1.5 wt%, where the catalyst reached its $ZnCl_2$ saturation point. BET analysis showed a decrease in surface area at increasing Zn load and as in the case of Pb it was concluded that zinc deposited non-selectively over the catalyst surface and not only on the active sites. Increasing the temperature above 340℃ resulted in losing of weight due to evaporation of $ZnCl_2$: after degassing for 16 hours at at 400℃, 50% of the Zn was already removed.

Moradi *et al.* [103] exposed vanadia supported catalysts to submicron aerosols of $ZnCl_2$. The particles were prepared by spraying an aqueous solution of $ZnCl_2$ (25 g/l) and had a mean diameter equal to 0.70 μm. The particle load was around 20 mg/m^3 at room temperature and the total exposure time was 31 hours. SEM pictures and X-ray mapping of Zn of the catalysts exposed at 300℃ showed the formation of a thick layer (*i.e.* 6-8 μm) on the catalysts outer surface and an entire penetration depth around 5 μm. This ability in penetrating the pore structure of the wall was explained considering the fact that at these temperature the $ZnCl_2$ is a melt (melting point 275℃) and can easily move through the porous structure of the catalyst. The activity of the doped catalysts was not found to decrease considerably. However no data about the final Zn concentration were reported.

Regarding the effects of hydrogen chloride, HCl, on the SCR activity, these are different and dependent on the reaction temperature [95]. According to the definition of poison, HCl can be considered as such for vanadia-based catalysts since it can react with the lower vanadium oxides formed by the reduction of V_2O_5 by NH_3. Their interaction with gaseous HCl forms both VCl_4 and VCl_2 which are volatile and can be found in the outlet gas. Thus HCl "removes" the vanadia active sites from the catalyst surface. Moreover, Lisi *et al.* [102] noticed that this effect was more evident at increasing values of vanadia content. They thus concluded that weaker V=O terminals associated with polyvanadate species at higher V content are more attackable by HCl.

6 Conclusions

In the last two decades tremendous work has been carried out in order to find the best solution for NO abatement at stationary combustion processes. Both primary and secondary measures have been developed with

different results. Among these cleaning techniques, the SCR of NO by NH_3 on vanadia-based catalysts is an effective process which has obtained an incredible commercial success, eventhough it presents disadvantages, like the use of an expensive and toxic reagent, and the activity in the SO_2 oxidation.

Thanks to the above mentioned commercial success, a great amount of resourses has been invested in the development of always more performing vanadia-based catalysts, through the understanding of the nature of the active sites, the mechanisms of reaction under different conditions, and the evidences of the deactivation rates experienced at full-scale.

Nowadays, the main challenge for this family of catalysts is their application to fuels different from coal or oil and to non-stationary processes. Power plants firing secondary fuels (*e.g.* biomass, wastes) in addition to the traditional ones, are increasing in number. When applied to these systems, the vanadia-based catalysts quite often present unacceptable deactivation rates. The causes of deactivation are many and not fully understood. Both chemical and physical deactivation can play a role depending on the different compounds introduced by the fuels used in the combustion process. As it results from the deactivation studies carried out, alkali and alkaline earth metals and arsenic are the most dangerous poisons for the vanadia-based catalysts. However, expecially in the case of waste-firing, deactivation by phosphorus and heavy metals has to be carefully taken into consideration. Only by understanding the different deactivation mechanisms, effective measures to slow these down as much as possible could be adopted. Moreover, also the regeneration of the spent catalysts could become a more used practice.

References

[1] H. Bosch and F. Janssen. Catalytic reduction of nitrogen oxides - A review on the fundamentals and technology. *Catalysis Today*, 2(4):369–532, 1988.

[2] V.I. Parvulescu, P. Grange, and B. Delmon. Catalytic removal of no. *Catalysis Today*, 46:233–316, 1998.

[3] R. Delmas, D. Serca, and C. Jambert. Global inventory of NO_x sources. *Nutrient Cycling in Agroecosystems*, 48:51–60, 1997.

[4] J.A. Miller and C.T. Bowman. Mechanism and modeling of nitrogen chemistry in combustion. *Prog. Energy Combust. Sci.*, 15:287–338, 1989.

[5] P. Glarborg, A.D. Jensen, and J.E. Johnsson. Fuel nitrogen conversion in solid fuel fired systems. *Progress in Energy and Combustion Science*, 29:89–113, 2003.

[6] H.N. Soud and K. Fukasawa. Developments in the NO_x abatement and control. IEA Coal Research, London, United Kingdom, 1996.

[7] Coalpower: world coal fired power plants and FGD and NO_x control installations database on cd-rom. IEA Coal Research, London, United Kingdom, 1995.

[8] R. Rodenhausen. Case study: choosing selective catalytic reduction as a preferred technology for the destruction of NO_x. *Environmental Progress*, 18:260–266, 1999.

[9] S. Khan, G. Shroff, J. Tarpara, and R. Srivastava. Scr applications: addressing coal characteristic concerns. EPRI-DOE-EPA, 1997.

[10] P. Forzatti. Present status and perspectives in de-NO_x SCR catalysis. *Applied Catalysis A: General*, 222:221–236, 2001.

[11] M. Kleemann, M. Elsener, M. Koebel, and A. Wokaun. Investigation of the ammonia adsorption on monolithic SCR catalyst by transient response analysis. *Applied Catalysis*, 27:231–242, 2000.

[12] H. Flora, J. Barkley, G. Janik, B. Marker, and Cichanowicz. Status of 1 MW SCR pilot plant tests at Tennessee valley authority and new york state electric & gas. Proceeding of the 1991 joint symposium on stationary combustion NO_x control, March 1991.

[13] J. Ando. Flue gas cleaning technology of the world. Coal Mining Research Institute, 1990.

[14] E. Tronconi. Interaction between chemical kinetics and transport phenomena in monolithic catalysts. *Catalysis Today*, 34:421–427, 1997.

[15] J.W. Beeckman and L.L. Hegedus. Design of monolith catalysts for power plant NO_x emission control. *Ind. Eng. Chem. Res.*, 30:969–978, 1991.

[16] F. Janssen and R. Meijer. Quality control od deNO_x catalysts. Performance testing, surface analysis and characterization of deNO_x catalysts. *Catalysis Today*, 16:157–185, 1993.

[17] G. Busca, G. Ramis, and V. Lorenzelli. FT-IR study of the surface properties of polycrystalline vanadia. *Journal of Molecular Catalysis*, 50:231–240, 1989.

[18] L.J. Alemany, M.A. Banares, M.A. Larrubia, M.C. Jiménez, F. Delgado, and J.M. Blasco. Vanadia-titania systems: morphological and structural properties. *Materials Research Bulletin*, 31(5):513–520, 1996.

[19] G. Ramis, C. Cristiani, A.S. Elmi, P. Villa, and G. Busca. Characterization of the surface properties of polycrystalline WO_3. *Journal of Molecular Catalysis*, 61:319–331, 1990.

[20] L. Lietti. Reactivity of V_2O_5-WO_3/TiO_2 de-NO_x catalysts by transient methods. *Applied Catalysis B: Environmental*, 10:281–297, 1996.

[21] L. Lietti, J.L Alemany, P.Forzatti, G. Busca, G. Ramis, E. Giamello, and F. Bregani. Reactivity of V_2O_5-WO_3/TiO_2 catalysts in the selective catalytic reduction of nitric oxide by ammonia. *Catalysis Today*, 29:143–148, 1996.

[22] L.J. Alemany, L. Lietti, N. Ferlazzo, P. Forzatti, G. Busca, E. Giammello, and F. Bregani. Reactivity and physicochemical characterization of V_2O_5-WO_3/TiO_2 De-NO_x catalysts. *Journal of Catalysis*, 155:117–130, 1995.

[23] L. Casagrande, L. Lietti, I. Nova, P. Forzatti, and A. Baiker. SCR of NO by NH_3 over TiO_2-supported V_2O_5-MoO_3 catalysts: reactivity and redox behavior. *Applied Catalysis B: Environmental*, 22:63–77, 1999.

[24] P. Ciambelli, M.E. Fortuna, D. Sannino, and A. Baldacci. The influence of sulphate on the catalytic properties of V_2O_5-TiO_2 and WO_3-TiO_2 in the reduction of nitric oxide with ammonia. *Catalysis Today*, 29:161–164, 1996.

[25] L. Lietti, J. Svachula, P. Forzatti, G. Busca, G. Ramis, and F. Bregani. Surface and catalytic properties of vanadia-titania and tungsta-titania systems in the selective catalytic reduction of nitrogen oxides. *Catalysis Today*, 17:131–140, 1993.

[26] G. Ramis, G. Busca, and P. Forzatti. Spectroscopic analysis of titania-tungsta-vanadia deNO_xing catalysts. *Applied Catalysis B: Environmental*, 1:L9–L13, 1992.

[27] G. Ramis, G. Busca, C. Cristiani, L. Lietti, P. Forzatti, and F. Bregani. Characterization of tungsta-titania catalysts. *Langmuir*, 8:1744–1749, 1992.

[28] L. Lietti, G. Ramis, F. Berti, G. Toledo, D. Robba, G. Busca, and P. Forzatti. Chemical, structural and mechanistic aspects on NO_x SCR over commercial and model oxide catalysts. *Catalysis Today*, 42:101–116, 1998.

[29] L.J. Alemany, F. Berti, G. Busca, G. Ramis, D. Robba, G.P. Toledo, and M. Trombetta. Characterization and composition of commercial V_2O_5-WO_3-TiO_2 SCR catalysts. *Applied Catalysis B: Environmental*, 10:299–311, 1996.

[30] G. Ramis, G. Busca, V. Lorenzelli, and P. Forzatti. Fourier transform infrared study of the adsorption and coadsorption of nitric oxide, nitrogen dioxide and ammonia on TiO_2 Anatase. *Applied catalysis*, 64:243–257, 1990.

[31] N.-Y. Topsøe. Characterization of the nature of surface sites on vanadia-titania catalysts by FTIR. *Journal of Catalysis*, 128:499–511, 1991.

[32] S.T. Choo, Y.G. Lee, I.-S. Nam, S.-W. Ham, and J.-B. Lee. Characteristic of V_2O_5 supported on sulfated TiO_2 for selective catalytic reduction of NO by NH_3. *Applied Catalysis A: General*, 200:177–188, 2000.

[33] L.J. Alemany, M.A. Ba n ares, E. Pardo, F. Martín-Jimé nez, and J.M. Blasco. Morphological and structural characterization of a titanium dioxide system. *Materials Characterization*, 44:271–275, 2000.

[34] I. Georgiadou, N. Spanos, Ch. Papadopoulou, H. Matralis, Ch. Kordulis, and A. Lycourghiotis. Preparation and characterization of various titanias (anatase) used as supports for vanadia-supported catalysts. *Colloids and Surfaces A: Physicochem. Eng. Aspects*, 98:115–165, 1995.

[35] G.T. Went, L.-J. Leu, and A.T. Bell. Quantitative structural analysis of dispersed vanadia species in TiO_2(Anatase)-supported V_2O_5. *Journal of Catalysis*, 134:479–491, 1992.

[36] G.T. Went, L.-J. Leu, R.R. Rosin, and A.T. Bell. The effects of structure on the catalytic activity and selectivity of V_2O_5/TiO_2 for the reduction of NO by NH_3. *Journal of Catalysis*, 134:492–505, 1992.

[37] G. Madia, M. Elsener, M. Koebel, F. Raimondi, and A. Wokaun. Thermal stability of vanadia-tungsta-titania catalysts in the SCR process. *Applied Catalysis*, 39:181–190, 2002.

[38] N.-Y. Topsøe, H. Topsøe, and J. A Dumesic. Vanadia/Titania catalysts for selective catalytic reduction (SCR) of nitric oxide by ammonia. combined temperature programmed in situ FTIR and on-line mass spectroscopy studies. *Journal of Catalysis*, 151:226–240, 1995.

[39] N.-Y. Topsøe, H. Topsøe, and J. A Dumesic. Vanadia/Titania catalysts for selective catalytic reduction (SCR) of nitric oxide by ammonia. studies od active sites and formulation of catalytic cycle. *Journal of Catalysis*, 151:241–252, 1995.

[40] G. Ramis, G. Busca, F. Bregani, and P. Forzatti. Fourier transform infrared study of the adsorption and coadsorption of nitric oxide, nitrogen dioxide and ammonia on vanadia-titania and mechanism of selective catalytic reduction. *Applied Catalysis*, 64:259–278, 1990.

[41] B.M. Weckhuysen. Chemistry, spectroscopy and the role of supported vanadium oxides in heterogeneous catalysis. *Catalysis Today*, 78:25–46, 2003.

[42] G. Busca, L. Lietti, G. Ramis, and F. Berti. Chemical and mechanistic aspects of the selective catalytic reduction of NO_x by ammonia over oxide catalysts: A review. *Applied Catalysis B: Environmental*, 18:1–36, 1998.

[43] L. Lietti, I. Nova, G. Ramis, L. Dell'Acqua, G. Busca, E. Giamello, P. Forzatti, and F. Bregani. Characterization and reactivity of V_2O_5-MoO_3/TiO_2 de-NO_x SCR catalysts. *Journal of Catalysis*, 187:419–435, 1999.

[44] G. Ramis, L. Yi, and G. Busca. Ammonia activation over catalysts for the selective catalytic reduction of NO_x and selective catalytic oxidation of NH_3. an FT-IR study. *Catalysis Today*, 28:373–380, 1996.

[45] M.A. Larrubia, G. Ramis, and G. Busca. An FT-IR study of the adsorption of urea and ammonia over V_2O_5-MoO_3-TiO_2 SCR catalysts. *Applied Catalysis B: Environmental*, 27:L145–L151, 2000.

[46] M.A. Centeno, I. Carrizosa, and J.A. Odriozola. NO-NH_3 coadsorption on vanadia/titania catalysis: determination of the reduction degree of vanadium. *Applied Catalysis B: Environmental*, 29:307–314, 2001.

[47] S.M. Jung and P. Grange. DRIFTS investigation of V=O behavior and its relations with the reactivity of ammonia oxidation and selective catalytic reduction of NO over V_2O_5 catalyst. *Applied Catalysis B: Environmental*, 36:325–332, 2002.

[48] U.S. Ozkan, Y. Cai, and M.W. Kumthekar. Mechanistic studies on vanadia catalysts for the selective catalytic reduction of nitric oxide using N-15 and O-18 isotopic labeling. Symposium on NO_x reduction 207th National Meeting, American Chemical Society, March 1994.

[49] I. Nova, L. Lietti, E. Tronconi, and P. Forzatti. Dynamics of SCR reaction over TiO_2-supported vanadia-tungsta commercial catalyst. *Catalysis Today*, 60:73–82, 2000.

[50] L. Lietti, I. Nova, S. Camurri, E. Tronconi, and P. Forzatti. Dynamics of the SCR-DeNO_x reaction by transient-response method. *AIChE Journal*, 43(10):2559–2570, October 1997.

[51] L.G. Pinaeva, A.P. Suknev, A.A. Budneva, E.A. Paukshtis, and B.S. Bal'zhinimaev. On the role of oxygen in the reaction of NO reduction by NH_3 over monolayer V_2O_5-TiO_2 catalyst. *Journal of Molecular Catalysis A: Chemical*, 112:115–124, 1996.

[52] N.-Y. Topsøe, M. Anstrom, and J.A. Dumesic. Raman, FTIR and theoretical evidence for dynamic structural rearrangements of vanadia/titania DeNOx catalysts. *Catalysis Letters*, 76:11–20, 2001.

[53] M. Anstrom, J.A. Dumesic, and N.-Y. Topsøe. Theoretical insight into the nature of ammonia adsorption on vanadia-based catalyst for SCR reaction. *Catalysis Letters*, 78:281–289, 2002.

[54] M. Anstrom, N.-Y. Topsøe, and J.A. Dumesic. Density functional theory studies of mechanistic aspects of the SCR reaction on vanadium oxide catalysts. *Journal of Catalysis*, 213:115–125, 2003.

[55] T. Homann, T. Bredow, and K. Jug. Adsorption of small molecules on the anatase(1 0 0) surface. *Surface Science*, 555:135–144, 2004.

[56] K. Jug, T. Homann, and T. Bredow. Reaction mechanism of the selective catalytic reduction of NO with NH_3 and O_2 to N_2 and H_2O. *J. Phys. Chem.*, 108:2966–2971, 2004.

[57] T. Bredow, T. Homann, and K. Jug. Adsorption of NO, NH_3 and H_2O on V_2O_5/TiO_2 catalysts. *Res. Chem. Intermed.*, 30:65–73, 2004.

[58] A. Miyamoto, M. Inomata, A. Hattori, T. Ui, and Y. Murakami. A molecular orbital investigation of the mechanism of the NO- NH_3 reaction on vandium oxide catalyst. *Journal of Molecular Catalysis*, 16(3):315–333, 1982.

[59] M. Takagi, T. Kawai, M. Soma, T. Onishi, and K. Tamaru. The mechanism of the reaction between NO_x and NH_3 on V_2O_5 in the presence of oxygen. *Journal of Catalysis*, 50(3):441–446, 1977.

[60] M. Calatayud, B. Mguig, and C. Minot. Modeling catalytic reduction of NO by ammonia over V_2O_5. *Surface science reports*, 55:169–236, 2004.

[61] M. Gasior, J. Haber, T. Machej, and T. Czeppe. Mechanism of the reaction NO + NH_3 on V_2O_5 catalysts. *Journal of Molecular Catalysis*, 43(3):359–369, 1988.

[62] C.U.I. Odenbrand, S.T. Lundin, and L.A.H. Andersson. Catalytic reduction on nitrogen oxides 1. The reduction of NO. *Applied Catalysis*, 18(2):335–352, 1985.

[63] J.A. Dumesic, N.-Y Topsøe, T. Slabiak, P. Morsing, B.S. Clausen, E. Tornqvist, and H. Topsøe. Proc. of 10th International Congress on Catalysis, Budapest, 1993.

[64] J. Marangozis. Comparison and analysis of intrinsic kinetics and effectiveness factors for the catalytic reduction of NO with ammonia in the presence of oxygen. *Ind. Eng. Chem. Res.*, 31:987–994, 1992.

[65] A.M. Efstathiou and K. Fliatoura. Selective catalytic reduction of nitric oxide with ammonia over V_2O_5/TiO_2 catalyst: A steady-state and transient kinetic study. *Applied Catalysis B: Environmental*, 6:35–59, 1995.

[66] M. Koebel and M. Elsener. Selective catalytic reduction of NO over commercial deNO_x-catalysts: experimental determination of kinetic and thermodynamic parameters. *Chemical Engineering Science*, 53(4):657–669, 1998.

[67] L.J. Pinoy and L.H. Hosten. Experimental and kinetic modelling study of DeNOx on an industrial V_2O_5-WO_3/TiO_2 catalyst. *Catalysis Today*, 17:151–158, 1993.

[68] V. Tufano and M. Turco. Kinetic modelling of nitric oxide reduction over a high-surface area V_2O_5-TiO_2 catalyst. *Applied Catalysis B: Environmental*, 2:9–26, 1993.

[69] C.U.I. Odenbrand, A. Bahamonde, P. Avila, and J. Blanco. Kinetic study of the selective reduction of nitric oxide over vanadia-tungsta-titania/sepiolite catalyst. *Applied Catalysis B: Environmental*, 5:117–131, 1994.

[70] R. Willi, B. Roduit, R.A. Koeppel, A. Woakun, and A. Baiker. Selective reduction of NO by NH_3 over vanadia-based commercial catalyst: parametric sensivity and kinetic modelling. *Chemical engineering science*, 51(11):2897–2902, 1996.

[71] J.A. Dumesic, N.-Y. Topsøe, H. Topsøe, Y. Chen, and T. Slabiak. Kinetics of selective catalytic reduction of nitric oxide by ammonia over vanadia/titania. *Journal of Catalysis*, 163:409–417, 1996.

[72] B. Roduit, A. Wokaun, and A. Baiker. Global kinetic modeling of reactions occurring during selective catalytic reduction of NO by NH_3 over vanadia/titania-based catalysts. *Ind. Eng. Chem. Res.*, 37:4577–4590, 1998.

[73] H. Kamata, Takahashi K., and C.U. Odenbrand. Kinetics of the selective reduction of NO with NH_3 over a $V_2O_5(WO_3)/TiO_2$ commercial SCR catalyst. *Journal of Catalysis*, 185:106–113, 1999.

[74] J. Svachula, N. Ferlazzo, P. Forzatti, E. Tronconi, and F. Bregani. Selective reduction of NO_x by NH_3 over honeycomb deNOxing catalysts. *Ind. Eng. Chem. Res.*, 32:1053–1060, 1993.

[75] I. Nova, L. Lietti, E. Tronconi, and P. Forzatti. Transient response method applied to the kinetic analysis of the DeNO$_x$-SCR reaction. *Chemical Engineering Science*, 56:1229–1237, 2001.

[76] L. Lietti, I. Nova, E. Tronconi, and P. Forzatti. Transient kinetic study of the SCR-DeNO$_x$ reaction. *Catalysis Today*, 45:85–92, 1998.

[77] J. Brück and H.-G. Lintz. Combined kinetic and potentiometric measurements of the reduction of nitrogen monoxide on vanadia titania catalysts. *Chemical Engineering and Processing*, 38:571–577, 1999.

[78] M.D. Amiridis, I.E. Wachs, G. Deo, J.-M. Jehng, and D.S. Kim. Reactivity of V_2O_5 catalysts for the selective catalytic reduction of NO by NH_3: influence of vanadia loading, H_2O, and SO_2. *Journal of Catalysis*, 161:247–253, 1996.

[79] N.-Y. Topsøe. Influence of water on the reactivity of vanadia/titania for catalytic reduction of no$_x$. *Journal of Catalysis*, 134:742–746, 1992.

[80] M.A. Buzanowski and R.T. Yang. Simple design of monolith reactor for selective catalytic reduction of NO for power plant emission control. *Ind. Eng. Chem. Res.*, 29:2074–2078, 1990.

[81] E. Tronconi and P. Forzatti. Adequacy of lumped parameter models for SCR reactors with monolith structure. *AIChE Journal*, 38:201–210, 1992.

[82] E. Tronconi, P. Forzatti, J.P. Gomez Martin, and S. Malloggi. Selective catalytic removal of NO_x: a mathematical model for design of catalyst and reactor. *Chemical Engineering Science*, 47:2401–2406, 1992.

[83] A. Santos, A. Bahamonde, M. Schmid, P. Avila, and F. Garcia-Ochoa. Mass transfer influences on the design of selective catalytic reduction (SCR) monolithic reactors. *Chemical Engineering and Processing*, 37:117–124, 1998.

[84] A. Beretta, C. Orsenigo, N. Ferlazzo, E. Tronconi, and P. Forzatti. Analysis of the performance of plate-type monolithic catalysts for selective catalytic reduction deNO$_x$ applications. *Ind. Eng. Chem. Res.*, 37:2623–2633, 1998.

[85] E. Tronconi and A. Beretta. The role of inter- and intra-phase mass transfer in the SCR-DeNO$_x$ reaction over catalysts of different shapes. *Catalysis Today*, 52:249–258, 1999.

[86] S.T. Kolaczkovski. Measurement of effective diffusivity in catalyst-coated monoliths. *Catalysis Today*, 83:85–95, 2003.

[87] J.W. Beekman. Measurement of the effective diffusion coefficient of nitrogen monoxide through porous monolith-type ceramic catalysts. *Ind. Eng. Chem. Res.*, 30:428–430, 1991.

[88] N. Wakao and J.M. Smith. Diffusion in catalyst pellets, 1962.

[89] B. Roduit, A. Baiker, F.Bettoni, J. Baldyga, and A. Wokaun. 3D modeling of SCR of NO_x by NH_3 on vanadia honeycomb catalysts. *AIChE Journal*, 44:2731, 1998.

[90] C.H. Bartholomew. Mechanisms of catalyst deactivation. *Applied Catalysis A: General*, 212:17–60, 2001.

[91] P. Forzatti and L. Lietti. Catalyst deactivation. *Catalysis Today*, 52:165–181, 1999.

[92] A.K. Neyestanaki, F. Klingstedt, T. Salmi, and D.Y. Murzin. Deactivation of post-combustion catalysts, a review. *Fuel*, 83:395–408, 2004.

[93] E. Kurkela. Formation and removal of biomass-derived contaminants in fluidized-bed gasification processes. *VTT Publications*, 287:47, 1996.

[94] I. Nova, L. dall'Acqua, L. Lietti, E. Giamello, and P. Forzatti. Study of thermal deactivation of a de-NO_x commercial catalyst. *Applied Catalysis B: Environmental*, 35:31–42, 2001.

[95] J.P. Chen, M.A. Buzanowski, and R.T. Yang. Deactivation of the vanadia catalyst in the selective catalytic reduction process. *J. Air Waste Manage. Assoc.*, 40:1403–1409, 1990.

[96] J.P. Chen and R.T. Yang. Mechanism of poisoning of the V_2O_5/TiO_2 catalyst for the reduction of NO by NH_3. *Journal of Catalysis*, 125:411–420, 1990.

[97] J. Blanco, P. Avila, C. Bahamonde, J.A. Odrizola, J.F. Garcia de la Banda, and H. Heinemann. Influence of phosphorus in vanadium-containing catalyasts for NO_x removal. *Applied Catalysis*, 55:151–164, 1989.

[98] S. Pritchard, S. DiFrancesco, S. Kaneko, N. Kobayashi, K. Suyama, and K. Iida. Optimizing SCR catalyst design and performance for coal-fired boilers. Presented at EPA/EPRI 1995 joint symposium stationary combustion NO_x control, May 16-19 1995.

[99] L. Lietti, P. Forzatti, G. Ramis, G. Busca, and F. Bregani. Potassium doping of vanadia/titania de-NO_xing catalysts: Surface characterization and reactivity study. *Applied Catalysis B: Environmental*, 3:13–35, 1993.

[100] Y. Zheng, A.D. Jensen, and J.E. Johnsson. Laboratory investigation of selective catalytic reduction catalysts: deactivation of potassium compounds and catalyst regeneration. *Ind. Eng. Chem. Res.*, 43:941–947, 2004.

[101] H. Kamata, K. Takahashi, and C.U.I. Odenbrand. The role of K_2O in the selective reduction of NO with NH_3 over $V_2O_5(WO_3)/TiO_2$ commercial selective catalytic reduction catalyst. *Journal of Molecular Catalysis A: Chemical*, 139:189–198, 1999.

[102] L. Lisi, G. Lasorella, S. Malloggi, and G. Russo. Single and combined deactivating effect of alkali metals and HCl on commercial SCR catalysts. *Applied Catalysis B: Environmental*, 50:251–258, 2004.

[103] F. Moradi, J. Brandin, M. Sohrabi, M. Faghihi, and M. Sanati. Deactivation of oxidation and SCR catalysts used in flue gas cleaning by exposure to aerosols of high- and low melting point salts, potassium salts and zinc chloride. *Applied Catalysis B: Environmental*, 46:65–76, 2003.

[104] R. Khodayari and C.U.I. Odenbrand. Deactivation and regeneration of SCR catalysts used in bio fuel plants. Proceedings of the 5^th European Conference on Industrial Furnace and Boilers, volume II, April 2001.

[105] Y. Zheng, A.D. Jensen, and J.E. Johnsson. Deactivation of V_2O_5-WO_3-TiO_2 SCR catalyst at a biomass-fired combined heat and power plant. *Applied Catalysis B: Environmental*, 60:261–272, 2005.

[106] L.L. Baxter, T.R. Miles, T.R. Miles Jr., B.M. Jenkins, T. Milne, D. Dayton, R.W. Bryers, and L.L. Oden. The behavior of inorganic material in biomass-fired power boilers: field and laboratory experiences. *Fuel Processing Technology*, 54:4778, 1998.

[107] K. Wieck-Hansen, P. Overgaard, and O.H. Larsen. Cofiring coal and straw in a 150 MW_e power boiler experiences. *Biomass and Bioenergy*, 19:395–409, 2000.

[108] K.A. Christensen and H. Livbjerg. A field study of submicron particles from the combustion of straw. *Aerosol Science and Technology*, 25:185–199, 1996.

[109] K.A. Christensen, M. Stenholm, and H. Livbjerg. The formation of submicron aerosol particles, HCl and SO_2 in straw-fired boilers. *Aerosol Science and Technology*, 29:421–444, 1998.

[110] R. Khodayari and C.U.I. Odenbrand. Regeneration of commercial TiO_2-V_2O_5-WO_3 SCR catalysts used in bio fuel plants. *Applied Catalysis B: Environmental*, 30:87–99, 2001.

[111] R. Khodayari and C.U.I. Odenbrand. Regeneration of commercial SCR catalysts by washing and sulphation: effect of sulphate groups on the activity. *Applied Catalysis B: Environmental*, 33:277–291, 2001.

[112] J.E. Staudt, T. Engelmeyer, W.H. Weston, and R. Sigling. The impact of arsenic on coal fired power plants equipped with SCR. Presented at ICAT Forum 2002, Houston, February 12-13 2002.

[113] K. Rigby, R. Johnson, R. Neufert, G-Pajonk, E. Hums, A. Klatt, and R. Sigling. SCR catalyst design issues and operating experience: coals with high arsenic concentrations and coals from Powder River Basin. Proceedings of 2000 international joint power generation conference, Miami Beach, Florida, July 23-26 2000.

[114] M. Ichiki. Poisoning kinetics by arsenic on the $DeNO_x$ catalysts. Proceedings of the international conference on power engineering, Kobe, Japan, November 9-13 2003.

[115] F.C. Lange, H. Schmelz, and H. Knózinger. Infrared-spectroscopic investigations of selective catalytic reduction catalysts poisoned with arsenic oxide. *Applied Catalysis B: Environmental*, 8:245–265, 1996.

[116] E. Hums. Effects of As_2O_3 on the phase composition of V_2O_5-MoO_3-TiO_2 (anatase) $DeNO_x$ catalysts. *Ind. Eng. Chem. Res.*, 30:1814–1818, 1991.

[117] E. Hums. Mechanistic effects of arsenic oxide on the catalytic components $DeNO_x$ catalysts. *Ind. Eng. Chem. Res.*, 31:1030–1035, 1992.

[118] E. Hums. Deactivation behavior of SCR $DeNO_x$ catalysts - basis for the development of a new generation of catalysts. Symposium on NO_x Reduction, 207th National Meeting, American Chemical Society, San Diego, CA, March 13-18 1994.

[119] E. Hums. Understanding of deactivation behavior of $DeNO_x$ catalysts: a key to advanced catalyst applications. *Kinetics and Catalysis*, 39:603–606, 1998.

[120] J. Beck, J. Brandenstein, S. Unterberger, and K.R.G. Hein. Effects of sludge and meat and bone meal co-combustion on SCR catalysts. *Applied Catalysis B: Environmental*, 49:15–25, 2004.

[121] H. Kamata, K. Takahashi, and C.U.I. Odenbrand. Surface acid property and its relation to scr activity of phosphorus added to commercial $V_2O_5(WO_3)/TiO_2$ catalyst. *Catalysis Letters*, 53:65–71, 1998.

[122] J. Beck, R. Muller, J. Brandenstein, B. Matschenko, J. Matschke, S. Unterberger, and K.R.G. Hein. The behaviour of phosphorus in flue gases from coal and secondary fuel co-combustion. *Fuel*, 84:1911–1919, 2005.

[123] R. Khodayari. Selective catalytic reduction of NO_x: Deactivation and regeneration studies and kinetic modelling of deactivation. Doctoral Thesis, Department of Chemical Engineering II, Lund University, Institute of Technology, April 2001.

[124] R. Khodayari and C.U.I. Odenbrand. Deactivating effects of lead on the selective catalytic reduction of nitric oxide with ammonia over a $V_2O_5/WO_3/TiO_2$ catalyst for waste incineration applications. *Ind. End. Chem. Res.*, 37:1196–1202, 1998.

Appendix B

Paper I

Available online at www.sciencedirect.com
ScienceDirect
Applied Catalysis B: Environmental 83 (2008) 110–122
APPLIED CATALYSIS B: ENVIRONMENTAL
www.elsevier.com/locate/apcatb

Deactivation of vanadia-based commercial SCR catalysts by polyphosphoric acids

Francesco Castellino [a], Søren Birk Rasmussen [b,1], Anker Degn Jensen [a,*], Jan Erik Johnsson [a], Rasmus Fehrmann [b]

[a] *Department of Chemical Engineering, Technical University of Denmark, Building 229, DK-2800 Kgs. Lyngby, Denmark*
[b] *Chemistry Department, Technical University of Denmark, Building 207, DK-2800 Kgs. Lyngby, Denmark*

Received 7 January 2008; received in revised form 8 February 2008; accepted 13 February 2008

Abstract

Commercial vanadia-based SCR monoliths have been exposed to flue gases in a pilot-scale setup into which phosphoric acid has been added and the deactivation has been followed during the exposure time. Separate measurements by SMPS showed that the phosphoric acid formed polyphosphoric acid aerosols, which were characterized by particle number concentrations in the order of 1×10^{14} #/m^3 at 350 °C and diameters <0.1 μm. Three full-length monoliths have been exposed to flue gases doped with 10, 100 and 1000 ppmv H_3PO_4 for 819, 38 and 24 h, respectively. At the end of the exposure the relative activities were equal to 65, 42 and 0%, respectively. After exposure, samples of the spent monoliths have been characterized by ICP-OES, Hg-porosimetry, SEM–EDX and in situ EPR. The results showed that the polyphosphoric acids chemically deactivate the vanadia-based catalysts by decreasing the redox properties of the catalyst surface and by titrating the number of V(V) active species. When plate-shaped commercial catalysts have been wet impregnated with different aqueous solutions of H_3PO_4 obtaining *P/V* ratios in the range 1.5–5, the relative activity for the doped catalysts in the whole *P/V* range was 0.85–0.90 at 350 °C. These results show that the presence of phosphor compounds in the flue gas may be much more harmful than indicated by simple wet chemical impregnation by phosphoric acid. The reason has been found in the nature of the polyphosphoric acid aerosol formed in the combustion process, which cannot be reproduced by the wet impregnation process.

Keywords: SCR catalyst deactivation; Polyphosphoric acid; Vanadia; EPR; SMPS

1. Introduction

Biomass and waste (co)-firing with fossil fuels and NO_x reduction by selective catalytic reduction (SCR) are two practices of increasing application at stationary power stations, which, however, present some economical and technical challenges. Firing of secondary fuels such as biomass, meat and bone meal (MBM), sewage sludge and urban wastes is seen as a way to recover energy while decreasing the net CO_2 emissions. In countries like Denmark and Sweden this practice is forced by local regulations. NO_x emissions are also strictly limited by national regulations, rendering the utilization of secondary measures like the SCR process necessary.

In the SCR process ammonia is injected into the flue gas and the gas is passed over a catalyst at 300–400 °C [1]. Here the undesired NO_x is reduced to molecular nitrogen according to the following global reactions:

$$4NH_3 + 4NO + O_2 \rightarrow 4N_2 + 6H_2O \quad (1.1)$$

$$2NO_2 + 4NH_3 + O_2 \rightarrow 3N_2 + 6H_2O \quad (1.2)$$

Since NO accounts for roughly 95% of the total NO_x fraction at typical SCR conditions, reaction (1.1) can be considered the dominant SCR reaction.

Commercial catalysts are mainly constituted by vanadium oxide (V_2O_5) supported on a titania (TiO_2) carrier. The total load of V_2O_5 is around 1–5 wt.% depending on the specific application. WO_3 and MoO_3 are also added to the final composition improving both chemical and physical properties

* Corresponding author. Tel.: +45 45 25 28 41; fax: +45 45 88 22 58.
E-mail address: aj@kt.dtu.dk (A.D. Jensen).
[1] Present address: Instituto de Catálisis y Petroleoquímica, CSIC, c/Marie Curíe 2, Cantoblanco 28049 Madrid, Spain.

0926-3373/$ – see front matter © 2008 Elsevier B.V. All rights reserved.
doi:10.1016/j.apcatb.2008.02.008

of the catalyst. The catalysts are normally shaped into channels with hydraulic diameters up to 9 mm depending on the fly ash load. A widely accepted mechanism of reaction for these catalysts at typical industrial operating conditions was proposed by Topsøe et al. [2,3]. This involves adsorption of NH_3 on Brønsted acid sites, activation of adsorbed ammonia by V=O species and subsequently reaction with gaseous or weakly adsorbed NO.

The SCR technology was first developed and optimized for fossil fuels applications: in the case of pure coal combustion, a catalyst at high dust position has an expected lifetime of up to 5 years. However, when applied at biomass or waste firing the SCR catalysts are reported to experience much faster rates of deactivation [4,5].

Deactivation of SCR catalyst can be due to poisoning, fouling, surface masking, and sintering according to the particular application. Phosphorus is known as a poison for the vanadia-based catalysts. Its poisoning strength was tested in the laboratory both using model V_2O_5–TiO_2 and commercial vanadia-based catalysts [6,7]. Generally authors report that poisoning by P is moderate. At 300 °C, a model 5% V_2O_5–TiO_2 catalyst wet impregnated with aqueous solution of H_3PO_4 lost about 30% of activity when $P/V = 1$ [6]. Moreover, Kamata et al. [7] found that P is able to some extent to form Brønsted acid sites, which are still able to adsorb ammonia, and could then actively participate in the SCR reaction. Blanco et al. [8] pointed out the negative influence of P on the surface area of vanadia-based honeycomb catalysts extruded with phosphoric acid. However, catalysts extruded with H_3PO_4 and having up to 12.3 wt.% P showed almost the same activity as a P-free catalyst. Beck et al. [9] analyzed SCR catalysts exposed at full-scale plants to flue gases from co-combustion of P-rich fuels (i.e. MBM, sewage sludge) and coal. The catalysts had up to 4.9 wt.% P_2O_5 on the external surface and both a decreased surface area and total pore volume. The authors regarded P as one of the main components responsible for the deactivation of the catalysts and hypothesized the following mechanisms of deactivation by P: (i) poisoning by gaseous P_2O_5 and/or H_3PO_4; (ii) pore condensation by polyphosphoric acids; (iii) deposition of alkali phosphates glasses. However, the catalysts were exposed to ill defined conditions and in the presence of other known poisons (e.g. K). Hence it was not possible to clearly point out the main mechanism of deactivation by P and its importance in the simultaneous presence of other deactivating species.

At the time of the writing, the addition of phosphorus compounds to biomass combustion processes is under investigation by Danish power companies [10,11]. It is suggested that this could be an effective measure to reduce the deposition of fly ash on the superheater surfaces, increasing the efficiency of biomass firing. In fact, during biomass combustion the fly ash is rich in K (mainly KCl and K_2SO_4) and has low melting points that make it particularly sticky at the temperatures of the superheater section. Addition of P and Ca has been found to form ashes in the P–K–Ca system with higher melting points and consequently lower tendency to deposit on the superheater exchangers. However, in this case the flue gas could experience an important increase in total P-concentration [12]. Therefore all the potential drawbacks of this addition process have to be carefully examined at both lab- and pilot-scale, prior to any full-scale applications in the presence of an SCR reactor.

The main objective of this work was to investigate the deactivating effect of P under well defined and realistic operating conditions, thus helping the Danish power companies in foreseeing the potential effects of the P addition process on the SCR catalysts. Full-length commercial SCR monoliths have been exposed for more than 800 h to a flue gas doped with different water solutions of *ortho*-phosphoric acid in a pilot-scale SCR setup. The activity of the monoliths has been periodically tested during exposure and the deactivation mechanisms by P have been pointed out.

2. Experimental

In order to verify the condensation of *ortho*-phosphoric acid and have an online measurement of the activity of a SCR catalyst, a water solution of H_3PO_4 has been injected in a hot flue gas from a natural gas burner. The resulting mixture was then passed over a commercial SCR monolith, and the activity was periodically measured.

2.1. Catalysts

Commercial corrugated-type monoliths and plates obtained from Haldor Topsøe A/S were used in this study. The catalysts were based on V_2O_5 (up to 5 wt.%) and tungsten oxide (WO_3, up to 9 wt.%) dispersed on a fiber reinforced TiO_2 carrier. The monoliths had a size of 75 mm × 75 mm × 500 mm. The hydraulic diameter of the channels was 6.44 mm and the wall thickness of about 1.0 mm. Pieces of both the fresh and spent monoliths have been cut from both the inlet and the outlet in order to study their local properties under well defined reacting conditions in a laboratory fixed bed reactor. In order to run activity tests on powdered samples, they have been gently crushed in a mortar and the particle fraction in the range 105–125 μm has been collected by sieving. Plate-shaped catalysts were doped with H_3PO_4 at three different levels by a wet impregnation method at room temperature under a vacuum of 0.8 bar absolute pressure to allow the solution to evenly penetrate into the catalyst pores. The catalyst plates had a dimension of 1 mm × 50 mm × 150 mm. They were dried at 120 °C for 1 h and then calcined at 400 °C for 4 h under a stream of 1 L/min of N_2. The different P/V ratios obtained were measured by inductively coupled plasma optical emission spectroscopy (ICP-OES) and were equal to 1.8, 2.9 and 4.7.

2.2. SCR pilot plant

A schematic of the SCR pilot plant is shown in Fig. 1. The setup runs slightly below atmospheric pressure (5–8 mbar) for safety reasons. Natural gas is burned in the presence of excess air. The flue gas exiting the burner at 950–1000 °C is then led to a high temperature pipe, where the phosphoric acid solution is

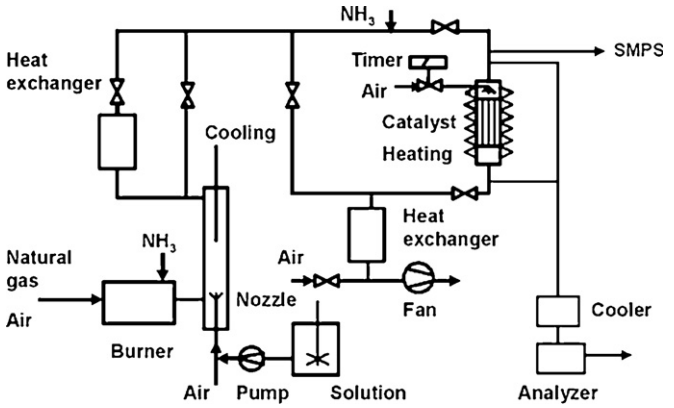

Fig. 1. Schematic drawing of the pilot-scale setup for catalyst monolith deactivation test.

injected. This is done by pumping the desired solution through a water-cooled lance inserted in the high temperature pipe having a two-fluid nozzle at the outlet. Here the water solution meets a flow of compressed air (also added through the lance) and is thus sprayed into the flue gas.

The temperature of the flue gas at the inlet of the SCR reactor can be controlled by adjusting the flow passing through a heat exchanger. For minor adjustments, or simply to avoid that a fraction of the flue gas experiences too low temperature affecting particle condensation rates, the temperature can be controlled by simply adjusting the position of bayonet heat exchanger inserted on the other side of the high temperature pipe. The gas flow is measured by a pitot tube situated at the inlet of the SCR reactor. A throttle valve is used to bypass part of the flue gas and get the desired flow through the reactor.

Ammonia is added into the burner in order to obtain a NO concentration of ~500 ppmv at the SCR reactor inlet. If NH_3 was not added, only 80 ppmv of NO would have been present.

The reactor is a squared duct where the catalyst element is vertically supported. In order to have a constant temperature along the whole element, two electric heating wires with temperature control are installed around the reactor. In this way the temperature difference between the inlet and the outlet of the reactor was always kept less than 3 °C.

Plate-shaped catalysts have been exposed to the P-rich flue gases by placing them in the pipe downstream the SCR reactor using a squared-plate-holder designed for this purpose.

2.3. H_3PO_4 addition

The addition of H_3PO_4 to the flue gas was performed by spraying different acid water solutions through a nozzle as described above. The solutions were prepared by diluting 85% H_3PO_4 (Fluka Inc.) with distilled water. Three catalyst elements have been exposed to 10, 100 and 1000 ppmv H_3PO_4. In this work they will be identified by the labels "P10", "P100" and "P1000", respectively. The letters "T" and "B" added at the end of the labels will indicate a sample cut respectively from the top (first 5 cm) or the bottom (last 5 cm) of element. In all tests, the solution feed was fixed at 1.25 L/h and the acid concentrations were 0.018, 0.18 and 1.8 mol/L, respectively. During the 100 ppmv test, five catalyst plates were also exposed. They will be referred as P100plate in this work.

2.4. Activity measurements

The rate of SCR reaction at typical industrial reacting conditions has been assumed to follow an Eley-Rideal mechanism of reaction with NH_3 adsorbed on the catalyst surface and NO reacting from the gas-phase. The following expression for the rate of reaction, r_{NO}, can then be derived:

$$-r_{NO}\left(\frac{\text{mol}}{\text{m}^3\text{s}}\right) = kc_{NO}\frac{K_{NH_3}c_{NH_3}}{1+K_{NH_3}c_{NH_3}} \tag{1.3}$$

where k (1/s) is the rate constant, c_{NO} and c_{NH_3} (mol/m^3) are the concentrations of NO and NH_3, respectively, and K_{NH_3} (m^3/mol) is the adsorption constant for NH_3 on the catalyst surface. The fraction term on the right-hand side of Eq. (1.4) is the NH_3 coverage of the catalytic surface, θ_{NH_3}.

At the pilot plant, the activities of the catalysts were measured at 350 °C in the presence of about 500 ppmv NO, 600 ppmv NH_3, 10 vol.% O_2, 6 vol.%. CO_2, and about 10 vol.% H_2O. During activity measurements (where not stated differently) the flow through the SCR reactor was normally kept at 40 Nm^3/h. At this flow the gas velocity in the channel was about 6.5 m/s at 350 °C, thus similar to the velocities used at full-scale applications, and up to 50% external mass transfer limitations have been estimated.

Since ammonia in our measurements is added in excess with respect to NO (i.e. $NH_3/NO \approx 1.2$), the NH_3 coverage, θ_{NH_3}, can be assumed equal to one and the reaction rate can be regarded as pseudo-first order with respect to NO and zero order with respect to NH_3. Therefore, directly from the fractional NO conversion, X, it is possible to calculate an observed catalyst activity constant, k', that includes both the influence of external and internal mass transfer:

$$k'\left(\frac{\text{mL}}{\text{g s}}\right) = -\frac{F_{gas}}{m_{cat}}\ln(1-X) \tag{1.4}$$

where F_{gas} is the gas flow rate (mL/s), m_{cat} is the weight of catalyst (g). The degree of deactivation can be then calculated as the ratio k/k_0 between the activity constant of the catalyst during exposure, k, and the one measured for the fresh element, k_0, right before starting the poison addition.

In the laboratory, powderized samples have been tested for activity in a packed bed quartz micro-reactor with a diameter equal to 10 mm. Around 0.07 g of powder has been used during activity measurement with a total flow equal to 2.8 NL/min constituted by 500 ppmv NO, 600 ppmv NH_3, 5% O_2 and 1.4% H_2O in N_2. Activity measurements have been performed in the temperature range 250–400 °C. The catalyst activity has been calculated according to Eq. (1.5) and the deactivation as the ratio between the activity constant of the spent catalyst and the one measured for the fresh one. At 350 °C, the observed activity constant for the fresh catalyst was found only 10% less than the one calculated in the total absence of mass transfer limitations. The latter value was calculated by extrapolating at higher

temperatures the Arrhenius fitting obtained in the range 250–330 °C. No NH_3 oxidation has been measured up to 350 °C during an empty reactor test. In the case of the plates, the activity tests were carried out in another quartz reactor with a diameter equal to 18 mm. The plates were cut into 15 mm × 15 mm bits. Only one bit, corresponding to around 0.17 g of catalyst, was used for each measurement. This was placed in the center of the reactor and supported by small glass indentations especially designed for the purpose. The total flow and gas composition used during the activity measurements on plates were the same as the ones used for the powders. In previous tests carried out at different flows, it has been shown that when 2.8 NL/min were used, the rate of reaction could be assumed not limited by external mass transfer limitations up to 350 °C.

During all activity measurements, the NO concentration in the dry mixture was measured by conventional UV analyzers (Rosemount NGA 2000).

2.5. Ammonia chemisorption

NH_3 chemisorption is the first step of the reaction mechanism [2,3]. Therefore, NH_3 chemisorption studies have been made to investigate the mechanism of deactivation due to polyphosphoric acid deposition. The tests were carried out in our laboratories using the fixed bed quartz reactor and the catalyst plates. The complete SCR gas mixture described in the previous section was prepared. All the mixture components but NO were then let into the reactor and passed over the catalyst for 30 min. During this time, the catalyst surface got saturated with NH_3. After this saturation period, the NH_3 addition was shut off and the NO flow was added to the rest of the mixture. Reaction between NO and the previously chemisorbed NH_3 then took place and the amount of NH_3 on the catalyst was calculated from the amount of NO reduced.

2.6. Aerosol measurements

To get a better understanding of polyphosphoric acids formation, aerosols measurements have been carried out at the SCR pilot plant. The particle concentration and size distribution were measured by a Scanning Mobility Particle Sizer (SMPS, TSI Inc.), which included an Electrostatic Classifier (Model 3080) and a Condensation Particle Counter (Model 3775). Particle sampling was carried out at the inlet of the SCR reactor by an ejector sampler running with dry, particle-free air. In this system the particle-containing flue gas was at the same time cooled and diluted. In this way: (i) water condensation was prevented by keeping the sample well above the water dew point; (ii) the rate of coagulation in the sample line was effectively decreased by several orders of magnitude; (iii) overloading of both the impactor and the SMPS was prevented. The dilution ratio, needed to know the real particle concentration in the flue gas, was obtained by measuring the CO_2 concentration both in the flue gas and in the diluted sample. The aerosol measurements were carried out during addition of H_3PO_4 in the range 10–400 ppmv.

2.7. Catalyst characterization

Small pieces of catalyst were cut from the ends of both fresh and exposed monoliths and characterized with respect to bulk chemical composition, mercury porosimetry and physical appearance by a scanning electron microscope (SEM).

The chemical composition was obtained by ICP-OES at the laboratory of DONG Energy A/S and Haldor Topsøe A/S. Prior to the measurements, the samples were cut to 1.5 cm × 1.7 cm and dried at 105 °C for 2 h before analysis.

The total pore volume and the pore size distribution of the different catalyst sample were made by mercury intrusion in a Micromeritics Autopore II 9220 porosimeter. SEM–EDX analysis was performed at the Teknologisk Institut using a Zeiss Ultra55 and an Oxford ISIS with a Pentafet X-ray detector.

2.8. In situ EPR spectroscopy

Samples (∼0.030 g) of both the fresh and the exposed monoliths at the pilot plant (P10 and P100) were placed into a micro-reactor cell specially designed for high temperature EPR measurements using a Bruker ER 4114 HT cavity [13,14]. The spectra were recorded in situ at 350 °C in a flow of around 100 mL/min simulated flue gas. After thermal equilibration, the catalysts were first exposed to a reactant gas composition consisting of 1000 ppmv NO, 3.5% O_2, 3% H_2O in N_2. After acquisition of a spectrum at stationary conditions, 1000 ppmv NH_3 was added to the gas mixture. Again after acquisition at stationary conditions, NO was omitted from the reactant gas and the final spectrum was recorded. Spectra were recorded with 1024 points from 2500 to 4500 G, using a time constant of 82 ms and a total sweep time of 84 s. The resonance frequencies were around 9.534 GHz. Modulation frequency and amplitude were 100 kHz and 8.12 G, respectively.

3. Results

3.1. Aerosol measurements at the pilot-scale setup

Table 1 summarizes the main results of the SMPS measurements carried out. In Fig. 2 the particle size distribution (PSD) for the tests with 10, 50, 100 and 400 ppmv of H_3PO_4 are shown. In all the measurements the PSD consisted of only one clear peak. The mean particle size, which was calculated from the total number concentration, was found to vary in the range 25–70 nm and was increasing with the acid concentration in the flue gas. The order of magnitude of the total particle number concentration was equal to 1×10^{14} particles/m^3. A blank measurement where only distilled water was sprayed into the setup has also been performed. The results of this measurement showed the presence of particles with a mean diameter equal to 5.81 nm. The total particle number concentration was more than 10 times lower than the one measured when adding 10 ppmv of acid. Table 1 also reports the total P-concentration in the particles measured by the SMPS, together with the ratio between this concentration and the total P injected as H_3PO_4.

Table 1
Performed SMPS experiments

Experiment		SMPS results			
H_3PO_4 added (ppmv)	P-added (g/m^3)	Particle mean diameter (nm)	Particle total concentration ($\#/m^3$)	P-content (g/m^3)	P-inlet fraction (%)
10	0.006	25.0	3.76E+14	0.003	50
20	0.012	31.8	4.63E+14	0.008	66
30	0.018	36.2	5.20E+14	0.013	72
40	0.024	39.7	5.42E+14	0.018	75
50	0.030	42.8	5.82E+14	0.024	80
70	0.042	46.9	6.30E+14	0.034	81
100	0.061	50.1	6.14E+14	0.041	67
200	0.121	59.4	7.13E+14	0.085	70
300	0.181	63.6	7.63E+14	0.103	57
400	0.243	66.9	8.14E+14	0.127	52

The P-content of the particles has been calculated by assuming the particles at the azeotropic mixture (P_2O_5 = 92.4 wt.%). T = 350 °C.

The P-content of the particles has been calculated by assuming the particles constituted by 92.4 wt.% P_2O_5. The reasons for this assumption will be clearer in Section 4.1. The particle density, ρ, has then been calculated as

$$\rho = (0.7102 + 0.01617\,P_2O_5\ \text{wt.}\%) - (11.7E-4 - 6.00E-6P_2O_5\ \text{wt.}\%)T$$

where T is the temperature in °C [15]. From the values reported in Table 1, it can be seen that 50–81% of the injected P reaches the catalyst in the particles. Apparently, the mass fraction of P that reaches the inlet of the SCR reactor goes through a soft maximum around 70 ppmv. The remaining may be in the gas-phase or is deposited on the walls of the setup before the catalyst.

3.2. Activity tests at the pilot-scale setup

The three catalyst elements P10, P100 and P1000 have been exposed for 819, 38 and 24 h, respectively. Prior to exposure, each element has been exposed to a ''clean'' flue gas for at least 1 week or until its activity had reached a stable value. The different values of activity for the fresh elements have then been used to calculate the relative activity of each catalyst element.

The results of the different deactivation tests are presented in a chronological order.

3.2.1. Exposure to 1000 ppmv H_3PO_4

The addition of 1000 ppmv H_3PO_4 was carried out for 24 h. During the first 2 h of exposure, the activity of the catalyst element was continuously measured. The results of the measurement are shown in Fig. 3. As it can be seen from this, the relative activity rapidly decreased as soon as the P-rich flue gas was flowing through the SCR reactor. After only 2 h the element lost already 33% of its original activity. At the end of the acid addition, the monolith showed no activity at all. The

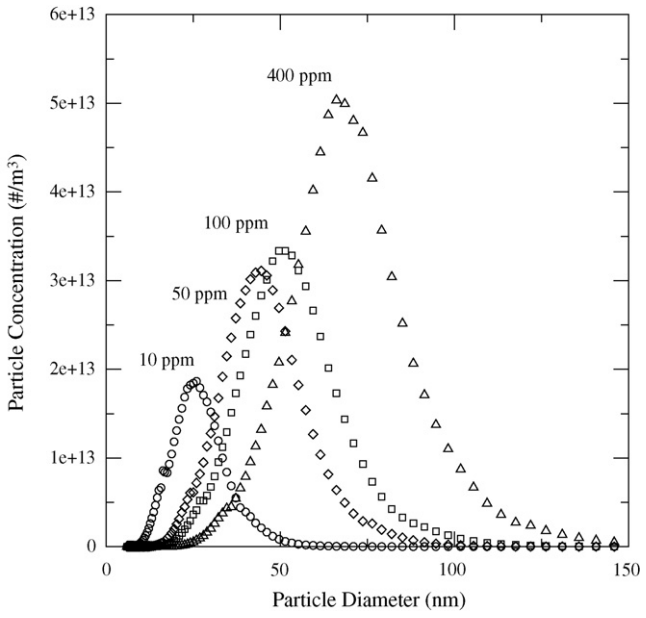

Fig. 2. Particle size distribution of polyphosphoric acids measured at the SCR reactor inlet at different H_3PO_4 addition by SMPS. T = 350 °C.

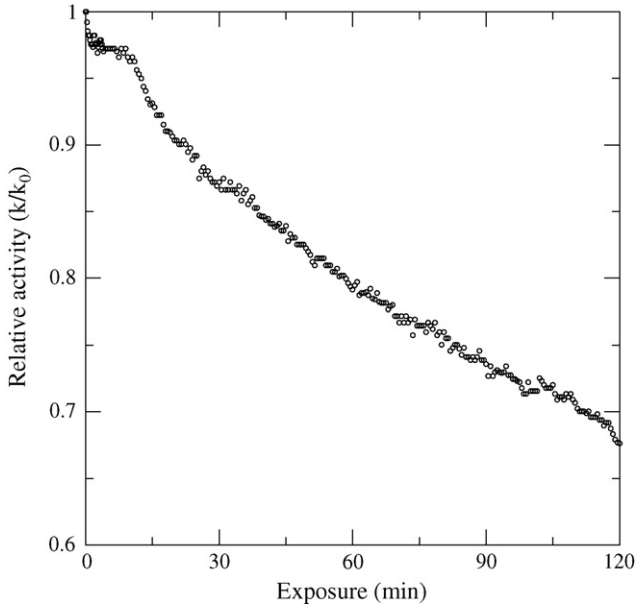

Fig. 3. Relative activity of the P1000 element during the first 2 h of exposure. T = 350 °C. Total flow 40 N m^3/h. Gas composition on dry basis NO = 496 ppmv, NH_3 = 735 ppmv, O_2 = 10 vol.%, CO_2 = 6 vol.%, N_2 balance. 10 vol.% H_2O.

results show that high level of P in the flue gas may be very harmful to the catalyst.

This test had a tremendous impact on the whole setup. A lot of acid was found deposited on the setup pipe walls and therefore an extensive cleaning was carried out before starting the test at lower acid concentrations.

3.2.2. Exposure to 10 ppmv H_3PO_4

The addition of 10 ppmv H_3PO_4 corresponds to about 32 mg/Nm^3 of P_4O_{10} in the flue gas, which is well below the expected P_4O_{10} concentration (3500 mg/Nm^3) assuming a 4% co-firing thermal share of sewage sludge with a P-content of 7% and a solid–gas conversion equal to 50% [9]. Fig. 4 shows the decrease in relative activity of the exposed catalyst element. A fresh monolith was charged and exposed to a "clean" flue gas for about 430 h. This time was required in order to get a steady value for the NO conversion. However, the element had already lost about 28% of its original activity, probably due to deposit remaining in the setup even after the cleaning. The addition of 10 ppmv H_3PO_4 was then started. The exposure to the flue gas containing 10 ppmv H_3PO_4 further deactivated the catalyst. However this deactivation was found to be rather slow. Globally, the relative activity leveled off at around 65%, meaning that the element lost 7% of activity since the start of the exposure to 10 ppmv H_3PO_4. The results indicate that low levels of P in the flue gas may not be very harmful to the catalyst.

During the activity measurements, a transient in the NO conversion was noted when NH_3 was added. This phenomenon was even more evident during the exposure to 100 ppmv H_3PO_4, and will be therefore presented in the next section.

3.2.3. Exposure to 100 ppmv H_3PO_4

The addition of 100 ppmv H_3PO_4 was carried out for only 38 h. After this time, the element was exposed to a clean flue gas for additional 433 h. Table 2 reports the activity measurements carried out. During all the measurements, the NO conversion was found to first go through a maximum and then reach a steady level at lower values as a function of time. In Table 2, both the maximum and steady state are reported. Fig. 5 shows the activity measurement carried out after 134 h of operating time. Here, the NO concentration in the flue gas is plotted against the time of the activity measurement. For times less than 0, no ammonia is present in the flue gas and about 514 and 484 ppmv NO are present at the reactor inlet and outlet, respectively. This difference was simply due to dilution of the flue gas with ambient air entering the setup from the pipe flanges. At time 0, around 600 ppmv of NH_3 are added to the flue gas and, as a result of the SCR reaction, the NO concentration starts decreasing until it reaches a concentration of 218 ppmv, corresponding to a NO conversion, X, of 55% and a relative activity, k/k_0, of 0.91. However, right after reaching this value, the NO concentration in the flue gas starts increasing and reaches a steady-state value at 333 ppmv after about 1 h. In the meantime, the NO concentration at the inlet was measured twice in order to verify that the NO transient was not due to changes in the inlet values. In both cases, this was found equal to about 504 ppmv. This value was only 10 ppmv lower than the initial one and could have been caused by only few degrees change in the burner. At steady state, neglecting the small change in NO inlet concentration, the NO conversion, X, was equal to 0.31, corresponding to a relative activity, k/k_0, equal to 42%. After having reached the steady state, the amount of NH_3 to the SCR reactor was doubled. Interestingly, the relative activity of the element increased to 50%. Since ammonia is introduced as a pure gas, it is excluded that the drop in NO concentration shown in Fig. 5 is due to dilution of the flue gas. This effect is more likely related to changes in the NH_3 adsorption properties of the P100 surface.

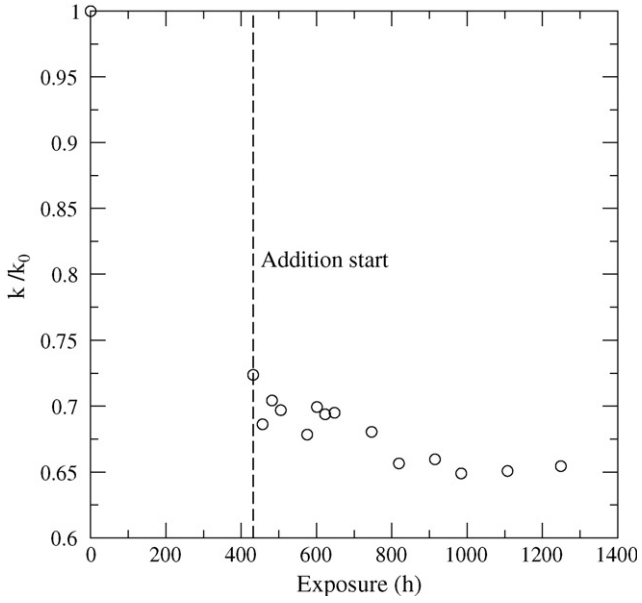

Fig. 4. Relative activity of P10 at 350 °C as a function of exposure time. Total flow 40 N m^3/h. Average gas composition NO = 500 ppmv, NH_3 = 735 ppmv, O_2 = 10 vol.%, CO_2 = 6 vol.%, and 10 vol.% H_2O in N_2.

Table 2
Results of the activity measurements performed with the P100 element

Operating time (h)	H_3PO_4 addition (h)	X		k/k_0	
		Max	Steady state	Max	Steady state
0	0	0.585	0.585	1	1
20	20	0.569	0.390	0.957	0.562
134	38	0.549	0.312	0.905	0.425
158	38	0.531	0.366	0.861	0.518
180	38	–	0.369	–	0.523
471	38	0.535	0.388	0.871	0.558

From the analysis of the activity measurements reported in Table 2, it is possible to see that at increasing time of H_3PO_4 exposure, both the maximum and the steady-state value of NO conversion are decreasing. However, when the element was exposed to a H_3PO_4-free flue gas for some time, it slowly regained some activity. In fact, both the maximum and the steady-state values of NO conversion increased, indicating that part of the deposited acid causing the deactivation is slowly leaving the catalyst.

As it will be discussed later, it is believed that this element is clearly showing effects of chemical deactivation due to

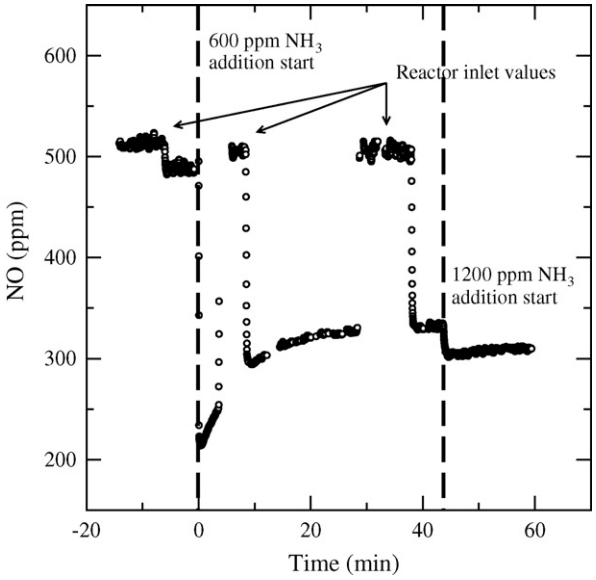

Fig. 5. Activity measurement for P100 at 350 °C and 50 N m^3/h after 134 h of operating time. Gas composition on dry basis NO = 515 ppmv, NH_3 = 600–1200 ppmv, O_2 = 11 vol.%, CO_2 = 5.6 vol.%, N_2 balance. 10 vol.% H_2O.

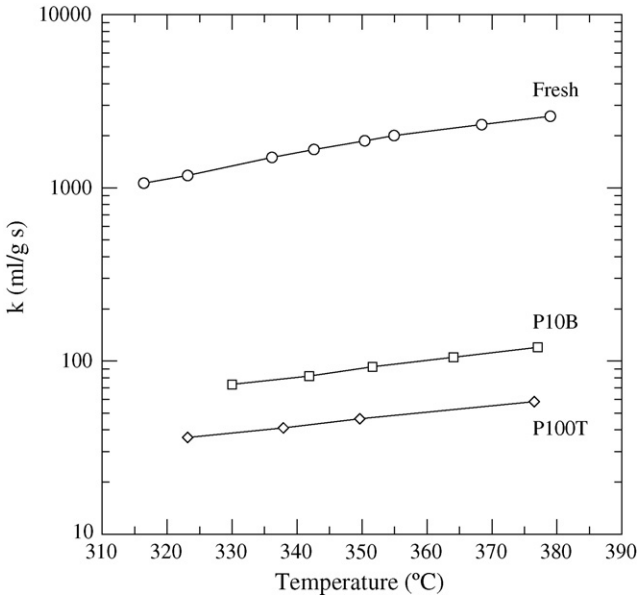

Fig. 6. Activity test on powderized samples. Total flow 2.8 N L/min. NO = 521 ppmv, NH_3 = 622 ppmv, O_2 = 5.2%, H_2O = 1.47%, N_2 balance. Catalyst mass W = 0.072 g.

polyphosphoric acids associated with the transient in NO conversion and due to the formation of V–P–O–NH_3 species, which are not or less active in the reduction of NO than the original sites. Finally, it is worth noting that the NO transient was fully reproducible provided that the NH_3 was shut off for about 1 h. If the element was exposed to an NH_3-free flue gas for shorter times before NH_3 was reintroduced in the flue gas, the NO transient was still present, but the measured maximum NO conversion was lower. This shows that it takes quite some time for the surface complexes to be consumed.

3.3. Lab-scale investigations

3.3.1. Activity tests on catalyst deactivated at the pilot-scale setup

The activity tests on powderized spent and fresh monoliths are shown in Fig. 6. The plot only reports the results in the temperature range 320–380 °C, where external and internal mass transfer have been estimated not to limit the observed reaction rate. Therefore, the values reported in the plot represent the pseudo-first order intrinsic reaction rate constants. Both the powderized P10B and P100B showed an extreme deactivation: at 350 °C they retained only 5 and 2.6% of their original activity, respectively.

3.3.2. Activity tests on wet impregnated plates

The relative activities of the three different impregnated plates were found in the range 0.85–0.90. Even though the *P*/*V* ratios (i.e. 1.8, 2.9 and 4.7) for these plates were comparable to the ones measured on the monoliths P10 and P100 (Table 3), their deactivation was much lower, in agreement with other works [6,7] where both model and commercial catalysts have been doped by a wet impregnation method. The results indicate

Table 3
Results of the bulk and surface chemical analysis, and of the Hg-porosimetry for the fresh and spent monoliths.

	Monolith						Plate	
	Fresh	P10T	P10B	P100T	P100B	P1000B	Fresh	P100plate
Bulk chemical analysis								
V (% w/w)	1.60	1.66	2.85	3.12	1.87	0.70	1.00	0.87
P (% w/w)	0.01	3.29	3.02	4.17	4.19	18.70	0.10	6.07
P/*V* (mol/mol)		3.26	1.74	2.20	2.10	43.94		11.48
Surface chemical analysis								
V (% w/w)	2.1	3.1	3.3	3.9	2.7	1.1		
P (% w/w)	0.0	5.4	4.4	7.9	6.3	21.8		
P/*V* (mol/mol)	0.0	2.8	2.2	3.3	3.9			
Hg-porosimetry								
Total intrusion volume (mL/g)	0.71	0.57	0.58	0.42	0.53	0.06	0.82	0.44
Total pore area (m^2/g)	36.84	31.16	22.77	19.60	30.67	5.42	73.05	17.19
Catalyst bulk density (g/mL)	0.96	1.15	1.14	1.38	1.17	2.11	0.89	1.20
Porosity (%)	68.60	65.27	66.47	57.73	61.96	11.83	73.02	53.02

that when P does not experience temperatures higher than the calcination temperature used during the doping process, it is not present on the catalyst surface as a polyphosphate. Its deactivating strength is therefore limited.

3.3.3. NH_3 chemisorption tests

Fig. 7 shows the results of the NH_3 chemisorption test performed at 350 °C with a sample cut from P100plate and a fresh plate of the same type. As it can be seen from the plot, the amount of NH_3 adsorbed on the P-deactivated sample was much higher than on the fresh sample. In fact, the P-deactivated sample is able to adsorb about five times more NH_3 than the fresh catalyst. This is in agreement with the increased acidity of the catalyst surface due to deposition of the polyphosphoric acids. However, the activity measurements show that the NH_3 adsorbed on the polyphosphates is much less active (or even non-active), which indicates that in the chemisorption test this NH_3 acts mainly as a reservoir.

3.4. In situ EPR spectroscopy

Fig. 8 shows the in situ EPR spectra of VO^{2+} present on the samples taken from exposure tests of the fresh, P10 and P100 elements measured at 350 °C. Vanadium in oxidation states +5 and +3 are both invisible in EPR at these temperatures. The oxidising mixture NO, O_2, H_2O in N_2 is leaving the active oxo-vanadium species present on the catalyst surface mainly in their oxidation state +5. Under these conditions, the spectrum of the fresh catalyst exhibits a broad band from polymeric surface vanadium species. Superimposed on this, a spectrum exhibiting poorly resolved hyperfine structure is observed. The latter appears to be from dimeric V(IV) species, with only the most significant peaks clearly visible. No significant presence of monomeric V(IV) species at this temperature under oxidising conditions is observed. During exposure to NH_3-containing gases, the redox chemistry of the fresh catalyst surface is not altered at all, as shown by the identical spectra, which were recorded during exposure to the different gas mixtures.

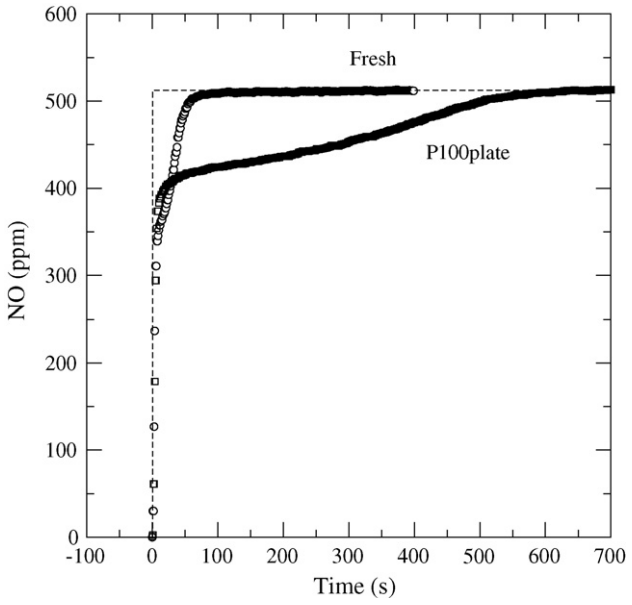

Fig. 7. NH_3 chemisorption test on fresh and P100 mini plate samples at 350 °C. Total flow 2.75 N L/min. NO = 501 ppmv, NH_3 = 601 ppmv, O_2 = 5%, N_2 balance. Catalyst mass W = 0.45 g.

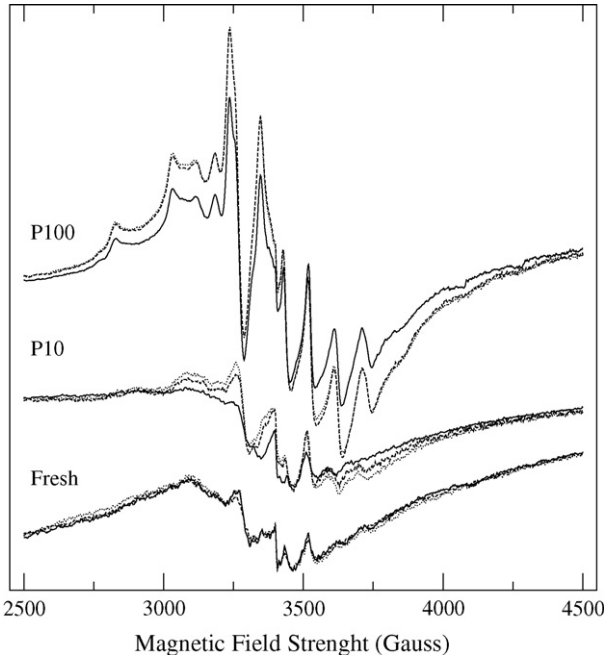

Fig. 8. In situ EPR spectra acquired at 350 °C of catalyst samples taken from pilot plant tests fresh, P10 and P100, exposed to various simulated flue gas compositions. Gas composition: 1000 ppmv NO (—), 1000 ppmv NO + 1000 ppmv NH_3 (···), 1000 ppmv NH_3 (- - -) and 3.5% O_2, 3% H_2O in N_2.

The P10 sample essentially shows the same spectrum as the fresh catalyst after equilibration in the oxidising NO, O_2, H_2O, N_2 atmosphere. However, unlike the uncontaminated sample, the exposure to an NH_3-containing mixture caused an increase in VO^{2+} (or $(VO^{2+})_n$) content. In particular, the spectrum of the sample equilibrated in the SCR gas mixture exhibited the greatest difference from oxidising conditions.

Contrarily to the previous results, P100 showed a significantly increased broad band of polymeric $(VO^{2+})_n$ species even during exposure to the oxidising gas mixture. Superimposed on this signal, a new but recognisable contribution from monomeric VO^{2+} species is observed.

3.5. Catalyst characterization

The V- and P-content on both the surface and bulk of the fresh and doped catalyst are shown in Table 3. The results of the mercury porosimetry are also reported in Table 3. In all the tested cases, the P-levels in the bulk were found slightly higher at the inlet compared to the outlet of the catalyst element, according to both the higher particle concentration and the higher mass transfer due to the developing flow and higher level of turbulence.

The P-content of the P100 element was found slightly higher than the one measured for the P10 (i.e. about 4 wt.% against 3 wt.%). Considering the big difference in exposure time for the two experiments (819 h vs. only 38 h), and assuming a linear

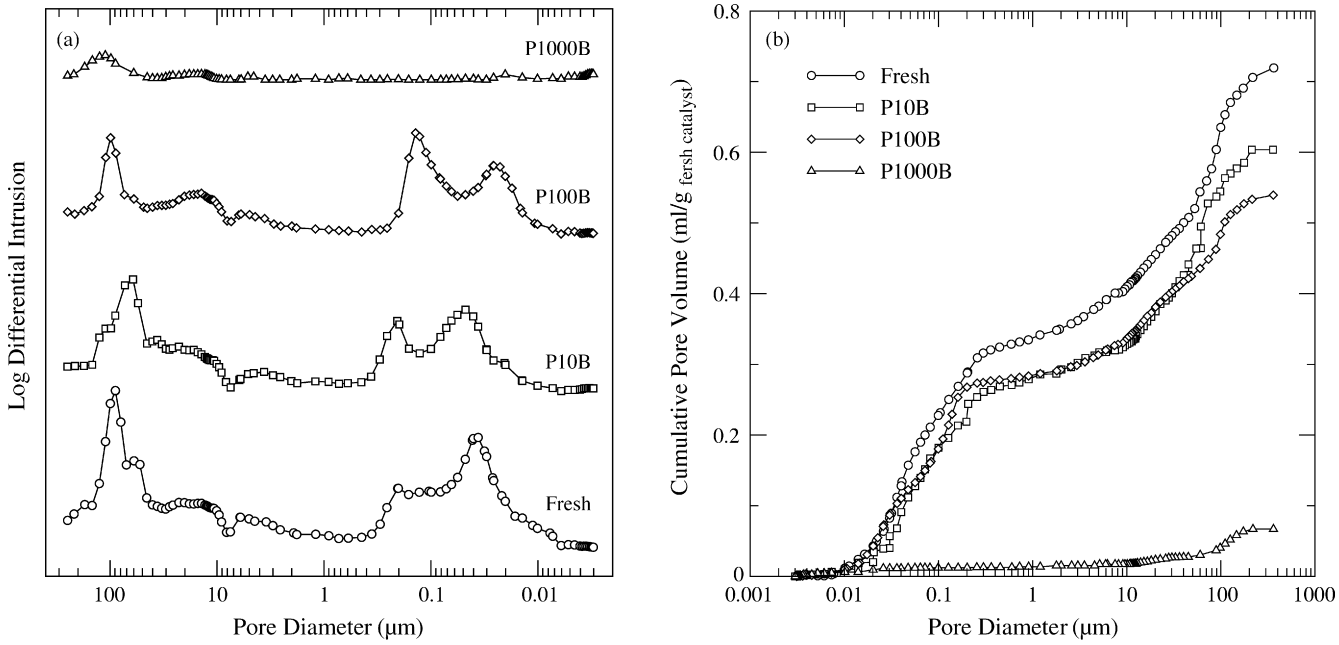

Fig. 9. Pore size distribution and cumulative intrusion volume measured by Hg-porosimetry with different monolithic samples.

and constant deposition of P vs. time, it can be calculated that the overall accumulation rates have been 0.09%/day and 2.6%/day for P10 and P100, respectively. Assuming a first order process for the particle deposition (i.e. the fraction of deposited particles not depending on the total particle concentration number) and making the conservative assumption that the particle formed during the addition of 10 ppmv H_3PO_4 have the same diffusivity of the bigger particles formed in the presence of 100 ppmv H_3PO_4, the deposition rate for the 100 ppmv H_3PO_4 test should have been only 10 times higher than the one with 10 ppmv H_3PO_4. As calculated before, the P-accumulation on P100 was instead found 29 times the P-accumulation on P10. This fact, as it will be discussed later, is considered as an indication that the overall P-accumulation is the result of a balance between particle deposition and deposit hydrolysis followed by P-vaporization from the sample.

According to the results obtained by Hg-porosimetry shown in Fig. 9, the deposition of polyphosphoric acid produced a shift toward smaller pore diameters in the pore size distribution for the different monoliths, pointing out the occurrence of physical deactivation due to pore blocking and condensation. In fact, it appears that the smaller pores at 40–50 nm of the bimodal mesoporous system are filled during P-addition, and a partial blocking of the interparticulate pore structure happened for P10 and P100. Furthermore, large crystalline formation has filled the void space in the macro-cracks above 100 μm. For the P10 a shift towards smaller macropores is observed due to this, whereas for the P100, a more dispersed destruction of the entire pore system is observed.

Overall, the total intrusion volume (TIV) was found to decrease at increasing P-content (Fig. 10).

The physical deactivation pointed out by the Hg-porosimetry measurements has also been confirmed by SEM analysis of the exposed catalysts (Fig. 11). From these it can be seen that the surface of P100 looks uniformly covered by a glassy layer, whereas the porous structure of titania is more defined on the surface of P10. Instead, on this latter, some needle-shaped crystals are present. The analysis of these crystals by EDX showed enrichment in both P and V.

Fig. 12 shows the distribution of P into the walls of P10B and P100B as measured by EDX at the points shown in Fig. 11. P was found to penetrate the whole catalyst wall in both cases. In particular, the P-content in P100B was found constant around a value of 6.1 wt.%. Differently, the concentration profile measured on P10B showed a gradient in P-concentration in

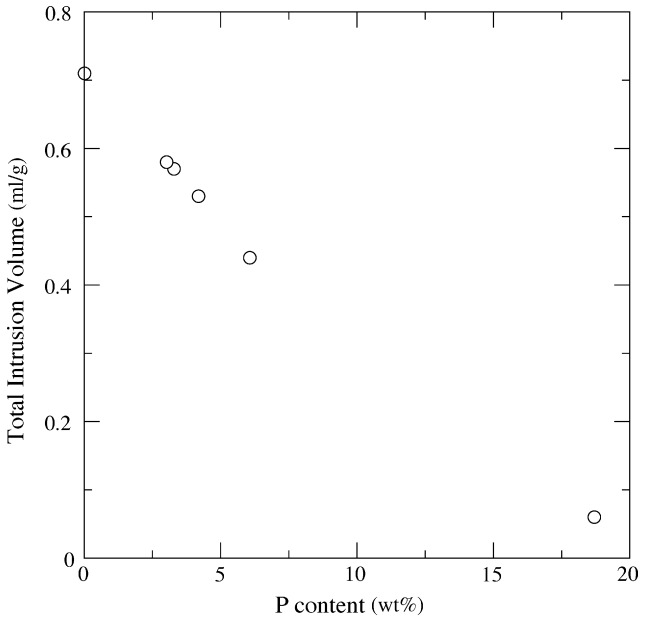

Fig. 10. Total intrusion volume measured by Hg-porosimetry as a function of P-content measured in the bulk of the different spent monoliths.

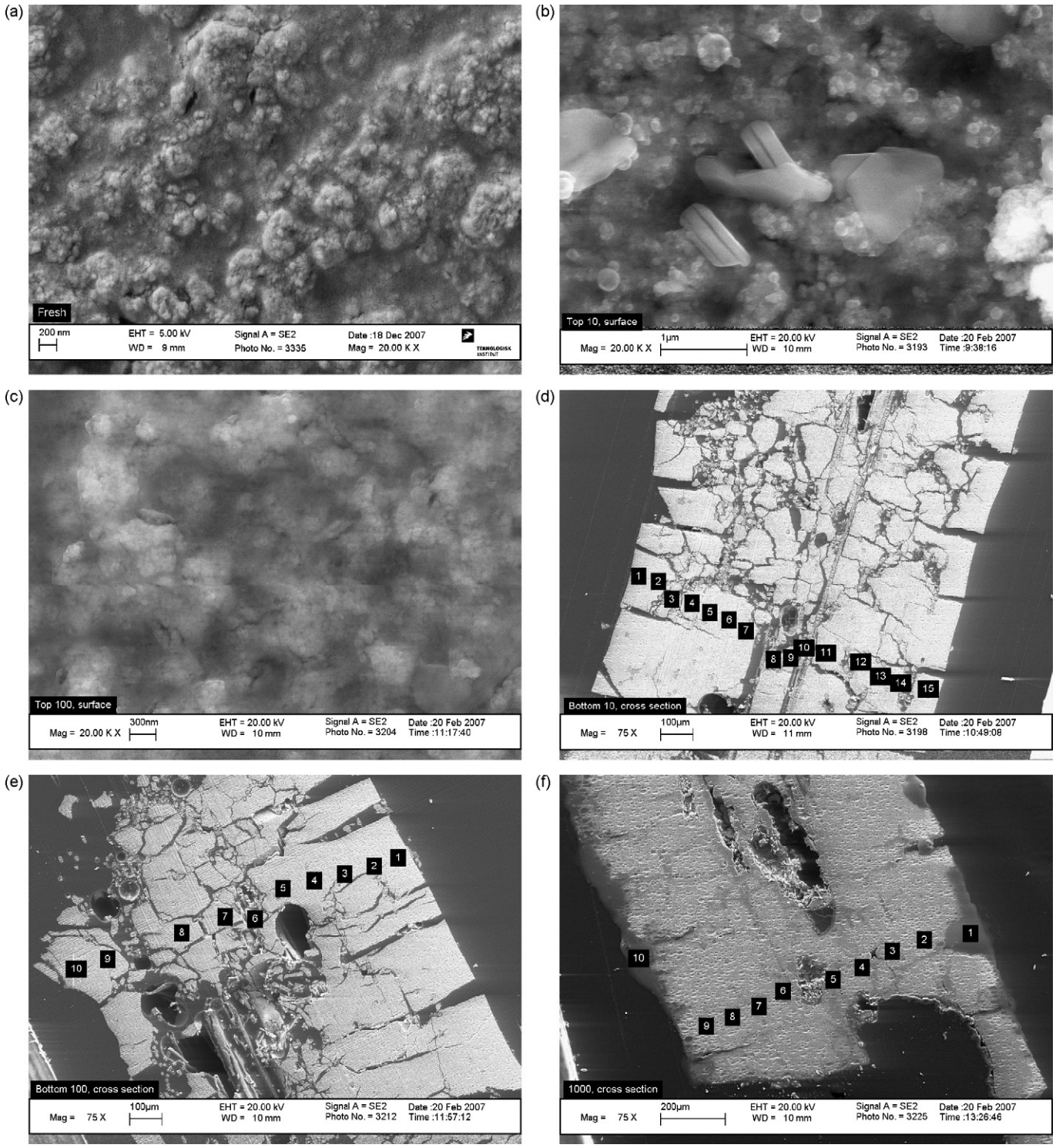

Fig. 11. SEM analysis of fresh and spent catalyst: (a) fresh surface; (b) P10T surface; (c) P100T surface; (d) P10B wall cross-section; (e) P100B wall cross-section and (f) P1000B wall cross-section.

the proximity of the surface, normally indicating a diffusion limited process in P-accumulation. However, in some points in the middle of the wall, especially in the proximity of a macropore, the P-concentration was found again higher. Overall, the average P-content in P10B wall was equal to 3.1 wt.%.

4. Discussion

A higher degree of deactivation was obtained by exposure to polyphosphoric acid aerosols at the pilot plant compared to the one obtained by wet impregnation of H_3PO_4 aqueous solutions. This indicates the importance in understanding the mechanism

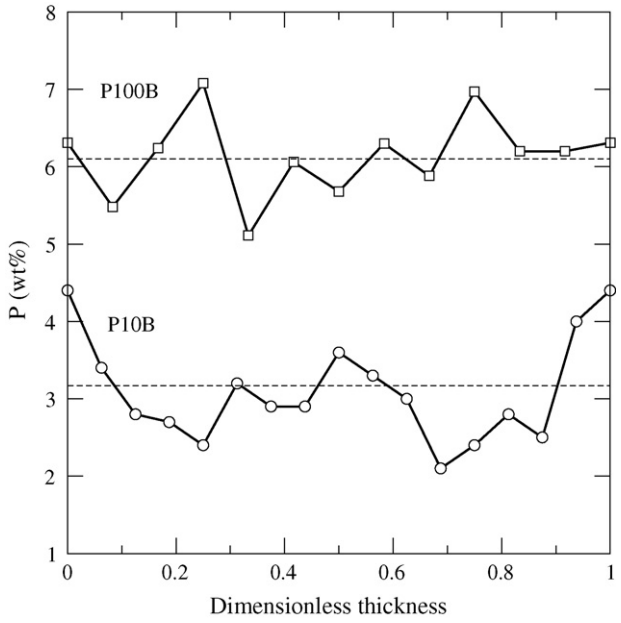

Fig. 12. P-content measured by EDX across some catalyst walls shown in Fig. 11.

of formation of these particles and their influence on the activity of the vanadia-based catalysts. Apparently the real poisoning strength of P is not reproduced by the wet impregnation method normally used to dope both model and commercial catalysts.

4.1. Polyphosphoric acids formation and deposition

The measured particles had very small mean diameters and a total particle number concentration in the order of 1×10^{14} #/m^3 indicating their formation by homogeneous nucleation from the gas-phase. Condensation on particles already present (i.e. the ones measured during the blank measurement) cannot be completely excluded. However, this cannot be regarded as the main mechanism of particle formation since already at the lower acid concentrations (i.e. 10 ppmv), the particle number concentration was more than 10 times higher than the one found during the blank test. Furthermore, due to the very small size of the particles measured during the blank test, their mass fraction in the deposits can be neglected.

In order to explain the particle formation experienced, the formation of polyphosphoric acid will be here discussed based on Ref. [16]. The phosphoric acid molecule H_3PO_4 can be written as $1/2P_2O_5{\cdot}3H_2O$ and thus be considered as a 72.5% P_2O_5 solution having a boiling point temperature at 255 °C. When exposed to higher temperatures, water can evaporate until an azeotropic mixture consisting of 92.4% P_2O_5 is formed. This azeotropic mixture has a much higher boiling point at 864 °C. This water evaporation and the subsequent increase of P_2O_5 concentration is the result of condensation reactions taking place between the H_3PO_4 molecules in the gas-phase producing chains of poly-, pyro-, tri-, and *meta*-phosphoric acid, as follows:

$$2H_3PO_4 \rightarrow H_4P_2O_7 + H_2 \quad (1.5)$$

$$H_3PO_4 + H_4P_2O_7 \rightarrow H_5P_3O_{10} + H_2O \quad (1.6)$$

Due to their higher boiling point temperatures, the polyphosphoric acids may condense according to their vapor pressure when the gas cools down to the SCR reactor temperature.

Fig. 13 shows a plot of the partial pressure of different polyphosphoric acids as a function of P_2O_5 content [17]. Since particles have been found at the reactor inlet even at the lowest acid concentration of 10 ppmv, and considering the high temperatures (>850 °C) experienced in the spraying section of the setup, it is assumed that the composition of the deposited particles is equal to the azeotropic mixture. In this way, around 50–81% of the injected P-mass, was collected at the inlet of the SCR reactor. In the absence of a direct measurement of the P-content in the gas-phase, it is difficult to completely exclude and/or quantify the presence of gaseous P-species at the reactor inlet. Considering the equilibrium between the gas- and the liquid-phase as described by Fig. 13, no condensation with 10 ppmv H_3PO_4 is expected since this would have needed a supersaturated atmosphere in order to take place. However, this was not the case. Moreover, the fraction of P calculated from the particle number concentration measured by the SMPS was found in the range 50–81%. If it is assumed that at low acid concentrations the rest of the injected P is in the gas-phase, this should have been close to zero at increasing acid concentrations. However, as shown in Table 1, the collected P-fraction at 400 ppmv H_3PO_4 was almost the same as the one at 10 ppmv.

It is therefore assumed that: (i) the injected H_3PO_4 reacted in the gas-phase forming an azeotropic mixture of polyphosphoric

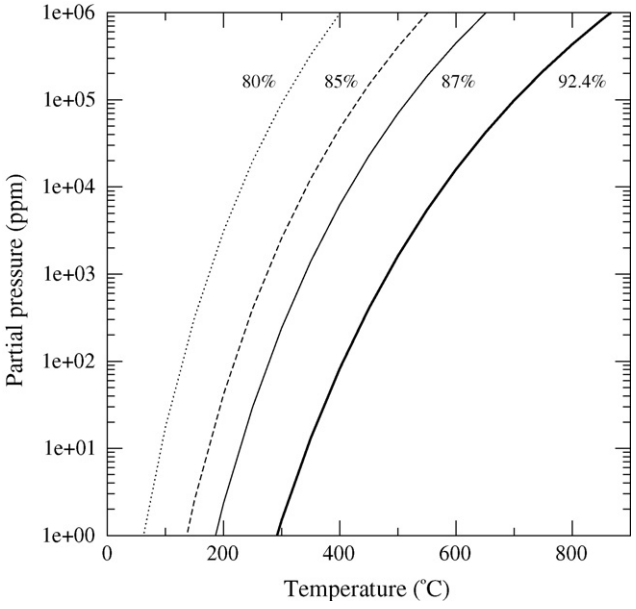

Fig. 13. Vapor pressure of polyphosphoric acids as a function of temperature at different P_2O_5 weight content. The lines are calculated by extrapolating at lower pressures the equation fitting the experimental data found at higher partial pressures [17].

acids; (ii) nucleation of polyphosphoric acid happened at temperatures <500 °C; (iii) almost all the acid was present in the liquid-phase and (iv) the differences found between the total P-mass injected and the P-mass measured at the SCR reactor inlet was mainly due to particle deposition on the pipe walls leading to the SCR reactor.

Due to their submicron dimensions, the particles are very mobile and can diffuse towards the catalyst walls, deposit on the catalyst surface and even penetrate into the pore structure by capillary forces. Once deposited, however, some of the deposited polyphosphoric acid may be hydrolyzed in the presence of the flue gas moisture forming H_3PO_4 which evaporates from the catalyst. The resulting P-accumulation rate is therefore a balance between the particle deposition and evaporation of phosphoric acid. The hydrolysis of polyphosphoric acid in water is known to be a slow process and dependent on different factors, such temperature, chain length and pH [16]. Therefore the P-accumulation in the catalyst walls will be mainly controlled by the particle deposition rate at high total particle numbers, while deposit evaporation at low deposition rates and low total particle number concentrations becomes relatively more important.

Taking into account all these facts, together with the different P-concentration profiles measured by EDX on P10 and P100 (Fig. 12), it is possible to conclude that evaporation of phosphorus compounds effectively limited the P-accumulation in the P10 case and that the profile measured in the wall is the net result of deposition and evaporation. The deposition rate during the 100 ppmv H_3PO_4 addition was much faster than evaporation leading to a fast accumulation of P in the wall.

4.2. Deactivation mechanisms

The high P-concentration found in the bulk of the exposed catalysts, the even P-distribution measured along the catalyst walls, the decrease in TIV measured by Hg-porosimetry at increasing P-concentrations and the SEM analysis of the different catalyst surfaces, all point to the occurrence of physical deactivation due to surface masking, pore blocking and condensation, in agreement with previous investigations about P-deactivation. However, the transient in NO conversion observed during every activity measurements clearly points out the occurrence of a simultaneous chemical deactivation mechanism.

The in situ EPR measurements carried out with the fresh catalysts have shown that the different gas compositions are not able to change the redox properties of the surface. In particular, during the SCR reaction, the V(V) species are continuously reduced during formation of the reaction intermediates and then re-oxidised by O_2 [2,3]. The fact that this sample, when exposed to the complete SCR mixture, does not show an increased number of V(IV) species can be explained assuming that at 350 °C the rate of re-oxidation of the active V(IV) species in the redox cycle of the mechanism is high enough to keep the vanadium as V(V). In other words, this behaviour confirms the literature consensus [1] that at this temperature, the order of reaction of oxygen is zero.

Under oxidising conditions, P10 practically exhibited the same spectrum as the fresh sample. However, when P10 was exposed to the complete SCR gas mixture, the number of $(VO^{2+})_n$ species slightly increased. This indicates that the SCR reaction is occurring, but that the re-oxidation step is significantly slower than for the fresh catalyst.

Contrarily to the previous results $(VO^{2+})_n$ species are present as a stable phase on the catalyst surface of the P100 sample already under oxidising conditions, suggesting that the VO^{2+} on P10 and P100 are exposed to two distinctly different phosphor species. Furthermore, the concentration of V(IV) is increased when NH_3 is added to the mixture and the SCR reaction takes place. The most likely explanation for this is that the intermediate V(IV) species, which are consistently formed during the SCR reaction [2,3], are being trapped by phosphate interactions, since it appears unlikely that phosphates alone should be able to reduce the V(V) compounds. This indicates that the deposited phosphates interact with parts of the active oxo-vanadium species, forming vanadyl-phosphate species which will not take part in the reaction anymore, thus inducing chemical deactivation by titration of the active species.

By considering this chemical deactivation, together with the effect of intra-particle diffusion limitations, the transient in NO conversion can be explained. As shown in Fig. 5, at the very beginning of the NH_3 addition, the monolith P100 still presents a relative good activity. As reported in Table 2, when the NO conversion goes through the maximum, the relative activity is equal to 0.91. The lost 9% of activity is mainly due to physical deactivation only. However, the V(IV) species which were initially formed during the SCR reaction, are then stabilized in complexes which are formed with the deposited polyphosphoric acids. NH_3 can then be considered as the responsible for this titration of active sites since it initiates their reduction due to the SCR reaction. This titration is assumed to happen first at the outer catalyst wall, since it is where the SCR reaction is first happening. The intrinsic rate of reaction then starts decreasing at the outer wall due to the formation of NH_3–P–V species and the reagents have to diffuse further into the catalyst walls in order to find active sites where to react. The steady-state is finally reached when equilibrium between the formed P–V– complexes, the active V-species and NH_3 is reached along the catalyst wall. In the case shown in Fig. 5 and reported in Table 2, the additional 48% of activity which has been lost has to be considered due to chemical deactivation.

NH_3 is controlling the stability of the formed and inactive complexes. In fact, the NO transient during the activity measurement can only be reproduced if NH_3 has been taken off the flue gas for the time required by these complexes to completely disappear. Moreover, as shown in Fig. 5, further NO conversion can be obtained by increasing the NH_3 partial pressure, but again this will first show a maximum and then a steady-state level at lower values. This additional activity at higher NH_3 partial pressures can be related to the NH_3 adsorption constant of the catalyst surface, which is changed due to the presence of the polyphosphoric acids. As shown in Fig. 7, the amount of chemisorbed NH_3 is increased due to the polyphosphoric acid deposition. However this additional

adsorbed NH_3 can be assumed either *less active*, in agreement with Kamata et al. [7], or inactive, simply constituting an NH_3 storage on the surface. In the latter case, it has first to jump on an active site prior to react. Regarding the increased activity, which was measured when the NH_3 concentration was increased, it can then be argued that, due to the increased number of sites for the NH_3 chemisorption, the coverage of NH_3 appearing in Eq. (1.4) has become less than one at the typical condition of our activity measurements.

Finally, the reason for P100 for showing a more pronounced transient than P10 has to be found in: (i) a higher P-content in P100 and a consequent slower diffusivity due to the decreased pore sizes; (ii) a higher degree of polymerization of the deposits in P100 due to the faster deposition compared to the hydrolysis rate; (iii) a more uniform distribution of P in the P100 walls.

5. Conclusions

When exposed to the high temperatures of a combustion process, the H_3PO_4 molecules eventually released in the gas-phase start condensation reactions forming polyphosphoric acids. These species are characterized by higher melting point temperatures than the typical SCR reaction temperatures and are found in a liquid-phase at the SCR reactor inlet. Condensation of these species has been estimated to happen at temperatures lower than 500 °C. Therefore, there is a high probability that the formed aerosols will be characterized by high number concentrations of submicron liquid particles, due to the short time passing between the nucleation burst and the SCR reactor inlet. These particles therefore have high diffusivities and a high deposition rates on the monolith walls.

Deactivation by polyphosphoric acid has been found to follow both a physical and a chemical deactivation. Surface masking, fouling, pore blocking and condensation are definitely important contributions to catalyst deactivation. Once deposited on the catalyst outer surface, they are very mobile and can even be sucked into the walls by capillary forces. The P-accumulation, and consequently the implied deactivation, is however limited by the rate of hydrolysis of the deposits themselves. The H_2O present in the flue gas, at the SCR temperatures can break down the polyphosphoric acid chains and free some H_3PO_4 back in the gas-phase.

The physical deactivation, however is not the only effect responsible for the overall measured deactivation levels. Supported by the transient behaviour in NO reduction measured during activity tests with mass transfer-limited-catalysts, and in situ EPR analysis of the spent catalysts, it has been found that the deposited polyphosphoric acids tend to both increase and stabilize the number of *non-active* V(IV) species, which are formed as intermediate during the SCR reaction. Moreover, part of the NH_3 present in the gas-phase preferentially adsorbs on the polyphosphoric acids and is only less active in the reduction of NO.

The results obtained in this work constitute the first reference about deactivation of vanadia-based catalysts explicitly due to polyphosphoric acid alone. It is believed they show the real deactivating potential of P, when this is present in the flue gas during post-treatment of combustion processes, which has been found much more poisonous than indicated by wet impregnated tests.

Acknowledgments

This work is part of the CHEC (Combustion and Harmful Emission Control) Research Center funded a.o. by the Technical University of Denmark, the Danish Technical Research Council, the European Union, the Nordic Energy Research, Dong Energy A/S, Vattenfall A.B., F L Smidth A/S, and Public Service Obligation funds from Energinet.dk and the Danish Energy Research program. In particular, it is supported by the PSO project ‘‘Deactivation of SCR Catalysts by Additives’’ (PSO Elkraft FU-4205). Supply of the catalyst samples by Haldor Topsøe A/S is gratefully acknowledged.

References

[1] V.I. Parvulescu, P. Grange, B. Delmon, Catal. Today 46 (1998) 233–316.
[2] N.-Y. Topsøe, H. Topsøe, J.A. Dumesic, J. Catal. 151 (1995) 226–240.
[3] N.-Y. Topsøe, J.A. Dumesic, H. Topsøe, J. Catal. 151 (1995) 241–252.
[4] Y. Zheng, A.D. Jensen, J.E. Johnsson, Appl. Catal. B: Environ. 60 (2005) 261–272.
[5] Y. Zheng, A.D. Jensen, J.E. Johnsson, Appl. Catal. B: Environ. (2008), doi:10.1016/j.apcatb.2008.02.019.
[6] J.P. Chen, M.A. Buzanowski, R.T. Yang, J. Air Waste Manage. Assoc. 40 (1990) 1403–1409.
[7] H. Kamata, K. Takahashi, C.U.I. Odenbrand, Catal. Lett. 53 (1998) 65–71.
[8] J. Blanco, P. Avila, C. Barthelemy, A. Bahamonde, J.A. Odriozola, J.F. Garcia de la Banda, H. Heinemann, Appl. Catal. 55 (1989) 151–164.
[9] J. Beck, J. Brandenstein, S. Unterberger, K.R.G. Hein, Appl. Catal. B: Environ. 49 (2004) 15–25.
[10] P.A. Jensen, L.H. Sørensen, G. Hu, J.K. Holm, F. Frandsen, U.B. Henriksen, Technical University of Denmark, KT-Report No. 0504, 2005.
[11] L. Tobiasen, R. Skytte, L.S. Pedersen, S.T. Pedersen, M.A. Lindberg, Fuel Process. Technol. 88 (2007) 1108–1117.
[12] J. Beck, R. Muller, J. Brandenstein, B. Matschenko, J. Matschke, S. Unterberger, K.R.G. Hein, Fuel 84 (2005) 1911–1919.
[13] K.M. Eriksen, R. Fehrmann, N.J. Bjerrum, J. Catal. 132 (1991) 263–265.
[14] M.Y. Kustova, S.B. Rasmussen, A.L. Kustov, C.H. Christensen, Appl. Catal. B: Environ. 67 (2006) 60.
[15] T.D. Farr, Phosphorus Properties of the Element and Some of Its Compounds, Tennessee Valley Authority, Chemical Engineering Report No. 8, U.S. Government Printing Office, Washington, DC, 1950. From http://www.innophos.com.
[16] J.R. Van Wazer, Phosphorus and its Compounds, Interscience Publisher, New York, 1958.
[17] E.H. Brown, C.D. Whitt, Ind. Eng. Chem. 44 (1952) 615–618.

Appendix C

Paper II

This report has been submitted to the peer-reviewed international journal *Applied Catalysis B: Environmental.*

Influence of Reaction Products of K-getter Fuel Additives on Commercial Vanadia-based SCR catalysts

Part I: Potassium Phosphate

Francesco Castellino, Anker Degn Jensen[1], Jan Erik Johnsson, Rasmus Fehrmann[a]

Department of Chemical and Biochemical Engineering, Technical University of Denmark, DK-2800 Kgs. Lyngby, Denmark
[a]Center for Sustainable and Green Chemistry, Department of Chemisty, Technical University of Denmark, Building 207, DK-2800 Kgs. Lyngby, Denmark

Abstract
Commercial vanadia-based full-length monoliths have been exposed to aerosols formed by injection of K_3PO_4 (dissolved in water) in a hot flue gas (T > 850°C) from a natural gas burner. Such aerosols may form when burning fuels with high K- and P-content, or when P-compounds are mixed with biomass as a K-getter additive. The formed aerosols have been characterized by using both a SMPS system and a low pressure cascade impactor, showing a dual-mode volume-based size distribution with a first peak at around 30 nm and a second one at diameters > 1 μm. The different peaks have been associated with different species. In particular, the particles related to the 30 nm peak are associated to condensed phosphates, whereas the larger particles are associated to potassium phosphates. Two monoliths have been exposed during addition of 100 and 200 mg/Nm^3 K_3PO_4 for 720 and 189 hours respectively. Overall, deactivation rates up to 3 %/day have been measured. The spent catalysts have been characterized by bulk chemical analysis, Hg-porosimetry and SEM-EDX. NH_3-chemisorption tests on the spent elements and activity tests on catalyst powders obtained by crushing the monoliths have also been carried out. The catalyst characterization has shown that poisoning by K is the main deactivation mechanism. The results show that binding K in K-P salts will not reduce the rate of catalyst deactivation.
Keywords: $DeNO_x$ SCR catalysts, catalyst deactivation, vanadia, biomass, potassium poisoning, polyphosphoric acids.

1. Introduction

1.1. The K-getters Fuel Additives

The release of K-salts during biomass combustion is known to cause several problems to the boiler equipment downstream the boiler, thus limiting the application of this CO_2-neutral process [1]. Among these problems, the fast deposition rate on the super-heater exchangers of highly corrosive ashes is by far the most undesired. When biomass (e.g.

[1] Corresponding author. Telephone: +45 45 25 28 41. Fax: +45 45 88 22 58. E-mail: aj@kt.dtu.dk.

straw and wood) is fired, the potassium in the fuel, which is released in the gas-phase during combustion, forms aerosols of pure KCl and K_2SO_4 [2,3]. Potassium chloride has a relatively low melting point (i.e. 776°C) and is therefore found in a melted-phase at the temperatures of the super-heater exchangers, making the ashes sticky. Ash deposition on the exchanger surfaces is therefore enhanced, causing a decrease in steam production efficiency. A periodical removal of these deposits, however, might not be sufficient in order to re-establish the original heat flux across the heat exchanger surfaces. In fact, since Cl is included in the formed deposits, these are very corrosive and a complete substitution of the tubing system might then be required in a shorter time than anticipated.
In order to limit these problems, Danish and Swedish power companies are currently evaluating the addition of different compounds to the biomass which are able to bind the potassium into particles with higher melting temperatures, while releasing the chlorine in the gas-phase as HCl [4,5]. Sørensen et al. [6] developed a process where additives mainly constituted by P and Ca were mixed with the biomass in order to create the reaction conditions in the boiler at which the potassium gets captured in a phase consisting of $K_2O•CaO•P_2O_5$. As shown in Table 1, the compounds belonging to this system have melting points well above 1000°C and will thereby not be found as melts at the super-heater section. Initial tests performed by feeding straw mixed with different additive compositions to an entrained flow reactor have shown a reduction of 74-98% of the level of Cl in the deposits when the molar ratios of P/(K+Na) and P/Ca in the resulting fuel mixture were in the ranges 1.9-3.2 and 0.8-0.9 respectively [7]. This seems very promising from a deposition and corrosion point of view, but the addition process apparently requires an excess of both P and Ca with respect to the alkali fraction.

1.2. Additives Influence on the SCR Vanadia-based Catalysts

Changes in fly ash composition due to the addition of P- and Ca-compounds might also have an effect on the equipment downstream the superheaters that must be adressed. Particularly sensitive to changes in both the fly ash content and composition is the selective catalytic reduction (SCR) process used for the abatement of the NO_x fraction of the flue gas [8]. This process relies on the ability of ammonia to selectively reduce the undesired NO_x present in the flue gas to molecular nitrogen according to the following global reactions:

$$4\,NH_3 + 4\,NO + O_2 \rightarrow 4\,N_2 + 6\,H_2O \qquad (1.1)$$

$$2\,NO_2 + 4\,NH_3 + O_2 \rightarrow 3\,N_2 + 6\,H_2O \qquad (1.2)$$

The most active and selective catalysts are mainly constituted by vanadium pentoxide (V_2O_5, total load varying between 1-5 %wt. depending on the specific application), supported on a titania (TiO_2, anatase form) carrier. These are normally shaped into monoliths with parallel channels with hydraulic diameters up to 9 mm, which allows operation even in the presence of fly ash loads (>10 g/Nm^3) relevant for suspension firing before ESP with only low pressure drops over the reactor. A widely accepted mechanism of reaction for these catalysts at typical industrial operating conditions was proposed by Topsøe et al. [9,10]. This involves adsorption of NH_3 on Brønsted acid sites, activation of adsorbed ammonia by V=O species and subsequently reaction with gaseous or weakly

adsorbed NO. Deactivation of vanadia-based catalysts can be due to poisoning, fouling, surface masking, pore blocking and sintering according to the particular application. In most of these cases, however, the fly ash plays an important role since it may act both as physical deactivating agent, and as a carrier for different chemical deactivating species. For instance K, which according to different studies is a very strong poison for the vanadia-based SCR catalysts [3,11-17], is present as solid particles at the SCR reactor inlet. Therefore the observed rate of deactivation is directly related to the fluid dynamics controlling the rate of particle deposition. However, important as well is the rate of particle/poison penetration into the catalyst walls, and this is more likely related to the way the K-fraction is bound to the particle itself. For instance, up to 1%/day deactivation has been measured both at a biomass-fired combined heat and power plant [3] and in a pilot plant [17] where K was present as aerosols of pure KCl and K_2SO_4. Contrary, accordingly to coal firing experience, when K is mainly bound to non-soluble silica-aluminates, the deactivation proceeds at much slower rates. In order to explain the influence of the particle composition on the different deactivation rates experienced, Zheng et al. [3] suggested that this is related to the K-mobility at the SCR temperatures. The reason for the good mobility of KCl and K_2SO_4 was found in the Hüttig and Tamman temperatures of these compounds. These two temperatures are normally used to estimate the temperatures at which sintering starts [18] and are calculated with the following empirical expressions:

$$T_{Hüttig} = 0.3\ T_{melting}$$
$$T_{Tamman} = 0.5\ T_{melting}$$

When the Hüttig temperature is reached, atoms at vacancies start being mobile. When the Tamman temperature is eventually reached, the atoms in the bulk start showing mobility. According to their Hüttig and Tamman temperatures, the atoms forming the KCl and K_2SO_4 deposits may then be expected to be mobile at the SCR temperatures, and therefore react with the catalyst surface and further diffuse on it.

The discussion above indicates that binding K to ashes with higher melting temperatures by the addition process may reduce the rate of deactivation by decreasing the poison penetration in the catalyst walls. On the other hand, the increased P- and Ca-levels induced by the additive process could to some extent counterbalance this positive effect. P and Ca are known to be deactivating species for the vanadia-based SCR catalysts [11,12,19-22]. The excess levels of P with respect to the alkali fraction in the resulting fuel mixture required by the addition process might lead to an undesired formation of polyphosphoric acids. In a previous investigation [22] the formation and deactivating mechanisms of polyphosphoric acids have been reported. H_3PO_4 was found to form aerosols of viscous liquid polyphosphoric acids with diameters < 0.1 μm due to homogeneous nucleation occurring at temperatures < 500°C. These results were in agreement with the higher P-concentrations found in the submicron particles when coal was co-fired with P-rich secondary fuels at full-scale [23], or simply mixed with P-compounds and burned in an electrically heated plug flow reactor [24]. The polyphosphoric acid particles were characterized by very fast deposition rates due to both the high particle number and their high diffusivity due to their small size, and they caused a fast deactivation of the catalyst by both physical and chemical deactivation [22]. In particular, the chemical deactivation was

related to the stabilization of V(4+) species formed as intermediate during the SCR reaction by the polyphosphoric acids. However, no other species (apart from O_2, CO_2, H_2O and N_2) were present in the flue gas during the tests, leaving the question about the formation of polyphosphoric acids in a *non-clean* system still open.

1.3. Objectives

This work is part of a project, which aims at evaluating the effects of the addition of Ca-, P-based K-getter species on the vanadia-based SCR catalysts. This paper focuses on the potassium phosphate system, since in this system some of the potential reaction products of the K-getter fuel additives are found. The results of the investigations carried out by exposing full-length commercial SCR monoliths to a flue gas doped with K_3PO_4 in a pilot-scale SCR setup for up to 700 hours are reported. The second part of the work will focus on the simultaneous addition of KCl, $Ca(OH)_2$, H_3PO_4 and H_2SO_4 in the flue gas, to simulate a more complete full-scale addition process.
Apart from estimating the potential effect of the addition process on the SCR catalysts, the tests shown in this paper offer the possibility: (i) to provide further input to the mechanism of K-deactivation by aerosols; (ii) to determine the possible formation of polyphosphoric acids and thereby provide additional information about the P-release during combustion.

2. Experimental

2.1. Catalysts

Commercial corrugated-type monoliths obtained from Haldor Topsøe A/S were used in this study. The catalysts were based on V_2O_5 (up to 5 wt%) and tungsten oxide (WO_3, up to 9 wt%) dispersed on a fiber reinforced TiO_2 carrier. The monoliths had a size of 75 mm x 75 mm x 500 mm. The hydraulic diameter of the channels was 6.44 mm and the wall thickness was 1.0 mm. Pieces of both fresh and spent monoliths have been cut from both the inlet and the outlet in order to study their local properties under well defined reaction conditions in a laboratory fixed bed reactor. In order to run activity tests on powdered samples, they have been gently crushed in a mortar and the particle fraction in the range 105-125 μm has been collected by sieving.

2.2. SCR Pilot Plant

The SCR pilot plant setup used for this investigation is the same as described in [22]. Its main parts are a natural gas burner for flue gas production, a lance for injecting liquid solutions, a square duct hosting a full length commercial monolith and a NH_3 supply system. NH_3 is injected both in the burner to produce the desired NO concentration at the reactor inlet, and in the flue gas duct leading to the reactor for the NO reduction. A soot blowing system running with compressed air is installed at the SCR reactor inlet to keep the monolith channels open.

2.3. K_3PO_4 Addition

The addition of K_3PO_4 to the flue gas was performed by spraying water solutions through a two-fluid nozzle. The solutions were prepared by dissolving K_3PO_4 (reagent grade ≥98%,

Sigma®) in distilled water. Two catalyst elements have been exposed to 100 and 200 mg/Nm^3 K_3PO_4. In this work they will be identified by the labels "KP100" and "KP200" respectively. The letters "T" and "B" added at the end of the labels will indicate a sample cut respectively from the top (first 10 cm) and the bottom (last 10 cm) of the element. In all tests, the salt concentration in the solutions was fixed at 21 g/L and the solution feed rate was then varied in order to get the desired concentration in the flue gas (i.e. 0.25 and 0.5 L/h to get 100 and 200 mg/Nm^3 respectively).

2.4. Aerosol Measurements

2.4.1. Scanning Mobility Particle Sizer

A Scanning Mobility Particle Sizer (SMPS, TSI Inc.), which included an Electrostatic Classifier (Model 3080) and a Condensation Particle Counter (Model 3775) was used to measure the particle concentration and size distribution during the exposure to K_3PO_4. Particle sampling was carried out at the inlet of the SCR reactor by an ejector sampler running with dry, particle-free air. In this system the particle-containing flue gas was at the same time cooled and diluted thereby preventing: i) water condensation; ii) particle coagulation in the sample line by effectively decreasing its rate by several orders of magnitude; iii) overloading of both the impactor and the SMPS. The dilution ratio, required to know the real particle concentration in the flue gas, was obtained by measuring the CO_2 concentration both in the flue gas and in the diluted sample.

2.4.2. Low Pressure Cascade Impactor

A 10-stage Berner-type low pressure cascade impactor (LPI) with an aerodynamic diameter range of 0.03-12.7 μm connected to a vacuum pump was used. The flow through the LPI was controlled by a critical orifice and was equal to 22.49 L/min at 25°C and atmospheric pressure. The flue gas was sampled directly at the reactor inlet without any dilution. Therefore the sampling line and the LPI were heated to 90°C in order to avoid any water condensation. Deposited particles were collected on aluminum foils coated with a thin film of Apiezon H grease. The grease served to limit bouncing of the particles and was added using a dilute toluene solution of the grease. The toluene was evaporated from the foils by drying these in an oven at 140°C for 2 hours. The sampling time was equal to 60 minutes, which allowed a suitable collection of particle mass. The weight gains from the deposited particles on each foil were determined by a Sartorius M5D-000V001 microbalance. The foils were finally analyzed by electron dispersive X-ray analysis for chemical composition.

2.5. Activity Measurements

The rate of the SCR reaction at typical industrial reaction conditions has been assumed to follow an Eley-Rideal mechanism of reaction with NH_3 adsorbed on the catalyst surface and NO reacting from the gas phase. The following expression for the rate of reaction, r_{NO}, can then be derived:

$$-r_{NO}\left[\frac{mol}{m_{cat}^3 s}\right] = kc_{NO}\frac{K_{NH_3}c_{NH_3}}{1+K_{NH_3}c_{NH_3}} \qquad (1.3)$$

where k [1/s] is the rate constant, c_{NO} and c_{NH_3} [mol/m^3] are the concentrations of NO and NH_3 respectively, and K_{NH_3} [m^3/mol] is the adsorption constant for NH_3 on the catalyst surface. The fraction term on the right-hand side of equation (1.3) is the NH_3 coverage of the catalytic surface, θ_{NH_3}.

At the pilot plant, the activities of the catalysts were measured at 350°C in the presence of about 500 ppmv NO, 600 ppmv NH_3, 10%v O_2, 6%v CO_2, and about 10%v H_2O. During activity measurements the flow through the SCR reactor was kept at 40 Nm^3/h. At this flow the gas velocity in the channels were about 6.5 m/s at 350°C, similar to the velocities used at full scale applications. At this velocity, up to 50% external mass transfer limitations have been estimated.

Since ammonia in our measurements is added in excess with respect to NO (i.e. $NH_3/NO \approx 1.2$), the NH_3 coverage, θ_{NH_3}, can be assumed equal to 1 and the reaction rate can be regarded as pseudo-first order with respect to NO and zero order with respect to NH_3. Therefore, directly from the fractional NO conversion, X, it is possible to calculate an observed catalyst activity constant, k', that includes both the influence of external and internal mass transfer:

$$k' \left[\frac{ml}{g\ s} \right] = -\frac{F_{gas}}{m_{cat}} \ln(1-X) \qquad (1.4)$$

where F_{gas} is the gas flow rate (ml/s), m_{cat} is the weight of catalyst (g). The degree of deactivation can then be calculated as the ratio k/k_0 between the activity constant of the catalyst during exposure, k, and the one measured for the fresh element, k_0, right before starting the poison addition.

In the laboratory, powdered samples have been tested for activity in a packed bed quartz micro-reactor with a diameter equal to 10 mm. Around 0.07 g of powder has been used during activity measurement with a total flow equal to 2.8 NL/min constituted by 500 ppmv NO, 600 ppmv NH_3, 5%v O_2 and 1.4%v H_2O in N_2. Activity measurements have been performed in the temperature range 250-400°C. The catalyst activity has been calculated according to equation (1.4) and the deactivation as the ratio between the activity constant of the spent catalyst and the one measured for the fresh one. At 350°C, the observed activity constant, k', for the fresh catalyst powder was found only 10% less than the one calculated in the total absence of mass transfer limitations. The latter value was calculated by extrapolating to higher temperatures a fit to the Arrhenius plot obtained in the kinetic regime in the range 250-330°C.

During all activity measurements, the NO concentration in the flue gas has been measured with a conventional UV analyzer (Rosemount NGA 2000).

2.6. Ammonia Chemisorption

NH_3 chemisorption is the first step of the reaction mechanism [9,10], and poisoning by K has been found to decrease the amount of chemisorbed NH_3. Therefore, NH_3 chemisorption tests have been periodically carried out at the pilot scale setup during the K_3PO_4 addition. The measurements have been made at 350°C and 40 Nm^3/h. Around 600 ppmv NH_3 have

been added to the flue gas and flow through the SCR reactor for 30 minutes in order to saturate the catalyst sites. Previous investigations made with the same catalysts showed that this period of time is sufficient to saturate all the sites available for NH_3 chemisorption on a fresh element. During this saturation period, only the NO produced by the natural gas combustion was present (i.e. ≈ 80 ppmv). After this time, the NH_3 was shut off and right after, around 500 ppm NO were produced by adding a stream of NH_3 to the burner. The amount of chemisorbed NH_3 can then be calculated by integrating over time the amount of reduced NO, due to the equimolar reaction between the gaseous NO and the chemisorbed NH_3.

2.7. Catalyst Characterization

Small pieces of catalyst were cut from the ends of both fresh and exposed monoliths and characterized with respect to bulk chemical composition, mercury porosimetry and physical appearance by a Scanning Electron Microscope (SEM).

The chemical composition was obtained by ICP-OES at the laboratory of DONG Energy A/S. Prior to the measurements, the samples were cut to 1.5 x 1.7 cm^2 and dried at 105 °C for 2 h before analysis.

The total pore volume and the pore size distribution of the different catalyst samples were made by mercury intrusion in a Micromeritics Autopore II 9220 porosimeter. SEM-EDX analysis was performed at the Danish Technological Institute using a Zeiss Ultra55 and an Oxford ISIS with a Pentafet X-ray detector.

3. Results

3.1. Aerosol Measurements at the Pilot-scale Setup

3.1.1. SMPS Measurements

Figure 1 shows the number-based and volume-based particle size distributions measured during the addition of 100 mg/Nm^3 K_3PO_4. According to the number-based distribution, the aerosols were characterized by a peak at around 30 nm. However, when the volume-based distribution is plotted instead, a second peak at higher diameter appears. In particular, it can be seen in Figure 1b that this second peak almost entirely extends outside the upper detection limit of the SMPS used. By assuming a density for these particles equal to the density of K_3PO_4 (i.e. 2.564 g/cm^3), the total mass measured by the SMPS would be equal to around 8% of the injected one. This low value indicates that a great part of the injected mass is present at the larger diameters not detectable by the SMPS. By fitting the data obtained with a lognormal distribution, the curve showed in Figure 1b can be obtained. The fitting has been made by minimization of

$$\sum_{d_p}\left[\psi_{V,SMPS}(d_p)-\psi_{V,logn}(d_p)\right]^2 \qquad 300\ nm \le dp \le 550\ nm \qquad (1.5)$$

where $\psi_{V,SMPS}$ is the volume distribution *dV/d(log dp)* calculated from the SMPS measurement, $\psi_{V,logn}$ is the fitted distribution. The mean diameter of the lognormal

distribution is equal to 1.25 μm. Overall, the total mass calculated is equal to around 40% of the injected K_3PO_4. Both the mean diameter and the total mass at the reactor inlet would then be comparable to previous tests carried out at this setup [17]. As will be discussed later, the presence of this dual mode particle distribution is related to the presence of mainly two different species, whose formation has followed different mechanisms.

3.1.2. Cascade Low Pressure Impactor Measurements

Tests with the LPI have been performed during both the KP100 and KP200 experiments. In all cases, the particles collected at the different stages were very liquescent and were therefore melting as soon as they were exposed to ambient air. The determination of the weight of the different foils was therefore problematic. Not only the foils were increasing their weight due to water adsorption. Some of them were at some point even loosing weight during their mass determination. This fact indicates that during exposure to ambient air at room temperature some gaseous species were released by the deposit. Due to these problems, the only partly useful indications obtained from the tests were those provided by the EDX analysis of the different foils reported in Table 2. Here, values of the K:P molar ratio in the range 3-3.5 were measured, which are slightly higher than the expected value of 3. Interestingly, the K:P values were increasing with the collected particle size (apart from the value measured on stage #6). These values may differ from the expected value of 3 simply because experimental uncertainity of the EDX measurements, but, recalling the particle size distribution measured by the SMPS, they may also indicate that part of the P was not collected on the lower impactor stages, probably because the remaining fraction was present in even smaller particles or in the gas phase.

3.2. Catalyst Characterization

3.2.1. Bulk and Surface Chemical Analysis

Table 3 reports the results of both the bulk and surface chemical analysis for the elements KP100 and KP200. The K-content in the bulk was varying in the range 0.8-2.5 wt%, whereas the P-content was varying in the range 0.4-0.8 wt%. Apart from the K-content in KP200, both the levels of K and P found in the bulk of the two elements were decreasing from the top to the bottom in agreement with both the higher particle concentration and the higher mass transfer due to the developing flow and higher level of turbulence at the top. About double levels of K were found on KP100 compared to KP200, whereas the levels of P were roughly the same. The calculated bulk K:P molar ratios were in the range 0.85-2.52 and therefore less than 3, which is the value introduced into the system by the K_3PO_4 molecule, indicating a different path for the accumulation of K and P in the catalyst walls.
Regarding the external surface composition measured by SEM-EDX shown in Table 3, very high concentrations of P have been found. In particular, the element KP200 reported P-concentrations up to 12.6 %wt. In the case of KP100, the P-content was ranging between 1.0 and 2.8 %wt. The cross sections of the samples KP100B and KP200T shown in Figure 2 have also been analyzed by SEM-EDX in order to measure the distributions of K and P along the catalyst walls. The results of the EDX measurements are shown in Figure 3a and Figure 3c. As shown in the plots, both the K- and P-content decrease as a function of catalyst wall depth, indicating a diffusion limited proces. Only in the case of KP100B, the

K-content is almost constant around 0.7 %wt throughout the analyzed wall thickness. However, the major difference between the K- and P-distributions is that, in the case of K, the concentration in the walls always appears to level off at a finite K-level (i.e. 0.7 %wt in the cases shown in Figure 3a), whereas the P-concentration decreases to zero. From these profiles, it appears that K tends to penetrate and remain in the catalyst wall, whereas P either is characterized by a slower mobility compared to K, or its penetration is counterbalanced by simultaneous evaporation of P as it was shown in our previous study [22]. As expected, in the presence of higher total K_3PO_4 concentrations in the flue gas, both K and P tend to accumulate on the outer catalyst surface.
Finally, Figure 3b and Figure 3d shows the calculated values for the K:V and P:V molar ratios, which can be used to estimate the local activities of the catalyst wall. According to values found in the literature [11,12], for K:V molar ratios equal to 0.2, up to 70% deactivation in the absence of mass transfer limitations can be expected.

3.2.2. Hg-porosimetry

The pore size distribution of the fresh and spent catalysts has been measured in order to clarify the presence of physical deactivation by pore blocking due to deposition of K-P particles. Figure 4 reports the results of this investigation. The PSD of the fresh catalyst is clearly a dual-mode distribution, with the first peak found in the region 0.6-300 μm at 90 μm, and the second one in the region 0.003-0.6 μm at 0.03 μm. This dual mode distribution is basically conserved in all spent catalyst samples. No major differences indicating pore blocking are found between the fresh and spent samples apart from the region 0.6-8 μm. Here, the spent samples consistently show almost no pores, whereas the fresh one has a considerable amount of them. In particular, the porosity for the fresh sample in this diameter range has been calculated to be equal to 6.93%. This value dropped to 1.35 and 0.89% for KP100T and KP100B respectively, and 1.32 and 1.19% for KP200T and KP200B respectively. However, no major difference in the total intrusion volume of the spent catalysts compared to the fresh sample was found (Table 3). This fact may indicate that the sample outer wall layer, which is the first that gets in contact with Hg during the measurement, had no pores in that range due to deposit build-up and/or pore blocking, but kept the original structure of the inner wall.

3.3. Deactivation at the Pilot-scale Setup

3.3.1. Activity Measurements

The results of the activity measurements carried out during exposure to 100 and 200 mg/Nm^3 K_3PO_4 are shown in Figure 5. Overall the measured deactivation rate was increasing according to the K_3PO_4 concentrations in the flue gas. In both cases, the deactivation was very fast at the beginning of the exposure: The two elements lost respectively 26 and 31% of their original activity during the first 72 h. After this initial period, the deactivation proceeded at slower but still appreciable rates.
The addition of 100 mg/Nm^3 was carried out for 720 h. After this period of time, the element was exposed to *clean* flue gas for additional 288 h, before it was taken out and characterized. The relative activity at the end of the addition time was 62%, corresponding to an overall deactivation rate of about 1.3%/day. During the subsequent exposure to the

clean flue gas, the element regained 9% of relative activity. In particular, 7% was regained after the first 24 h after the addition was shut off. During these 24 hours, the pressure drop over the monolith decreased by 11% indicating some cleaning of the channels due to soot blowing, which was continued after the addition stopped.
The addition of 200 mg/Nm^3 was carried out for only 280 h and was more problematic than the previous test. Due to the higher K_3PO_4 load, the two-fluid nozzle used for atomizing the water solution tended to clog due to salt deposition. In particular, the compressed air line right at the meeting point with the liquid solution was the one that had the higher tendency in getting clogged. When this happened, the solution was not correctly atomized and was eventually introduced as a liquid jet. The jet was then simply hitting the hot pipe walls right after the lance and forming massive deposits of salt. Clogging of the nozzle mainly happened two times: After 89 and 284 h from the addition start. In both cases, the activity measurement performed after the clogging showed an increased relative activity of the element compared to the previous test. These facts are in agreement with the result obtained with the element KP100, when this latter was exposed to a *clean* flue gas as discussed before. Overall, at the end of the experiment, the element KP200 had lost 22% of its original activity. However, the minimum relative activity was measured after 284 h during the last activity measurement before the nozzle clogged for the second time. Here the relative activity was equal to 73%, corresponding to a deactivation rate equal to about 2.3 %/day.

3.3.2. NH_3 Chemisorption Tests

Figure 6 shows the results of NH_3 chemisorption tests made with the element KP100 and KP200 during the addition of K_3PO_4. Since the amount of reduced NO is assumed equal to the amount of NH_3 chemisorbed on the catalyst surface, a longer time for the NO measured at the outlet to equalize to the value measured at the inlet indicates that more NH_3 is chemisorbed on the catalyst. From Figure 6 it can be seen that the fresh element was able to chemisorb a higher amount of NH_3, and that this was decreasing as a function of the exposure to K_3PO_4. In particular, after 408 h of exposure the amount of chemisorbed NH_3 on KP100 was about 54% of the fresh one. After 720 h, this further dropped to 47%. These results indicate that the deactivation was proceeding by deactivation of the sites for the NH_3 chemisorption.

3.4. Activity Measurements in the Laboratory

Figure 7 shows the activity measurements made with powdered samples cut from the top and the bottom of the element KP100, together with a measurement made on a fresh catalyst. The plot only reports the results in the temperature range 250-400°C, where external and internal mass transfer have been estimated not to limit the observed reaction rate for the doped samples. Due to its very high activity, the fresh sample is subjected to some mass transfer limitations (i.e. ≈ 10% at 350°C).
As expected from the K- and P-content of the KP100 monolith, the top of the catalyst is more deactivated than the bottom. At 350°C the relative activities for the top and the bottom of the element are equal to 9.1% and 30.0% respectively.

4. Discussion

4.1. K- and P-accumulation and Penetration Mechanisms

The bulk chemical analysis of the catalyst composition has shown a K:P molar ratio less than the theoretical value of 3, varying in the range 0.85-2.5. The same ratio was always lower than 1 on the outer surface. Assuming a reaction between the catalyst surface and the K_3PO_4 particles leading to accumulation of K in the wall and release of H_3PO_4 in the gas phase, in a similar way as the release of HCl from KCl on the catalyst surface [3], the resulting K:P molar ratio should have then been found higher than 3. This fact is clearly in contrast with the results of the bulk chemical analysis and indicates that the deposited particles are not only constituted by K_3PO_4.

Further confirming this fact is the dual-mode particle size distribution measured by the SMPS. As discussed above, both particles with a volume-based mean diameter around 30 nm and particles with diameters exceeding the upper limiting range of the SMPS were present in the gas. Simply based on their size, the following can be assumed for these two classes of particles:

1. Low particle diameters and high number concentrations indicate particle formation due to homogeneous nucleation in the gas phase. In other words, the particles with mean diameters of 30 nm are constituted by species which can be found in the gas phase at relatively high temperatures. Contrarily, particles with diameters up 1 μm are more likely formed due to salt crystallization during water evaporation from the atomized aqueous solution according to their different solubilities.
2. The deposition rate of the smaller particles is higher due to the higher diffusion coefficients for these particles. In the presence of differences in the chemical composition as a function of particle size, the element characterizing the population with the higher number concentration and smaller particle diameters will accumulate faster on the catalyst surface.

In the absence of a detailed determination of the particle chemical composition due to the encountered experimental limitations, the scenario plotted in Figure 8 is proposed.

1. *Condensate phosphates formation*. Potassium phosphate salts are reported to form condensate phosphates [25], here referred to as "KPO_x":

$$2\,K_3PO_4 \rightarrow K_4P_2O_7 + K_2O \qquad (1.6)$$

$$K_4P_2O_7 + K_3PO_4 \rightarrow K_5P_3O_{10} + K_2O \qquad (1.7)$$

   From these reactions K_2O is formed. According to equilibrium calculations performed in this work by using the commercial software FactSage 5.2, the formed K_2O will be converted to KOH by reacting with the flue gas moisture. At lower temperatures K_2CO_3 will be formed by reaction with CO_2.
2. *KH_2PO_4 formation*. Crystallization of salts which are not the thermodynamic stable phases under the conditions of crystallization is reported to be rather common for the potassium orthophosphate system [25]. This means that the salts formed during the fast water evaporation from every single K_3PO_4 solution drop sprayed into the flue gas may differ from the initial K_3PO_4. Table 4 shows the known P-K salts and

their solubility in water. In this, the solubility for KOH is also reported. As it can be seen, KH_2PO_4 is the salt with the lowest solubility. This indicates that this compound is the first that precipitates when water evaporates from a drop in the hot flue gas. The remaining K, which is not bound to the formed KH_2PO_4 will later precipitate as KOH. Part of the P may also lead to some H_3PO_4. After water evaporation, the formed aerosols will be heated by the surrounding flue gas, and both the formed KH_2PO_4 and KOH are then converted to the more stable K_2HPO_4 and K_2CO_3. At temperatures higher than 465°C the K_2HPO_4 will finally decompose. This decomposition may lead to formation of gaseous H_3PO_4 and solid K_2CO_3 by reaction with CO_2.

Both of these two scenarios foresee the formation of H_3PO_4, KPO_x, K-P-salts with K:P molar ratios lower than 3 and some K_2CO_3, at the expenses of some of the original K_3PO_4. Among these species, H_3PO_4 can be regarded as responsible for the formation of the aerosols with mean diameter equal to 30 nm. Similar results have in fact been obtained during our previous investigation [22]. In this way, the high P-content on the outer catalyst surface measured by SEM-EDX would be explained, since it would be due to the higher deposition rates for these small particles compared to the bigger ones, where K is concentrated. Regarding the presence of K_2CO_3, this cannot be proved by the tests carried out in this work. However, the relatively high K:P molar ratios measured on the impactor stages may be considered as an indication of the presence of P-free K-particles. Moreover, it can be argued that the gas released by the deposits collected with the impactor was CO_2. Most of the compounds present in Figure 8 are deliquescent, and therefore form a liquid solution when exposed to the ambient air, in agreement with the experience of the collected deposits. In this liquid solution then, release of CO_2 could be possible due to recombination of the species in the liquid phase, and could be favoured by the presence of acid compounds like the polyphosphoric acids.

The SEM-EDX of the catalyst wall cross sections indicate a faster net penetration for K compared to the one measured for P. Even though there still is an uncertainty about the real composition of the aerosols involved in the performed tests, and the presence of different species have been assumed, these different penetration rates are not likely associated to the presence of different species with different particle sizes and mobilities in the solid state. These are instead more likely associated with the different affinities between the elements K and P towards the acidic surface of the catalyst. It is here assumed that *solid-state acid-base reactions* are the major driving force responsible for reaction between the K-atoms from the particles and the catalyst surface. Since particles are deposited at the outer layers of the catalyst walls, a K-surface-gradient in the wall is first formed. This gradient is then responsible for the further penetration/distribution of the K-atoms by *surface diffusion*. On the other hand, P is included in acidic compounds. Consequently, acid-base reactions between the P-containing particles and the catalyst surface are not expected. The penetration of P is then mainly controlled by capillary forces applied on the viscous liquid phase the polyphosphoric acids are made of, and possibly K-P solid particle diffusion in the external layers of the catalyst walls. Furthermore, considering that the PO_x are hydrolyzed by the flue gas moisture at the reactor temperature releasing gaseous H_3PO_4 [22], the P-concentration in the wall will approach zero as observed. This would in fact be the result of

combined particle deposition and P-evaporation. The P which is included in K-P salts might also leave the particle as H_3PO_4 when the K reacts with the catalyst surface.

4.2. Deactivation Mechanism

The exposure of the commercial monoliths used in this work to a flue gas containing aerosols of K- and P-species has rapidly lowered the activity of the tested elements. In the absence of particles, the deactivation did not continue any further. On the contrary, when the exposure was performed without any K_3PO_4 addition, some reactivation of the catalysts was observed (9%). These facts indicate that (i) the aerosols are necessary to get any deactivation; (ii) reversable physical deactivation by outer surface fouling is contributing to the measured deactivation. According to the K-content measured by SEM-EDX analysis and the activity measurements made on powders, an agreement with the poisoning data from the literature has been found. For instance, the SEM-EDX analysis for the sample KP100B showed a constant K:V value of 0.2 along the whole wall. For the same sample, the relative intrinsic activity measured on powder was equal to 30% at 300°C (Figure 7), in good agreement with previous studies of K-poisoning [11, 12]. This fact and the results of the NH_3 chemisorption tests indicate that the deactivation measured is mainly due to poisoning by K via blocking of the active sites for NH_3 chemisorption as reported in previous works [3,11-15]. The influence of poisoning by polyphosphoric acid is in this work not significant due to: (i) the relative low levels of P found due to simultaneous hydrolysis of the deposited acids; (ii) their relative low poisoning strength compared to K; (iii) a possible lowering of the deactivation strength of the polyphosphates due to the presence of K.

Physical deactivation due to pore blocking or surface masking by particle deposition is not likely to be the main mechanism responsible for the deactivation measured, but it is clearly contributing to the overall deactivation as indicated by the partial reactivation obtained by exposing the spent monoliths to clean flue gas while soot blowing. In particular, the almost complete disappearance of the pores in the range 0.6-8 μm for all the spent catalysts, together with the small loss (i.e. 6%) of the total intrusion volume are indications of the formation of an outer fouling layer. With up to 12 %wt P found on the outer catalyst surface, and since the polyphosphoric acids are viscous liquids at the SCR temperature [22], it is believed that they are playing an important role in the formation of this fouling layer by gluing togheter the different deposited particles. In general, an efficient soot blowing system is required not only to keep the channels opened, but also to clean their external surface.

5. Conclusion

K_3PO_4 has been indicated as a potential product of combustion of biomass mixed with P- and Ca-based K-getter additives for reducing fouling and corrosion problems on superheater surfaces at power stations. In order to evaluate whether the formation of this compound might also have a positive effect on the vanadia-based SCR catalysts by limiting the fast fast rate of deactivation normally experienced with KCl or K_2SO_4, K_3PO_4 has been added in a hot flue gas at a SCR pilot scale setup and the activity of two commercial vanadia-based monoliths has been followed as a function of exposure time.

During the performed tests, different K- and P-compounds have been formed from the originally injected K_3PO_4. A dual-mode volume-based particle distribution with peaks at around 30 nm and at diameters > 1 μm has been measured at the SCR reactor inlet. The distribution of K and P in the different particles has thereby influenced the rate of deposition and accumulation of the species in the exposed catalysts. In order to explain the high P-concentrations and low K:P molar ratios found on the outer catalyst surface, the smaller particles have been associated with liquid phase phosphates (PO_x and KPO_x), whereas the larger ones have been associated to potassium phosphates formed during evaporation of water from the injected droplets.
Deactivation rates up to 3%/day have beeen measured. K has been found to penetrate the whole catalyst wall indicating that this is not strongly bound to the particles and relatively fast reacts with the catalyst surface and subsequently penetrates the catalyst wall by surface diffusion. The NH_3 chemisorption studies have shown that the deactivation has mainly proceeded via K-poisoning by blocking the sites for NH_3 adsorption. All these data recall the mechanism of deactivation previously reported during exposures to KCl and K_2SO_4 and therefore indicate that binding K to P by the addition process does not seem to be an advantageous solution with respect to the vanadia-based SCR catalysts.
Poisoning by polyphosphoric acids is not clearly seen in this investigation due to both the relatively low P-content in the catalyst and the low poisoning strenght compared to K. However, Hg-porosimetry has revealed the occurrence of fouling and pore mouth blocking at the outer catalyst surface. It is believed that the polyphosphoric acids play an important role in the formation of this layer by gluing together the deposited particles and should therefore be considered a fouling promoter.

Acknowledgments

This work is part of the CHEC (Combustion and Harmful Emission Control) Research Center funded a.o. by the Technical University of Denmark, the Danish Technical Research Council, the European Union, the Nordic Energy Research, Dong Energy A/S, Vattenfall A.B., F L Smidth A/S, and Public Service Obligation funds from Energinet.dk and the Danish Energy Research program. In particular, this work is supported by the PSO project "Deactivation of SCR Catalysts by Additives" (PSO Elkraft FU-4205). Supply of the catalyst samples by Haldor Topsøe A/S is gratefully acknowledged.

References

[1] L.L. Baxter, T.R. Miles, T.R. Miles Jr., B.M. Jenkins, T. Milne, D. Dayton, R.W. Bryers, L.L. Oden, Fuel Processing Technology 54 (1998) 4778.
[2] K.A. Christensen, H. Livbjerg, Aerosol Science and Technology 25 (1996) 185-199.
[3] Y. Zheng, A.D. Jensen, J.E. Johnsson, Applied Catalysis B: Environmental 60 (2005) 261-272.
[4] Å. Kling, C. Andersson, Å. Myringer, D. Eskilsson, S.G. Järås, Applied Catalysis B: Environmental 69 (2007) 240-251
[5] L. Tobiasen, R. Skytte, L.S. Pedersen, S.T. Pedersen, M.A. Lindberg, Fuel Processing Technology 88 (2007) 1108-1117.

[6] L. Sørensen, J. Fjellerup, U. Henriksen, International Publication Number WO 01/05911 A2 (2001).
[7] P.A. Jensen, L.H. Sørensen, G. Hu, J.K. Holm, F. Frandsen, U.B. Henriksen. Technical University of Denmark (2005) KT-Report No. 0504.
[8] V.I. Parvulescu, P. Grange, B. Delmon, Catalysis Today 46 (1998) 233-316.
[9] N.-Y. Topsøe, H. Topsøe, J.A. Dumesic, Journal of Catalysis 151 (1995) 226-240.
[10] N.-Y. Topsøe, J.A. Dumesic, H. Topsøe, Journal of Catalysis 151 (1995) 241-252.
[11] J.P. Chen, M.A. Buzanowski, R.T. Yang, J. Air Waste Manage. Assoc. 40 (1990) 1403-1409.
[12] J.P. Chen, R.T. Yang, Journal of Catalysis 125 (1990) 411-420.
[13] L. Lietti, P. Forzatti, G. Ramis, G. Busca, F. Bregani, Applied Catalysis B: Environmental 3 (1993) 13-35.
[14] H. Kamata, K. Takashi, C.U.I. Odenbrand, Journal of Molecular Catalysis A: Chemical 139 (1999), 189-198.
[15] R. Khodayari, C. Andersson, C.U.I. Odenbrand, L.H. Andersson, in: Proceeding of the Fifth European Conference on Industrial Furnace and Boilers, vol. II, 11-14 April 2000, Espinho, Porto, Portugal, 2000.
[16] Y. Zheng, A.D. Jensen, J.E. Johnsson, Ind. Eng. Chem. Res. 43 (2004), 941-947.
[17] Y. Zheng, A.D. Jensen, J.E. Johnsson, Applied Catalysis B: Environmental 83 (2008) 186-194.
[18] J.A. Moulijn, A.E. van Diepen, F. Kapteijn, Applied Catalysis A: General 212 (2001) 3–16.
[19] J. Blanco, P. Avila, C. Barthelemy, A. Bahamonde, J.A. Odriozola, J.F. Garcia de la Banda, H. Heinemann, Applied Catalysis 55 (1989) 151-164.
[20] H. Kamata, K. Takahashi, C.U.I. Odenbrand, Catalysis Letters 53 (1998) 65-71.
[21] J. Beck, J. Brandenstein, S. Unterberger, K.R.G. Hein, Applied Catalysis B: Environmental 49 (2004) 15-25.
[22] F. Castellino, S.B. Rasmussen, A.D. Jensen, J.E. Johnsson, R. Fehrmann, Applied Catalysis B: Environmental 83 (2008) 110-122.
[23] J. Beck, R. Müller, J. Brandenstein, B. Matschenko, J. Matschke, S. Unterberger, K.R.G. Hein, Fuel 84 (2005) 1911-1919.
[24] J. Beck, S. Unterberger, Fuel 86 (2007) 632-640.
[25] J.R. Van Wazer. Phosphorus and Its Compounds, Interscience Publisher, New York, 1958.

Figure Captions

Figure 1: Number-based (a) and volume-based (b) particle size distributions measured by SMPS at the reactor inlet during addition of 100 mg/Nm^3 K_3PO_4. T = 350°C.
Figure 2: SEM picture of the cross section of KP100B (a) and KP200T (b).
Figure 3: K- and P-content and K:V and P:V molar ratios along the KP100B and KP200T walls as measured by SEM-EDX.
Figure 4: Pore size distribution for fresh and spent samples measured by Hg-porosimetry.
Figure 5: Relative activity as a function of exposure time. Total flow: 40 Nm^3/h. Gas composition: NO = 500 ppmv, NH_3 = 600 ppmv, O_2 = 10%v, CO_2 = 6%v, and 10%v H_2O in N_2.
Figure 6: NH_3 chemisorption test for the element exposed to 100 mg/Nm^3 K_3PO_4 at different times during the exposure.
Figure 7: Activity measurements on powder samples. Total flow: 2.8 NL/min. NO = 521 ppmv, NH_3 = 622 ppmv, O_2 = 5.2%, H_2O = 1.47%, N_2 balance. Catalyst mass W = 0.072 g.
Figure 8: Possible reactions during heating of K_3PO_4 solution droplets. The compounds in bold boxes are the ones most likely found at the SCR reactor inlet.

Table 1: Possible products of biomass combustion and relative melting temperatures in the presence of K-getter fuel additives.

	T_m, °C
$K_4P_2O_7$	1105
$K_2CaP_2O_7$	1143
K_3PO_4	1340
$KCaPO_4$	1560
$K_4Ca(PO_4)_2$	1645
$Ca_3(PO_4)_2$	1670

Table 2: K- and P-content measured on different impactor stages by EDX. The particles were collected during addition of 100 mg/Nm3 K_3PO_4.

Impactor stage number	**Particle Diameter, nm**	**K, a%**	**P, a%**	**K/P molar**
4	1488	47.31	13.8	3.48
5	754	51.22	15.39	3.33
6	382	48.66	16.65	2.92
7	193	48.49	14.82	3.27
8	98	47.49	14.8	3.21
9	49	44.08	14.71	3.00

Table 3: Bulk, surface and Hg-porosimetry analysis for the fresh and spent monoliths.

	Fresh	**KP100T**	**KP100B**	**KP200T**	**KP200B**
Total exposure time, h		720	720	189*	189*
Bulk chemical analysis					
V, % wt/wt	1.60	2.46	1.61	1.76	2.70
K, % wt/wt	0.0	2.45	1.44	0.80	0.90
P, % wt/wt	0.01	0.77	0.46	0.75	0.40
K/P, mol/mol		2.52	2.46	0.85	1.79
K/V, mol/mol		1.30	1.17	0.59	0.44
P/V, mol/mol		0.31	0.47	0.70	0.24
Surface chemical analysis					
V, % wt/wt	2.1	2.1	3.5	2.4	2.2
K, % wt/wt	0.0	1.7	0.8	6.2	2.1
P, % wt/wt	0.0	2.8	1.0	12.6	6.2
K/P, mol/mol		0.5	0.7	0.4	0.3
K/V, mol/mol	0.0	1.1	0.3	2.7	1.2
P/V, mol/mol	0.0	2.2	0.5	7.1	4.5
Hg porosimetry					
Total Intrusion Volume, ml/g	0.71	0.71	0.67	0.67	0.64
Total Pore Area, m^2/g	36.84	37.04	37.65	48.66	39.46
Catalyst Bulk Density, g/ml	0.96	0.94	1.01	1.03	1.11
Porosity, %	68.60	66.92	67.66	69.64	70.78

*) This exposure time does not include the lance blocking.

Table 4: Solubility and melting temperature for different K-species.

	Solubility g/100 g H_2O	**Melting Temperature ℃**
K_3PO_4	106	1340
K_2HPO_4	168	dec.
KH_2PO_4	25	253
KOH	121	406
K_2CO_3	111	891

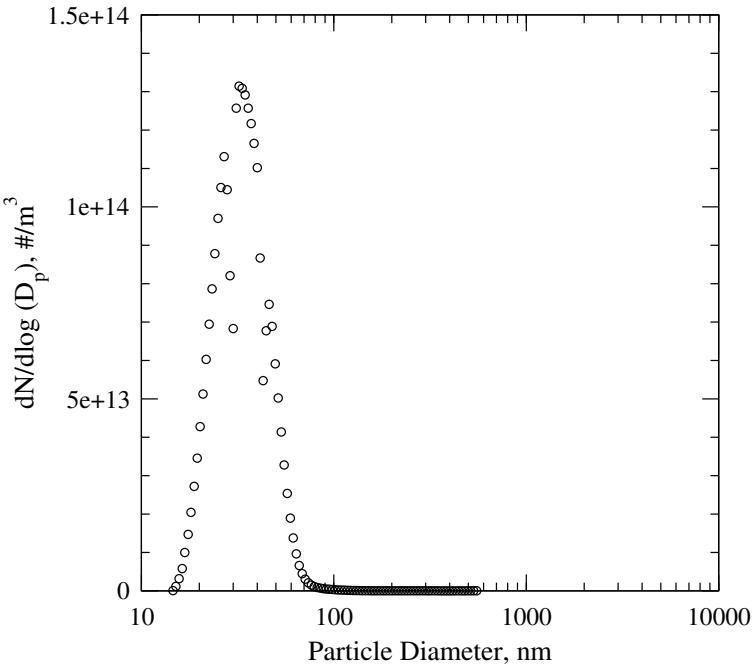
1.5e+14
1e+14
5e+13
0
dN/dlog (D_p), #/m^3
10
100
1000
10000
Particle Diameter, nm

a)

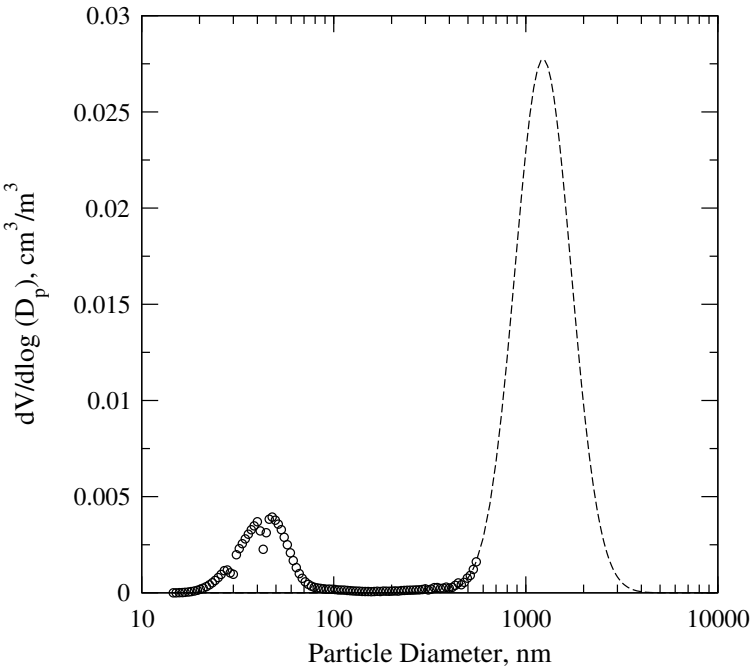
0.03
0.025
0.02
0.015
0.01
0.005
0
dV/dlog (D_p), cm^3/m^3
10
100
1000
10000
Particle Diameter, nm

b)

Figure 1

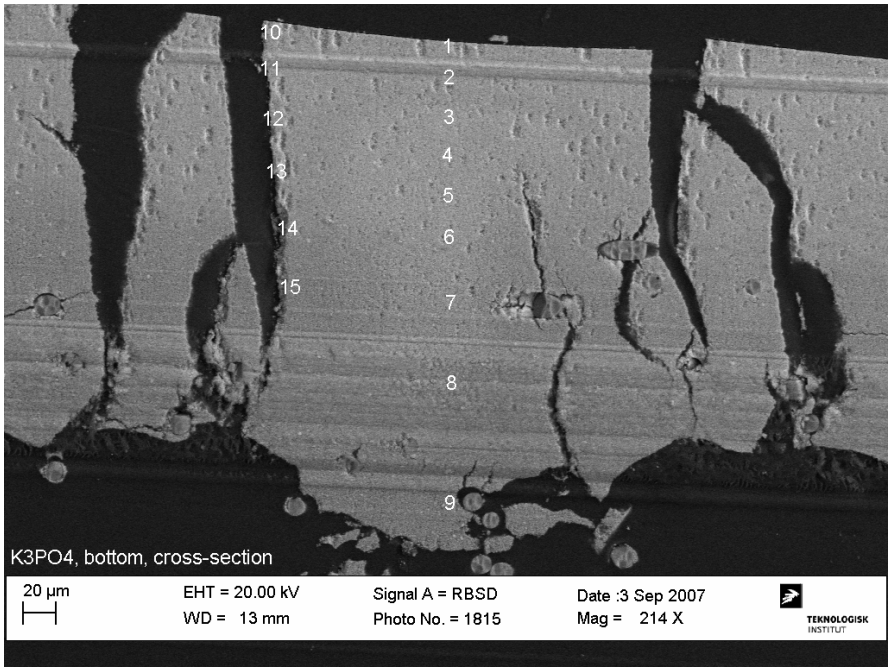
10
11
12
13
14
15
1
2
3
4
5
6
7
8
9
K3PO4, bottom, cross-section
20 µm
EHT = 20.00 kV
WD = 13 mm
Signal A = RBSD
Photo No. = 1815
Date :3 Sep 2007
Mag = 214 X
TEKNOLOGISK INSTITUT

a)

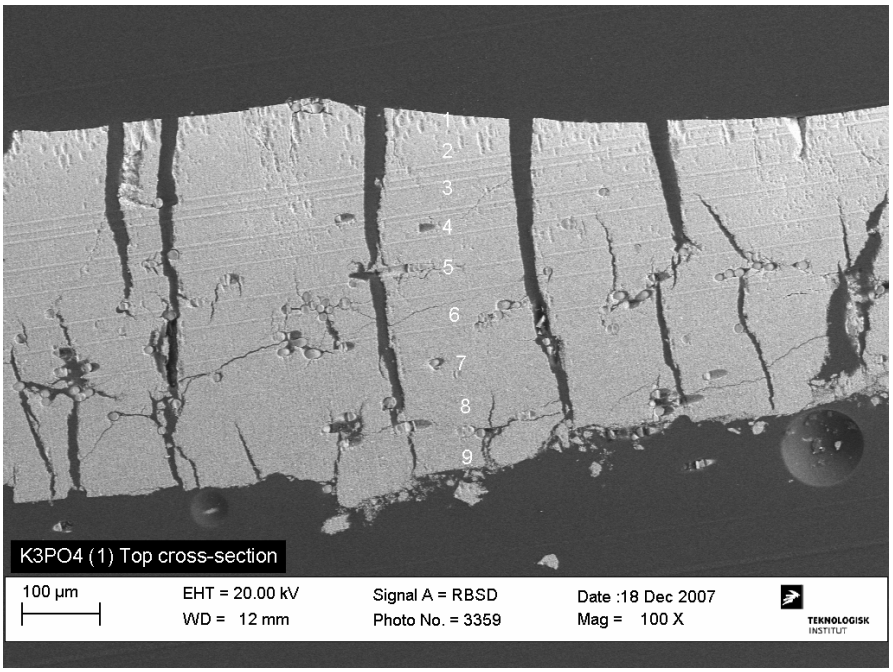
1
2
3
4
5
6
7
8
9
K3PO4 (1) Top cross-section
100 µm
EHT = 20.00 kV
WD = 12 mm
Signal A = RBSD
Photo No. = 3359
Date :18 Dec 2007
Mag = 100 X
TEKNOLOGISK INSTITUT

b)

Figure 2

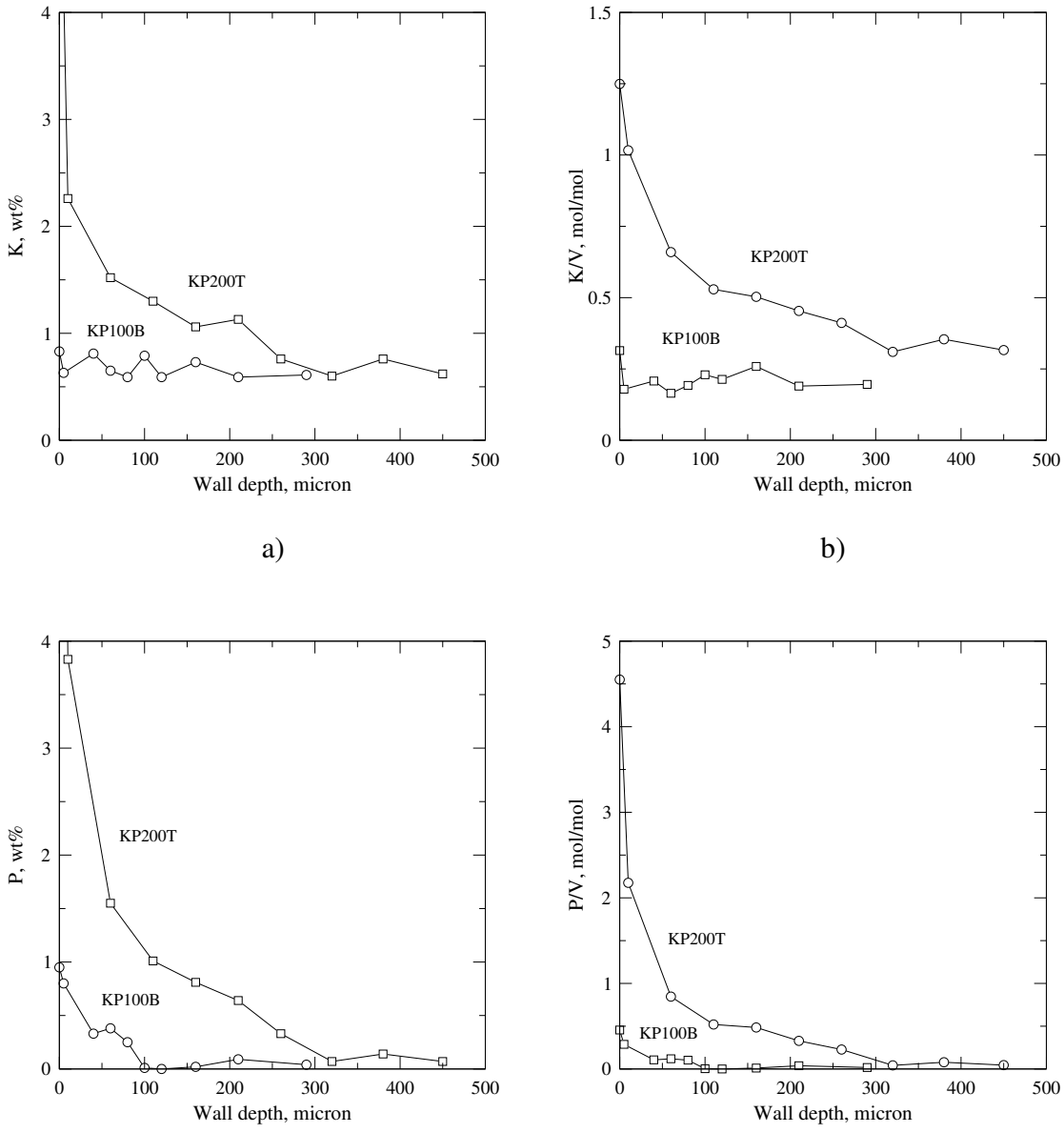
K, wt%
Wall depth, micron
KP200T
KP100B
a)
K/V, mol/mol
Wall depth, micron
KP200T
KP100B
b)
P, wt%
Wall depth, micron
KP200T
KP100B
c)
P/V, mol/mol
Wall depth, micron
KP200T
KP100B
d)

Figure 3

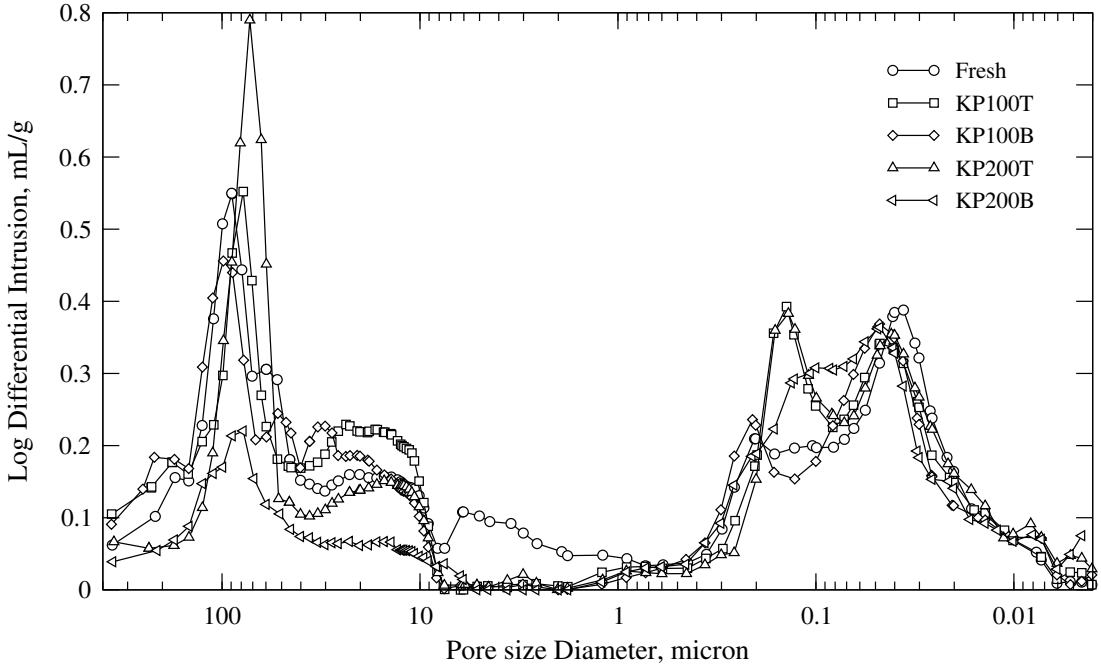
Log Differential Intrusion, mL/g
0.8
0.7
0.6
0.5
0.4
0.3
0.2
0.1
0
100
10
1
0.1
0.01
Pore size Diameter, micron
Fresh
KP100T
KP100B
KP200T
KP200B

Figure 4

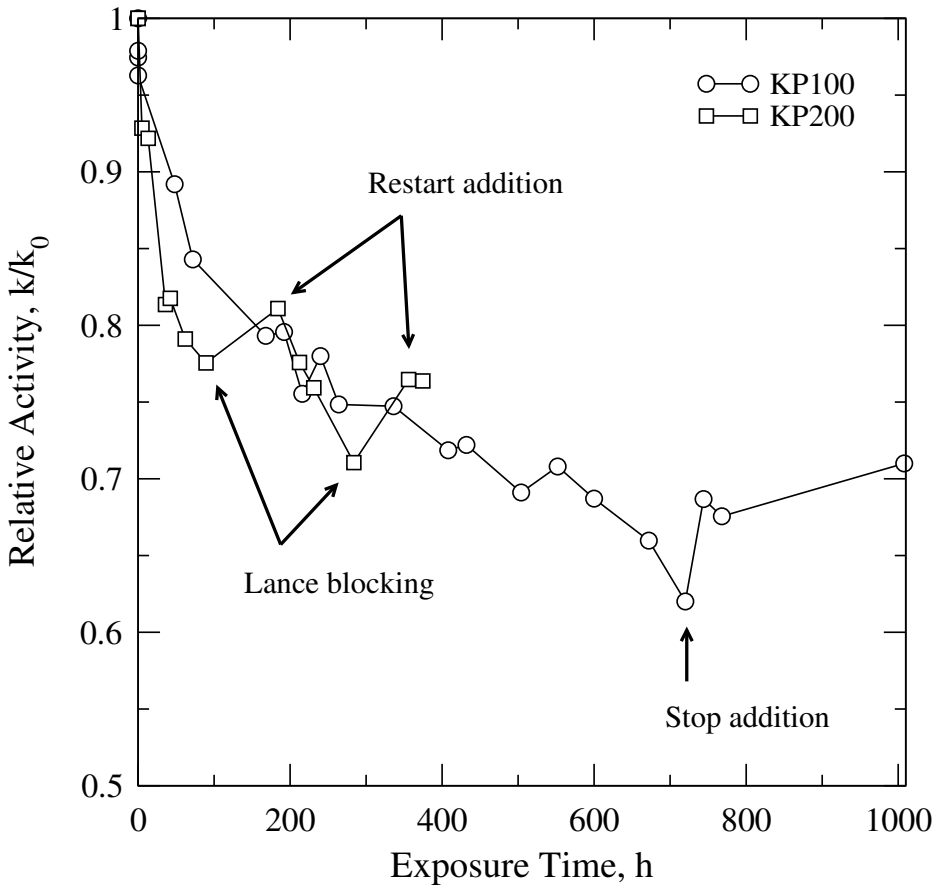
KP100
KP200
Restart addition
Lance blocking
Stop addition
Relative Activity, k/k0
Exposure Time, h
1
0.9
0.8
0.7
0.6
0.5
0
200
400
600
800
1000

Figure 5

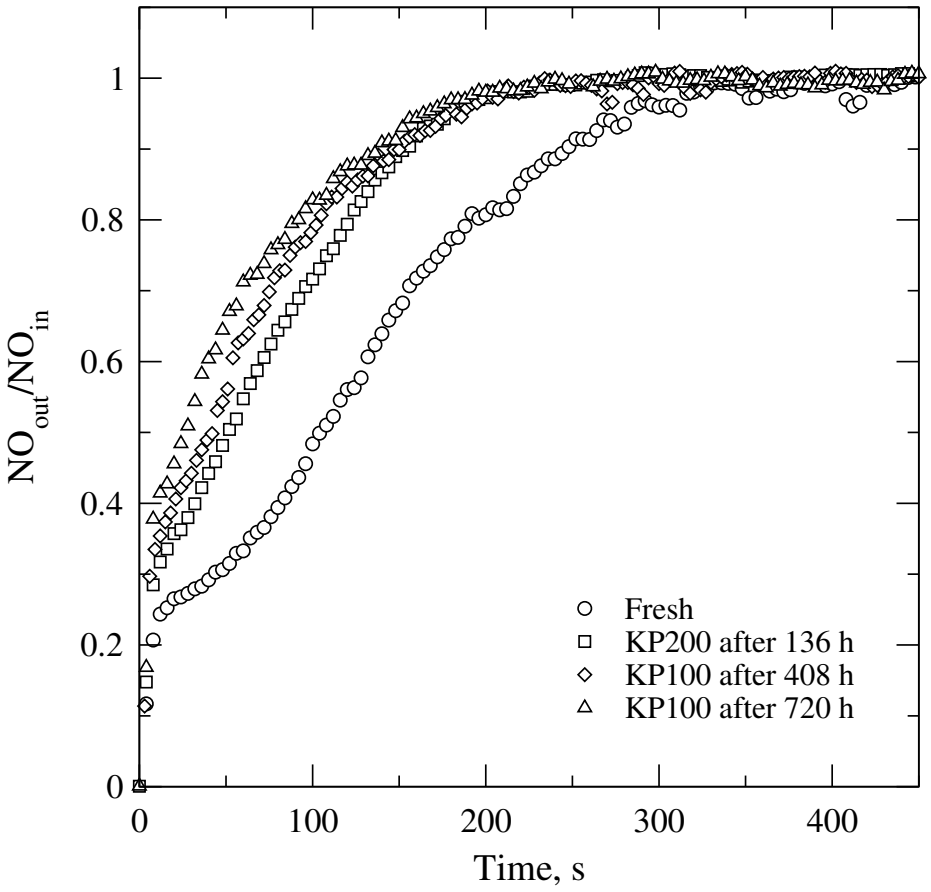
1
0.8
0.6
0.4
0.2
0
0
100
200
300
400
Time, s
NO_out/NO_in
Fresh
KP200 after 136 h
KP100 after 408 h
KP100 after 720 h

Figure 6

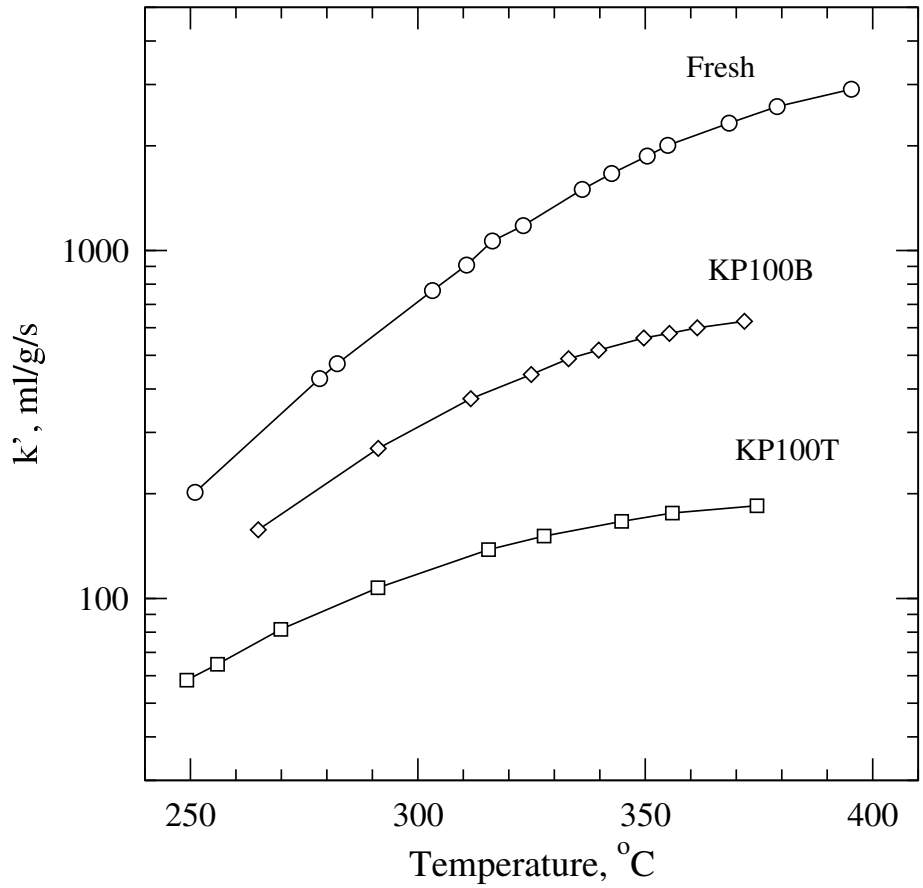
Fresh
KP100B
KP100T
1000
100
k', ml/g/s
250
300
350
400
Temperature, °C

Figure 7

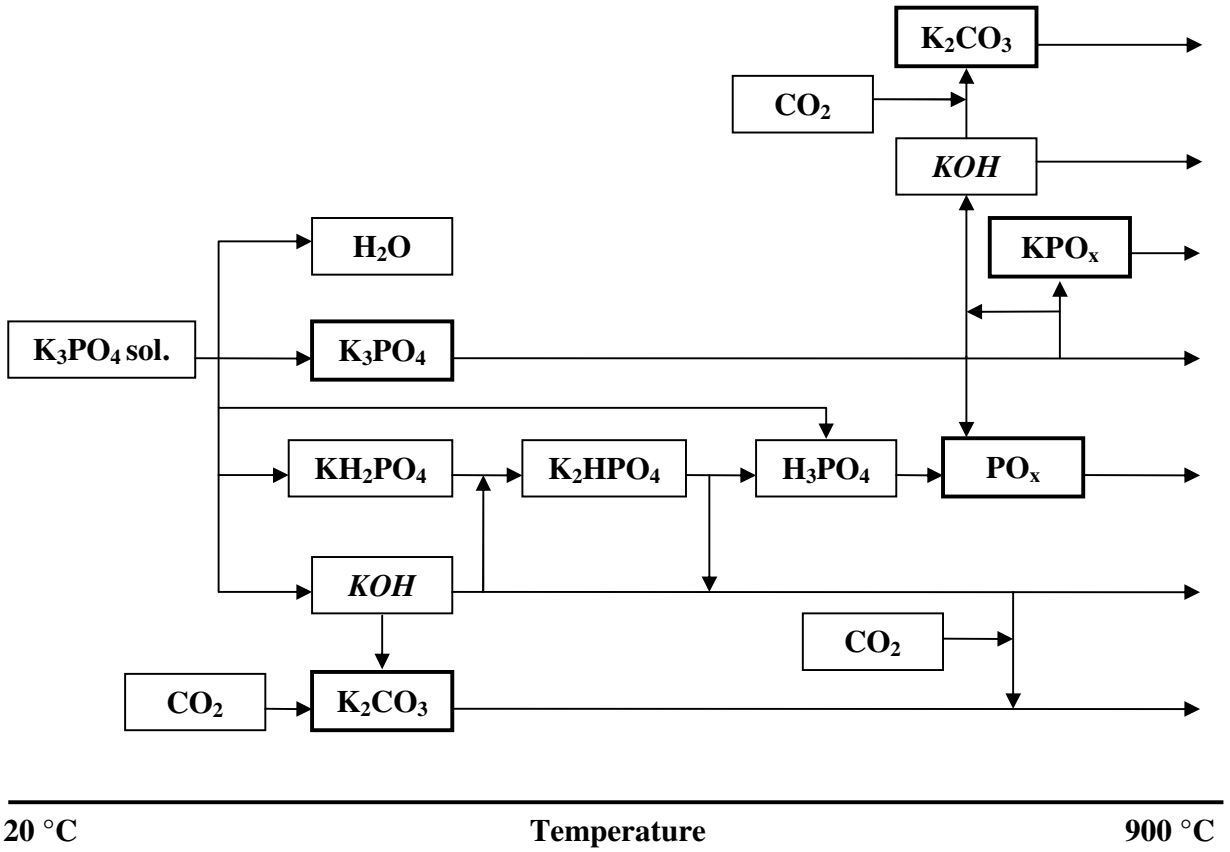
K2CO3
CO2
KOH
H2O
KPOx
K3PO4 sol.
K3PO4
KH2PO4
K2HPO4
H3PO4
POx
KOH
CO2
CO2
K2CO3
20 °C
Temperature
900 °C

Figure 8

Appendix D

Paper III

This report has been submitted to the peer-reviewed international journal *Applied Catalysis B: Environmental.*

Influence of Reaction Products of K-getter Fuel Additives on Commercial Vanadia-based SCR catalysts

Part II: Simultaneous Addition of KCl, $Ca(OH)_2$, H_3PO_4 and H_2SO_4 in a Hot Flue Gas at a SCR Pilot-scale Setup

Francesco Castellino, Anker Degn Jensen[1], Jan Erik Johnsson, Rasmus Fehrmann[a]

Department of Chemical Engineering, Technical University of Denmark, Building 229, DK-2800 Kgs. Lyngby, Denmark
[a]Center for Sustainable and Green Chemistry, Department of Chemisty, Technical University of Denmark, Building 207, DK-2800 Kgs. Lyngby, Denmark

Abstract

A commercial V_2O_5-WO_3-TiO_2 corrugated-type SCR monolith has been exposed for 1000 hours in a pilot-scale setup to a flue gas doped with KCl, $Ca(OH)_2$, H_3PO_4 and H_2SO_4 by spraying a water solution of the components into the hot flue gas. The mixture composition has been adjusted in order to have P/K and P/Ca ratios equal to 2 and 0.8 respectively. At these conditions, it is suggested that all the K released during biomass combustion gets captured in P-K-Ca particles and the Cl is released in the gas phase as HCl, thus limiting deposition and corrosion problems at the superheater exchangers during biomass combustion. Aerosol measurements carried out by using a SMPS and a low pressure cascade impactor have shown two distinct particle populations with volume-based mean diameters equal to 12 and 300 nm, respectively. The small particles have been associated to polyphosphoric acids formed by condensation of H_3PO_4, whereas the larger particles are due to P-K-Ca salts formed during evaporation of the water solution. No Cl has been found in the collected particles. During the initial 240 h of exposure, the catalyst element lost about 20 % of its original activity. The deactivation then proceeded at slower rates, and after 1000 h the relative activity loss had increased to 25 %. Different samples of the spent catalyst have been characterized after 453 h and at the end of the experiment by bulk chemical analysis, Hg-porosimetry and SEM-EDX. NH_3-chemisorption tests on the spent elements and activity tests on catalyst powders obtained by crushing the monolith have also been carried out. From the characterization, it was found that neither K nor Ca were able to penetrate the catalyst walls, but only accumulated on the outer surface. Poisoning by K has then been limited to the most outer catalyst surface and did not proceed at the fast rates known for KCl. This fact indicates that binding K in P-K-Ca compounds is an effective way to reduce the influence of alkali metals on the lifetime of the vanadia-based SCR catalysts. On the other hand, P-deposition was favoured by the formation of the polyphosphoric acids, and up to 1.8 %wt. P was found in the catalyst walls. Deactivation by polyphosphoric acids proceeded at about 0.2 %/day and finally accounted for about 8 % of the overall deactivation. However, the measured relative

[1] Corresponding author. Telephone: +45 45 25 28 41. Fax: +45 45 88 22 58. E-mail: aj@kt.dtu.dk.

activity reached a steady state level during the last 240 h of exposure indicating that the P-concentration in the bulk reached a saturation level due to simultaneous hydrolisys of the polyphosphoric acids.
Keywords: SCR, deactivation, vanadia, KCl, polyphosphoric acid, biomass.

1. Introduction

As described in Part I of this work [1], changes in the fly ash composition during biomass combustion are seen as a potential solution to both deposition and corrosion problems encountered on the super-heaters at power plants. These problems are mainly due to the formation of KCl aerosols experienced during biomass combustion, which are formed during cooling of the flue gas. The above mentioned changes in the ash composition may involve the addition of P- and Ca-compounds in the boiler in order to create the reacting conditions at which (i) the K released by the biomass during combustion is captured in P-K-Ca compounds having higher melting temperatures than KCl; and (ii) the Cl is released in the gas phase as HCl. Initial tests on P-Ca additives have shown up to 74-98% reduction in the Cl content of the deposits when the molar ratios of P/(K+Na) and P/Ca in the resulting fuel mixture were in the ranges 1.9-3.2 and 0.8-0.9 respectively [2]. For instance, similar values may be obtained by cofiring straw with about 13% meat and bone meal (MBM) on an energy basis.

The addition of these P- and Ca-compounds during biomass combustion and the corresponding changes in both ash load and composition may also have a beneficial effect on the fast SCR catalyst deactivation normally experienced during biomass combustion [3,4]. Here K, which is known as one of the strongest poisons for the vanadia-based catalysts normally used in the SCR process [5-11], once deposited as submicron particles of KCl and K_2SO_4, is found to easily diffuse inside the catalyst wall and thereby deactivate the active sites. The diffusion of K, as shown in Part I of this work, apart from being related to the submicron particles, is directly dependent on how strongly K is bound to the particle itself. In this sense, capturing K into P-K-Ca particles may decrease the amount of K that is released to the catalyst surface and deactivate it. These particles will in fact have higher melting temperatures and potentially a higher stability.

On the other hand, both Ca and P are known as deactivating compounds for the vanadia-based SCR catalysts [5,6,12-15]. Having a relatively weak poisoning strenght, Ca is normally considered as a physically deactivating specie since during combustion it forms very stable compounds constituting the fly ash, which tend to block the pore structure of the catalyst wall. Furthermore, sulfation of the deposited Ca is often referred to form a fouling layer on the outer catalyst surface. On the other hand, P may act both as chemical and physical deactivating species according to the compounds it may form during combustion. When polyphosphoric acids (PO_x) are formed, physical deactivation by pore blocking and surface masking is enhanced by the liquid viscous nature of these compounds. Furthermore, chemical deactivation at high concentrations (i.e. >100 ppmv) may be very fast and involves blocking of the catalytic cycle via formation of non-active V(4+) species [15]. Increasing the concentration in the flue gas of P and Ca by the addition process, which as stated above may require an excess of both species, may then lead to undesired deactivating effects. This may counterbalance the possible positive effects obtained by binding K into P-K-Ca particles.

The aim of this study is to evaluate the potential effects of the P, Ca addition process on the SCR catalysts by exposing a commercial vanadia-based SCR monolith to a flue gas

doped with K, Ca and P for 1000 hours and following its activity as a function of exposure time.

2. Experimental

A water solution of KCl, $Ca(OH)_2$, H_3PO_4 and H_2SO_4 has been injected in a hot flue gas (T > 900°C) from a natural gas burner. The resulting flue gas was then passed over a commercial SCR monolith, and the activity was periodically measured.
Both the setups and experimental procedures employed in the tests reported in this paper are the same as those described in Part I of this work, and are here only briefly introduced. For further details, see ref. [1].

2.1. Catalysts

Commercial corrugate-type monoliths obtained from Haldor Topsøe A/S were used in this study. The catalysts were based on V_2O_5 (up to 5 wt%) and tungsten oxide (WO_3, up to 9 wt%) dispersed on a fiber reinforced TiO_2 carrier. The monoliths had a size of 75 mm x 75 mm x 500 mm. The hydraulic diameter of the channels was 6.44 mm and the wall thickness of about 1.0 mm. Pieces of both the fresh and spent monoliths have been cut from the spent monolith in order to study their local properties under well defined reaction conditions in a laboratory fixed bed reactor. In order to run activity tests on powder samples, they have been gently crushed in a mortar and the particle fraction in the range 105-125 μm has been collected by sieving. The first and last 5 cm of the element were cut after 453 hours of exposure, and the rest of the element was recharged in the reactor and the exposure restarted. In the following, they will be referred to as "ADD1T" and "ADD1B", respectively. Two more samples were then cut at the end of the test from the first and last 5 cm of the recharged element. They will be referred to as "ADD2T" and "ADD2B", respectively.

2.2. SCR Pilot Plant

The SCR pilot plant setup used for this investigation is the same as described in [15]. It mainly consists of a natural gas burner for the flue gas production, a lance for spraying the aqueous solution, a square duct hosting a full length monolith and a NH_3 supply system. NH_3 is injected both in the burner to produce the desired NO concentration at the reactor inlet, and in the flue gas duct leading to the reactor for the NO reduction. Channel blocking is avoided by a soot blowing system installed at the reactor inlet.

2.3. K-P-Ca-S Addition

In order to simulate the addition process, the molar P:K and P:Ca ratios in the flue gas have been fixed to 2 and 0.8 respectively. The KCl concentration has been fixed to 10 mg/Nm^3. Accordingly, 13, 26 and 20 mg/Nm^3 of $Ca(OH)_2$, H_3PO_4 and H_2SO_4 have been added. The addition has been carried out by preparing a water solution of the above listed compounds with the following concentrations: KCl = $6.7 \cdot 10^{-3}$ mol/L, $Ca(OH)_2$ = $1.7 \cdot 10^{-2}$ mol/L, H_3PO_4 = $1.3 \cdot 10^{-2}$ mol/L, H_2SO_4 = $1.0 \cdot 10^{-2}$ mol/L. Since the total flue gas flow at the injection point was equal to 50 Nm^3/h, the solution feed has been fixed to 1 L/h. Only 40 Nm^3/h were then let through the catalyst element during the whole exposure.

2.4. Aerosol Measurements

Aerosol measurements were performed by using both a Scanning Mobility Particle Sizer (SMPS, TSI Inc.), which included an Electrostatic Classifier (Model 3080) and a Condensation Particle Counter (Model 3775), and a 10-stage Berner-type low pressure cascade impactor (LPI) with an aerodynamic diameter range of 0.03-12.7 μm connected to a vacuum pump. Sampling for the SMPS was made at the SCR reactor inlet by an ejector sampler running with dry, particle-free air. In the case of the LPI, the flue gas was sampled directly at the reactor inlet without any dilution. Both the sampling line and the LPI were therefore heated at 90°C in order to avoid any water condensation.

2.5. Activity Measurements

The rate of the SCR reaction at typical industrial reaction conditions has been assumed to follow an Eley-Rideal mechanism of reaction with NH_3 adsorbed on the catalyst surface and NO reacting from the gas phase. The following expression for the rate of reaction, r_{NO}, can then be derived:

$$-r_{NO}\left[\frac{mol}{m^3 s}\right] = kc_{NO}\frac{K_{NH_3}c_{NH_3}}{1+K_{NH_3}c_{NH_3}} \qquad (1.1)$$

where k [1/s] is the rate constant, c_{NO} and c_{NH_3} [mol/m^3] are the concentrations of NO and NH_3 respectively, and K_{NH_3} [m^3/mol] is the adsorption constant for NH_3 on the catalyst surface. The fraction term on the right-hand side of equation (1.1) is the NH_3 coverage of the catalytic surface, θ_{NH_3}.

At the pilot plant, the activities of the catalysts were measured at 350°C in the presence of about 500 ppmv NO, 600 ppmv NH_3, 10%v O_2, 6%v CO_2, and about 10%v H_2O. During activity measurements the flow through the SCR reactor was kept at 40 Nm^3/h, corresponding to about 6.5 m/s of gas velocity at 350°C in the channels.

Since ammonia in our measurements is added in excess with respect to NO (i.e. $NH_3/NO \approx 1.2$), the NH_3 coverage, θ_{NH_3}, can be assumed equal to 1 and the reaction rate can be regarded as pseudo-first order with respect to NO and zero order with respect to NH_3. Therefore, directly from the fractional NO conversion, X, it is possible to calculate an observed catalyst activity constant, k', that includes both the influence of external and internal mass transfer:

$$k'\left[\frac{ml}{g\ s}\right] = -\frac{F_{gas}}{m_{cat}}\ln(1-X) \qquad (1.2)$$

where F_{gas} is the gas flow rate (ml/s), m_{cat} is the weight of catalyst (g). The degree of deactivation can then be calculated as the ratio k/k_0 between the activity constant of the catalyst during exposure, k, and the one measured for the fresh element, k_0, right before starting the poison addition.

In the laboratory, powdered samples have been tested for activity in a packed bed quartz micro-reactor with a diameter equal to 10 mm. Around 0.07 g of powder has been used during activity measurement with a total flow equal to 2.8 NL/min constituted by 500 ppmv NO, 600 ppmv NH_3, 5% O_2 and 1.4% H_2O in N_2. Activity measurements have been performed in the temperature range 250-400°C. The catalyst activity has been calculated according to equation (1.2) and the deactivation as the ratio between the activity constant of the spent catalyst and the one measured for the fresh one.

During all activity measurements, the NO concentration in the flue gas has been measured with a conventional UV analyzer (Rosemount NGA 2000).

2.6. Ammonia Chemisorption

NH_3 chemisorption tests have been periodically carried out at the pilot scale setup during the addition of the additive mixture. The measurements have been made at 350°C and 40 Nm^3/h. Around 600 ppmv NH_3 has been added to the flue gas to the SCR reactor for 30 minutes in order to saturate the catalyst surface. During this saturation period, only the NO produced by the natural gas combustion was present (i.e. ≈ 80 ppmv). After this time, the NH_3 was shut off and right after, around 500 ppm NO was produced by adding a different stream of NH_3 to the burner. The amount of chemisorbed NH_3 can then be calculated by integration over time the amount of reduced NO, due to the equimolar reaction between the gaseous NO and the chemisorbed NH_3.

2.7. Catalyst Characterization

Small pieces of the catalyst were cut from the ends of both fresh and exposed monoliths and characterized with respect to bulk chemical composition, mercury porosimetry and physical appearance by a Scanning Electron Microscope (SEM).
The chemical composition was obtained by ICP-OES at the laboratory of DONG Energy A/S. Prior to the measurements, the samples were cut to 1.5 x 1.7 cm^2 and dried at 105 °C for 2 h before analysis.
The total pore volume and the pore size distribution of the different catalyst samples were made by mercury intrusion in a Micromeritics Autopore II 9220 porosimeter. SEM-EDX analysis was performed at Teknologisk Institut using a Zeiss Ultra55 and an Oxford ISIS with a Pentafet X-ray detector.

3. Results

3.1. Aerosol Measurements at the Pilot-scale Setup

3.1.1. SMPS Measurements

Figure 1 shows the particle size distribution (PSD) measured by the SMPS. The number-based distribution is characterized by a peak around 9 nm. Due to their small sizes, these particles are very mobile and are expected to have fast deposition rates on the catalyst surface. The volume-based distribution, which is proportional to the mass carried by the different particles, shows instead the presence of two distinct peaks. The first one has a mean diameter equal to 12 nm, whereas the second one has a peak around 300 nm. This second peak is clearly representing most of the volume/mass of the total PSD. From Figure 1b it is possible to see that the total volume distribution is somewhat cut off due to a lower efficiency in sampling bigger particles due to the non-isokinetic conditions. By fitting the SMPS data with a lognormal distribution, the expected complete PSD has been obtained. The fitting has been made by minimization of

$$\sum_{d_p}\left[\psi_{V,SMPS}(d_p)-\psi_{V,logn}(d_p)\right]^2 \qquad 20\ nm \le dp \le 300\ nm \qquad (1.3)$$

where $\psi_{V,SMPS}$ is the volume distribution *dV/d(log dp)* calculated from the SMPS measurement, $\psi_{V,logn}$ is the fitted distribution. The mean diameter of the lognormal distribution is equal to about 400 nm. Particles bigger than 1 μm are also expected as shown by the dashed curve in Figure 1b.
The dual-mode volume-based PSD measured by SMPS indicate the presence of mainly two classes of compounds:

1. The first one is constituted by small particles and high concentration numbers due to homogeneous nucleation of gaseous species. This class of particles accounts for about 6% of the total volume measured by the SMPS.
2. The second class is constituted by bigger particles with low total concentration numbers. Their formation is likely due to salt crystallization during water evaporation from the atomized solution at the injection point. This class accounts for about 94% of the total volume measured by the SMPS.

Due to their different mobility and number concentrations, these two particle classes contribute differently to the species accumulation and penetration into the catalyst walls.

3.1.2. Low Pressure Cascade Impactor Test

The results of the tests made with the LPI are shown in Figure 2 and reported in Table 1. Here a mass based particle size distribution with a peak at around 200 nm can be seen. This value is lower than the one measured by the SMPS, and the difference is believed to be due to experimental uncertainties associated with the different sampling techniques and equipments. Particle deposition was found to happen at every single impactor stage as indicated by the non-zero particle concentration in the whole particle diameter range. The total mass concentration was about 10 mg/Nm^3. The EDX chemical analysis of the collected deposits showed no Cl in any of the impactor stage, indicating that Cl was effectively released to the gas phase prior to enter the SCR reactor. From the analysis of the element distribution shown in Figure 2, it can be seen that both Ca and P are distributed in the particle diameter range 25-3000 nm and are instead not found at higher diameters, where only K and S are found, probably due to the formation of some K_2SO_4. For each impactor stage, the different P:K, P:Ca, K:S and K:Ca molar ratios have been calculated and compared with the ones present in the injected solution. As it can be seen in Table 1, both P:Ca and K:S molar ratios have been found constant at around 0.65 and 1.55 respectively throughout the whole particle size range, with only some exceptions for the P:Ca ratio at the first and second impactor stage. Simply based on these values it is not possible to identify the exact composition of the formed salts. However, by comparing the results with both the P:K and P:Ca injected, it is possible to conclude that some P is missing. This result might indicate the formation of gaseous P-compounds or the preferential formation of particles with diameters out of the impactor range, for instance having the volume-based mean diameter at 12 nm measured by the SMPS.

3.2. Catalyst Characterization

3.2.1. Bulk and Surface Chemical Analysis

Table 2 reports the results of both the bulk and surface analysis of samples taken from the exposed monolith at two different exposure times. According to the results obtained from the bulk elemental analysis, P is, among the different species, the one that has accumulated the most in the catalyst walls: On average, the P-accumulation rate is equal to $1.4 \cdot 10^{-3}$ wt%/h, corresponding to about 4% of the incoming P mass. Regarding the Ca and S, the elemental bulk analysis did not show any important increase of these two species in the exposed samples. In fact, apart from ADD1T, the contents of Ca and S were similar to the ones measured for the fresh catalyst, indicating very low accumulation rates for these two elements. The same can be said for the Cl, where the levels were below the lower detection limits for all tested samples.

The results of the EDX surface chemical analysis showed the presence of all the added elements on the outer surface of the catalyst wall. P was again the element most present with a concentration in the range 1.7-4.7 wt%. These values are higher than the total P found in the bulk. As it will be seen later, the reason for the difference is in the decreasing P-concentrations measured along the cross-section of the catalyst wall. As stated before, Ca and S are normally found in the bulk of the fresh catalyst, but are not seen on the outer surface of the walls by EDX. This fact indicates that their presence might be due to the glass fibers, which are reinforcing the catalyst support. All the exposed samples showed instead some Ca and S also on the outer surface indicating that some deposition of these elements did happen during the exposure to the additive mixture. K was also found on the outer surface. The highest maximum level was found on ADD2B, where this was equal to 0.3 wt%, corresponding to a K:V molar ratio equal to 0.2. Interestingly, the K-content on the surface of ADD1T and ADD1B was not much different from the final values indicating that K-accumulation did not proceed at the same rates as at the beginning. The results for the P:K and P:Ca ratios in the catalyst with the ratios in the injected solution indicates an enhanced accumulation of P in the catalyst walls.

3.2.2. SEM Analysis

Aerosol deposition on the outer catalyst surface has been confirmed by the SEM picture taken of the different samples and are shown in Figure 3. In the case of ADD1T shown in Figure 3a, most of the characteristic macro-cracks were even filled with particles. However, these particles which were deposited in the catalyst macro-cracks were able to penetrate the pores for only 20-30 μm, as shown in Figure 3b for ADD1B, indicating that clogging of the macro-cracks did not necessarily require the complete filling of their pore volume. Figure 3c shows a picture at higher magnifications of the deposits found in the macro-cracks.

At the end of the exposure, the appearance of the catalyst surface had changed. The SEM analysis made after 1000 h of exposure revealed the presence of layer on the outer catalyst surface. Figure 4 shows the surface of the catalyst at different magnifications, together with pictures taken of a fresh sample at the same magnifications for comparison. This layer was revealed by the presence of unusual cracks on the surface as shown in Figure 4a and Figure 4b. As can be seen from these pictures, this layer appears as a compact phase about 2-3 μm thick. The comparison with the fresh sample surface clearly confirms the presence of this deposit covering the original catalyst surface. In fact, only the zones revealed by the deposit breakage somewhat recall the porous structure seen on the fresh sample. The EDX analysis of the zones underneath the formed layer, which were revealed by the outer layer cracks, had a reduced content of P compared to the top of the compact layer itself: In the exposed zones the P-content was found equal to around 1 wt%, whereas the average P-content of the surface was equal to 3 wt%.

Cross-sections of the catalyst sample have also been analyzed by SEM-EDX in order to measure the distribution of the different elements inside the catalyst walls. The P-distribution for the sample ADD1B and ADD2T are shown in Figure 5. The measured profiles were those typical for diffusion limited processes, with the P-concentrations levelling off within the first 100 μm of the catalyst wall. In the figure, it can also be seen how the P-levels have increased according to the longer exposure in the sample ADD2T.

Regarding K and Ca, they were not found inside the catalyst walls indicating the inability of these elements in diffusing into the catalyst material. Sulfur was constantly ranging inside the walls between 0.4 and 0.5 wt%, identical to the values found for a fresh sample.
Overall, the results obtained from the cross-sectional analysis clearly indicate i) the ability of P in penetrating the whole catalyst wall; ii) the inability of K and Ca once deposited on the outer surface, to further diffuse inside the wall.

3.3. Deactivation at the Pilot-scale Setup

3.3.1. Activity Measurements

Three activity measurements made after 0, 191 and 1 000 h of exposure respectively are shown in Figure 6. As it can be seen, apart from the different final conversions obtained, which are also dependent on different total catalyst mass due to the cut after 453 h, the conversion curve obtained at 1000 h differs from the other two curves because it first goes through a maximum value right after the NH_3 introduction, and then reaches a steady state value after about 2 minutes of exposure to NH_3. All the activity measurements made after around 300 h of exposure to the additive mixture have shown this behaviour. No NO conversion transient was instead measured at shorter exposure times, as shown by the activity tests made at 0 and 191 h of exposure. This NO transient was found in a previous investigation to be related to the deposition of polyphosphoric acids in the catalyst wall and the consequent titration of V(5+) active sites by formation of P-V(4+) species during exposure to NH_3 [15]. From both the aerosol measurements and the catalyst characterization presented so far, it is clear that also in this case the transient can be associated to the PO_x. In order to isolate the PO_x effect on the overall degree of deactivation, for each activity measurement both a maximum and a steady-state relative activity have been calculated. The results of the calculation are shown in Figure 7. As it can be seen, the two curves started been distinguishable from each other after about 300 h of exposure. Figure 8 shows a plot of the difference between the "Max X" and the "Steady-state" curve shown in Figure 7. In the plot, the y-axis has been labelled "Relative activity - PO_x effect" in order to underline that the curve represents the deactivation explicitly due to the polyphosphoric acids poisoning. As it can be seen, this mechanism of deactivation first increased at a calculated rate of 0.2 %/day, and then started levelling off after about 750 h of exposure, indicating that the catalyst wall probably got saturated with polyphosphoric acids. At the end of the exposure, the percentage of total deactivation that could be associated to poisoning by PO_x can be estimated equal to about 6-7%.
Apart from the quantification of the so called "PO_x effect", another important conclusion can be made from Figure 7. Since the appearance of the NO conversion transient, the "Max X" relative activity has constantly remained around 81% throughout the whole exposure. In fact, 19% of the original activity was lost after the first 191 h of exposure, where no NO transient was measured. This result indicates that the components causing the fast drop of activity at the beginning of the exposure did not cause any further deactivation during the rest of exposure.

3.3.2. NH_3 Chemisorption Tests

The performed NH_3 chemisorption tests made before the first cut are reported in Table 3, together with the observed steady-state relative activity for comparison, in order to

understand the mechanism of deactivation that caused the steep initial decrease in relative activity. According to the NH_3 chemisorption tests, the 19% decrease of activity measured after 260 h of exposure was accompanied by a loss of only 16% in the total chemisorbed NH_3. If poisoning by K and/or Ca was the main responsible for the measured deactivation, being the monolith operating under both external and internal mass transfer limitations, which are partially masking its effect on the intrinsic rate of reaction, a higher decrease in the relative amount of chemisorbed NH_3 compared to the decrease in relative activity would have been measured. In particular, assuming (i) a square root dependency between intrinsic rate of reaction and the observed rate of reaction, valid for mass-transfer-limited reactions; and (ii) a linear relation between the chemisorbed NH_3 and the intrinsic activity, it can be calculated that poisoning only accounted for 8% of the lost activity. The remaining 11% was instead due to physical deactivation by pore blocking and surface masking.
After the first cut, a relative increase of chemisorbed NH_3 was instead measured. For instance, the element increased its capacity in chemisorbing NH_3 of about 39% in the last 600 h of exposure. This increase in chemisorbed NH_3 did however not induce any increase in activity, which was instead decreasing due to the PO_x effect discussed in the previous section. On the other hand, this increase in chemisorbed NH_3 caused a decrease in the NH_3 coverage at the NH_3 partial pressures (i.e. 600 ppm) normally used during the activity measurements. As shown in Equation (1.1), the rate of NO reaction is dependent on the NH_3 coverage of the catalyst surface and can be assumed zero order in NH_3 only when the NH_3 coverage is total. Figure 9 shows a standard activity measurement made after 1096 h of total exposure (i.e. after 1000 h exposure to the doped flue gas and 96 hours exposure to a clean flue gas) followed by a test with the double amount of NH_3 introduced (i.e. 1200 ppmv). The decreased NO measured at the reactor outlet when the ammonia partial pressure was doubled clearly indicates an increase in the reaction rate due to a higher NH_3 coverage at higher NH_3 partial pressures. For a fresh catalyst, no difference in NO conversion is seen for NH_3 concentrations > 600 ppmv.

3.4. Activity Measurements in the Laboratory and Hg-porosimetry Tests

Activity tests on powder samples have been carried out in the laboratory in order to identify the extent of deactivation measured on the monolith due to poisoning. Figure 10 shows an Arrhenius plot of the activities of the fresh and spent catalyst samples exposed for 453 h. The samples ADD1T and ADD1B had a relative activity of 27% and 75% respectively. These values were constant in the whole temperature range as indicated by the same activation energy calculated from the Arrhenius plot (i.e. 63 kJ/mol), pointing at the occurrence of *non-selective* poisoning, mainly proceeding by changing the mass transport characteristic of the catalyst [16].
Physical deactivation by formation of the external layer has been pointed out by the Hg-porosimetry analysis. Figure 11 shows the pore size distribution for the fresh sample and ADD2B, which, as shown by the SEM pictures, presented a fouling layer on its external surface. As it can be seen in the figure, the ADD2B sample did not present any pores in the range 0.3-8 μm. However the total intrusion volume did not differ between the two samples. This fact indicates that the outer surface of the ADD2B sample only presents pores smaller than 0.3 μm due to the formation of the fouling layer. It is believed that the formation of the fouling layer has smoothed the catalyst external area by pore mouth closure.

4. Discussion

4.1. Polyphosphoric Acids Formation

Based on the results obtained in a previous investigation about deactivation by polyphosphoric acids [15] and the results just described in this work (i.e. aerosol formation by homogeneous nucleation, NO conversion transient, increased amount of chemisorbed NH_3, reduced NH_3 coverage), there is no doubt about their formation during the exposure to the additive mixture

The reasons for their formation during this particular test can be various, but they would all require the formation of gaseous H_3PO_4 and its exposure to temperatures higher than 600-700°C. It is believed that some of the compounds which were formed during evaporation of the water from the atomized droplets went through decomposition at increasing temperatures and released some H_3PO_4 in the gas phase. This latter might also have been formed directly during the spraying process. At the end of the polyphosphoric acid investigation [15], it was not clear whether the formation would have been possible in a system including other different elements, or whether the formation was the result of the simplified flue gas composition used in those tests. The results obtained in this investigation have shown that the formation of polyphosphoric acids was possible in our system at the given P/K and P/Ca ratios. Depending on their concentration, polyphosphoric acids may constitute a high risk for a fast deactivation of the vanadia-based SCR catalysts, since for concentrations corresponding to 100 ppmv H_3PO_4, their deposition might already be too fast compared to the rate of hydrolysis at SCR reaction conditions.

4.2. Particle Deposition and Penetration

The volume-based particle size distributions measured by the SMPS and the SEM pictures of the deposits have shown the presence of two distinct classes of particles. The first one with a volume-based mean diameter equal to 12 nm, and the second one with a volume-based mean diameter equal to 400 nm. Due to both a higher number concentration and a higher diffusion coefficient, the first class of particles is depositing faster than the other. By associating these particles to the polyphosphoric acids, which are liquid at the SCR temperatures, it can be assumed that the P found inside the catalyst walls is mainly due to their depositions and penetration due to capillary forces. On the other hand, the complete absence of Ca and K inside the walls is an indication that: i) these elements are present in the bigger particles (i.e. $d_p > 0.1$ μm) which have lower deposition rates and practically no penetration ability; ii) they are tightly bound to the particles themselves. This latter indication is particularly interesting since it further supports the mechanism of deactivation by K proposed in previous works [3,11]. It is now clear that the K present in the particles which are deposited on the outer surface of the catalyst needs to be released from the particles on atomic scale by interactions with the catalyst surface. It is only afterwards that K can diffuse inside the walls by surface concentration gradients. Particle diffusion is not likely to happen since the same mechanism would have also been active in this investigation, due to the similar particle sizes involved in the tests. K and Ca are instead accumulating on the outer surface. Due to the higher concentration of P found on the formed fouling layer, it is likely that the K-Ca-(P) crystals are dissolved in the polyphosphoric acids forming the molten-looking layer. From the present data it is not possible to know whether this outer layer would have continued growing or whether its depth had reached a steady value. From the

cracks found during the SEM analysis, it appears that some of it has fallen apart, but this could have happened during the cooling of the monolith and may not happen during normal operation.
Regarding the S-content, the SO_2 levels measured in the flue gas were approximately the ones calculated by assuming the entire S added by the solution to be completely converted to SO_2. Therefore it is believed that the additional S found on the outer surface of the catalyst is due to sulphation reactions between the deposits and the gaseous SO_2. Moreover, since no additional S has been found inside the catalyst wall where only P had accumulated, it is assumed that the sulphation reaction preferentially takes place with K and Ca giving K_2SO_4 and $CaSO_4$ respectively.

4.3. Deactivation Mechanism

Based on the results presented, it can be concluded that the deactivation measured during this investigation followed different mechanisms, each of them acting in different periods of time. During the first 200 h of exposure, the steep decrease in observed deactivation (i.e. – 2.4%/day) was due to (i) poisoning by K and Ca of the outer catalyst surface; (ii) blocking of the macro-cracks and surface fouling by particle deposition. Both these deactivation mechanisms are caused by particle deposition on the catalyst outer surface with subsequent direct and indirect blocking of the active sites. Due to the pore blocking, the diffusion of both reactants and products is slowed down and, even though the inner layers of the wall are still very active since not attacked by the poison, they are less accessible. This mechanism of deactivation, however, is not expected to cause any further deactivation in the long term provided that the formed deposit layer will (i) keep some porosity, and (ii) not increase its thickness.
For exposure time > 300 h, the observed deactivation was instead due to poisoning by polyphosphoric acids and initially proceeded at 0.2 %/day and ceased after about 750 h of exposure. Based on both the size and number concentration of the particles which have been assigned to the polyphosphoric acids (i.e. the peak around 9 nm) and the aerosols measurements made at different H_3PO_4 concentrations in a previous investigation [15], it can be estimated that these were counting for about 3-4 ppmv P during the test reported in this work, i.e. half of the total P injected in the flue gas. At these low concentrations, the P-accumulation in the catalyst walls is limited by the hydrolysis of the polyphosphoric acids at the SCR temperature due to the gas moisture [15]. Therefore, it is believed that the relative activity levelled off due to a saturation of the catalyst wall obtained due to simultaneous deposition and hydrolysis.
Based on these considerations, it is not expected that further deactivation due to the just discussed mechanisms would have been measured if the exposure was continued.

5. Conclusion

Simultaneous addition of KCl, H_3PO_4, $Ca(OH)_2$ and H_2SO_4 in a hot flue gas has been carried out for 1000 h in a SCR pilot scale setup and the activity of a commercial SCR catalyst has been followed as a function of exposure time. The test has been used to estimate the effects of the potential products of the K-getter additives addition process during biomass combustion.
In the test carried out, the P/K and P/Ca molar ratios have been fixed to values of 2 and 0.8 respectively suggested in the literature.
Either K or Ca did not penetrate the catalyst walls but only accumulated on the external catalyst surface. Poisoning by K and Ca was therefore limited to the most outer wall

layers. It has been estimated that 8% of initial relative activity (i.e. 1/3 of the overall deactivation measured at the end of the test) was lost due to this mechanism.
At the chosen experimental conditions, formation of polyphosphoric acids has been favoured and about half of the total P has been estimated to be present in these compounds, which formed aerosols with volume-based mean diameter equal to 12 nm. The known deactivating effects of the polyphosphoric acids (i.e. NO transient, reduced NH_3 coverage) have been identified: After the initial loss of activity, they controlled the overall deactivation rate, which was about 0.2 %/day. However, due to their relatively low concentration and the simultaneous occurrence of hydrolysis at the SCR reaction condition, the catalyst reached a saturation point after about 750 h of exposure. No additional deactivation was then measured in the following 250 h of addition.
Based on the results obtained in this work, it can be concluded that binding K into P-K-Ca compounds is an effective way of reducing the deactivation rates normally experienced during biomass combustion. Reactions between K and the V active sites are in fact prevented, and so is the penetration of K in the catalyst walls by surface diffusion. However, in real applications, the formation of polyphosphoric acids needs to be controlled, since this may counterbalance the just mentioned positive effects. PO_x levels in the range 1-10 ppmv may still be acceptable since their deposition will be limited by their simultaneous hydrolysis, and a saturation level in the catalyst wall will be reached. This situation could however be different in the presence of higher K-concentrations in the flue gas. If the fraction of P forming the PO_x is mainly controlled by the P/K and P/Ca ratios, at higher K-contents the amount of formed PO_x could be higher and thereby lead to faster deactivation rates. More tests at different P/K and P/Ca ratios would be necessary to understand the formation of PO_x, and suggest the conditions to limit it.

Acknowledgments

This work is part of the CHEC (Combustion and Harmful Emission Control) Research Center funded a.o. by the Technical University of Denmark, the Danish Technical Research Council, the European Union, the Nordic Energy Research, Dong Energy A/S, Vattenfall A.B., F L Smidth A/S, and Public Service Obligation funds from Energinet.dk and the Danish Energy Research program. In particular, this work is supported by the PSO project "Deactivation of SCR Catalysts by Additives" (PSO Elkraft FU-4205). Supply of the catalyst samples by Haldor Topsøe A/S is gratefully acknowledged.

References

[1] F. Castellino, A.D. Jensen, J.E. Johnsson, Influence of Reaction K-getter Fuel Additives on Commercial Vanadia-based SCR Catalysts - Part I: Potassium Phosphate, Applied Catalysis B: Environmental, *submitted.*
[2] P.A. Jensen, L.H. Sørensen, G. Hu, J.K. Holm, F. Frandsen, U.B. Henriksen. Technical University of Denmark (2005) KT-Report No. 0504.
[3] Y. Zheng, A.D. Jensen, J.E. Johnsson, Applied Catalysis B: Environmental 60 (2005) 261-272.
[4] Å. Kling, C. Andersson, Å. Myringer, D. Eskilsson, S.G. Järås, Applied Catalysis B: Environmental 69 (2007) 240-251.
[5] J.P. Chen, M.A. Buzanowski, R.T. Yang, J. Air Waste Manage. Assoc. 40 (1990) 1403-1409.

[6] J.P. Chen, R.T. Yang, Journal of Catalysis 125 (1990) 411-420.
[7] L. Lietti, P. Forzatti, G. Ramis, G. Busca, F. Bregani, Applied Catalysis B: Environmental 3 (1993) 13-35.
[8] H. Kamata, K. Takashi, C.U.I. Odenbrand, Journal of Molecular Catalysis A: Chemical 139 (1999), 189-198.
[9] R. Khodayari, C. Andersson, C.U.I. Odenbrand, L.H. Andersson, in: Proceeding of the Fifth European Conference on Industrial Furnace and Boilers, vol. II, 11-14 April 2000, Espinho, Porto, Portugal, 2000.
[10] Y. Zheng, A.D. Jensen, J.E. Johnsson, Ind. Eng. Chem. Res. 43 (2004), 941-947.
[11] Y. Zheng, A.D. Jensen, J.E. Johnsson, Applied Catalysis B: Environmental 83 (2008) 186-194.
[12] J. Blanco, P. Avila, C. Barthelemy, A. Bahamonde, J.A. Odriozola, J.F. Garcia de la Banda, H. Heinemann, Applied Catalysis 55 (1989) 151-164.
[13] H. Kamata, K. Takahashi, C.U.I. Odenbrand, Catalysis Letters 53 (1998) 65-71.
[14] J. Beck, J. Brandenstein, S. Unterberger, K.R.G. Hein, Applied Catalysis B: Environmental 49 (2004) 15-25.
[15] F. Castellino, S.B. Rasmussen, A.D. Jensen, J.E. Johnsson, R. Fehrmann, Applied Catalysis B: Environmental 83 (2008) 110-122.
[16] E. Hums, Catalysis Today 42 (1998) 25-35.

Figure Captions

Figure 1: Number-based (a) and volume-based (b) particle size distributions measured by a SMPS at the reactor inlet during simulatneous addition of KCl (10 mg/Nm^3), $Ca(OH)_2$ (13 mg/Nm^3), H_3PO_4 (26 mg/Nm^3) and H_2SO_4 (20 mg/Nm^3). T = 350°C. The dashed line represents the lognormal distribution obtained by interpolation of experimental data.
Figure 2: Particle size distribution measured by a low pressure impactor at the reactor inlet during simulatneous addition of KCl (10 mg/Nm^3), $Ca(OH)_2$ (13 mg/Nm^3), H_3PO_4 (26 mg/Nm^3) and H_2SO_4 (20 mg/Nm^3). T = 90°C. The curves for each single element have been obtained knowing their concentration on each single stage from EDX analysis.
Figure 3: SEM images of catalyst samples taken after 453 h of exposure: a) ADD1T; b) ADD1B; c) ADD1B.
Figure 4: SEM images of: a,b) catalyst sample taken after 1000 h of exposure (ADD2B); c,d) fresh sample. Magnification: a,c) 2000X; b,d) 20000X.
Figure 5: P-concentration profile inside the spent catalyst walls.
Figure 6: Activity measurement made on fresh and spent monolith at 350 °C. Gas dry composition: NO = 500 ppmv, NH_3 = 600 ppmv, O_2 = 10 %v, CO_2 = 6 %v. H_2O = 10 %v. Flow: 40 Nm^3/h.
Figure 7: Relative activity as a function of exposure time. The activity measurement were made at 350 °C. Gas dry composition: NO = 500 ppmv, NH_3 = 600 ppmv, O_2 = 10 %v, CO_2 = 6 %v. H_2O = 10 %v. Flow: 40 Nm^3/h.
Figure 8: PO_x deactivation effect as a function of exposure time. The data points represent the difference between "Max X" and "Steady-state X" curves in Figure 6.
Figure 9: Activity measurement on spent catalyst exposed for 1000 hours to the doped flue gas and 96 additional hours to a clean flue gas. T = 350°C. Gas dry composition: NO = 500 ppmv, NH_3 = 600-1200 ppmv, O_2 = 10 %v, CO_2 = 6 %v. H_2O = 10 %v. Flow: 40 Nm^3/h.
Figure 10: Activity test on powder samples. Catalyst mass, W = 0.07 g. Total flow F = 2.8 NL/min. Gas composition: NO = 500 ppmv, NH_3 = 600 ppmv, O_2 = 5%, H_2O =1.4% in N_2.
Figure 11: Pore size distribution measured by Hg-porosimetry.

Table 1: EDX analysis performed on the foils of the impactor stages.

Stage	**Particle Diameter**	**P/K**	**P/Ca**	**K/S**	**K/Ca**
#	*nm*	*mol/mol*	*mol/mol*	*mol/mol*	*mol/mol*
1	11391	0.08	17.22	1.63	211.61
2	5773	0.06	1.42	1.76	23.63
3	2931	0.33	0.72	1.67	2.18
4	1488	0.62	0.68	1.44	1.10
5	754	1.60	0.63	1.23	0.39
6	382	2.53	0.60	1.28	0.24
7	194	1.33	0.63	1.52	0.47
8	98	1.22	0.61	1.88	0.50
9	50	1.35	0.66	1.63	0.49
10	25	1.08	0.66	1.64	0.61
Addition		2	0.8	0.67	0.4

Table 2: Bulk, surface and Hg-porosimetry analysis for the fresh and spent monoliths.

	Fresh	**ADD1T**	**ADD2T**	**ADD2B**	**ADD1B**
Axial Position, cm		5	10	40	45
Additive Exposure, h		453	1 000	1 000	453
Bulk chemical analysis					
V %, wt/wt	1.6	2.4	1.9	1.8	1.7
K %, wt/wt	-	0.1	0.2	0.1	< 0.1
P %, wt/wt	-	0.7	1.8	1.3	0.5
Ca %, wt/wt	1.7	2.1	1.9	1.7	1.8
S %, wt/wt	0.3	0.4	0.4	0.3	0.3
Cl %, wt/wt	< 0.1	< 0.1	< 0.1	< 0.1	< 0.1
Surface chemical analysis					
V %, wt/wt	2.10	3.84	3.35	1.93	2.04
K %, wt/wt	-	0.22	0.25	0.33	0.12
P %, wt/wt	-	1.67	4.67	3.10	1.72
Ca %, wt/wt	-	0.41	0.36	1.17	0.11
S %, wt/wt	0.66	0.67	0.71	1.39	0.36
Cl %, wt/wt	-	-	-	-	-

Table 3: Relative chemisorbed NH_3 and relative activity as a function of exposure time.

Time *h*	**NH_3^*** *mol/kg*	**$NH_3^* / NH_3^*{}_0$**	**k_{ss}/k_0**
0	0.033	1.00	1.00
260	0.028	0.84	0.81
333	0.028	0.84	0.80
357	0.029	0.86	0.82

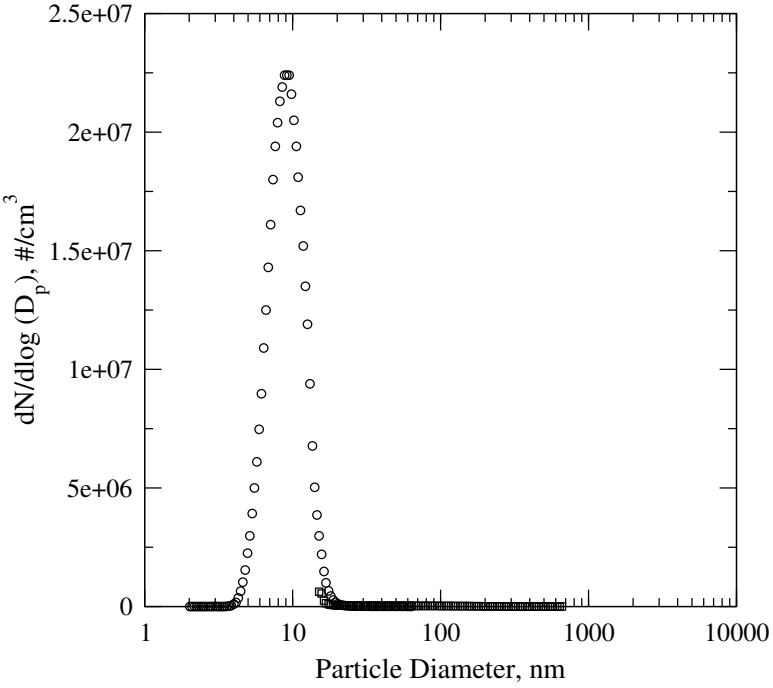
2.5e+07
2e+07
1.5e+07
1e+07
5e+06
0
dN/dlog (D_p), #/cm^3
1
10
100
1000
10000
Particle Diameter, nm

a)

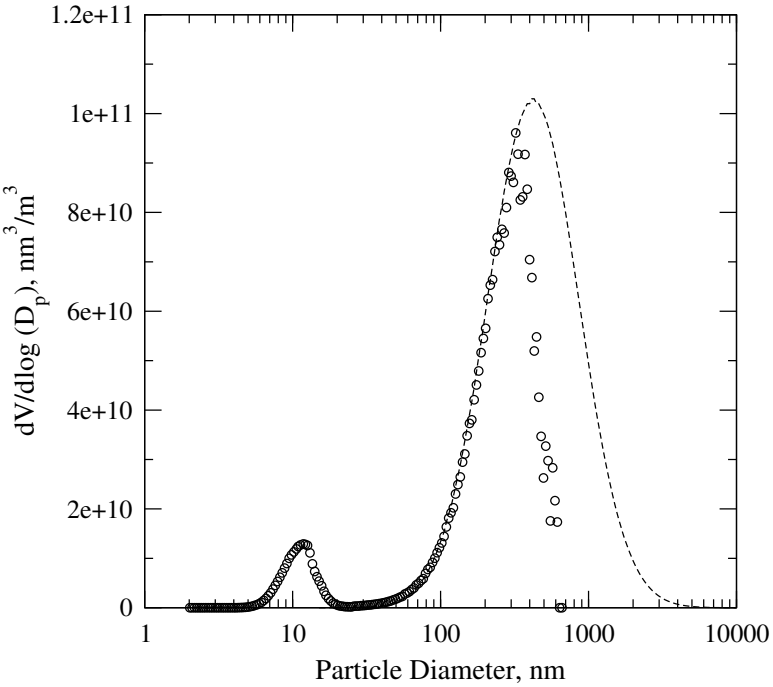
1.2e+11
1e+11
8e+10
6e+10
4e+10
2e+10
0
dV/dlog (D_p), nm^3/m^3
1
10
100
1000
10000
Particle Diameter, nm

b)

Figure 1

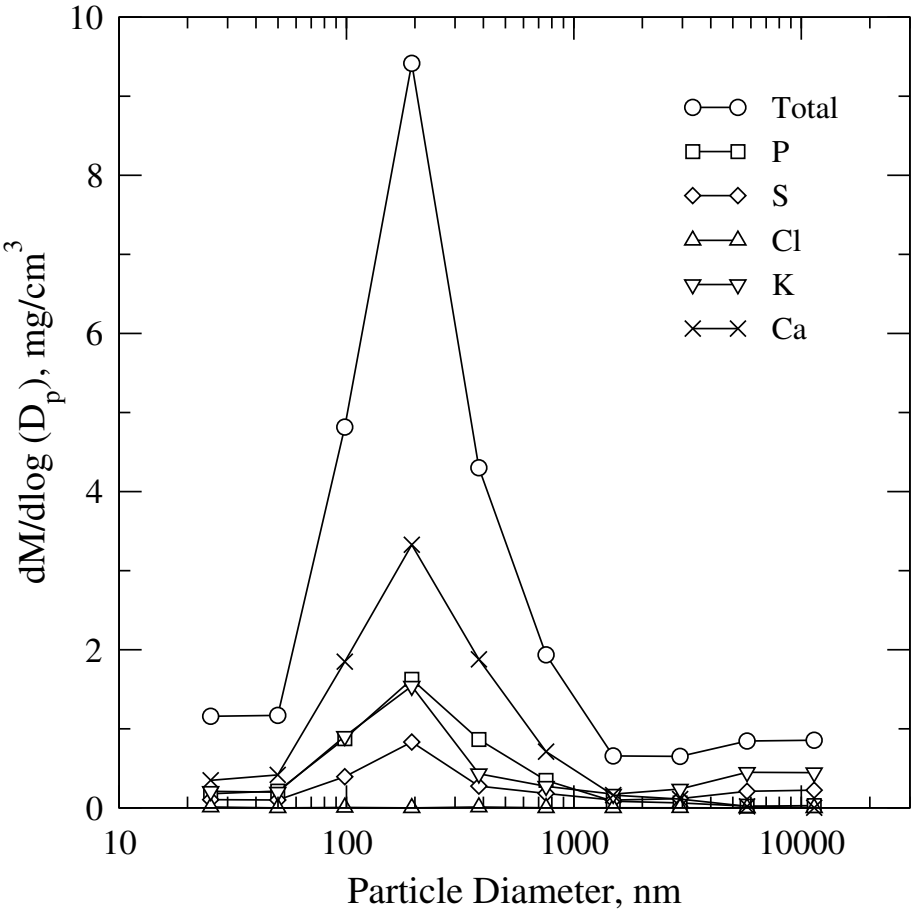
10
8
6
4
2
0
10
100
1000
10000
Particle Diameter, nm
dM/dlog (D_p), mg/cm^3
Total
P
S
Cl
K
Ca

Figure 2

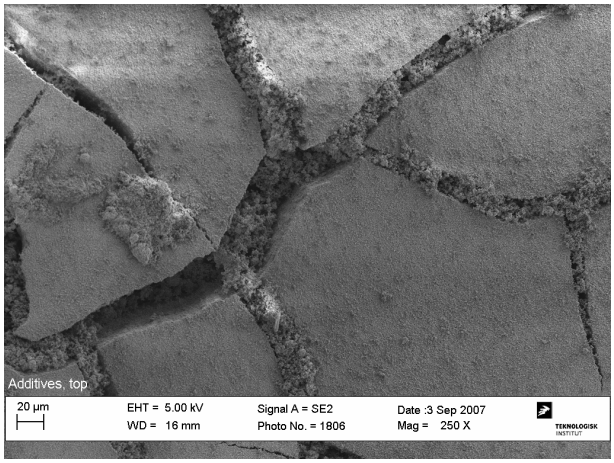
Additives, top
20 µm
EHT = 5.00 kV
WD = 16 mm
Signal A = SE2
Photo No. = 1806
Date :3 Sep 2007
Mag = 250 X
TEKNOLOGISK INSTITUT

a)

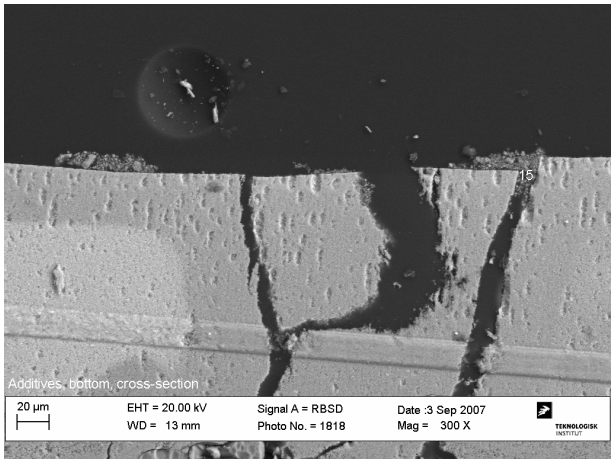
Additives, bottom, cross-section
20 µm
EHT = 20.00 kV
WD = 13 mm
Signal A = RBSD
Photo No. = 1818
Date :3 Sep 2007
Mag = 300 X
TEKNOLOGISK INSTITUT

b)

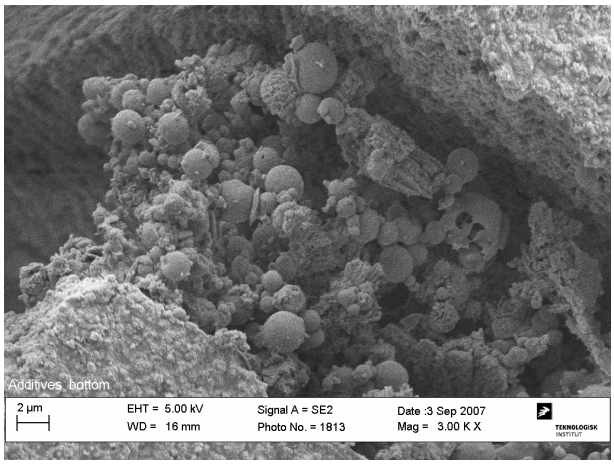
Additives, bottom
2 µm
EHT = 5.00 kV
WD = 16 mm
Signal A = SE2
Photo No. = 1813
Date :3 Sep 2007
Mag = 3.00 K X
TEKNOLOGISK INSTITUT

c)

Figure 3

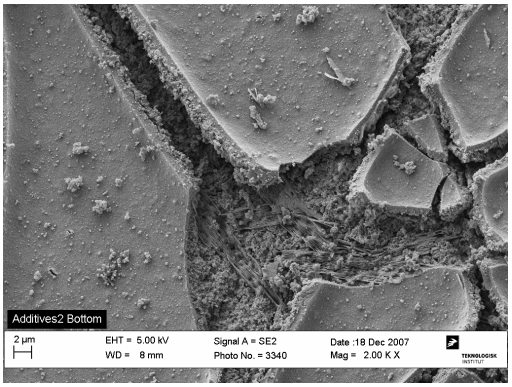

a)

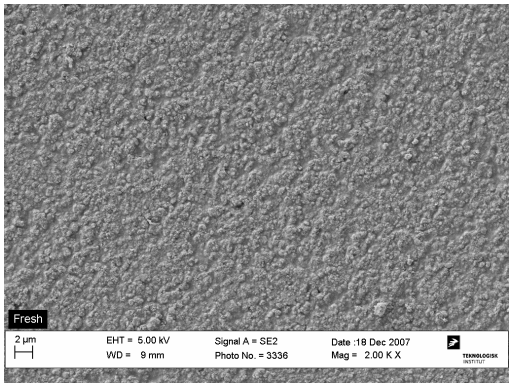

c)

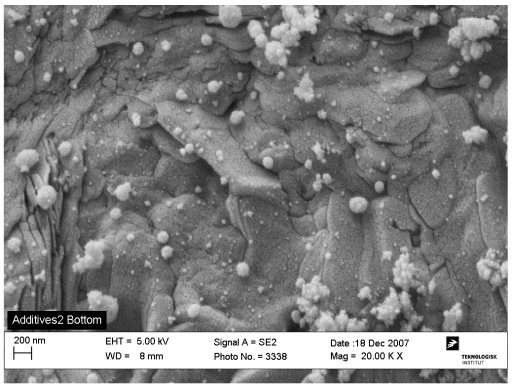

b)

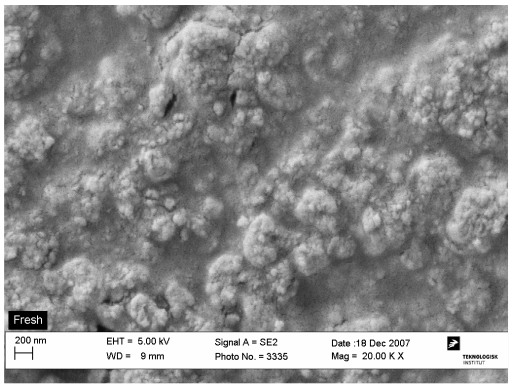

d)

Figure 4

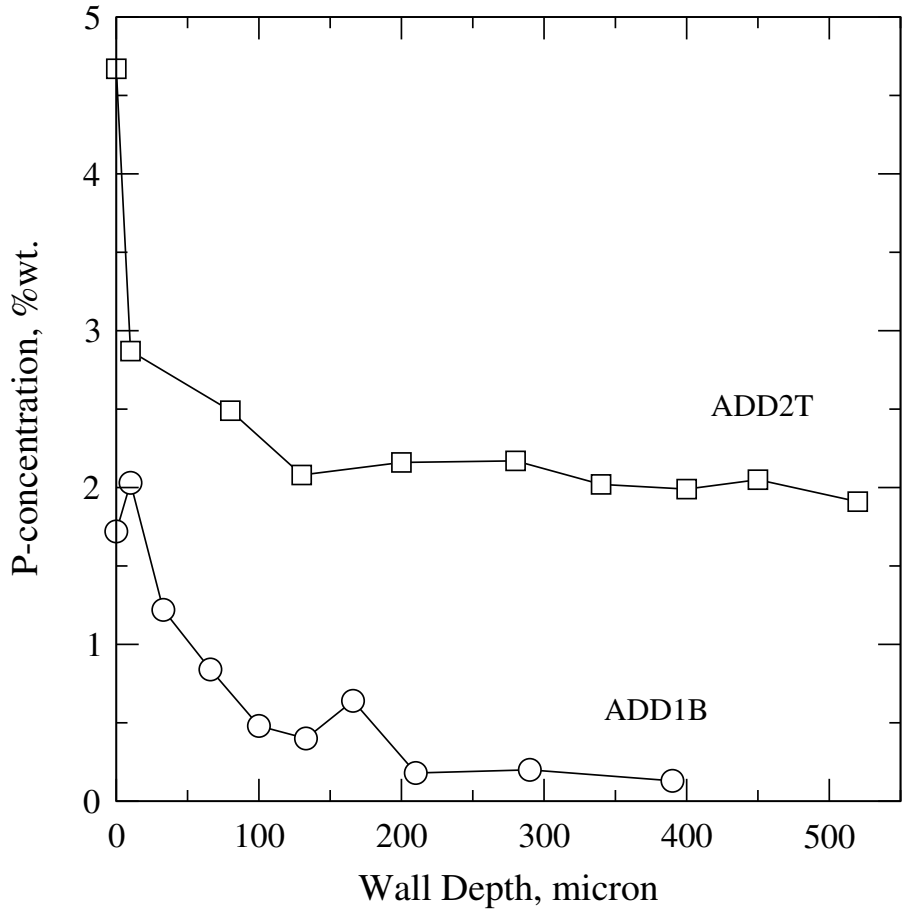
P-concentration, %wt.
Wall Depth, micron
ADD2T
ADD1B
0
1
2
3
4
5
0
100
200
300
400
500

Figure 5

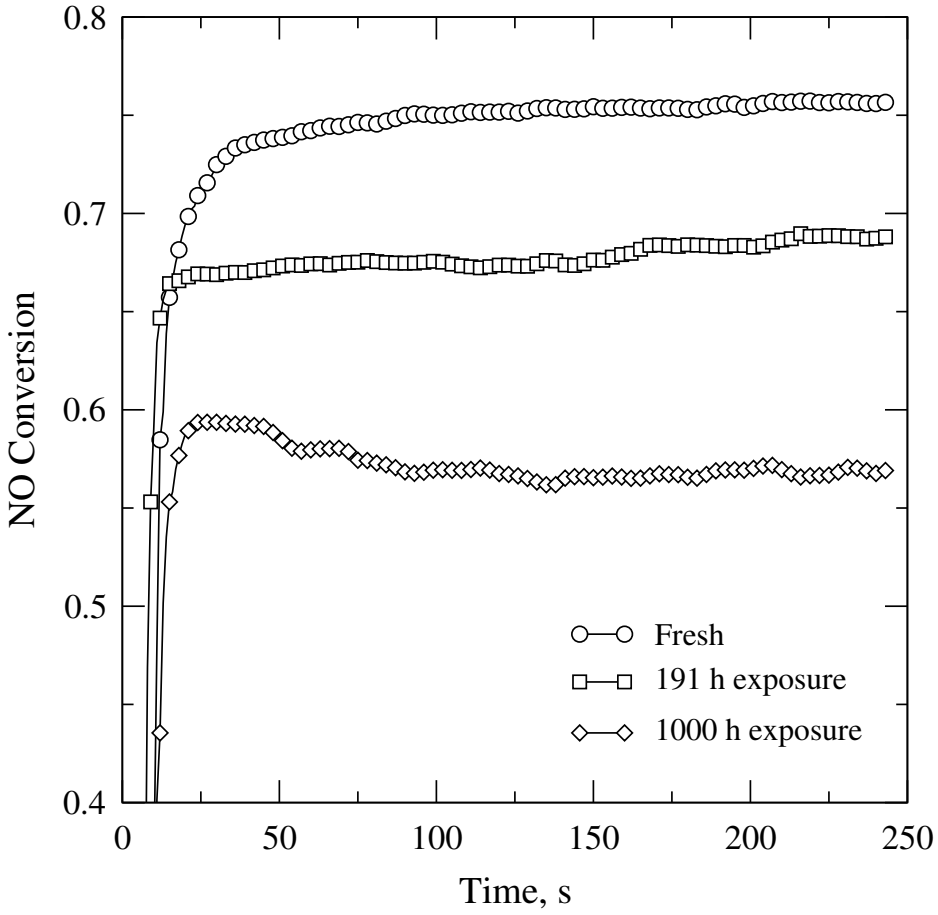
0.8
0.7
0.6
0.5
0.4
NO Conversion
0
50
100
150
200
250
Time, s
Fresh
191 h exposure
1000 h exposure

Figure 6

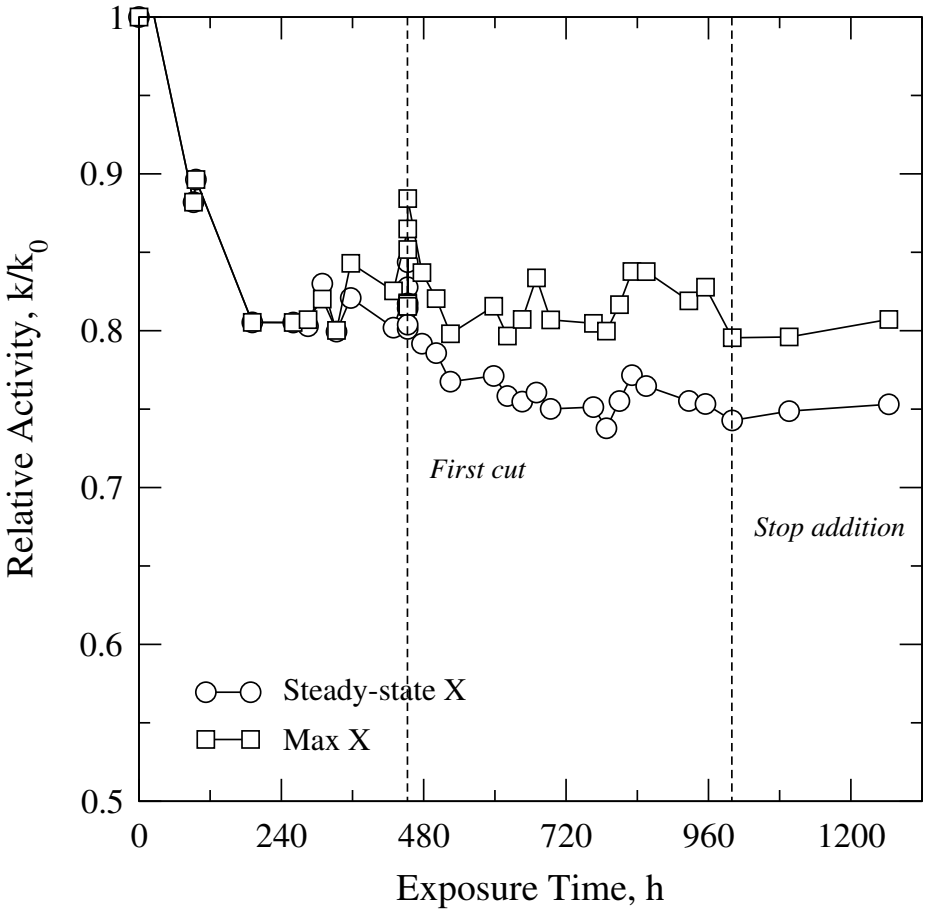
1
0.9
0.8
0.7
0.6
0.5
Relative Activity, k/k0
0
240
480
720
960
1200
Exposure Time, h
First cut
Stop addition
Steady-state X
Max X

Figure 7

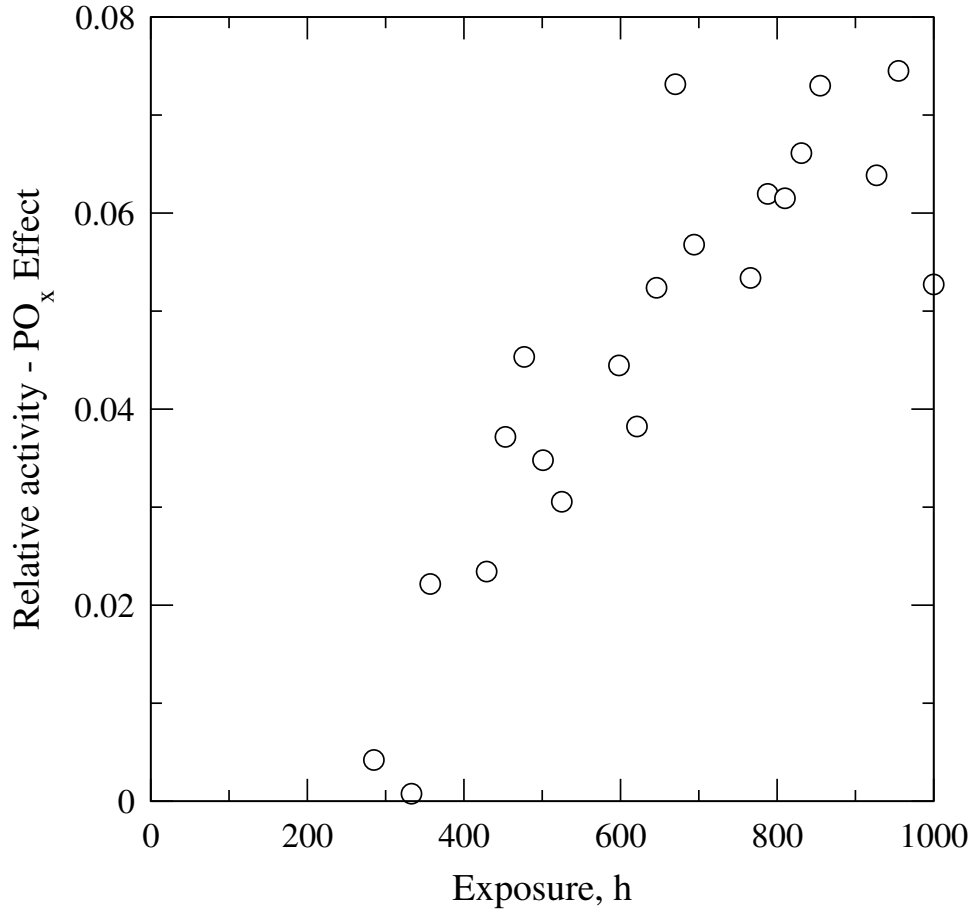
0.08
0.06
0.04
0.02
0
Relative activity - PO$_x$ Effect
0
200
400
600
800
1000
Exposure, h

Figure 8

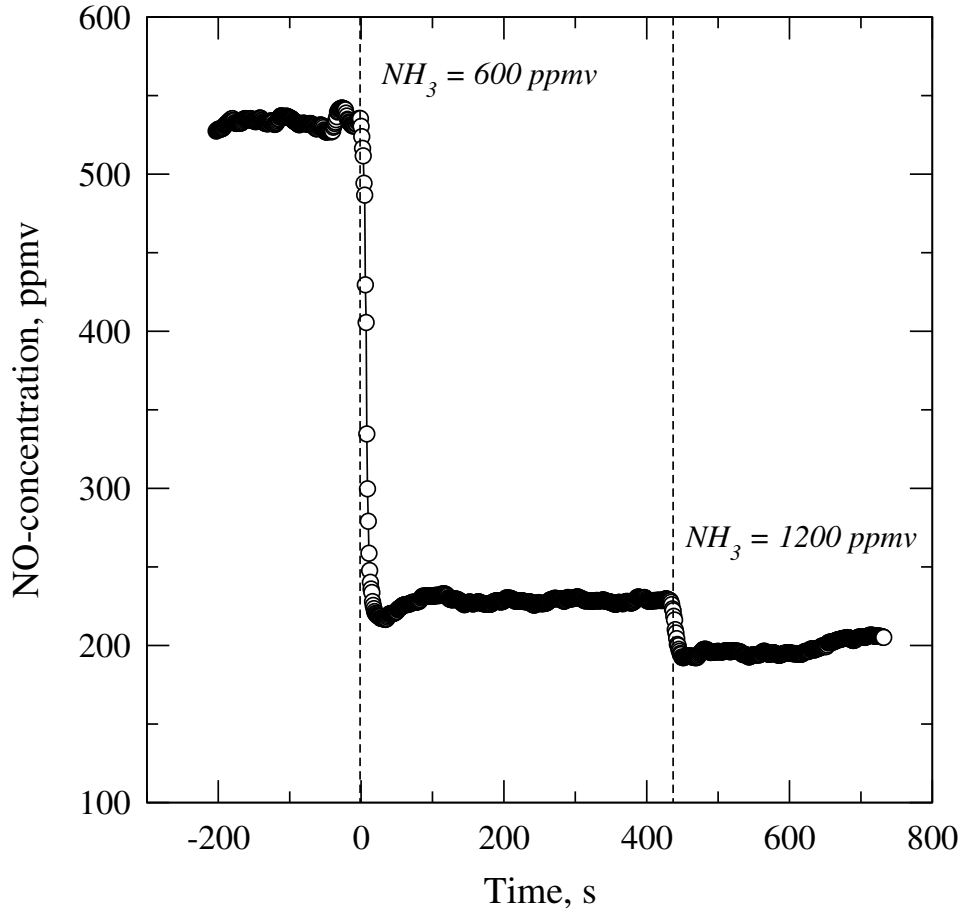
600
500
400
300
200
100
NO-concentration, ppmv
NH_3 = 600 ppmv
NH_3 = 1200 ppmv
-200
0
200
400
600
800
Time, s

Figure 9

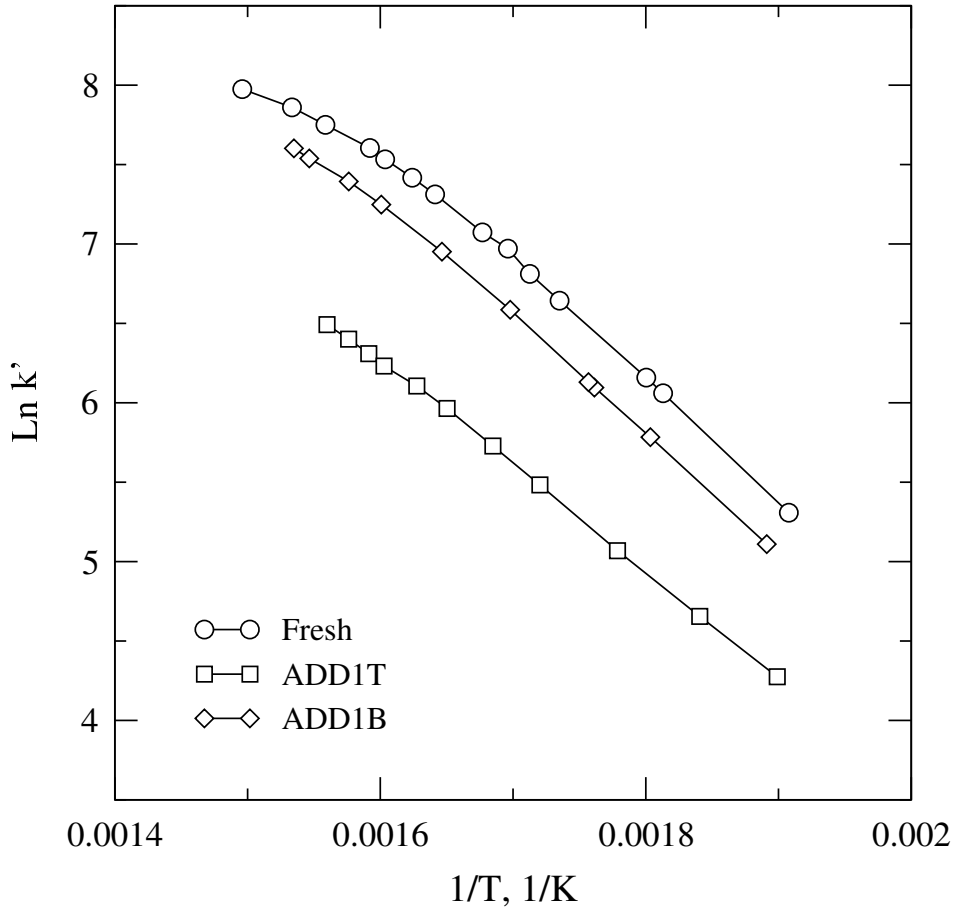

Figure 10

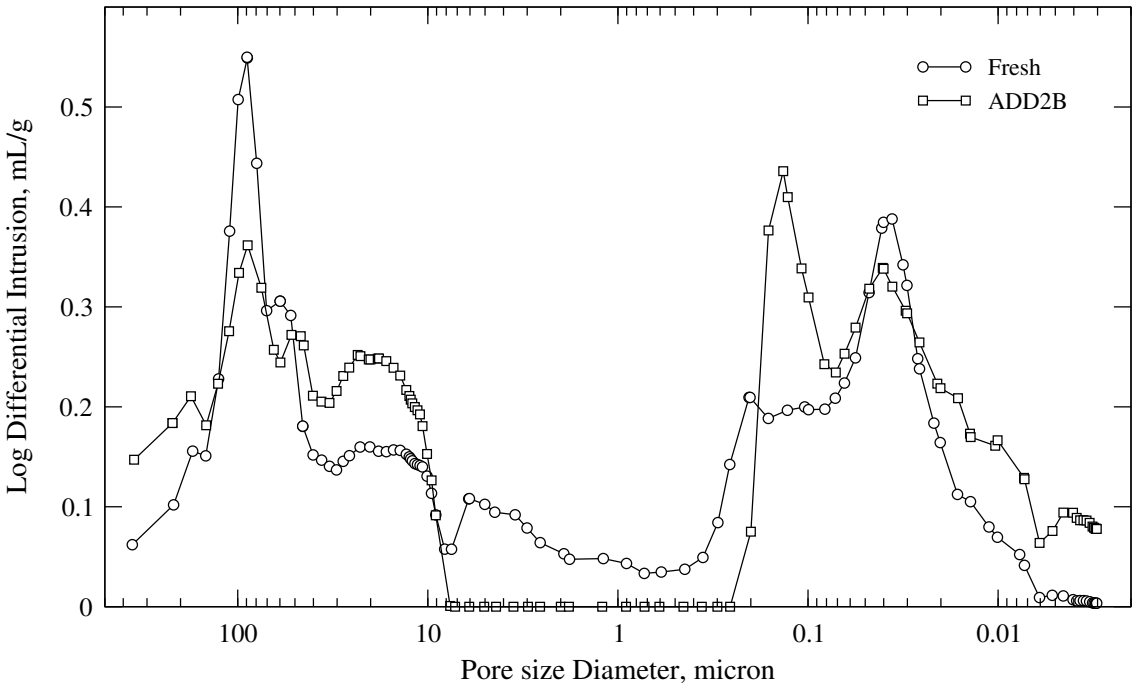
Fresh
ADD2B
Log Differential Intrusion, mL/g
0
0.1
0.2
0.3
0.4
0.5
100
10
1
0.1
0.01
Pore size Diameter, micron

Figure 11